Doctorate Dissertation
博士論文

The Early-phase Photometric Behavior of Type Ia Supernovae and Its Implications

（Ia 型超新星の早期測光観測とその解釈）

A Dissertation Submitted for Degree of Doctor of Philosophy
December　2018

平成 30 年 12 月博士（理学）申請

Department of Astronomy, Graduate School of Science,
The University of Tokyo

東京大学大学院理学系研究科天文学専攻

Jian Jiang
姜　継安

Doctorate Dissertation

The Early-phase Photometric Behavior of Type Ia Supernovae and Its Implications

Jian Jiang

Department of Astronomy
Graduate School of Science
The University of Tokyo

December 2018

I dedicate this thesis to my parents
for their encouragement,
endless support,
and unconditional love.

Acknowledgement

Firstly, I would like to express my sincerest gratitude to my advisor Prof. Mamoru Doi for the earnest inculcation and support of my Ph.D study, for his patience and encouragement, and for his immense knowledge. I am also very grateful to his trust to let me carry out scientific projects by myself and his guidance of how to become an independent researcher.

I am profoundly grateful to Profs. Keiichi Maeda and Toshikazu Shigeyama, for their earnest guidance and insightful comments in my research, which significantly broaden my knowledge not only on the stellar evolution and the physics of supernovae but also on the skills of scientific writing. I could not have imagined having better collaborators for my Ph.D study.

Heartfelt thanks go to Dr. Tomoki Morokuma, Profs. Nozomu Tominaga, Masaomi Tanaka, Naoki Yasuda, Drs. Ken'ichi Nomoto, Izumi Hachisu, and Naotaka Suzuki for the support and inspiring discussions in astronomical observations, pipeline development, theories, and so on.

Gratitude is extended to oversea MUSSES members including Profs. Željko Ivezić, Saurabh W. Jha, Pilar Luiz-Lapuente, Paolo A. Mazzali, Maximilian Stritzinger, Ferdinando Patat, Jeremy R.

Mould, Lifan Wang, Andrew Connolly, Drs. Dietrich Baade, Peter Yoachim, Chris Ashall, David Jones, and all astronomers and engineers who supported observations related to my research.

I would also like to thank my fellow labmates, Drs. Yasuhito Hashiba, Mitsuru Kokubo, Kazuma Mitsuda and my friends Tao Wang, Xing Lu, Yi Yang, and Shibo Shu. I have studied a lot about astrophysics and astronomical observations/instrumentations from discussions and chatting with them.

Finally, special thanks go to my parents, especially for my mother, Yeming Fang, for their support, understanding, and encouragement throughout my time in Todai, and inspiring me to pursue my dream. I love them so much, and I would not have made it this far without them.

Abstract

As one of the most spectacular explosive phenomena in the Universe, the type Ia supernova (SN Ia) has been thought to originate from the thermonuclear explosion of a carbon-oxygen white dwarf in a binary system. Even though SNe Ia have been widely applied as the cosmic distance indicator and helped us to discover the accelerating expansion of the Universe, their progenitor and the physics leading to the explosion are still under debate. Recent theoretical simulations have indicated that SNe Ia discovered within a few days of their explosions (hereafter "early-phase SNe Ia") play an irreplaceable role in tackling the long-standing explosion and progenitor issues of the SN Ia, thus inspiring me to carry out relevant studies with time-domain surveys which are specialized for discovering early-phase SNe Ia.

Despite the great scientific importance of early-phase SNe Ia, relevant studies have not been well conducted because the dimness of early-phase SNe Ia makes them hard to be discovered. Thanks to the excellent survey performance of the Kiso Wide Field Camera (KWFC) mounted on the 1.05-m Kiso Schmidt telescope and the Hyper Suprime-Cam (HSC) on the 8.2-m Subaru telescope, systematical investigations of the early-phase photometric behavior of SNe Ia were carried out by joining the "**KI**so **S**upernova **S**urvey" (**KISS**) project and leading two specific survey projects, the "**S**urvey with **K**WFC for **Y**oung **S**upernovae" (**SKYS**) and the "**MU**lti-band **S**ubaru **S**urvey for **E**arly-phase **S**Ne Ia" (**MUSSES**).

In order to test the feasibility of running an early-phase SNe Ia-targeted survey, a series of observations through two supernova projects with Kiso/KWFC, KISS and SKYS, were carried out in 2015. During seven-months observations, total 13 SN candidates were discovered and four of them were confirmed as early-phase supernovae. Photometric/spectroscopic information obtained from KWFC and other follow-up facilities indicate that three of them are early-phase SNe Ia (KISS15m, KISS15n, and SKYS6) in different SN Ia subclasses. The early-phase photometry together with follow-up observations enables us to study the intrinsic connection/difference between different SN Ia subclasses from a unique perspective.

The discovery of three early-phase SNe Ia in our KWFC observations demonstrated the feasibility of conducting an early-phase SNe Ia-targeted survey with wide-field imagers and thus inspired us to further investigate early-phase SNe Ia with the best survey facility in the world, the Subaru/HSC. A specialized early-phase SNe Ia survey project with Subaru/HSC, MUSSES, was launched out in April, 2016. The MUSSES project includes survey observations with the 8.2-m Subaru telescope and follow-up observations with more than 10 ground-based telescopes all over the world. In the first observing run, 12 early-phase SN candidates were discovered. In particular, the multiband Subaru/HSC survey and follow-up observations indicated that a promi-

nent but red flash at early phase followed with peculiar spectral features of a normal-brightness SN Ia, MUSSES1604D (SN 2016jhr), are in conflict with predictions by previously proposed physical scenarios. Further analysis with numerous computational simulations suggested that all peculiarities of MUSSES1604D can be naturally explained by a supernova explosion that is triggered by a detonation of a thin helium shell of its progenitor star (the so-called He-shell detonation scenario). This finding not only indicates the multiple origins of the light-curve excess found in early-phase SNe Ia but also provides robust evidence of one kind of explosion mechanism of SNe Ia for the first time.

Inspired by the discovery of MUSSES1604D, further investigations of early-phase SNe Ia that show additional brightness enhancements (hereafter "early-excess SNe Ia") were carried out. With the most complete early-phase SN Ia sample so far, we carried out a statistical study of early-excess SNe Ia (11 in total, and five of them are newly confirmed) for the first time. The study indicated that previously discovered early-excess SNe Ia show a clear preference for specific SN Ia subclasses. In particular, the early-excess feature shown in all six luminous (91T- and 99aa-like) SNe Ia is in conflict with the viewing angle dependence predicted by the companion-ejecta interaction scenario. Instead, such a high early-excess fraction is likely related to the explosion physics of luminous SNe Ia; i.e., a more efficient detonation happening in the progenitor of luminous SNe Ia may consequently account for the early-excess feature powered by the radiation from a ^{56}Ni-abundant outer layer. The diversity of early-excess features shown in different SN Ia subclasses suggests multiple origins of the discovered early-excess SNe Ia, challenging their applicability as a robust progenitor indicator. Further understanding of the early-excess diversity relies not only on multiband photometry and prompt-response spectroscopy of individual early-excess SNe Ia but also on investigations of the general early-phase light-curve behavior of each SN Ia subclass.

In the next decade, time-domain astronomy will become one of the most popular branches in astronomy, and pioneering work on early-phase SNe Ia and other kinds of rapid transients can be carried out by using Subaru/HSC and Kiso/Tomo-e Gozen camera. With the forthcoming Tomo-e Gozen transient survey and the MUSSES-FAST, an innovative transient survey that uniquely combines two top-level survey facilities (i.e. HSC and Tomo-e Gozen camera) for the rapid transients study, systematical investigations of dozens of early-phase SNe Ia will be achieved in the next few years. New breakthroughs in not only SNe Ia but also other branches of time-domain astronomy can be expected with the ongoing and forthcoming transient surveys in the near future.

Contents

List of Figures

List of Tables

1 Introduction

1.1 The History of Supernova Studies

The observation of supernova (SN) has a long history. The first reliable record of an SN can be dated back to AD185, the SN 185, which is recorded in the "Book of the Later Han" by Chinese astronomers. In the next hundreds of years, a few SNe occurred in the Milky Way were well recorded by astronomers from several countries, such as SN 1054, which is well known by its remnant, the Crab Nebula. In AD 1604, Johannes Kepler observed the last Milky Way SN so far, SN 1604, the so-called "Kepler's Supernova". In 1885, the first extragalactic SN, SN 1885A, was discovered in the Andromeda Galaxy, also known as the Messier 31 (M31). The finding of SN 1885A not only refreshed our understanding of the nature of the SN, but implied a likely extragalactic distance of M31. Since then, more and more observations have been carried out on these spectacular explosive phenomena in our universe.

As the booming development of astronomy and instrumentation, a number of extragalactic SNe were discovered in the 20th century. In 1941, Rudolph Minkowski firstly defined two branches of the SN in terms of whether the hydrogen absorption is shown in their spectra or not—the Type I (without hydrogen absorptions) and the Type II (with hydrogen absorptions) SN. Based on Minkowski's work, more advanced classification criteria have been proposed by using both spectroscopic and photometric features of the SN. For the type I SN class, it can be further classified into type Ia, type Ib, and type Ic subclasses by using the silicon and the helium features. For the classification of the type II SN, both photometric and spectroscopic information needs to be taken into account. A flowchart of how to classify an SN is shown in Figure 1.

In 1930s, Walter Baade and Fritz Zwicky firstly proposed that the high energy of the SN may originate from a process that a massive star evolves to a neutron star (Baade and Zwicky, 1934). They also suggested to use the SN as the "standard candle" because of the "identical" intrinsic peak luminosity for the first time. Such an idea made a profound influence on the supernova cosmology developed half a century later. From late 1960s to 1980s, theoretical studies on the type Ia supernova (SN Ia), stepped into a golden era—Finzi and Wolf (1967) proposed that an SN Ia occurs once a white dwarf (WD) reaches the Chandrasekhar mass limit. In the following 20 years, different kinds of SN Ia explosion and progenitor models have been proposed to further explain the observational properties of SNe Ia (e.g. Arnett, 1969, Whelan and Iben, 1973, Nomoto, 1982a, Nomoto et al., 1984; see section 1.2 for more details).

Another memorial date in the SN history is Feb. 24, 1987, when the brightest SN since 1604, the SN 1987A, was discovered in the Large Magellanic Cloud. The extremely close distance of SN 1987A provided a great opportunity of comprehensively investigating a local SN and testifying various theoretical models (Hillebrandt 1987; Shigeyama 1987; Chevalier 1987; Protheroe 1987; Barbiellinin 1987; Schaeffer 1987; Oyama 1987).

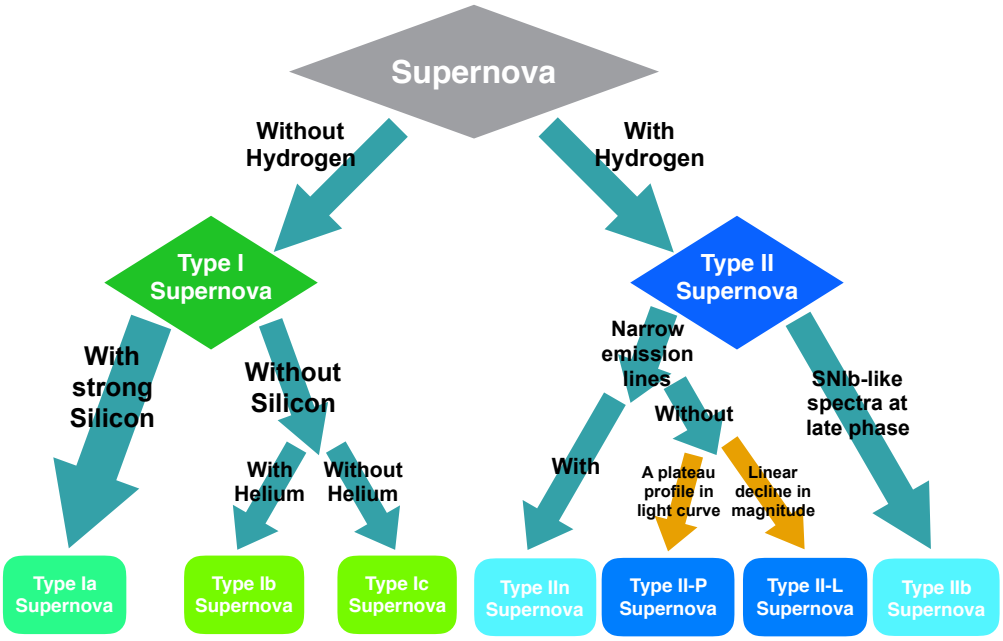

Figure 1: The classification of supernovae. By using the hydrogen P Cygni profile, the SN can be classified into two types—Type I (without hydrogen) and Type II (with hydrogen). For a type I SN, if distinct silicon absorption lines can be identified (especially in the around/post-maximum phase), it will be classified as a type Ia supernova (SN Ia). For an SN that shows clear helium absorption rather than the hydrogen and silicon absorptions, it will be classified as a type Ib supernova (SN Ib). If a type I SN shows neither the distinct silicon nor helium absorption features, it is a type Ic supernova (SN Ic). For type II SNe, the light curve of a type II-P supernova shows a distinctive plateau phase that lasts for a few months. By contrast, the post-maximum light curve of a type II-L supernova declines almost linearly in magnitude. In addition to using the light-curve diversity, further classifications of type II SNe rely on their spectral features. If a type II SN has intermediate- or narrow-width hydrogen emission lines, it is so-called a type IIn supernova. If the late-phase spectra of a type II SN show high similarity to those of type Ib SNe, it is a type IIb supernova. Peculiar SNe II (e.g. SN 1987A) and super luminous supernovae are not shown in the plot.

As more and more SNe Ia have been found, the specific photometric behavior of SNe Ia suggests the possible use of the SN Ia as the cosmological distance indicator. Pskovskii firstly proposed that the shape of the SN Ia light curve correlates with its peak absolute magnitude (Pskovskii, 1977, 1984)—once we properly derive the peak absolute magnitude based on the light-curve profile of an SN Ia, we are able to estimate its distance. A very important empirical relation of SNe Ia has been found by statistically investigating light curves of a number of well-observed SNe Ia in the early 1990s, the so-called "Phillips relation," which indicates a correlation between the B-band peak absolute magnitude and the decline rate in 15 days after the peak (i.e. $\Delta m_{15}(B)$). Thanks to this important work, SNe Ia can be used as a reliable distance indicator and applied into cosmology.

Several supernova survey programs were carried out in 1990s. The most representative two are Supernova Cosmology Project (SCP) and the High-z Team (HZT), which aim to use SNe Ia in a large redshift range ($0 \lesssim z \lesssim 1.0$) as a cosmological distance indicator to measure the expansion of the Universe. Finally, both groups discovered the accelerating expansion of the Universe (Perlmutter et al., 1997, 1999, Riess et al., 1998) and core investigators were awarded the 2011 Nobel Prize in Physics.

As the broad adoption of CCD arrays in astronomical observation in 2000s, several large transient survey projects, such as the Lick Observatory Supernova Search (LOSS, Li et al. 2000), the nearby Supernova Factory (SNFactory, Aldering et al. 2002), the Carnegie Supernova Program (CSP, Hammy et al. 2006), the SDSS-II Supernova Survey (SDSS SN Survey, Sako et al. 2008), the SuperNova Legacy Survey (SNLS, Pritchet et al. 2005), the Paloma Transient Factory (PTF; Rau et al. 2009) and the upgraded one, the intermediate Paloma Transient Factory (iPTF), and the All-Sky Automated Survey for Supernovae (ASAS-SN*) were carried out successfully. Breakthroughs on the origin of SNe Ia have been achieved with individual and statistical studies of well-observed SNe Ia. In particular, a growing number of SNe Ia discovered within a few days of their explosions provide unique information on the progenitor system and the explosion mechanism of SNe Ia (Nugent et al., 2011, Foley et al., 2012, Cao et al., 2015, Shappee et al., 2016, Marion et al., 2016, Hosseinzadeh et al., 2017, Jiang et al., 2017).

*$http://www.astronomy.ohio-state.edu/\ assassin/index.shtml$

1.2 The Early-phase Type Ia Supernova

1.2.1 Background of SNe Ia and the early-phase study

It has been widely accepted that SNe Ia originate from thermonuclear explosions of carbon-oxygen white dwarfs (C/O WDs) that have mass close to the Chandrasekhar-mass limit ($M_{\rm Ch}$) based on the good consistency between theoretical predictions and observations (Nomoto et al., 1984, Höflich and Khokhlov, 1996). Given that the birth mass of a C/O WD should be well below $M_{\rm Ch}$ (e.g. $\lesssim$1.1 $M_\odot$ (Umeda et al., 1999); also see Siess, 2006, Doherty et al., 2015), a mass-increasing process through interaction (e.g. gas accretion, merger, etc.) with the companion star is necessary before the primary C/O WD explodes as an SN Ia. However, the type of the companion star and the exact explosion physics are still under debate since none of the proposed scenario can perfectly explain all observational properties of SNe Ia (see Maoz et al. (2014), Maeda and Terada (2016) for a review).

The light curves of SNe Ia are powered by the radioactive decay of ^{56}Ni $\rightarrow$ ^{56}Co $\rightarrow$ ^{56}Fe (Arnett, 1982), which show specific width-luminosity relation in general—the wider the SN light curve, the brighter the luminosity is (i.e the Phillips relation). Although some stellar parameters such as metallicity (Timmes et al., 2003), mass ratio of carbon to oxygen of the WD (Umeda et al., 1999), the transition density from deflagration to detonation (Hillebrandt and Niemeyer, 2000), etc. during the SN explosion may affect the total amount of ^{56}Ni, and thus the luminosity of SNe Ia, the significant light-curve and spectral differences between specific SN Ia subclasses require multiple physical origins to explain the observed diversity of SNe Ia.

Observationally, although a large number of SNe Ia have been discovered and well investigated so far, the photometric/spectroscopic information on SNe Ia soon after their explosions (hereafter the "early-phase SNe Ia"*) is still limited. Theoretically, the early light curve and spectral information of SNe Ia play an irreparable role in understanding the long-standing progenitor and explosion mechanism issue of SNe Ia. However, given that most of transient surveys rely on 1-m or even smaller telescopes to easily achieve a large field of view, the faintness of SNe Ia at early phase makes them hard to be observed. Until 2018, about two dozen of SNe Ia have been successfully discovered and intensively followed up soon after their explosions thanks to powerful and well-organized transient survey projects such as the iPTF, which opened a new door of the SNe Ia study.

Early-phase SNe Ia can be divided into two branches according to their early light-curve be-

*Throughout this thesis, we define the "early-phase" is within about three days of the SN explosion.

havior: early-excess SNe Ia (hereafter EExSNe Ia), light curves of which show additional luminosity enhancement in the early phase, and non-EExSNe Ia, which show smoothly rising light curves from the beginning. To avoid the overlap with the main text of this thesis*, the next subsection focus on the introduction of previous studies of early-phase SNe Ia that do not show early-excess feature ("non-EExSNe Ia") and the main scientific objectives of early-phase SNe Ia study is summarized in §1.2.3.

1.2.2 An overview of non-EExSNe Ia study

SN 2011fe and SN 2014J are two nearest SNe Ia since 1972 (after the discovery of the SN Ia, SN 1972E). Both of them have been discovered soon after their explosions, which provide a great opportunity to carry out very detailed investigations of SNe Ia from the very early epoch. SN 2011fe, a normal-type SN Ia occurred in an extremely nearby spiral galaxy, known as the M101 (Figure 2), is the best observed SN Ia so far. The earliest photometry indicates the SN was discovered with the brightness $\sim$1000 times fainter than its peak, which provides a significant constraint on its progenitor system (Nugent et al., 2011, Li et al., 2011) based on the model of the interaction between the rapidly expanding ejecta and the companion star (the "companion-ejecta interaction" scenario (Kasen, 2010), hereafter companion-interaction scenario; see §1.2.3). Spectroscopically, Parrent et al. (2012) obtained a spectrum at $\sim$1.2 days after the explosion and successfully discriminate the C II λ6580 line and O I λ7774 line, suggesting a large amount of unburned material at the outermost region of the SN ejecta. Although the early follow-up observation of SN 2014J has not been very well performed compared with that of SN 2011fe, a discrepancy between the early-phase light-curve fitting and the typical simple-power-law model (Zheng et al., 2014) not only contradicts with the fireball and the single-zone model (Arnett, 1982, Riess et al., 1999a,b) but also suggests a possible diversity of the early light-curve behavior of SNe Ia.

In addition to the study of individual early-phase SN Ia, statistical investigations were conducted by using relatively early SNe Ia discovered from large survey projects. However, due to the incomplete early-phase information for most of samples, quantitative analysis has not been performed yet (Hayden et al., 2010, Bianco et al., 2011, Ganeshalingam et al., 2011). The first specific statistical study on the photometric behavior of early-phase SNe Ia was carried out by Firth et al. (2014). By investigating a dozen of early-phase light curves of SNe Ia, they found that the rising index n of early-phase light curve has extremely large scatter by adopting a simple-power-law fitting method ($L \propto t^n$), which contradicts with previous observations and theoretical predictions (Arnett 1982; Riess et al. 1999; Piro 2012, 2013, 2014).

*A detailed investigation of previously discovered EExSNe Ia is shown in Chapters 3 and 4.

The *Kepler* Space Telescope that was designed for the exoplanet search also made a contribution on the early-phase SN Ia observations. Thanks to the high survey cadence and the deep imaging capability of *Kepler*, three SNe Ia have been well observed from very early time (Olling et al., 2015). Similar to the early light curve of SN 2011fe, their single-band light curves also show smooth rising behavior, indicating a small radius companion of the progenitor system in case a non-degenerate companion is survived after the explosion. However, the lack of multiband photometric and spectroscopic observations prevents us from investigating their properties in detail.

Figure 2: A picture of SN 2011fe and its host galaxy, M101. SN 2011fe is one of the nearest and the best-observed extragalactic SNe Ia so far, which provided an unprecedented opportunity to systematically investigate the early-phase photometric/spectroscopic behavior of SNe Ia. Image credit: B. J. Fulton, Las Cumbres Observatory Global Telescope Network.

In addition to the studies of these "common" early-phase SNe Ia, recent discoveries of nearly a dozen of SNe Ia that show peculiar light-curve behavior in the early phase, i.e. the EExSNe Ia, also made great breakthroughs on both the progenitor and explosion issue of SNe Ia (Cao

et al., 2015, Marion et al., 2016, Hosseinzadeh et al., 2017, Jiang et al., 2017, Jiang et al., 2018, Miller et al., 2018; see following chapters for details).

1.2.3 Scientific objectives of early-phase SNe Ia study

The progenitor issue and implications from the early-phase photometry

Figuring out the progenitor of SNe Ia is one of the most important topics of SN Ia study. Even though Finzi and Wolf (1967) proposed that an SN Ia occurs once the mass of a white dwarf (WD) reaches the Chandrasekhar limit, the mechanism that how a WD grows to such a massive WD was unclear at that time. Whelan and Iben (1973) firstly proposed that a WD may grow to the Chandrasekhar mass limit through the stable accretion from a non-degenerate companion star (e.g. a main/sub-sequence star or a red giant star), the so-called single degenerate progenitor model (SD model) has thus been proposed. In 1984, another prevalent progenitor model known as the double degenerate progenitor model (DD model) has been proposed by Iben and Tutukov (1984) and Webbink (1984), which suggested that the mass of the primary C/O WD can reach the Chandrasekhar limit through the merger of two WDs and thus accounts for the SN Ia explosion. In the past 40 years, other possible scenarios relying on specific progenitor system and explosion mechanism, such as the core-degenerate (CD) scenario (Sparks and Stecher, 1974), the double detonation (DDet) scenario (Nomoto, 1984, Woosley and Weaver, 1994), the WD-WD collision scenario (Thompson, 2011), etc. have been proposed to explain the long-standing progenitor issue. Generally speaking, SD and DD are two widely-accepted scenarios among them in terms of a relatively good consistency with observations.

However, the debate between the SD and DD models has been lasted for a long time since neither of them can perfectly explain observational results. For the DD model, a major issue is that the high accretion rate under such a scenario may lead to the off-center ignition and then burning off carbon to oxygen and neon. Further accretion approaching to the Chandrasekhar mass limit will drive electron capture on magnesium and neon, leading to an "accretion-induced collapse" due to the gravitational instability. Finally, a neutron star, rather than an SN Ia, will be generated (Nomoto and Iben, 1985, Saio and Nomoto, 1998, Shen et al., 2012). Moreover, the pure DD scenario also cannot easily explain the high SN Ia rate in our universe (Dahlen et al., 2008, Kuznetsova et al., 2008, Barbary et al., 2012, Rodney et al., 2014). However, in contrast to the SD scenario, the DD scenario shows an advantage in explaining the delay time distribution (DTD) of SNe Ia (Totani et al., 2008, Graur et al., 2011) and specific SN Ia subclasses, e.g. the 91bg-like subluminous SNe Ia (Pakmor et al., 2010).

For the SD model, a main issue is the lack of direct/indirect evidence of the existence of a

non-degenerate companion star. In recent years, searching the companion star before/after the supernova explosion have been carried out and there is no detection of the companion for typical SN Ia subclasses (Mattila et al., 2005, Leonard, 2007, Shappee et al., 2013, Lundqvist et al., 2013, 2015). However, we note that such a method is not an efficient way because of the limited SN Ia samples that can be used for the companion investigation and the difficulties of the companion discrimination in pre-/post-explosion images. Additionally, possible companion detections indeed have been reported for two peculiar subluminous SNe Ia, SN 2008ha and SN 2012Z (Foley et al., 2014, McCully et al., 2014), both belong to a newly-defined SN Ia subclass, the 02cx-like SNe Ia (or "SNe Iax"; Foley et al., 2013). Observational results may suggest that both SD and DD scenarios contribute to the formation of SNe Ia in the Universe.

In addition to directly finding the companion star, Kasen (2010) proposed that a prominent brightening in the first few days of the explosion can be observed under specific viewing directions due to the interaction between the expanding ejecta and a non-degenerate companion star (i.e. the companion-interaction scenario), which makes EExSNe Ia a powerful indicator of the SD progenitor system (Kasen, 2010, Maeda et al., 2014, Kutsuna and Shigeyama, 2015). Since then, surveys for EExSNe Ia have become particularly popular in time-domain astronomy. However, there was no report of the discovery of early-excess light curves until 2015.

A breakthrough of the SN Ia progenitor issue was achieved three years ago. The first reported EExSN Ia, iPTF14atg, has been suggested as strong evidence for the companion-ejecta interaction (Cao et al., 2015). Soon after, the companion-interaction scenario was also proposed as a likely origin of early excess of SN 2012cg and the recently discovered SN 2017cbv (Marion et al., 2016, Hosseinzadeh et al., 2017). However, since all three SNe Ia are not typical "normal" SNe Ia and their observational properties are somewhat different from the prediction by the companion-interaction scenario (Kasen, 2010) through an SD channel, their origins are still under debate. Further discussions on the relation between previously discovered EExSNe Ia and the companion-interaction scenario are given in Chapter 4.

A powerful indicator of the SNe Ia explosion physics

In the last three decades of the 20th Century, various kinds of models have been proposed to explain how an SN Ia explodes. Generally speaking, if the mass of a C/O WD reaches nearly the Chandrasekhar mass, it is likely that thermonuclear runaway starts near the center of the WD (Nomoto et al., 1984). Theoretically it is not clear if the thermonuclear flame proceeds as a deflagration or detonation wave from the first principle. However, an immediate detonation occurs in the Chandrasekhar-mass WD produces too much iron-peak elements (e.g. ^{56}Ni, one of the most important elements that powers the SN radiation through the nuclear decay)

to be compatible to the luminosity of an SN Ia and the Galactic chemical evolution (Arnett, 1969, Woosley et al., 1986). In order to explain such discrepancies, the deflagration was proposed. However, a pure deflagration process is too weak to produce a sufficient amount of ^{56}Ni (Timmes and Woosley, 1992, Livne, 1993). In order to address problems for both the pure deflagration and the pure detonation scenario, the so-called "delayed detonation model" (Khokhlov, 1991, Arnett and Livne, 1994, Höflich et al., 1995, 1998, Iwamoto et al., 1999), in which the deflagration finally transformed into the detonation at a fuel density of $\sim 10^7$ g cm^{-3}. In addition to the popular delayed-detonation model, other explosion mechanisms have been proposed to further explain specific SN Ia subclasses, e.g., the "failed deflagration model" for 02cx-like subluminous SNe Ia (Kromer et al., 2013), the double-detonation scenario for 91bg-like subluminous SNe Ia (Livne and Glasner, 1990, Woosley and Weaver, 1994, Shen and Bildsten, 2009), the "spin-up/down scenario" for "super-Chandrasekhar-mass" (super-$M_{\rm Ch}$) SNe Ia, and so on (see Hillebrandt and Niemeyer, 2000, Maeda, 2016 for details).

The early-phase information plays an irreplaceable role in testing various explosion models. Spectroscopically, physical parameters such as the total mass and spacial distribution of unburned carbon and the velocity of the outermost ejecta derived from early-phase spectra are good indicators of the explosion physics (Höflich et al., 2002, Gamezo et al., 2003, Röpke et al., 2007, Kasen et al., 2009). Photometrically, Piro et al. (Piro et al., 2010, Piro, 2012, Piro and Nakar, 2013, 2014, Piro and Morozova, 2016) proposed that the early-phase light-curve behavior can constrain the total mass and the distribution of ^{56}Ni at the outmost region of the SN ejecta. By using the best-observed early-phase SN Ia, SN 2011fe, they pointed that the expected configuration of ^{56}Ni can be achieved under specific explosion mechanisms.

Another interesting question about the SN Ia explosion is whether or not the initial ignition occurs at the center of the WD. A recent study by Firth et al. (2014) suggested a relatively large dispersion in the early-phase light curves, which cannot be naturally achieved with traditional explosion models. However, the off-center explosion model (Kuhlen et al., 2006, Maeda et al., 2010, Maeda et al., 2011) may account for the scatter of early-phase light curves—if the initial thermonuclear sparks are ignited at an offset from the center of the WD progenitor, such an asymmetric physical process finally results in extremely inhomogeneous radioactive element distribution near the surface of the progenitor. By taking into account the viewing-angle effect, the scatter in both early-phase light curve and color evolution could be explained.

From the early-excess perspective, if previously discovered early light-curve excesses are exclusively attributed to the companion-ejecta interaction is still under debate. For instance, Kromer et al. (2016) claimed that the spectra of iPTF14atg cannot be reproduced by the SD scenario but show good consistency with the prediction of merging two sub-Chandrasekhar-mass WDs.

If the progenitor system of iPTF14atg is not an SD system, then the early light-curve excess of iPTF14atg cannot be attributed to the companion-interaction scenario, and other effects should come into play. In addition to iPTF14atg, discrepancies between observed early-excess features and the companion-interaction model have been proposed for several EExSNe Ia (SN 2012cg, Shappee et al., 2018; SN 2017cbv, Hosseinzadeh et al., 2017; iPTF14bdn, Smitka et al., 2015; iPTF16abc, Miller et al., 2018). Theoretically, the interaction between dense circumstellar matter (CSM) and SN ejecta (Shen et al., 2012, Levanon et al., 2015, Levanon and Soker, 2017, Tanikawa et al., 2015, Piro and Morozova, 2016, Maeda et al., 2018) and vigorous mixing of radioactive ^{56}Ni in the outermost region of SN ejecta (Piro and Morozova, 2016) may produce a similar early-excess feature to that predicted by the companion interaction. For such cases, the early light-curve excess is not only an indicator of the SN Ia progenitor system but may suggest specific explosion mechanisms (Chapter 4). In particular, we firstly confirmed the physical connection between the early light-curve excess and specific explosion mechanism by investigating a normal-brightness EExSN Ia, MUSSES1604D (SN 2016jhr), that shows a prominent but red early excess and strong Ti II absorptions around the *B*-band maximum. The early excess of this peculiar object can be well explained by the radiation emitted from short-lived radioactive elements that were generated by the detonation at a thin helium shell of its primary WD at the very beginning, indicating the multiple origins of EExSNe Ia (see Chapter 3 for details).

A new perspective to investigate the diversity of SNe Ia

As more and more SNe Ia have been discovered in recent years, the photometric behavior of a considerable number of SNe Ia do not well follow the width-luminosity relation (Phillips, 1993) and thus prevents us from improving the accuracy of SNe Ia as the "standardizable candle" in cosmology. In general, SNe Ia can be classified into six branches mainly based on their photometric behavior: super-$M_{\rm Ch}$ SNe Ia (e.g. SN 2007if, SN 2009dc), 91T/99aa-like luminous SNe Ia (e.g. SN 1991T, LSQ12gdj), normal SNe Ia (e.g. SN 2005cf, SN 2011fe), "transitional" SNe Ia (e.g. iPTF13ebh, SN 2015bp), 91bg-like subluminous SNe Ia (e.g. SN 1991bg, SN 2005bl), and 02cx-like subluminous SNe Ia (e,g. SN 2002cx, SN 2008ha). Given that the SN Ia diversity is very likely caused by the multiple origins of the progenitor system and/or the explosion mechanism, figuring out the long-standing diversity issue of SNe Ia is somewhat an ultimate goal of the SN Ia study.

Systematically investigating the early light-curve behavior of different SN Ia subclasses brings us new ideas of the origin of the SN Ia diversity. As opposed to the early-excess discoveries in several SN Ia subclasses, there is no clear evidence of early-excess detection in normal SNe Ia so far. For example, a smooth-rising light curve of SN 2011fe from the very beginning provides a significant constraint on the companion type (Nugent et al., 2011, Li et al., 2011).

Non-detections of EEx in normal SNe Ia can be explained by either an intrinsically faint EEx due to a small nondegenerate companion star or an unfavorable viewing angle by chance under the companion-interaction scenario. However, such an observational fact is in contrast to the high EEx fraction* discovered in 91T/99aa-like SNe Ia, which may suggest intrinsic differences between some SN Ia subclasses. In Chapter 4, possible origins of the SN Ia diversity will be discussed from the early-excess perspective in detail.

In addition to the clear distinctions between different SN Ia subclasses, recent studies also suggested that the diversity may exist even in normal SNe Ia. By investigating the evolution of the velocity of Si II λ6355 line ($V_{Si\ II}$) using the so-called "average daily decreasing rate of $V_{Si\ II}$," Benetti et al. (2005) argued that normal SNe Ia likely have two different groups: the high-velocity-gradient (HVG) group and the low-velocity-gradient (LVG) group. Wang et al. (2009) also suggested that two groups (high-$V_{Si\ II}$ and low-$V_{Si\ II}$) may exist in normal SNe Ia after investigating $V_{Si\ II}$ around the *B*-band peak of 158 SNe Ia. In addition to the spectral diversity, the NUV−optial color diversity of normal SNe Ia has been reported by Milne et al. (2013, 2015). Interestingly, statistical analysis suggested that the above diversities of normal SNe Ia may have the connection in physics (Foley and Kasen, 2011, Foley et al., 2011, Milne et al., 2013). So far, there is no clear answer about the origin of the diversity shown in normal SNe Ia. One possible explanation is the viewing angle effect due to a specific explosion process, e.g., the off-center explosion scenario (Maeda et al., 2010; also see §2.4.4).

The early-phase observation is also important for figuring out the possible diversity among normal SNe Ia. For the C II λ6580 absorption feature, previous statistical studies (Parrent et al., 2011, Thomas et al., 2011, Folatelli et al., 2012, Silverman and Filippenko, 2012) found that the fraction of SNe Ia that show C II λ6580 absorption is correlated to the phase since the SN explosion, i.e. more SNe Ia show C II λ6580 feature in the early phase. Therefore, by statistically investigating the C II λ6580 feature in the early-phase spectra, we are able to further investigate if there exist two distinct groups in terms of the early C II λ6580 absorption feature. Moreover, given that more prominent scatters of the Si II λ6355 velocity and the NUV−optical color can be seen in the early phase, we may find new clues about the physical origin(s) of such diversities by systematically investigating the photometric/spectral behavior of a number of normal SNe Ia soon after their explosions.

*For SNe Ia in each subclass, an early-excess fraction is defined as the number fraction of EExSNe Ia over EExSNe Ia and well-observed early-phase SNe Ia that do not show early-excess features (i.e., non-EExSNe Ia, selected from papers and public resources) in the same subclass.

1.3 An Overview of the Thesis

Despite the great scientific importance of early-phase SNe Ia, relevant studies have not been well conducted because the dimness of early-phase SNe Ia makes them hard to be discovered. Thanks to the excellent survey performance of the Kiso Wide Field Camera (KWFC) and the Subaru Hyper Suprime-Cam (HSC), systematical investigations of the early-phase photometric behavior of SNe Ia have been carried out with survey projects which are optimized to search early-phase SNe—the **KI**so **S**upernova **S**urvey (**KISS**), the **S**urvey with **K**WFC for **Y**oung **S**Ne Ia (**SKYS**, Sep.–Nov. 2015), and the **MU**lti-band **S**ubaru **S**urvey for **E**arly-phase **S**Ne Ia (**MUSSES**, since April 2016). This thesis mainly focus on (1) the scientific outputs from three SNe surveys, (2) a further investigation based on all EExSNe Ia discovered so far, and (3) a future plan with forthcoming transient survey projects. An overview of the thesis is shown as follows.

Early-phase SNe Ia studies with two prior survey projects, KISS and SKYS that aim for testing the feasibility of the early-phase SNe Ia survey is summarized in Chapter 2. During the seven-months observations, total four early-phase SNe were successfully discovered. Light curves and spectra obtained from KWFC and other follow-up facilities indicated that three of them (KISS15m, KISS15n, and SKYS6) are early-phase SNe Ia and the other one (SKYS9) is an early-phase type IIP supernova. In particular, we discovered one of the youngest subluminous SNe Ia (KISS15m) and a peculiar luminous early-phase SN Ia (KISS15n). Detailed information and further discussions based on KWFC early-phase SNe Ia can also be found in Chapter 2.

Chapter 3 mainly introduces our early-phase SNe Ia survey with Subaru/HSC, MUSSES and its scientific output. The experience accumulated from KISS and SKYS was applied to this advanced early-phase SNe Ia survey project. The MUSSES project includes survey observations with the 8.2-m Subaru telescope and follow-up observations with other ground-based telescopes. In order to carry out such a large project, building the global collaboration is necessary. Collaborations with astronomers from different countries ensure real-time follow-up observations with more than 10 large-aperture telescopes all over the world.

The first MUSSES observing run was carried out from April to June, 2016. We discovered total 12 early-phase SN candidates during the Subaru observation, and especially, a very special early-phase SN Ia, the so-called MUSSES1604D (or SN 2016jhr, Figure 3), attracted our attention. The Subaru/HSC survey and follow-up observations indicated that early-phase light curves and abnormal spectral features of MUSSES1604D are in conflict with predictions by previously proposed scenarios. We finally found out that the peculiarities of MUSSES1604D

can be naturally explained by a supernova explosion that is triggered by a detonation of a thin helium shell of its progenitor star (the so-called "He-shell detonation" or "He-det" scenario). This finding provides robust evidence of one kind of explosion mechanism of SNe Ia for the first time, and thus opens a new door to the essential understanding of these spectacular phenomena in the Universe. The details of the study of MUSSES1604D can be found in §3.2, which was published in *Nature* on October 4th, 2017 (Jiang et al., 2017).

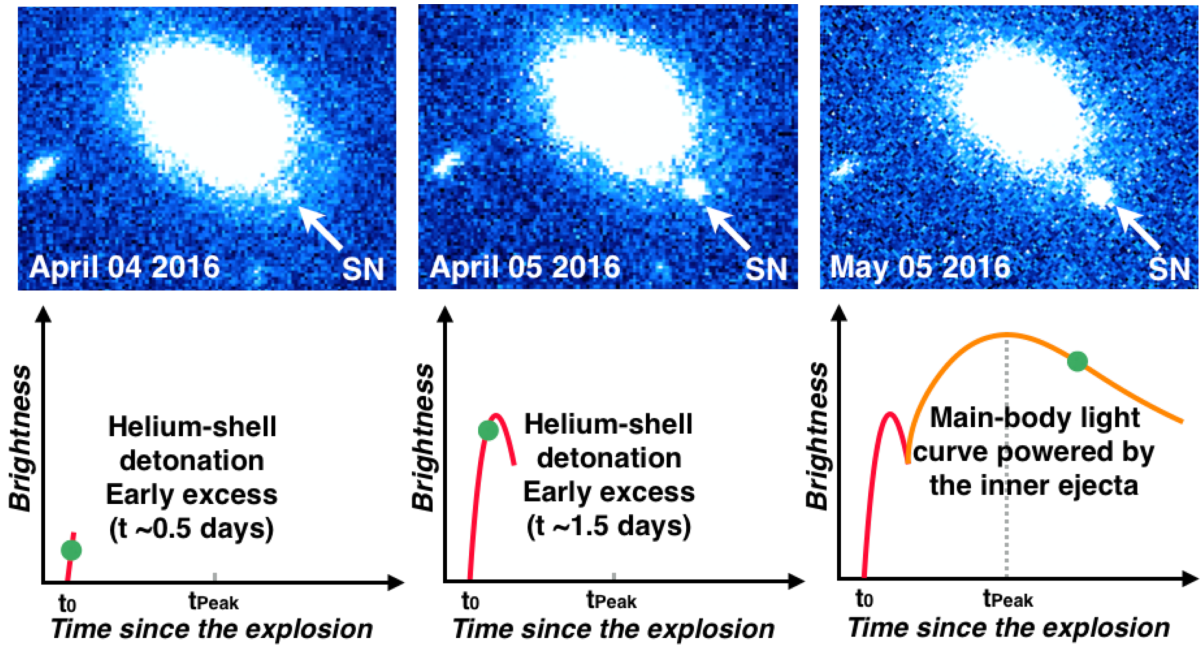

Figure 3: Images (upper panels) and schematic light curves (lower panels) of MUSSES1604D at specific epochs. Solid circles shown in light curves denote stages that the supernova was staying during observations.

With the most complete UV/optical early-phase SN Ia sample so far, we carried out the statistical study of EExSNe Ia (11 in total, and five of them are newly confirmed) for the first time. The study indicated that EExSNe Ia show clear preference for specific SN Ia subclasses and all luminous (91T- and 99aa-like) SNe Ia indeed show light-curve excess in the early phase. Given that the fraction of EExSNe Ia predicted by each early-excess scenario can be very different after taking into account the viewing angle effect, we further demonstrated the multiple origins of previously discovered EExSNe Ia by investigating early-excess fractions of SNe Ia in different subclasses. In particular, we found that an early-excess fraction of about 100% for luminous SNe Ia are likely due to the radiation from a larger amount of ^{56}Ni formed at the outermost region of the ejecta (i.e. the surface-^{56}Ni-decay scenario), which indeed can be interpreted by a popular explosion mechanism of luminous SNe Ia, the so-called gravitationally confined det-

onation scenario. Moreover, the connection between the surface-^{56}Ni-decay scenario and the luminous branch of SNe Ia suggests that the explosion mechanism of luminous SNe Ia may be different from that of other SN Ia subclasses. The relevant work has been published in *Astrophysical Journal* on October 3rd, 2018 (Jiang et al., 2018).

Prospects of early-phase SNe Ia studies with upcoming transient survey projects, the Tomo-e Gozen Transient Survey and the **MU**ltiple **S**imultaneous **S**urveys for **E**arly-phase **S**Ne and **FAS**ter **T**ransients (**MUSSES-FAST**, an upgrade version of MUSSES that makes the best use of the two top-level survey facilities in the world (i.e., Subaru/HSC and Kiso/Tomo-e) to study early-phase SNe and other rapid transients) are given in Chapter 5. Thanks to the excellent instrument performance and the well-designed survey strategy, new breakthroughs not only in early-phase SNe Ia but also in other area of time-domain astronomy can be achieved in the near future.

A summary of the thesis is given in Chapter 6. Supplementary information (preliminary results) on non-early-phase SN candidates and an early-phase SN IIP (SKYS9) discovered by the SKYS project is attached in the appendix.

Throughout the thesis we adopt the cosmological parameters H_0=70 km s^{-1} Mpc^{-1}, Ω_M=0.3, Ω_Λ=0.7. Without the specific notification, the AB and Vega magnitude are used for the SDSS *ugriz* and Johnson-Cousins *UBVRI* photometric system, respectively.

2 Searching for Early-phase SNe Ia with the Kiso Wide Field Camera

The Kiso Wide Field Camera (KWFC) is a wide-field imager on the prime focus of the Kiso 1.05-m Schmidt telescope. It is composed by eight 2k×4k CCDs (four SITe and four MIT Lincoln Laboratory (MIT/LL) CCDs, with a pixel size of 15μm and a pixel scale of $\sim$0.946 arcsec/pixel). A single exposure of Kiso/KWFC can cover 2.2 deg×2.2 deg sky area and the effective area is $\sim$4.6 deg^2. All CCDs are read out by the Kiso Array Controller (KAC; Sako et al., 2012). In the SLOW readout mode which is usually used for the SN survey, the readout noise is about 20 and 10 electrons RMS for SITe and MIT/LL CCDs, respectively. The CCD quantum efficiency is about 40–65% in *g*-band. The readout time in total is $\sim$125 seconds. KWFC is equipped with an automatic filter exchanger, which consists of an industrial robot arm and a 12-filters container. A sample image (180s exposure) is shown in Figure 4.

2.1 Kiso Supernova Survey (KISS)

The Kiso Supernova Survey (KISS) is a high-cadence wide-filed supernova survey with KWFC. The main scientific objective of KISS is to catch the earliest radiation of the core-collapse supernova (CCSN) in optical wavelengths, known as the supernova shock breakout, the intensity of which can be used to derive the physical properties of the progenitor star. The KISS project was carried out from April 2012 to September 2015. In average, about 100 dark/grey nights were allocated to KISS every year, and roughly half of the nights were shared with other scientific projects (Morokuma et al., 2014). The telescope is under maintenance from the middle of June to August every year due to the Japanese rainy season.

2.1.1 The Observing mode of KISS

To catch an SN shock breakout that only lasts for a few hours in the optical wavelengths (Campana et al., 2006), a high-cadence wide-field survey, an efficient candidate-filter system, and a well-organized follow-up network are highly required. Therefore, KISS adopted a different observing mode compared with that of typical supernova surveys. In brief, given the "blue color" and short timescale of an SN shock breakout and a high total throughput in *g* band of

Kiso/KWFC, KISS adopted a one-hour-cadence* g-band observing mode.

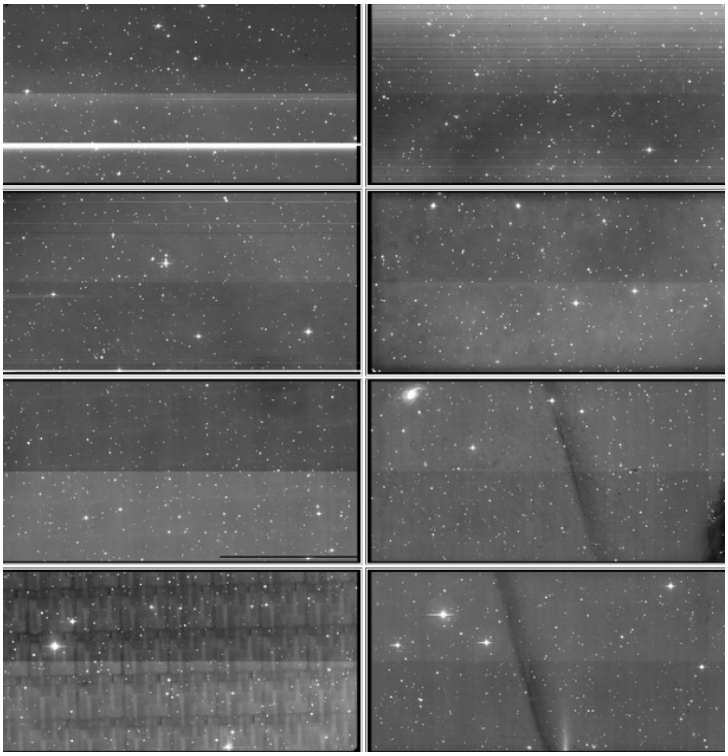

Figure 4: A g-band image taken by Kiso/KWFC in November, 2015 (1×1 binning, 180-sec on-source time. North is up and east is the left). The top four CCDs were made by SITe and the bottom four CCDs were produced by MIT/LL.

KISS's survey region was selected from SDSS imaging fields which show relatively higher star formation rate. The typical total star formation rate per KWFC field-of-view (FoV) is $\sim 20 M_{\odot}$ yr^{-1} at $z \lesssim 0.03$. For the transient selection, KISS used the SDSS archival images taken several years ago as the reference because of the higher spatial resolution and deeper limiting magnitude of the SDSS archival images. Given the seeing statistics in g band at the Kiso site ($\sim$3.3–5.3 arcsec full width of half maximum (FWHM) in usual; 3.9 arcsec FWHM at median), KISS adopted a 1×1 binning mode to achieve a finely sampled point spread function (PSF) of the KWFC image used for the image subtraction. The SLOW (for all 8 KWFC CCD chips) readout mode was applied for KISS to maximize the survey efficiency.

In general, KISS observed $\sim$20 different regions four or five times in a night. The exposure time

*The cadence is determined based on the radiative transfer calculation and previous observations (Tominaga et al., 2009, 2011, Schawinski et al., 2008, Gezari et al., 2008).

is three minutes for each pointing, reaching a g-band limiting magnitude of $\sim$20–21 mag (5-σ). In total, about 100 deg^2 sky area can be observed per night. For poor weather conditions (e.g., cloudy, windy, etc.), the survey was suspended and the telescope was used to observe bright SNe or nearby galaxy clusters and groups.

2.1.2 The KISS pipeline and transient selection

After the exposure, data reduction for each CCD image was conducted automatically by using a standard reduction pipeline (i.e., the KWFC pipeline) that includes overscan subtraction, overscan region trimming, bias subtraction, flat-fielding, and background subtraction. The bias and flat-field images were taken before/after the observation. Finally, the zeropoint and limiting magnitude was calculated by using the SDSS photometric catalog.

Comparing to KISS images (a g-band limiting magnitude of $\sim$20–21 mag (5-σ), 3.3–5.3 arcsec FWHM, and 0.946 arcsec/pixel), SDSS images with a finer pixel scale of 0.396 arcsec/pixel are deeper (a g-band limiting magnitude can reach $\sim$22.2 mag) and sharper ($\sim$1.4 arcsec FWHM in r band). Therefore, the SDSS archival g-band images taken before KISS observations were used as reference images for the image subtraction.

After the basic data reduction, the processed KWFC images were further analyzed with the KISS transient pipeline. At first, cosmic rays were removed from the reduced KWFC data using the publicly available code, L.A.Cosmic, developed by van Dokkum (2001). The SDSS reference image prepared in advance had to be rescaled to fit the KWFC images by using the software WCSremap[*], and then subtracted by the KWFC image with the software HOTPANTS[†]. For subtracted images, we only selected positive residuals with over 5-σ detections by the SExtractor software (Bertin and Arnouts, 1996). With the KWFC pipeline and the KISS transient pipeline, we were able to generate a transient catalog in about 15 minutes of each KWFC exposure. Note that more specific criteria were applied to further screen out false detections and non-astrophysical transients (see Morokuma et al. (2014) for details). Finally, only dozens of candidates of each KWFC exposure were left for the final inspection.

The remaining candidates were listed on a web page and ready for the last step—visually filtering the residual non-astrophysical sources and classifying reliable candidates into different classes (SNe, variable stars, AGNs, minor planets, etc.). In order to maximize the selection efficiency, astronomers, students, and astronomical amateurs in Japan work together to find interesting transient candidates. If an object was tagged as a young supernova candidate by

[*] *https://tdc-www.harvard.edu/wcstools/wcsprogs.html*
[†] *https://github.com/acbecker/hotpants*

multiple KISS members, follow-up observations were triggered.

2.1.3 Follow-up observations and the KISS collaboration

Since KWFC worked on the SN survey, follow-up observations by other telescopes were highly required. When a likely SN candidate was found by KISS, we triggered the simultaneous *g*-, *Rc*-, and *Ic*-band automatic imaging observations with the MITSuME imager on the Akeno 50-cm telescope (Kotani et al., 2005, Yatsu et al., 2007, Shimokawabe et al., 2008) for the further confirmation. If the SN candidate shown in the original KWFC image was successfully followed by KWFC and/or MITSuME in the next night, multiband imaging and spectroscopic follow-up observations were carried out through the KISS collaboration immediately.

The collaborative follow-up network included, in ascending order of the telescope aperture, the MITSuME on 50-cm telescope at Okayama Astrophysical Observatory (Yanagisawa et al., 2010), the Apogee AP-7 CCD camera (M70) on the 70-cm telescope of Sternberg Astronomical Institute, the KPNO 0.9-m telescope, the Lulin One-meter Telescope (LOT), the Atacama Near-Infrared Camera (ANIR; Motohara et al., 2010, Konishi et al., 2015) on the 1-m mini-TAO telescope (Sako et al., 2008, Minezaki et al., 2010), the HOWPol (Kawabata et al., 2008) and the HONIR (Sakimoto et al., 2012) on the 1.5-m Kanata telescope, the Kyoto Okayama Optical Low-dispersion Spectrograph (KOOLS; Yoshida, 2005) on the Okayama-188cm telescope, the Himalayan Faint Object Spectrograph (HFOSC) on the 2-m Himalayan Chandra Telescope (HCT), the Wide Field CCD Camera (WFCCD) on the Las Campanas 2.5-m du Pont telescope, the Andalucia Faint Object Spectrograph and Camera (ALFOSC) on the 2.5-m Nordic Optical Telescope (NOT), the Device Optimized for the LOw RESolution (DOLORES) on the 3.58-m Telescopio Nazionale Galileo (TNG; Barbieri, 1997), the FoldedPort Infrared Echellette (FIRE) spectrograph on the 6.5-m Magellan Baade Telescope, and the Faint Object Camera And Spectrograph (FOCAS; Kashikawa et al., 2002) on the 8.2-m Subaru telescope.

2.1.4 Searching for early-phase SNe Ia with KISS

Thanks to the high survey performance of Kiso/KWFC, more than 100 SN candidates were found (dozens of them have been spectroscopically confirmed) by KISS. However, since KISS was optimized for searching the SN shock breakout by adopting a high-cadence survey mode for about 100 deg^2 in a night, the observation indeed is not very efficient for searching early-phase SNe Ia. Therefore, we expected that a small number of early-phase SNe Ia can be discovered by the KISS project. Fortunately, two early-phase SNe Ia, KISS15m and KISS15n (Morokuma et al., 2015, Balam and Graham, 2015) have been discovered by KISS on April and May 2015,

respectively. Detailed observational information on two objects are shown in §2.3. However, as the rainy season came, no more early-phase SNe Ia discovered until the end of the KISS project (September 2015).

In order to further test the feasibility of running specific early-phase SNe Ia-targeted surveys with wide-field cameras and to keep enlarging the sample size of KWFC-discovered early-phase SNe Ia, a short-term KWFC survey project, SKYS, was carried in late 2015.

2.2 The Survey with KWFC for Young Supernovae (SKYS)

As the broad adoption of large-array CCD cameras in astronomical observations, great breakthroughs of the supernova study have been made through various transient survey programs in 2000's. Since early-phase SNe Ia are too faint to be easily discovered, we still barely understand the photometric behavior of SNe Ia soon after their explosions. Given the scientific importance of early-phase SNe Ia and the great survey performance of KWFC, an early-phase SNe Ia-targeted survey project, named as "**S**urvey with **K**WFC for **Y**oung **S**upernovae" (**SKYS**, PI: J. Jiang) was carried out in October and November 2015. As opposed to KISS that is optimized for catching the CCSN shock breakout with an hour-cadence survey mode, SKYS was designed for searching early-phase SNe Ia with a completely different observing mode.

2.2.1 The design of SKYS

There are two distinct advantages by using Kiso/KWFC to carry out early-phase SNe Ia survey. 1) As the 4th wide-field camera mounted on the 1-m class telescope by 2016, Kiso/KWFC has very good survey performance compared to that of most of telescopes in the world. 2) Thanks to a large amount of available observing time of Kiso/KWFC and well-organized follow-up observations, detailed investigations of KWFC-discovered early-phase SNe Ia can be easily carried out.

To maximize the survey efficiency of early-phase SNe Ia with the two-months KWFC observation, it is necessary to balance the total survey region and the observing cadence. Since SKYS aims to find SNe Ia within about 6 days of their explosions*, observing the same region with an interval longer than 6 days would miss some early-phase SNe Ia and decrease the visiting times for each region. On the other hand, even though observing the same region with very short

*Note: As a testing early-phase SNe Ia-targeted survey, the "early-phase" originally defined for SKYS is longer than that we used in other places of this thesis (i.e. within about three days of the SN explosion).

interval (e.g. hour-cadence) enables us to catch all early-phase SNe Ia in the survey region, the observing frequency is too high to maximize the survey efficiency for finding early-phase SNe Ia. Therefore, monitoring the same sky area in every 6 days ensures us to not only discover early-phase SNe Ia in the largest survey area but also monitor each area with a suitable time interval. Finally, total $\sim$1800 deg^2 SKYS survey area (corresponds to about 400 pointings) that has more than 6-hours visible time in either October or November was selected from SDSS- and KISS-observed regions (Figure 5). The survey region includes two parts, SKYS(A) and SKYS(B). The SKYS(A) region was prepared for observations in October and a large fraction of the SKYS(B) region were used for both October and November observing runs.

We carried out the *g*-band KWFC survey with on-source time of 180 seconds of a single exposure (a limiting magnitude of $\sim$20–21) by taking into account both the survey efficiency and follow-up capabilities of other telescopes. By using the transient pipeline and the online visual inspection system designed for KISS (§2.1.2), we started checking candidates in about one hour of each KWFC exposure. Once a likely SN candidate was discovered, we firstly carried out a KWFC follow-up observation to screen out non-early-phase SNe with specific selection criteria.

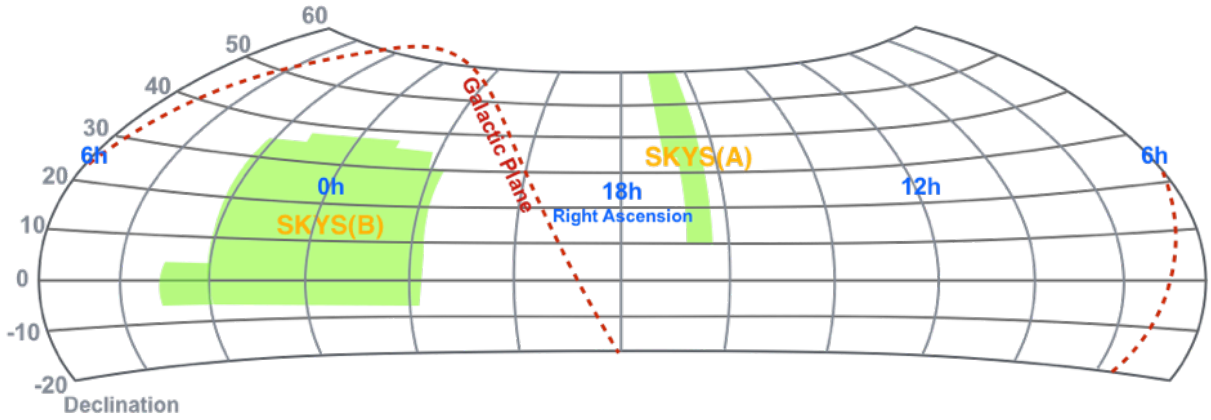

Figure 5: The survey region of SKYS (green color). SKYS(A) region is for observations in October and most of SKYS(B) region can be observed in two months with more than 6-hours visible time in a night. Since both regions have been observed by either SDSS or KISS before, we used the archival data as the reference to identify transients discovered by SKYS.

We made a set of criteria to efficiently select early-phase SN candidates. At first, we only focus on transient objects that have a significant offset from the center of their hosts to exclude rapidly variable AGNs. Then, we estimate the absolute magnitude of candidates based on the spectroscopic/photometric redshift of their host galaxies to further rule out other contaminations. For

candidates satisfied the above two conditions, we then confirmed if their brightness was significantly increased between two KWFC observations, i.e., with a rising speed $\lesssim -0.3$ mag day^{-1} quantitatively. Once an object passed all above criteria, we triggered multiband imaging and spectroscopic follow-up observations through SKYS follow-up network immediately. A flow chat of how SKYS worked is shown in Figure 6.

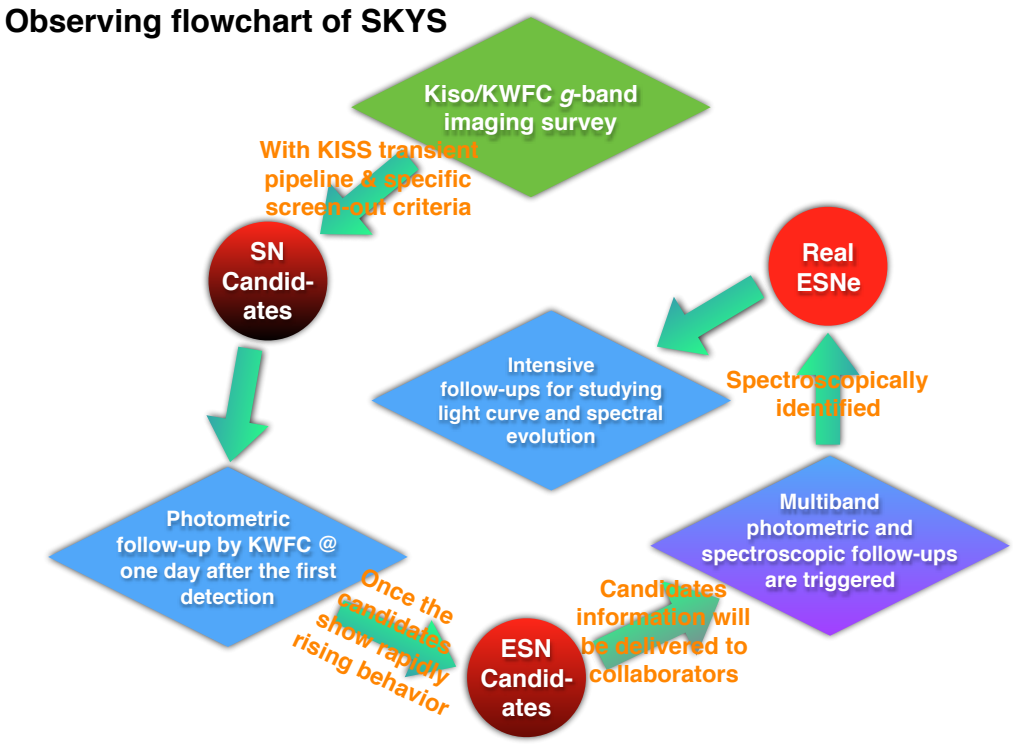

Figure 6: The flowchart of early-phase supernova (ESN) observations with SKYS.

2.2.2 Follow-up strategy and collaborations

Considering the unstable weather condition in Japan, it would be better to collaborate with both domestic and oversea telescopes to ensure that multiband photometric and spectroscopic follow-up observations can be carried out in time. For this reason, we joined the "Optical and Infrared Synergetic Telescopes for Education and Research" (OISTER) in Japan and collaborated with international collaborators to ensure the realtime follow-up observations of early-phase SNe discovered by SKYS.

1) The OISTER organization

OISTER is an organization that uses Japanese small/middle size (0.5-2-m class) telescopes to carry out intensive and/or high-flexibility-required observations. Therefore, a major scientific motivation of OISTER is to support time-domain observations, i.e., following up interesting transients.

Given the apparent magnitude of KWFC SNe and the capability of OISTER follow-up facilities, OISTER mainly worked on multiband imaging follow-up observations. In the optical band, we used Kiso/KWFC (g-, r-, i-, z-band observations), the MITSuME on the 50-cm telescopes in Okayama astronomical observatory and Akeno observatory (simultaneous g-, Rc-, and Ic-band automatic imaging observations), and the Multi-Spectral Imager (MSI) on the Prika telescope of Hokkaido University (B-, V-, R-, and I-band observations). For near-infrared follow-up observations, the Near-Infrared Camera (NIC) mounted on the 2-m NAYUTA telescope and the Simultaneous-3color InfraRed Imager for Unbiased Survey imager (SIRIUS) on the 1.4-m Infrared Survey Facility (IRSF) were used for simultaneous J-, H-, and K-band automatic imaging observations. The near-infrared imager and spectrograph (ISLE) mounted on the 188-cm telescope in Okayama astronomical observatory and the NIR camera on the 1-m telescope in Kagoshima University were also triggered for the J-, H-, and K-band observations. The optical and near-infrared simultaneous imager (HONIR) on the Kanata telescope of Hiroshima University was used for simultaneous I- and K-band observations.

2) International collaborations

The spectroscopy is crucial to identify transients found by imaging surveys. Since the apparent magnitudes of most KWFC SNe were fainter than 18 in optical band, we looked for international collaborations with 2–3 m class telescopes for the spectroscopy. Additionally, international collaborators also contributed to a part of imaging observations when the OISTER follow-up could not be well conducted due to the weather issue.

The "Yunnan Faint Object Spectrograph and Camera" (YFOSC) on the 2.4-m Lijiang telescope (LJT) of China is the major oversea follow-up facility for SKYS. YFOSC can take spectra for SNe brighter than $\sim$19 magnitude and multiband ($BVRIZ$) images of SNe brighter than $\sim$24 magnitude, respectively. Therefore, most of early-phase SNe discovered by SKYS can be followed by LJT/YFOSC. During the 2-months SKYS observation, LJT/YFOSC made contributions on both spectroscopic and photometric follow-ups of an early-phase SN IIP, SKYS9. Finally, we obtained a series of high signal to noise (S/N) ratio spectra and multiband images of SKYS9 with LJT/YFOSC (see the appendix for details).

Another main instrument for spectroscopy is the "SPectrograph for the Rapid Acquisition of Transients" (SPRAT) mounted on the 2-m Liverpool telescope, which is located at one of the best observational sites in the world, the La Palma Island. High S/N spectra taken by SPART helped us to confirm three SNe Ia (SKYS6, SKYS10, and SKYS11) and to study SKYS9 in the late phase. In addition to these two major spectroscopic facilities, we also got a high S/N spectrum of SKYS9 from Maeda et al. (proposal ID: S15B-055) by using the Subaru/FOCAS at about one month after the discovery of the SN.

Given that non-early-phase SNe (about one week or longer after the explosion) do not meet our scientific objectives, we only carried out *g*-band follow-ups with KWFC for those objects.

2.2.3 The observing log of SKYS

In fact, we suffered various kinds of troubles during the observation, mainly including: 1) the inevitable weather issues, such as cloudy, rainy, and extremely poor seeing, which occupied $\sim$50% observing time in total; 2) technical issues in both hardware and software, which occupied total $\sim$6% observing time; 3) an underestimation of the time of preparing SDSS templates, which led to an insufficient number of templates for the transient identification in the first 12 days of the observation and thus $\sim$11% observing time was lost. In general, the completeness of the SKYS project is $\sim$33%, which is comparable to our expectation (40% observable time).

As a result, we discovered 11 SN candidates based on their photometric behavior in the 26 full-night observations (a usable night fraction of $\sim$33%). Four of them were identified spectroscopically. In particular, we discovered one early-phase SN Ia (SKYS6) and one early-phase core-collapse SN (SKYS9), which is consistent with the expected number estimation by taking into account the SN rate in the local universe (Li et al., 2011) and early-phase photometric behavior of well-observed SN samples. The detailed situation during the October and November SKYS observing runs are recorded in Table 1.

Table 1: The observing log of SKYS

mm/dd	Observational Status	Effective Pointings	Completeness
10/06	unknown error happened from ∼22:00 (error code: 09)	5	6%
10/07	clear sky & very limited SDSS templates	11	14%
10/08	clear sky, but the seeing is bad (> 7.5" in average)	32	40%
10/09	weather turns bad from ∼25:00 & limited templates	14	17.5%
10/10	rainy and cloudy whole night	0	0%
10/11	cloudy whole night	0	0%
10/12	observational time less than 2 hours	22	27.5%
10/13	clear sky, but the seeing is bad (> 7.0" in average)	22	27.5%
10/14	clear sky, small error happened	48	60%
10/15	clear sky until ∼26:00 & limited templates	9	11.25%
10/16	clear sky all night & limited templates	28	35%
10/17	cloudy since ∼25:00 & limited templates	12	15%
10/18	clear sky almost all night	65	80%
10/19	clear sky almost all night	73	90%
10/20	later half night observation, cloudy from ∼26:10	33	66%
10/21	sharing with other observations, cloudy from ∼27:30	53	75%
11/05	clear all night, pointing deviation occurred, some images are useful	86	100%
11/06	3 hours clear, pointing deviation occurred again for most of images	7	10%
11/07	rainy	0	0%
11/08	rainy	0	0%
11/09	rainy	0	0%
11/10	clear sky in ∼7 hours	72	90%
11/11	cloudy & unknown error (no disk pace) since ∼25:00	40	50%
11/12	cloudy since ∼21:00	23	50%
11/13	rainy	0	0%
11/14	rainy	0	0%
11/15	clear all early half-night	44	100%
11/16	one-hour observable	7	15%
11/17	rainy	0	0%
11/18	rainy	0	0%
11/19	rainy & cloudy	0	0%
11/20	three hours multi-band follow-up observation	6	75%

Note. We mainly experienced weather and insufficient template issues in October 2015, which may be responsible to a relatively low SN detection rate in the October observing run. In November, we faced extremely bad weather and some technical issues, which also prevented us from arranging follow-up observations of an early-phase SN Ia, SKYS6, in time. Half-night observations were carried out on October 20, 21, and November 12–20, 2015.

2.3. KWFC Early-phase SNe Ia

In this section, the basic photometric information on three KWFC early-phase SNe Ia, KISS15m, KISS15n, and SKYS6 is presented. Given that the information of non-early-phase SN candidates (nine in total, two of them have been spectroscopically confirmed as SNe Ia discovered around/after their peak) and an early-phase SN IIP (SKYS9) do not meet the scientific purpose of this article, their properties are shown in the appendix as a reference.

2.3.1 Observations and data reduction

After the discovery of each early-phase SN Ia, over one month *g*-band observations were carried out with Kiso/KWFC. For spectral follow-up observations, three spectra of KISS15m and one pre-maximum spectrum for KISS15n through the KISS collaboration were obtained. Two spectra of SKYS6 were taken with LT/SPRAT and LJT/YFOSC, respectively. Interestingly, the spectra indicate that three early-phase SNe Ia belong to different subclass.

We adopted different methods for the photometry of KISS and SKYS SNe respectively. For two KISS SNe Ia, as both of them are far away from their host galaxies, the flux contamination from their hosts is negligible. In addition, since the apparent magnitude of KISS15m is close to the limiting magnitude of KISS, we stacked multiple images taken in the same night with the SWarp software (Bertin, 2010) to reduce the photometric error of such a faint object. Then, an aperture photometry was performed for both KISS15m and KISS15n using the APPHOT package in IRAF. In contrast to KISS SNe, SKYS SNe are either embedded in or located at the edge of their hosts. Therefore the galaxy subtraction procedure is necessary. Since SKYS SNe were bright enough even around the full moon night, the photometry of SKYS SNe was based on single-exposure images. For both KISS and SKYS observations, we used SDSS images at the same positions as templates and aligned the KWFC image with the SDSS template image through wcsremap before the imaging-subtraction process. Then, the image subtraction between KWFC images and corresponding SDSS images was conducted to get host-subtracted images of all SKYS SNe with HOTPANTS. Finally, a standard aperture photometry was performed on the residual SN with IRAF.

Spectroscopic and photometric information on three KWFC early-phase SNe Ia are respectively summarized in Tables 2 & 3 at the end of this section. Observational results of other SKYS SNe and candidates can be found in Tables 9–12 in the appendix. A general review of three KWFC early-phase SNe Ia is summarized in the following text of this section, and further discussions are given in §2.4.

KISS15m

A faint transient was discovered during the KISS observation on April 23, 2015 (UTC), located at the outermost region of a nearby galaxy, the NGC 4098, at z=0.024 (spectroscopic redshift). We classified it as an early phase SN candidate with a g-band absolute magnitude of ~ -15 during the discovery. Since the host galaxy is an early-type galaxy, we suspected that this object is a good early-phase SN Ia candidate. Therefore we conducted KWFC g-band follow-up immediately and confirmed that the object's brightness was increasing with a speed of ~ -0.4 mag/day. Such a fast brightening was in line with our expectation of an early-phase SN and we formally named it as KISS15m. Then, consecutive KWFC imaging follow-up observations (Figure 7) and spectroscopies through the KISS collaboration were triggered. On April 25, the NOT/ALFOSC took the first spectrum of KISS15m (Figure 8). Typical spectral features of 91bg-like SNe Ia, such as a red spectral energy distribution (SED), prominent Ti II absorptions around 4000 $\AA$ and Si II λ5972 line were easily distinguished even at the rising phase of the light curve. About one week later, we obtained a g-band peak absolute magnitude of -17.2 for KISS15m, and thus confirmed that the first observation was carried out at about 9 days before the g-band peak of KISS15m.

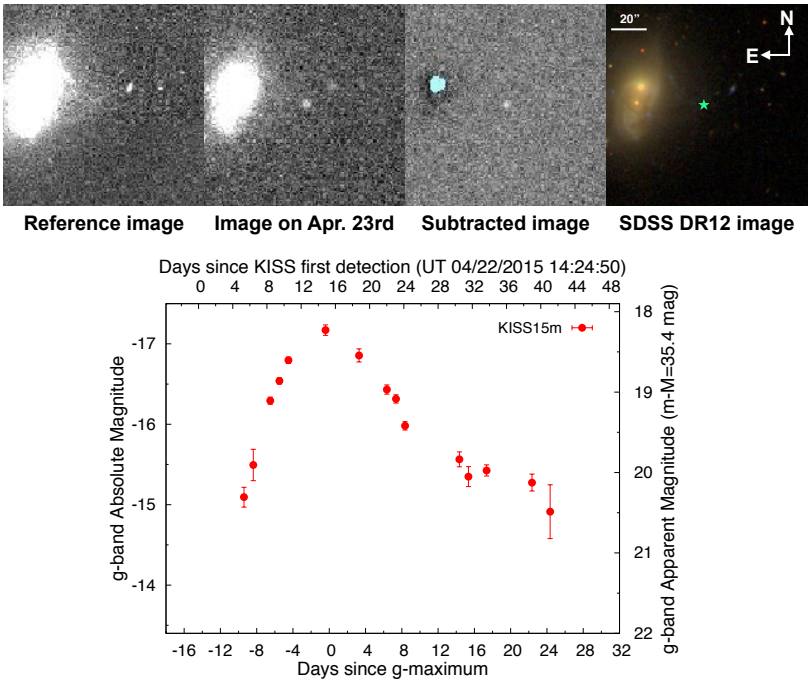

Figure 7: g-band observations of KISS15m. The upper panel (from left to right) shows the SDSS g-band reference image, the KWFC g-band image taken on Apr. 23, the subtracted image, and the SDSS DR12 color image at the same region. The location of KISS15m (RA $12^h06^m00^s.83$, Dec +20:36:18.4) is marked by a cyan star symbol. The lower panel is the g-band light curve obtained from our KWFC follow-up observations. The low luminosity and large Δm_{15} value ($\sim$1.8 in g-band) suggest that KISS15m is a subluminous (91bg-like) SN Ia.

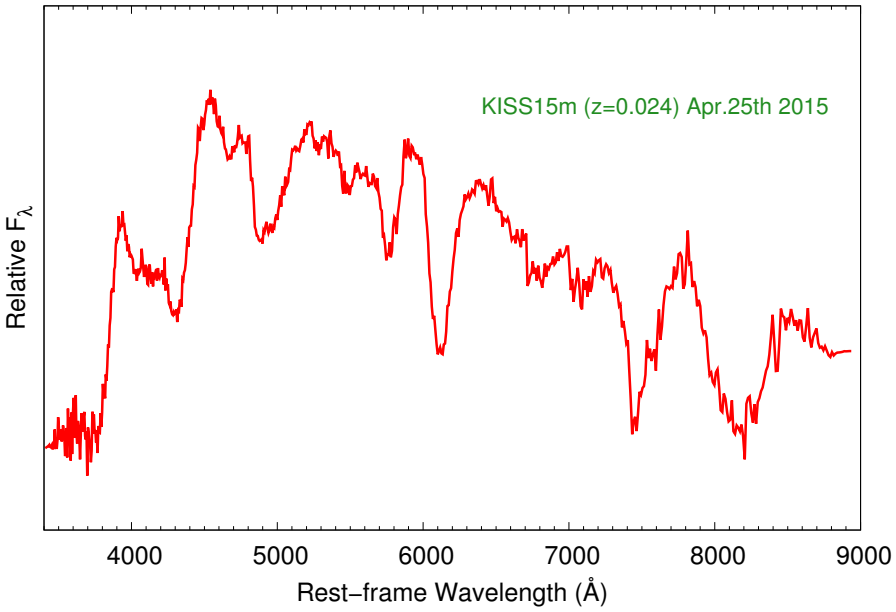

Figure 8: A spectrum of KISS15m taken by NOT/ALFOSC. Ti II absorptions at 4100–4400 $\AA$ and a strong Si II λ5972 absorption at the rising phase indicate that KISS15m is a 91bg-like subluminous SN Ia discovered in the early phase. Spectral evolution and discussions about KISS15m are shown in §2.4.

KISS15n

KISS15n was discovered in the Coma Cluster on May 10, 2015. Although we noticed KISS15n is an SN candidate, follow-up observations in next three days could not be carried out due to the poor weather in Kiso. Four days later, the brightness of KISS15n increased by ~ -1.2 mag (Figure 9), we then immediately triggered the spectroscopy and g-band follow-up observations for this early-phase SN candidate. A spectrum taken on May 15 showed a blue quasi-continuum with shallow absorption features of intermediate-mass elements (Figure 10). The SNID spectral fitting (Blondin and Tonry, 2007) of KISS15n matched with a super-$M_{\rm Ch}$ SN Ia, SN 2006gz at about 9 days before the maximum. On the other hand, the light-curve fitting also suggested that the brightness declining speed and the peak absolute magnitude of KISS15n are in line with 91T/99aa-like luminous SNe Ia. Given both photometric and spectroscopic properties we classify KISS15n as a transitional luminous SN Ia that may bridge typical luminous (91T/99aa-like) and super-$M_{\rm Ch}$ SNe Ia.

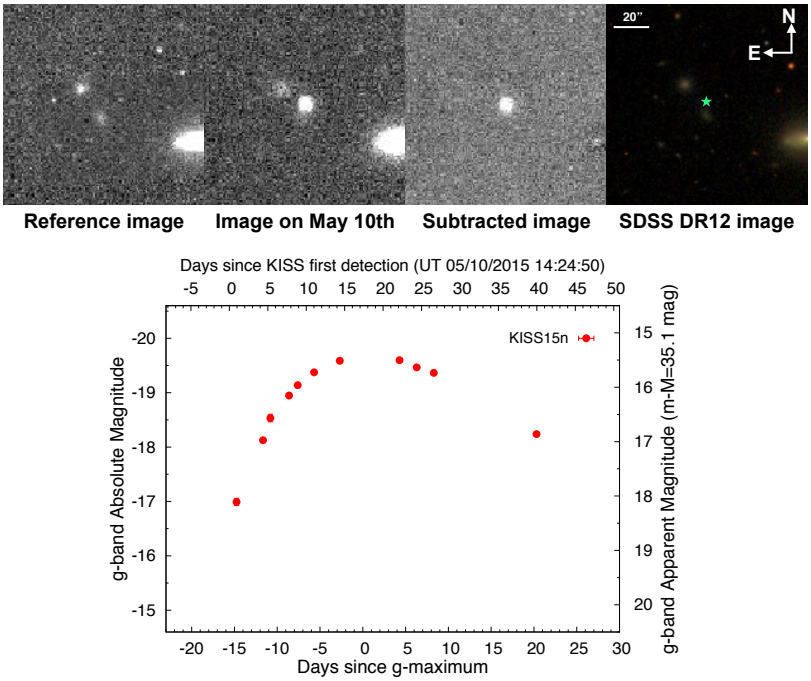

Figure 9: g-band observations of KISS15n. The upper panel (from left to right) shows the SDSS g-band reference image, the KWFC g-band image taken on May 10, the subtracted image and the SDSS DR12 color image at the same region. The position of KISS15n (RA $13^h00^m32^s.33$, Dec +27:58:41.0) is marked by a cyan star symbol. The lower panel is the g-band light curve obtained from our KWFC follow-up observations. The high luminosity and small $\Delta m_{15}(g)$ value ($\sim$0.8) indicate that KISS15n is a luminous SN Ia.

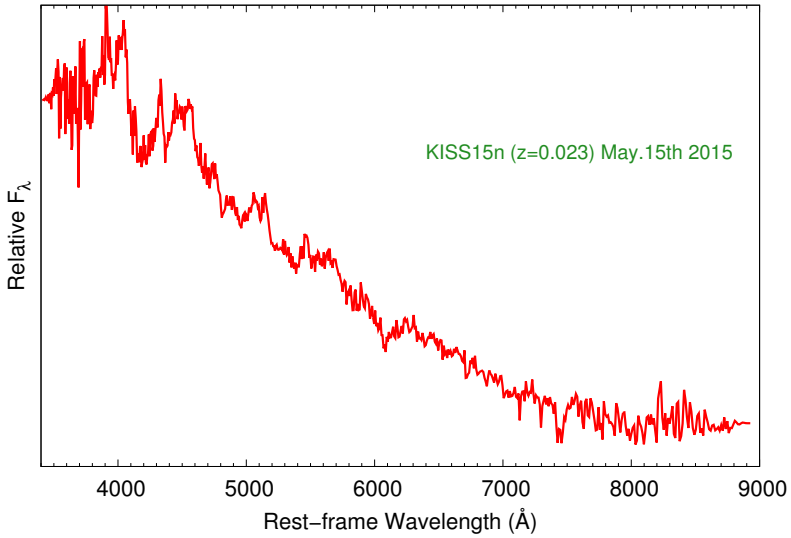

Figure 10: A pre-maximum spectrum of KISS15n taken by NOT/ALFOSC. The blue quasi-continuum spectral energy distribution (SED) with weak absorption features of iron and intermediate-mass elements (e.g. Si and S) suggest that KISS15n is a luminous SN Ia discovered in the early phase. Moreover, the clear C II λ6580 absorption and the low ejecta velocity are in line with the super-$M_{\rm Ch}$ SN Ia, SN 2006gz.

SKYS6

SKYS6 was discovered in the first night of our November observing run. Since the location of SKYS6 is close to the center of the host galaxy that is poorly investigated before, it is difficult to identify SKYS6 based on a single observation. Unfortunately, due to the continuous poor weather in Kiso, follow-up observations of SKYS6 were started about one week later. We identified that SKYS6 is an early-phase SN due to the significant brightness enhancement (~ -1.5 mag) in one week (Figure 11). The first spectrum (Figure 12) was taken on November 13 with LT/SPRAT, which is in line with normal SNe Ia at about one week before their maxima. Therefore, we classified SKYS6 as a normal SN Ia discovered within one week of the explosion.

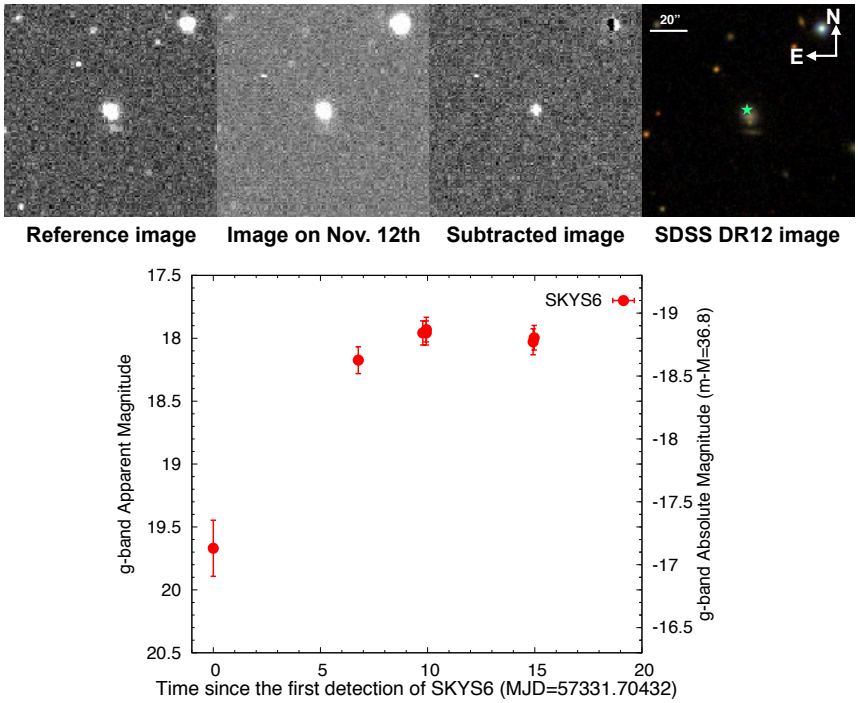

Figure 11: *g*-band observations of SKYS6. The upper panel (from left to right) shows the SDSS *g*-band reference image, the KWFC *g*-band image taken on November 12, the subtracted image and the SDSS DR12 color image at the same region. The position of SKYS6 (RA $02^h03^m44^s.31$, Dec +19:41:30.7) is marked by a cyan star symbol. The lower panel is the *g*-band light curve obtained from our KWFC follow-up observations, the peak magnitude of which suggests that SKYS6 is likely a normal-type SN Ia.

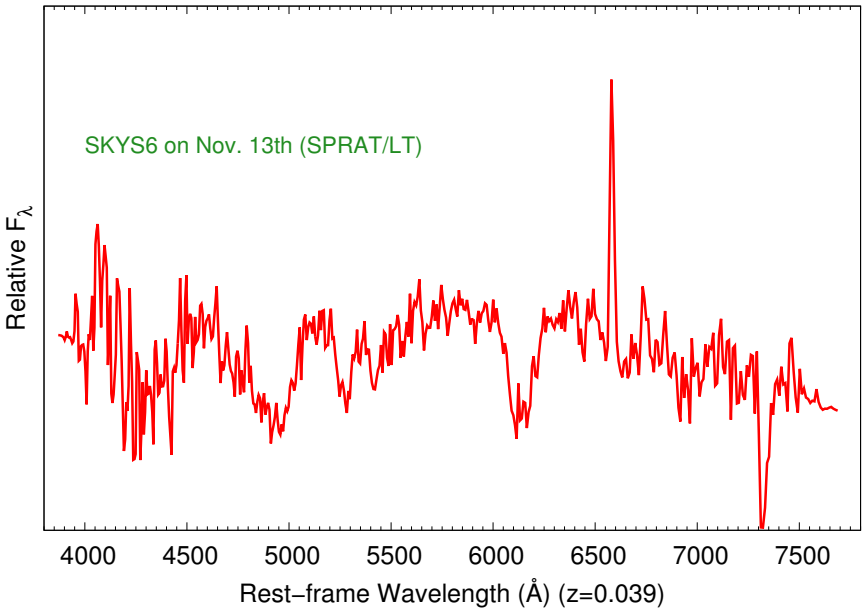

Figure 12: A spectrum of SKYS6 taken by LT/SPRAT on November 13. Typical absorption features of normal SNe Ia and a possible C II λ6580 line can be distinguished. Both spectral and light-curve fitting indicate that SKYS6 is a normal SN Ia discovered at about one week after the explosion.

Table 2: A Summary of Spectroscopies of KWFC Early-phase SNe Ia

Object	UT	Exp. Time (s)	Telescope	slit width (")	grism/filter
KISS15m	2015 Apr. 25	2400	NOT/ALFOSC[a]	1.0	#4 300 l/mm[b]
KISS15m	2015 Apr. 30	1800	NOT/ALFOSC[a]	1.0	#4 300 l/mm[b]
KISS15m	2015 May 09	2400	NOT/ALFOSC[a]	1.0	#4 300 l/mm[b]
KISS15n	2015 May 15	1800	NOT/ALFOSC[a]	1.0	#4 300 l/mm[b]
SKYS6	2015 Nov. 13	1800	LT/SPRAT	1.8	Red/4020longpass[c]
SKYS6	2015 Nov. 20	2100	LJT/YFOSC	2.5	#3[d]

Note.

[a] Spectroscopies for KISS15m and KISS15n were taken by NOT/ALFOSC, which were carried out by the Instituto de Astrofisica de Andalucia (IAA) under a joint agreement with the University of Copenhagen and NOTSA.

[b] The wavelength coverage and resolution of Grism#4 300 l/mm is 350–800 nm and 350, respectively.

[c] The LT/SPART "Red" configuration has much better performance on wavelengths above ∼6000Å, "4020longpass" is the abbreviation of "Edmund Optics 400nm longpass filter". The wavelength coverage and resolution is 400–800 nm and 350, respectively.

[d] The wavelength coverage and resolution of Grism#3 on LJT/YFOSC is 340–910 nm and 150, respectively.

Table 3: Photometric Information on Three KWFC Early-phase SNe Ia

Object	MJD[a]	UT	Filter	Magnitude[b]	Exp. Time (s)	Telescope
KISS15m	57134.47	2015 Apr. 22	*g*	20.31 ± 0.12	180×2	Kiso/KWFC
KISS15m	57135.47	2015 Apr. 23	*g*	19.92 ± 0.20	180×2	Kiso/KWFC
KISS15m	57137.45	2015 Apr. 25	*g*	19.11 ± 0.04	180×5	Kiso/KWFC
KISS15m	57138.45	2015 Apr. 26	*g*	18.86 ± 0.04	180×4	Kiso/KWFC
KISS15m	57139.46	2015 Apr. 27	*g*	18.60 ± 0.04	180×5	Kiso/KWFC
KISS15m	57143.57	2015 May 01	*g*	18.23 ± 0.07	180×4	Kiso/KWFC
KISS15m	57147.49	2015 May 05	*g*	18.54 ± 0.08	180×2	Kiso/KWFC
KISS15m	57150.55	2015 May 08	*g*	18.97 ± 0.06	180×2	Kiso/KWFC
KISS15m	57151.53	2015 May 09	*g*	19.08 ± 0.05	180×3	Kiso/KWFC
KISS15m	57152.51	2015 May 10	*g*	19.42 ± 0.05	180×3	Kiso/KWFC
KISS15m	57158.52	2015 May 16	*g*	19.84 ± 0.09	180×2	Kiso/KWFC
KISS15m	57159.53	2015 May 17	*g*	20.05 ± 0.12	180×3	Kiso/KWFC
KISS15m	57161.54	2015 May 19	*g*	19.97 ± 0.07	180×2	Kiso/KWFC
KISS15m	57166.65	2015 May 24	*g*	20.13 ± 0.11	180×4	Kiso/KWFC
KISS15m	57168.48	2015 May 26	*g*	20.49 ± 0.34	180×2	Kiso/KWFC
KISS15n	57152.55	2015 May 10	*g*	18.11 ± 0.07	180	Kiso/KWFC
KISS15n	57155.50	2015 May 13	*g*	16.97 ± 0.03	180	Kiso/KWFC
KISS15n	57156.71	2015 May 14	*g*	16.57 ± 0.07	180	Kiso/KWFC
KISS15n	57158.57	2015 May 16	*g*	16.15 ± 0.04	180	Kiso/KWFC
KISS15n	57159.60	2015 May 17	*g*	15.96 ± 0.04	180	Kiso/KWFC
KISS15n	57161.55	2015 May 19	*g*	15.73 ± 0.03	180	Kiso/KWFC
KISS15n	57164.70	2015 May 22	*g*	15.51 ± 0.05	180	Kiso/KWFC
KISS15n	57168.48	2015 May 29	*g*	15.50 ± 0.04	180	Kiso/KWFC
KISS15n	57171.47	2015 Jun. 01	*g*	15.64 ± 0.01	180	Kiso/KWFC
KISS15n	57176.51	2015 Jun. 03	*g*	15.73 ± 0.01	180	Kiso/KWFC
KISS15n	57188.52	2015 Jun. 15	*g*	16.86 ± 0.04	180	Kiso/KWFC
SKYS6	57331.70	2015 Nov. 05	*g*	19.67 ± 0.22	180	Kiso/KWFC
SKYS6	57338.47	2015 Nov. 12	*g*	18.17 ± 0.11	180	Kiso/KWFC
SKYS6	57341.48	2015 Nov. 15	*g*	17.96 ± 0.10	180	Kiso/KWFC
SKYS6	57341.64	2015 Nov. 15	*g*	17.96 ± 0.10	180	Kiso/KWFC
SKYS6	57346.63	2015 Nov. 20	*g*	18.03 ± 0.10	180	Kiso/KWFC
SKYS6	57346.68	2015 Nov. 20	*g*	18.00 ± 0.10	180	Kiso/KWFC
SKYS6	57353.46	2015 Nov. 27	*g*	18.38 ± 0.15	60	MITSuME
SKYS6	57354.55	2015 Nov. 28	*g*	18.47 ± 0.16	60	MITSuME
SKYS6	57357.46	2015 Dec. 01	*g*	18.72 ± 0.17	60	MITSuME
SKYS6	57341.46	2015 Nov. 15	*r*	17.76 ± 0.09	180	Kiso/KWFC
SKYS6	57346.63	2015 Nov. 20	*r*	17.68 ± 0.09	180	Kiso/KWFC
SKYS6	57341.47	2015 Nov. 15	*i*	18.20 ± 0.11	180	Kiso/KWFC
SKYS6	57346.58	2015 Nov. 20	*i*	18.32 ± 0.12	200	Kiso/KWFC
SKYS6	57341.47	2015 Nov. 15	*z*	18.85 ± 0.19	180	Kiso/KWFC
SKYS6	57346.59	2015 Nov. 20	*z*	18.30 ± 0.15	220	Kiso/KWFC

Note.

[a] The median time of stacked data (KISS15m and KISS15n) or a single exposure (SKYS6).

[b] AB magnitudes for SDSS *ugriz* filter.

2.4 Discussions on KWFC Early-phase SNe Ia

2.4.1 KISS15m: one of the youngest subluminous SNe Ia

Although about two dozen of SNe Ia have been discovered in a few days of their explosions, we are still puzzled by the early light curve of subluminous, especially the 91bg-like SNe Ia due to their fast evolving light curves and lower intrinsic brightness compared with other SN Ia subclasses. The early-phase SN Ia KISS15m, one of the youngest 91bg-like SNe Ia, brings us a good opportunity to investigate the rising behavior of this peculiar SN Ia class.

The distance and reddening of KISS15m

The location of KISS15m is far way from its host galaxy, NGC 4098. The large offset between the host and SN and the non-detection of narrow interstellar absorption lines in the SN spectra suggest the negligible extinction from the host galaxy. Therefore, we adopted only the Milky Way extinction at the direction of KISS15m as the total extinction, that is, $A_\lambda(g)$=0.11 mag (Schlafly and Finkbeiner, 2011).

For the distance uncertainty, NASA/IPAC Extragalactic Database (NED) indicates the recession velocity of NGC 4098 which has been corrected for the effects of the Local Group infall into the Virgo Cluster, the GA cluster, and the Shapley supercluster (Mould et al., 2000): $V_{Virgo+GA+Sharply}$=7852±32 km s^{-1}. The Hubble flow distance of NGC4098 is 112.2±7.9 Mpc, where H_0=70±5 km s^{-1} Mpc^{-1}, corresponding to a distance modulus μ=35.25±0.15 mag for KISS15m.

The photometry and spectral evolution of KISS15m

A comparison between *B*-band light curves of typical 91bg-like SNe Ia (including a model light curve made by P. Nugent*), a peculiar subluminous SN Ia SN 2007ax, and the *g*-band light curve of KISS15m is shown in Figure 13. The rest-frame *B*-band peak magnitude of KISS15m is same with that of SN 1999by after applying a K-correction of about -0.2 mag of 91bg-like SNe Ia at redshift of 0.024 (Takanashi et al., 2017). Fast-evolving light curves can be found for KISS15m ($\Delta m_{15}(g) \sim$1.8) and 91bg-like SNe Ia. With spectroscopic follow-up observations, we confirmed that KISS15m is a typical 91bg-like SN Ia discovered at about 9 days before the *g*-band peak.

*$https://c3.lbl.gov/nugent/nugent_templates.html$

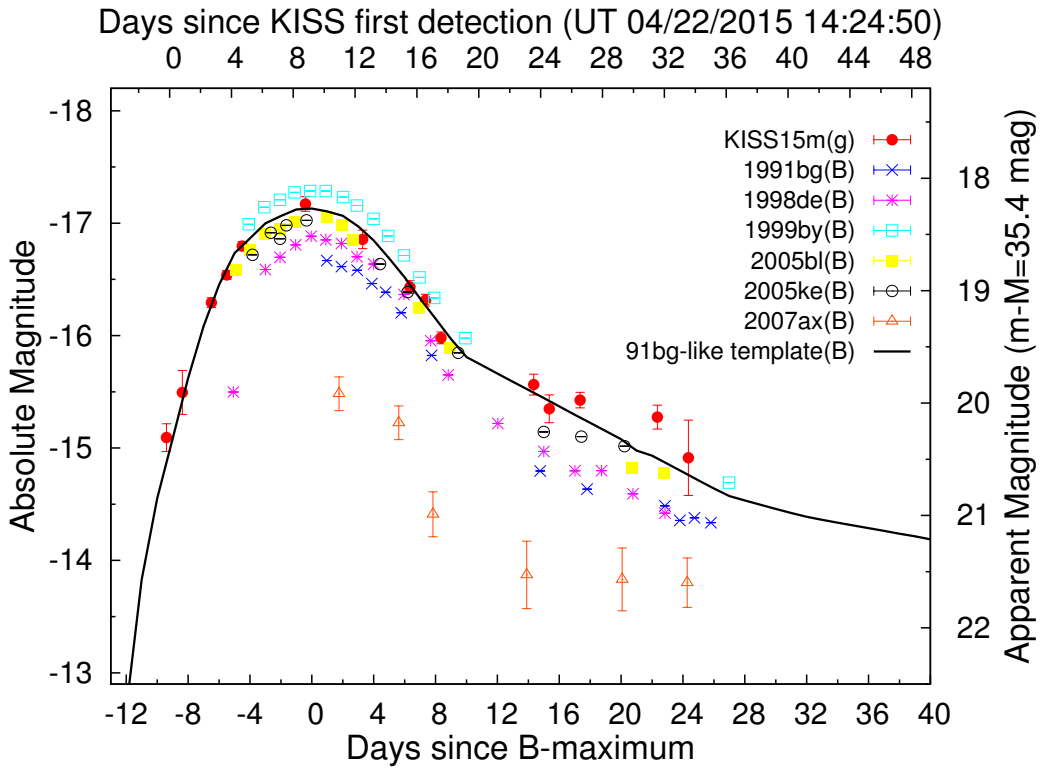

Figure 13: Light curves of KISS15m and other subluminous SNe Ia. The fast-evolving light curve suggests that KISS15m is a 91bg-like SN Ia discovered at a few days after the explosion. Data sources: SN 1991bg (Leibundgut et al., 1993); SN 1998de (Modjaz et al., 2001); SN 1999by (Vinkó et al., 2001); SN 2005bl (Taubenberger et al., 2008); SN 2005ke and SN 2007ax (Kasliwal et al., 2008).

The spectral evolution of KISS15m from -6 days to $+9$ days after the maximum is shown in Figure 14. The Ti II trough at $\sim$4100–4400 $\AA$ shown from the early phase and the rapid spectral evolution further indicate that KISS15m is a 91bg-like SN Ia. In addition, spectra of KISS15m are characterized by O I λ7774 absorption, which is commonly shown in rapid-decline SNe Ia (Figure 15). The large amount of oxygen remained in the SN ejecta can be explained by a low carbon burning efficiency during the SN explosion. However, given that the oxygen should originate from both the incomplete carbon burning and the progenitor itself (i.e. a C/O white dwarf), a quantitative analysis cannot be performed only based on the strength of the O I λ7774 line. Moreover, similar to other 91bg-like SNe Ia, such as SN 1991bg, SN 1998de, and SN 1999by (Filippenko et al., 1992, Leibundgut et al., 1993, Krisciunas et al., 2004, Modjaz et al., 2001, Vinkó et al., 2001), we cannot distinguish a clear flux deficit red-wards of the Si II λ6355 line, i.e. the C II λ6580 absorption, even in the earliest spectrum of KISS15m. We thus speculate that an efficient carbon-burning process might be achieved even for 91bg-like SNe Ia.

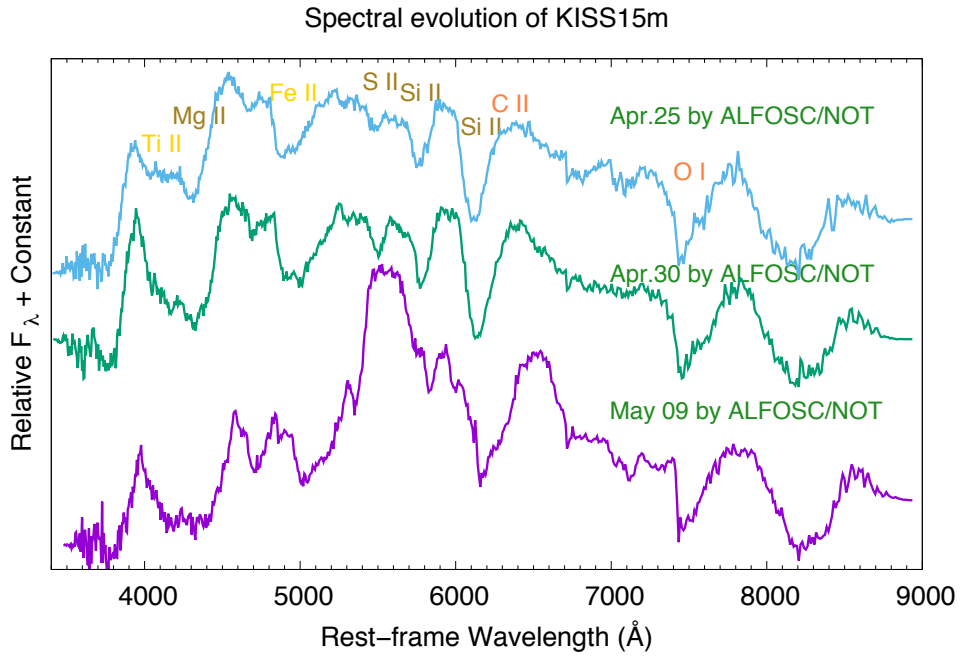

Figure 14: The spectral evolution of KISS15m. The Ti II trough at 4100–4400 *Å* from the early phase and the fast spectral evolution indicate that KISS15m is a 91bg-like SN Ia.

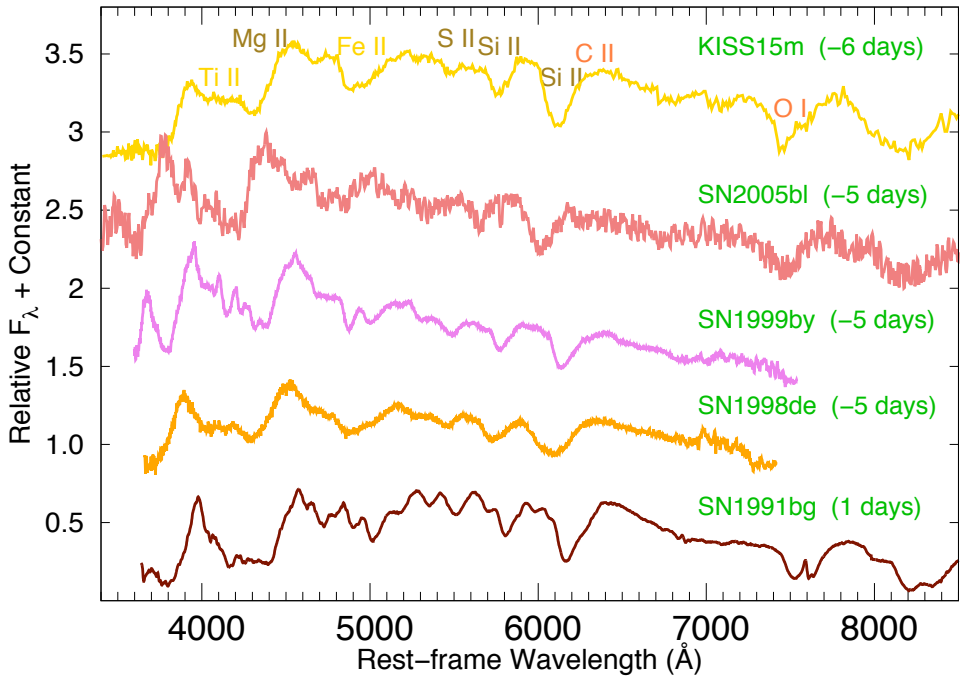

Figure 15: Pre/around-maximum spectra of 91bg-like SNe Ia. None of them show clear C II λ6580 absoption even in their pre-maximum spectra. Data sources: SN 2005bl (Taubenberger et al., 2008); SN 1999by and SN 1998de (Matheson et al., 2008); SN 1991bg (Asiago Supernova Catalogue, https://graspa.oapd.inaf.it).

2.4.2 KISS15n: bridging 91T/99aa-like and super-$M_{\rm Ch}$ SNe Ia?

Super-$M_{\rm Ch}$ SNe Ia are of special interest due to their abnormal photometric behavior, which challenges our common knowledge that SNe Ia originate from the thermonuclear explosion of near Chandrasekhar-mass C/O white dwarf. Observationally, a blue SED and slow-evolving light curve of the super-$M_{\rm Ch}$ SN Ia make a reminiscent of the typical luminous SN Ia subclass, 91T/99aa-like SNe Ia while the luminosity of the super-$M_{\rm Ch}$ SN Ia is even higher. Particularly, as opposed to 91T/99aa-like SNe Ia where C II lines are hardly distinguished even in the early phase, persistent C II absorptions can be commonly found in spectra of super-$M_{\rm Ch}$ SNe Ia. The peculiar luminous SN Ia, KISS15n, may enlighten us the physical connection between two SN Ia subclasses.

The distance and reddening of KISS15n

KISS15n was found in the Coma Cluster and far from centers of two closest galaxies, suggesting a low flux contamination from the host galaxy. Another possible host galaxy, COMAi130032.301p275841.02, shown in images taken by the Advanced Camera for Surveys (ACS) on the Hubble Space Telescope (Hammer et al., 2010) is nearly at the same position of KISS15n with an $F814W$ magnitude of about 25.2. If such a faint galaxy is the host of KISS15n, the reddening from the host may not be negligible. However, given a non-detection of narrow interstellar absorption lines in the spectrum of KISS15n, we adopted the Milky Way extinction on the direction of KISS15n as the total extinction, where $A_\lambda(g)$=0.035 mag (Schlafly and Finkbeiner, 2011).

Although the host of KISS15n is uncertain, the distance information of KISSn can be well constrained thanks to lots of previous work on the Coma Cluster. Here, we applied the same Hubble flow distance of the Coma Cluster to KISS15n. NASA/IPAC Extragalactic Database (NED) provides the recession velocity of the Coma Cluster which has been corrected for the effects of the Local Group infall into the Virgo Cluster, the GA cluster, and the Shapley supercluster (Mould et al. 2000): $V_{Virgo+GA+Sharply}$=7503$\pm$27 km s^{-1}. The Hubble flow distance of the Coma Cluster is 102.8$\pm$7.2 Mpc, corresponding to a distance modulus μ=35.06$\pm$0.15 mag for KISS15n, where H_0=70$\pm$5 km s^{-1} Mpc^{-1}.

The photometry and spectroscopy of KISS15n

A light-curve comparison between KISS15n (in both g and r band), super-$M_{\rm Ch}$ SNe Ia (SN 2007if and SN 2009dc; solid squares), normal-broad (SN 2012fr; diamonds), and the transitional type between 91T/99aa-like and super-$M_{\rm Ch}$ SNe Ia (or super-$M_{\rm Ch}$ SN Ia candidates, such as SN 2006gz, SN 2012dn, and LSQ12gdj; pentagons) is shown in Figure 16. All lu-

minous SNe Ia indeed show comparable $\Delta m_{15}(B)$ value, 0.8 mag or so. For KISS15n, the rest-frame B-band peak magnitude is almost the same with the g-band peak magnitude in the observer frame after applying the K-correction of luminous 91T/99aa-like SNe Ia at redshift of 0.024 (Takanashi et al., 2017). Its post-maximum light curve resembles to that of SN 2012dn (transitional) and SN 2012fr (normal-broad) but the rising speed is in between.

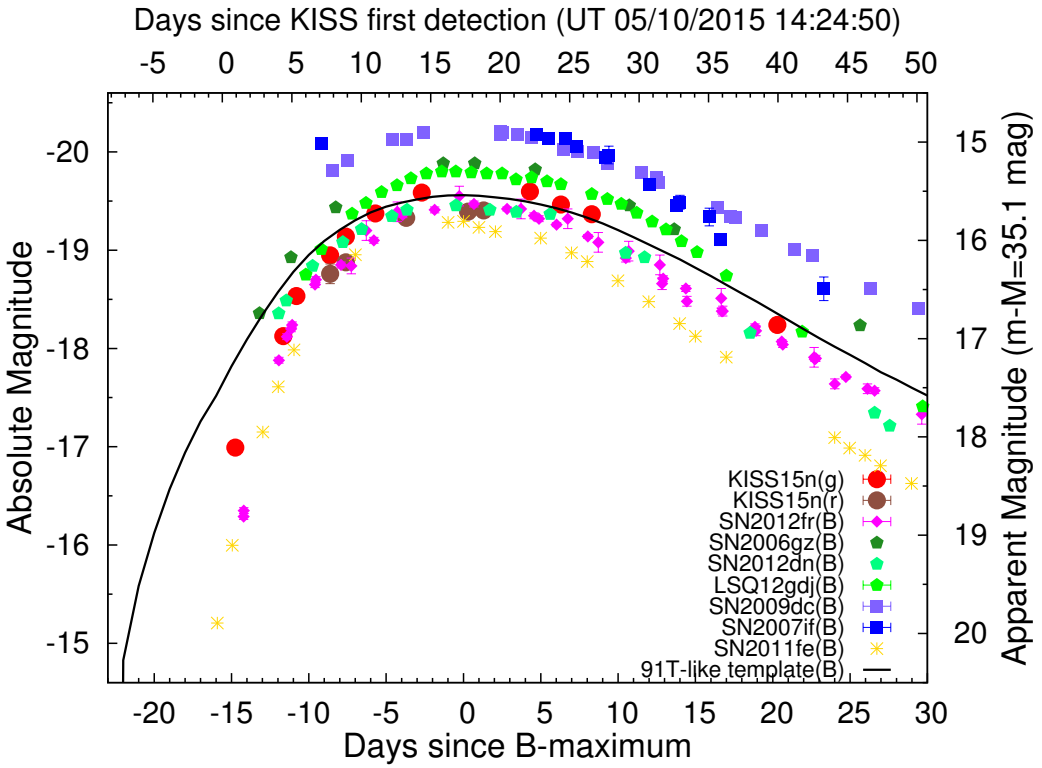

Figure 16: A light-curve comparison between KISS15n and other "slow-evolving" SNe Ia. The best-observed normal SN Ia, SN 2011fe is also included as a reference of a typical light curve of normal SNe Ia. In general, the rising-phase light curves show larger scatter than the post-maximum light curves between these luminous slow-evolving SNe Ia. Data sources: SN 2012fr (Childress et al., 2013); SN 2006gz (Hicken et al., 2007); SN 2012dn (Chakradhari et al., 2014); LSQ12gdj (Scalzo et al., 2014); SN 2009dc (Silverman et al., 2011); SN 2007if (Scalzo et al., 2014); SN 2011fe (Richmond and Smith, 2012).

A good similarity between SN 2006gz and KISS15n can be seen in their early spectra (Figure 17). A blue SED with plenty of iron and IME absorptions of the spectrum taken on May 15 (about 10 days before the g-band maximum) make a reminiscent of two super-$M_{\rm Ch}$ SN Ia candidates, SN 2006gz and SN 2012dn at the similar phase (Chakradhari et al., 2014). In contrast to 91T/99aa-like SNe Ia, more prominent and abundant IME absorptions are shown in early spectra of SN 2006gz and KISS15n, which further suggests that KISS15n is more close to a 06gz-like luminous SN Ia than a 91T/99aa-like luminous SN Ia.

The C II λ6580 feature in spectra of both KISS15n and SN 2006gz at t~-10 day are not clear. However, in terms of the spectral evolution of SN 2006gz by Hicken et al. (2007), the C II λ6580 line is very prominent at t=-14 days and then quickly disappeared in the following four days. Given the high spectral similarity between KISS15n and SN 2006gz, a possible absorption red-wards the Si II λ6355 of KISS15n may relate to the C II λ6580 line.

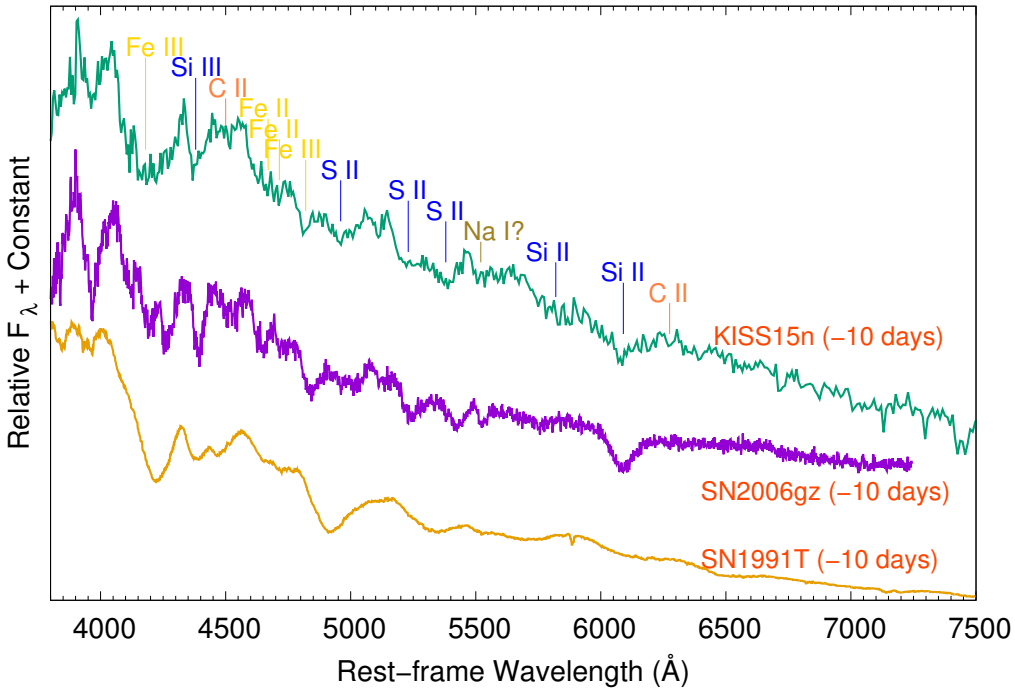

Figure 17: Spectra of KISS15n, SN 2006gz, and SN 1991T at about -10 days to their *B*-band maxima. Plenty of IME absorptions, clear Si II λ6355 line, and blue SED shown in the early spectrum of KISS15n are perfectly in line with those of SN 2006gz in the same epoch. The above spectral features are also similar to those of another transitional luminous SN Ia, SN 2012dn and a super-$M_{\rm Ch}$ SN Ia, SN 2009dc at about one week before their maxima but clearly different from the iron-dominant early spectra of SN 1991T. Additionally, high ejecta velocity derived from the Si II λ6355 and C II λ6580 lines of KISS15n also makes a reminiscent of SN 2006gz. Data sources: SN 1991T, Asiago Supernova Catalogue, https://graspa.oapd.inaf.it; SN 2006gz, Hicken et al. (2007).

Figure 18 gives the velocity evolution of Si II λ6355 and C II λ6580 line of SNe Ia in different subclasses. Velocities of Si II λ6355 line and possible C II λ6580 line of KISS15n are consistent with those of SN 2006gz but higher than another super-$M_{\rm Ch}$ SN Ia candidate, SN 2012dn in the early phase. Specifically, the velocity of C II λ6580 line is $\gtrsim$14,000 km s^{-1} at over 10 days before the maxima of both SN 2006gz and KISS15n, which is much higher than that of SN 2012dn at the same phase. The velocity of Si II λ6355 line for both SN 2006gz and KISS15n is around 13,000 km s^{-1} at t= -10 days, slightly higher than that of SN 2012dn. Such

values are significantly higher than those of super-$M_{\rm Ch}$ SNe Ia (e.g., SN 2003fg, SN 2007if, and SN 2009dc) and comparable to those of 91T/99aa-like SNe Ia (e.g. SN 2012cg, Marion et al., 2016; iPTF16abc, Miller et al., 2018) and normal SNe Ia (both low- and high-velocity groups; e.g., SN 1994D, Patat et al., 1996; SN 2002er, Kotak et al., 2005; SN 2012fr, Zhang et al., 2014) in the early phase.

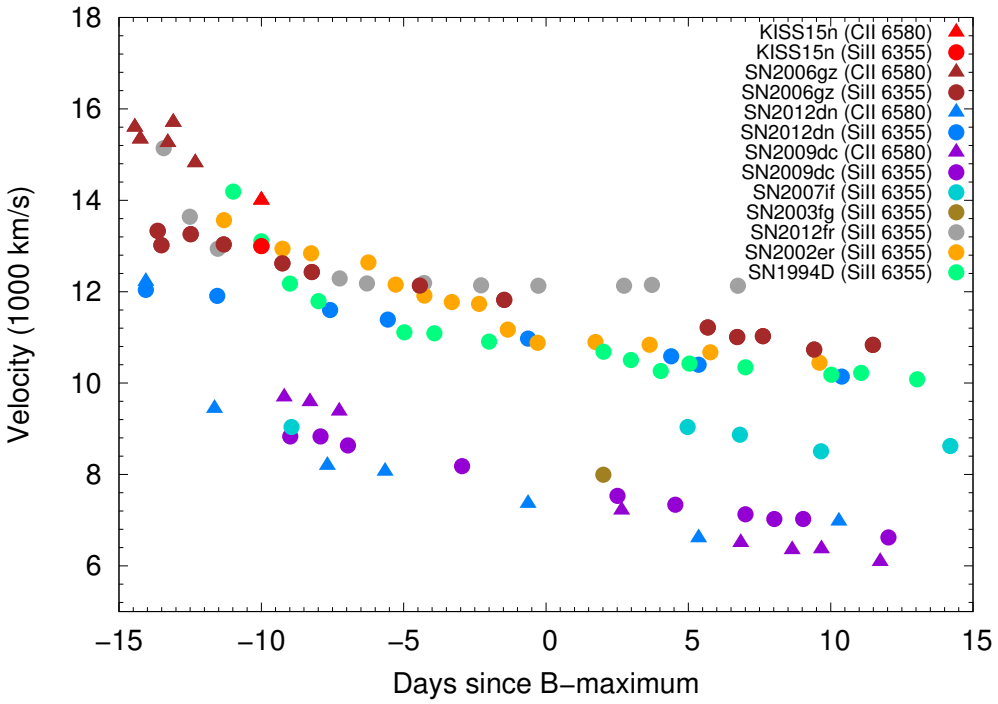

Figure 18: The C II λ6580 and Si II λ6355 line velocity evolution of SNe Ia in different subclasses. Velocities of the C II λ6580 line and Si II λ6355 line of KISS15n at t= -10 days are consistent with those of SN 2006gz but higher than super-$M_{\rm Ch}$ SNe Ia (SN 2003fg, SN 2007if, and SN 2009dc). Normal SNe Ia, such as SN1994D, SN 2002er, and SN 2012fr also show similar Si II λ6355 velocity to that of KISS15n at the same epoch. Data sources: SN2012dn, SN 2009dc, SN 2006gz, SN 2007if, and SN 2003fg (Chakradhari et al., 2014); SN 1994D (Patat et al., 1996); SN 2002er (Kotak et al., 2005); SN 2012fr (Zhang et al., 2014).

The pre-maximum spectrum suggests that KISS15n is more close to a 06gz-like SN Ia. In terms of the velocity evolution, 06gz-like SNe Ia show clear distinctions to super-$M_{\rm Ch}$ SNe Ia although both of them show very high luminosities and similar spectral features, which may imply an intrinsic difference between 06gz-like luminous SNe Ia and super-$M_{\rm Ch}$ SNe Ia. Due to the missing of very early spectral information of these rare objects, the early velocity evolution of 06gz-like and super-$M_{\rm Ch}$ SNe Ia is still unknown.

A remained uncertainty in the above discussion is the host of KISS15n. In contrast to KISS15m whose host galaxy can be easily identified, there are two bright galaxies near KISS15n. However, another possible host galaxy, COMAi130032.301p275841.02, is nearly at the same position of KISS15n but with an HST $F814W$ magnitude of $\sim$25.2. If the real host is the faintest one, the extinction influence may need to be taken into account and the intrinsic brightness of KISS15n can be higher. On the other hand, if the host of KISS15n is either of two bright galaxies with a negligible host extinction, the brightness of KISS15n indeed is comparable to that of 91T/99aa-like SNe Ia, suggesting that 06gz-like luminous SNe Ia may not always require a "super-$M_{\rm Ch}$" WD progenitor. If so, a specific explosion mechanism may be required to explain the brightness scatter of 06gz-like SNe Ia, for instance, an off-center explosion, an interaction with a confined circumstellar material (§4.3.2), etc. Statistically investigating early-phase photometric and spectroscopic behavior of luminous SNe Ia discovered by ongoing and forthcoming transient surveys will help us to figure out the intrinsic difference/connection between 91T/99aa-like, 06gz-like, and super-$M_{\rm Ch}$ SNe Ia.

2.4.3 SKYS6: a low-velocity normal SN Ia discovered in the early phase

As a large number of SNe Ia have been discovered in the last decade, diversities in normal SNe Ia have been noticed. Based on specific photometric/spectroscopic features, three popular classification methods of normal SNe Ia have been proposed: 1) the existence/duration of C II λ6580 absorption (Parrent et al., 2011, Thomas et al., 2011, Folatelli et al., 2012, Silverman and Filippenko, 2012); 2) the velocity evolution of specific absorption lines, e.g. Si II λ6355 (Benetti et al., 2005, Wang et al., 2009a); 3) the NUV$-$optical color evolution (Milne et al., 2013, 2015). The early-phase SN Ia SKYS6 can be classified as a low-velocity normal SN Ia.

The distance and reddening of SKYS6

We adopted the Milky Way extinction on the direction of SKYS6 as the total extinction ($A_\lambda(g)$=0.45 mag; Schlafly & Finkbeiner 2011) because of the non-detection of narrow interstellar absorption lines in its spectra.

Since SKYS6 has a relatively high redshift (z=0.042), the velocity uncertainty due to the peculiar motion is much smaller than the recession velocity of the host galaxy. Therefore, we only take into account the uncertainty of the Hubble constant (H_0=70$\pm$5 km s^{-1} Mpc^{-1}) for the distance estimation, which gives a Hubble flow distance of 186.6$\pm$13.3 Mpc, corresponding to a distance modulus μ=36.35$\pm$0.16 mag.

Photometry and spectroscopy of SKYS6

Given a negligible peak-magnitude difference between the rest-frame B-band and observed g-band light curve at redshift of 0.042 for non-subluminous SNe Ia (Takanashi et al., 2017), we make a light-curve comparison between SKYS6 (observer frame) and two normal SNe Ia, SN 2005cf and SN 2011fe in Figure 19 (light curves of two peculiar KWFC SNe Ia, KISS15m and KISS15n, are included as a reference). As can be seen in Figures 19 and 20, both light curves and spectra indicate that SKYS6 is a normal SN Ia. Although the single-band light curve with insufficient early-phase information prevents us from classifying SKYS6 with the NUV−optical color method and investigating its early light-curve behavior in detail, the C II λ6580 and Si II λ6355 absorption features can be discussed by using the spectra of SKYS6 at -6 days and $+1$ day after the peak.

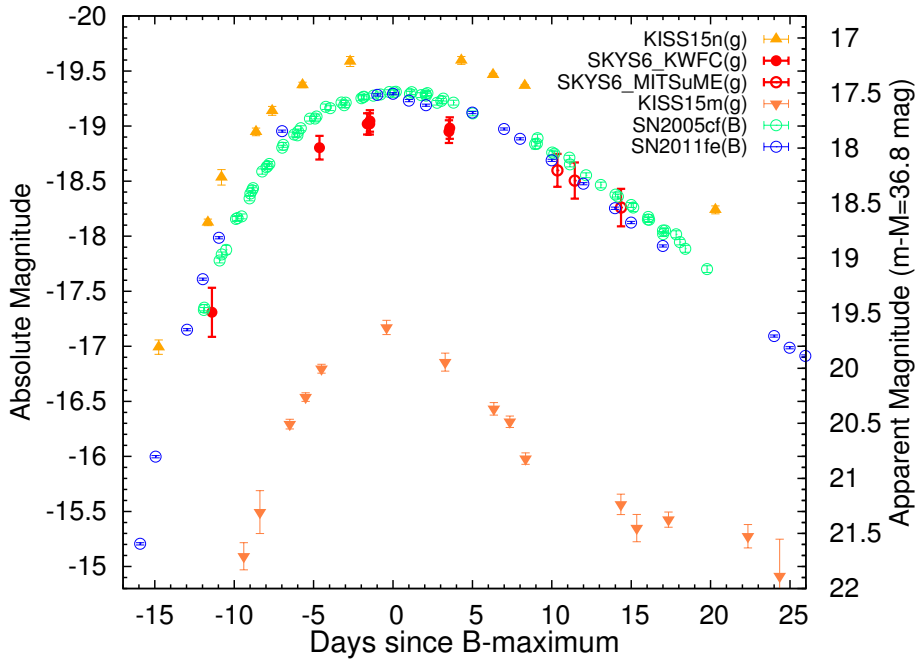

Figure 19: Light curves of SKYS6, two normal SNe Ia, SN 2005cf and SN 2011fe, 91bg-like subluminous SN Ia KISS15m, and 06gz-like luminous SN Ia KISS15n. SKYS6 is a normal SN Ia with a stretch factor of ∼0.93. Data sources: SN 2005cf (Wang et al., 2009b); SN 2011fe (Richmond and Smith, 2012).

Previous studies by Benetti et al. (2005) and Folatelli et al. (2012) suggested that the C II λ6580 absorption is commonly shown in SNe Ia that have relatively low Si II λ6355 line velocity before/around the maxima. By investigating the low S/N spectra of SKYS6 at -6 days and $+1$ day after the maximum, inconspicuous deficits toward to the red side of the Si II λ6355 line are

observed, possibly the C II λ6580 footprint. The velocity of the possible C II λ6580 line and Si II λ6355 line is as low as 13,300 km/s and 10,500 km/s at -6 days, respectively. According to the ejecta-velocity classification (Wang et al., 2009a), SKYS6 belongs to the low-velocity (LV) group and a slow Si II λ6355 velocity evolution of SKYS6 also resembles other LV SNe Ia (Taubenberger et al., 2011, Foley et al., 2011).

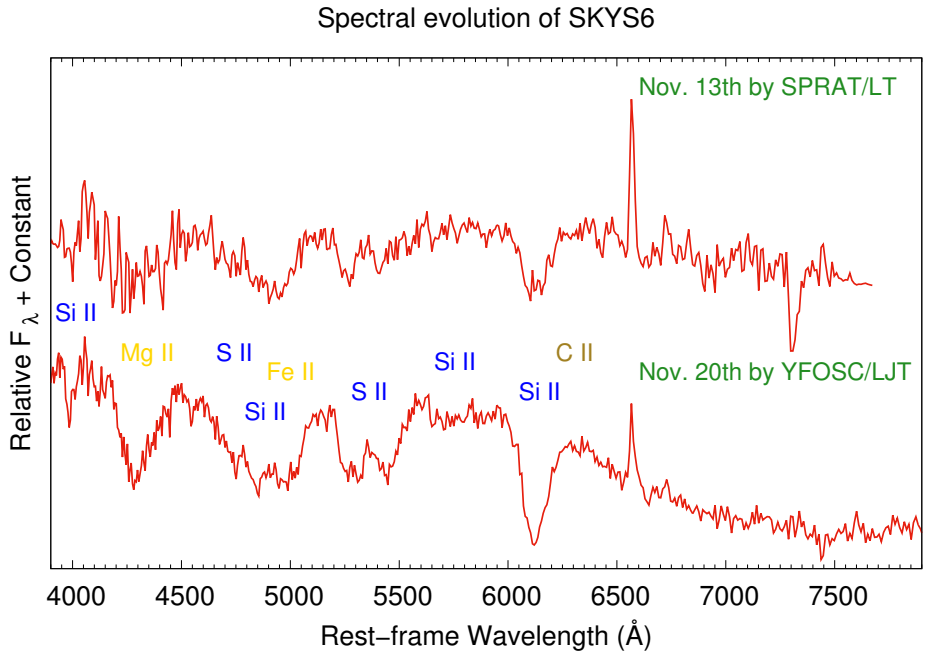

Figure 20: The spectra of SKYS6 at -6 days and $+1$ day after the maximum. Typical IME absorptions and a possible C II λ6580 absorption line can be found in two spectra. The velocity of Si II λ6355 line suggests that SKYS6 is a low-velocity normal SN Ia.

2.4.4 Further discussions and conclusions

Subluminous SNe Ia and their associated progenitor system

A subluminous EExSN Ia discovered by iPTF, iPTF14atg, was claimed as strong evidence of the single-degenerate (SD) scenario because of its peculiar light-curve behavior in the early phase (Cao et al., 2015). iPTF14atg was classified as a subluminous 02es-like subluminous SN Ia that shows much slower light-curve evolution than that of 91bg-like SNe Ia. Thanks to the prompt *Swift*/UVOT follow-up observations, an additional luminosity enhancement was found in the first few days after the explosion of iPTF14atg in UV and blue optical wavelengths, which is generally in line with the prediction of the companion-interaction scenario proposed by Kasen (2010). Given that KISS15m is one of the youngest 91bg-like SNe Ia discovered so

far, we make a further comparison between KISS15m, iPTF14atg, and other subluminous SNe Ia to seek for clues of the progenitor system of subluminous SNe Ia.

Spectroscopically, most of subluminous SNe Ia including KISS15m do not show persistent C II λ6580 feature. However, a rare number of subluminous SNe Ia, such as SN 2005bl and iPTF14atg, show C II λ6580 feature even around their maxima. Particularly, the C II λ6580 line of iPTF14atg is much more prominent than that of SN 2005bl and such an absorption can be clearly discriminated even at $\sim$30 days after the explosion (see Figure 4 in Cao et al., 2015), which indeed is commonly shown in 02es-like subluminous SNe Ia. If the progenitor system of iPTF14atg truly includes a nondegenerate companion, such a distinct absorption towards to the red side of the Si II λ6355 line may be contributed by not only the C II λ6580 but also the Hα absorption. Alternatively, such a feature may suggest a carbon-abundant environment for 02es-like SNe Ia. In that case, the companion of the progenitor system of iPTF14atg is more likely a C/O WD and thus the early-excess feature cannot be attributed to the companion-interaction scenario. By investigating whether or not the strength and duration of C II λ6580 line are correlated to the early light-curve behavior of 02es-like SNe Ia, we may find crucial evidence of the progenitor and explosion physics of this peculiar SN Ia subclass.

In order to explain the origin of various SN Ia subclasses, different progenitor systems and explosion mechanisms may need to be taken into account. In addition to the uncertain progenitor of 02es-like subluminous SNe Ia we discussed above, McCully et al. (2014) and Foley et al. (2014) reported that possible companions have been found at the same positions of two 02cx-like subluminous SNe Ia, SN 2008ha and SN 2012Z, indicating a possible connection between (some) subluminous SNe Ia and the SD scenario. On the other hand, recent simulations suggested that the violent merger of two sub-Chandrasekhar-mass WDs can explain the fast evolving light curves of subluminous 91bg-like SNe Ia quite well. Therefore, the multiple progenitor system is a likely reason of explaining the diversity of subluminous SNe Ia.

In addition to subluminous SNe Ia, the progenitor of normal and luminous SNe Ia is under debate as well. Further discussions on the progenitor system of luminous SNe Ia (i.e. 91T/99aa-like and super-$M_{\rm Ch}$ SNe Ia) based on their early light-curve behavior are given in Chapter 4.

Observing indicators for inconspicuous EExSNe Ia

g-band light curves of KISS15m and iPTF14atg are shown in Figure 21. Although iPTF14atg has a broader light curve and higher peak luminosity ($\sim$0.8 magnitude brighter) than those of KISS15m, it is still difficult to explain why the rising phase of iPTF14atg is significantly longer than that of all previously discovered subluminous and most of normal SNe Ia, e.g. SN 2011fe ($\sim$18 days). Considering a possible "dark phase" lasting for a few hours/days after the SN

explosion (Piro and Nakar, 2013, 2014, Zheng et al., 2014, Mazzali et al., 2014), radiation generated by a companion-ejecta interaction (or other early-excess scenarios) may brighten the dark phase, and thus extends the observable rising time of EExSNe Ia.

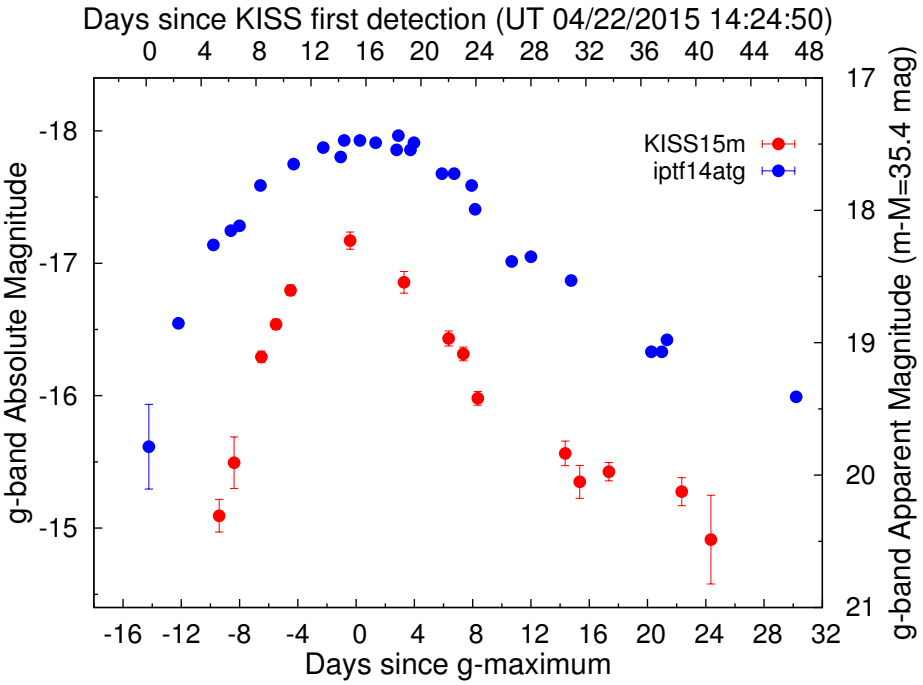

Figure 21: A *g*-band light-curve comparison between KISS15m and a 02es-like subluminous SN Ia, iPTF14atg. The rising time of iPTF14atg is much longer than that of other subluminous SNe Ia and most of normal SNe Ia which have much higher luminosities and "broader" (i.e. slower-evolving) light curves. A possible reason is that the radiation generated by a companion-ejecta interaction (or other early-excess scenarios) brightens the "dark phase" soon after the SN explosion and thus extends the observable rising time of EExSNe Ia.

Previous simulations indicated that the early light-curve excess is much stronger in UV and blue optical wavelengths for companion-interaction EExSNe Ia. For instance, even for a "WD – low-mass main-sequence star" progenitor system that corresponds to the most inconspicuous early light-curve excess, early $B-V$ color behavior still shows clear difference to that of non-EExSNe Ia (see Maeda et al., 2018 for details). Therefore, early-phase color information should be a good indicator to identify companion-interaction EExSNe Ia.

Since the strength of the companion-interaction early excess is correlated with both the configuration of the progenitor system (i.e. the distance between the WD and the companion) and the viewing direction from observers, it is difficult to confirm the origin of an early light-curve excess based on a single-band light curve. Systematically investigating the rising time, the post-maximum light-curve profile, and the early-color evolution should help us to distin-

guish inconspicuous EExSNe Ia to some extent. However, additional observational constraints (e.g. the early-phase spectroscopy) are necessary to further confirm whether an early excess originates from the companion-interaction scenario or other early-excess scenarios.

The off-center explosion scenario and possible impact on normal SNe Ia

As we mentioned in §2.4.3, the spectral information of SKYS6 may support the possible connection between unburned carbon footprint and low $V_{Si\ II}$ feature of normal SNe Ia. Statistical studies by Benetti et al. (2005) and Folatelli et al. (2012) suggested that the C II λ6580 feature is only shown in SNe Ia that have relatively low $V_{Si\ II}$ before/around the peak phase. Additionally, Foley et al. (2011) and Milne et al. (2013, 2015) pointed out that normal SNe Ia with relatively blue color commonly show C II absorptions and low $V_{Si\ II}$. All these findings imply that the diversities shown in normal SNe Ia may share the same origin in physics.

We infer that the off-center explosion scenario may account for the diversity issue of normal SNe Ia. Under the off-center explosion scenario, the scatter of Si II λ6355 line velocity can be well interpreted with the viewing angle effect (Maeda et al., 2010). Moreover, if the initial thermonuclear sparks are ignited at an offset from the center of the WD progenitor, such an asymmetric physical process will finally result in an inhomogeneous element distribution (both radioactive and unburned elements), especially at the outer layer of the ejecta. Therefore, dispersions of early-phase light curves, color evolution, and the carbon-feature duration shown in normal SNe Ia can be qualitatively explained by the off-center explosion scenario after taking into account the viewing angle effect.

Although the off-center explosion scenario is promising for interpreting the diversities of normal SNe Ia, early-phase light curves and spectral evolution predicted by 3D simulations are highly required to test if the viewing angle effect can attribute to all diversities quantitatively. Given that the luminosity of an SN Ia is correlated with the offset level of the initial ignition under the off-center explosion scenario (see §4.3.2 for further discussions), it is also necessary to constrain the offset range of normal-brightness SNe Ia when studying the relation between normal SNe Ia diversities and the viewing angle effect. Last but no least, other possibilities (e.g. the multiple progenitor systems) that may give rise to the diversities in normal SNe Ia should be investigated in the future.

In a word, the outputs from our surveys with Kiso/KWFC not only test the feasibility of the early-phase SNe Ia study with specialized wide-field survey observations but also enlighten us possible origins of the long-standing progenitor system, explosion physics, and diversity issues of SNe Ia.

3 Studying Early-phase SNe Ia with Subaru Hyper Suprime-Cam

3.1 Searching for Early-phase SNe Ia with a Deep, Wide Imaging Survey

Given the peerless survey capability of the Subaru/Hyper Suprime-Cam (HSC, Miyazaki et al., 2012) and the importance of early color information for tackling the long-standing progenitor and explosion issues of SNe Ia, we proposed a survey project that is optimized for studying early-phase SNe Ia with Subaru/HSC in 2015, the "**MU**lti-band **S**ubaru **S**urvey for **E**arly-phase **S**Ne Ia" (**MUSSES**).

3.1.1 The Subaru Hyper Suprime-Cam (HSC)

The Hyper Suprime-Cam (HSC, Figure 22) is a gigantic digital camera (height: $\sim$3 meters; weight: $\sim$3 tons) mounted on the 8.2-m Subaru telescope. HSC is composed by three major components: CCD Camera, Wide Field Corrector (WFC) and the Prime Focus Unit (PFU). A cross-sectional view of HSC is illustrated in Figure 23.

The camera consists of arrays of CCD sensors (116 in total), a cryogenic vacuum dewar, CCD readout electronics, filters, a shutter, and a filter exchanger unit. The CCD sensor is a highly sensitive 2K$\times$4K deep depletion Hamamatsu CCD. The camera has a total of 870 megapixels, covering a field-of-view (FoV) of $\sim$1.8 deg^2 (1.5 degrees in diameter). These CCDs are installed inside a vacuum cryogenic dewar and are operated at -100 °C where the dark current can be negligible.

WFC is designed to correct image smear (aberrations) occurred on the primary mirror located 16 m below the camera so that a sharp image over a wide FoV can be achieved. WFC is composed of five lenses and one atmospheric dispersion corrector element. The high quality of glasses and precision polishing technique ensure that HSC has an excellent image quality over the 498 mm diameter focal plane. All lenses (seven in total) are assembled together by the ceramic lens barrel.

The main function of PFU is to align the axis of the WFC and CCD dewar to the optical axis of the telescope at any altitude and to correct the field-rotation caused by tracking, which is crucial

to ensure the excellent image quality achieved by the WFC. To realize the precise motion of the PFU, a precision attitude control hexapod system that consists of six customized actuators is installed on the unit.

HSC saw the first light in 2012 and started to be served as an open-use facility of the Subaru telescope in 2014. Further information on HSC can be found in https://hsc.mtk.nao.ac.jp/ssp/instrument/.

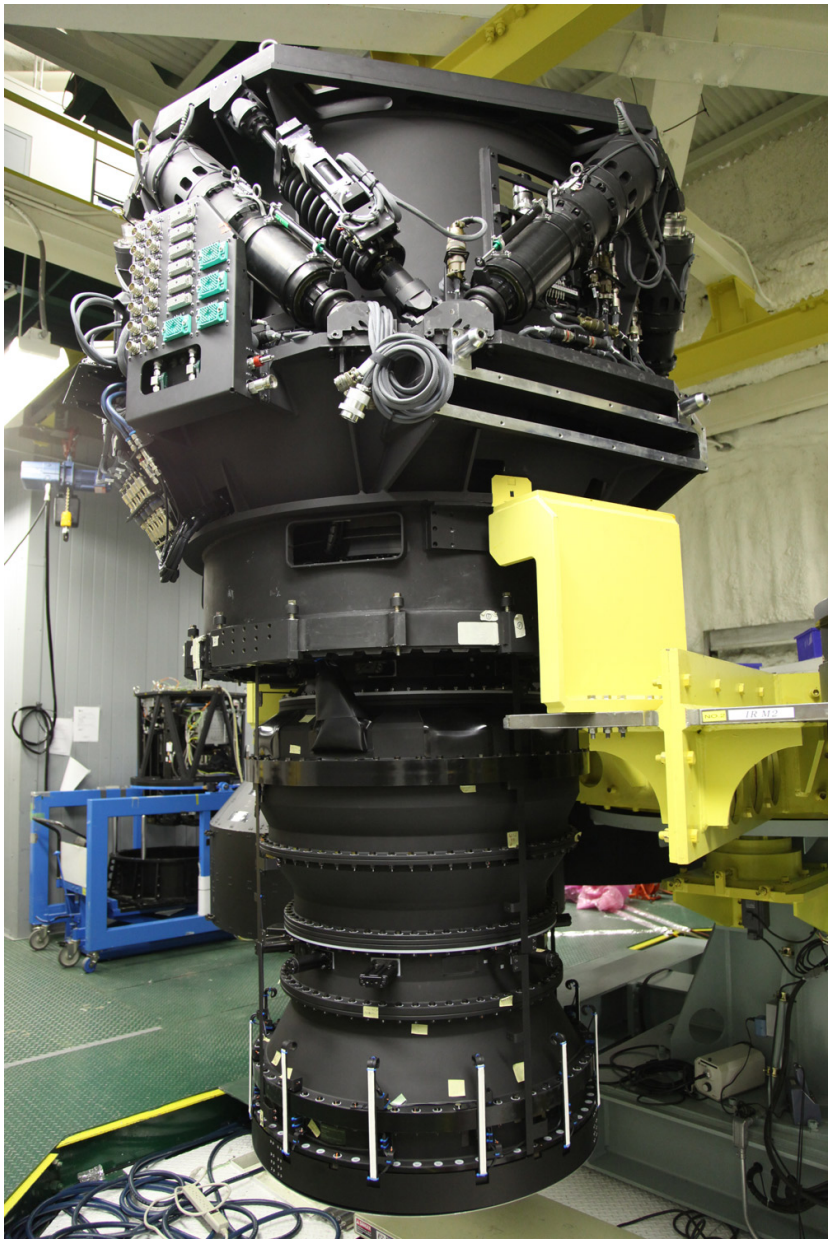

Figure 22: The Hyper Suprime-Cam. Credit: National Astronomical Observatory of Japan.

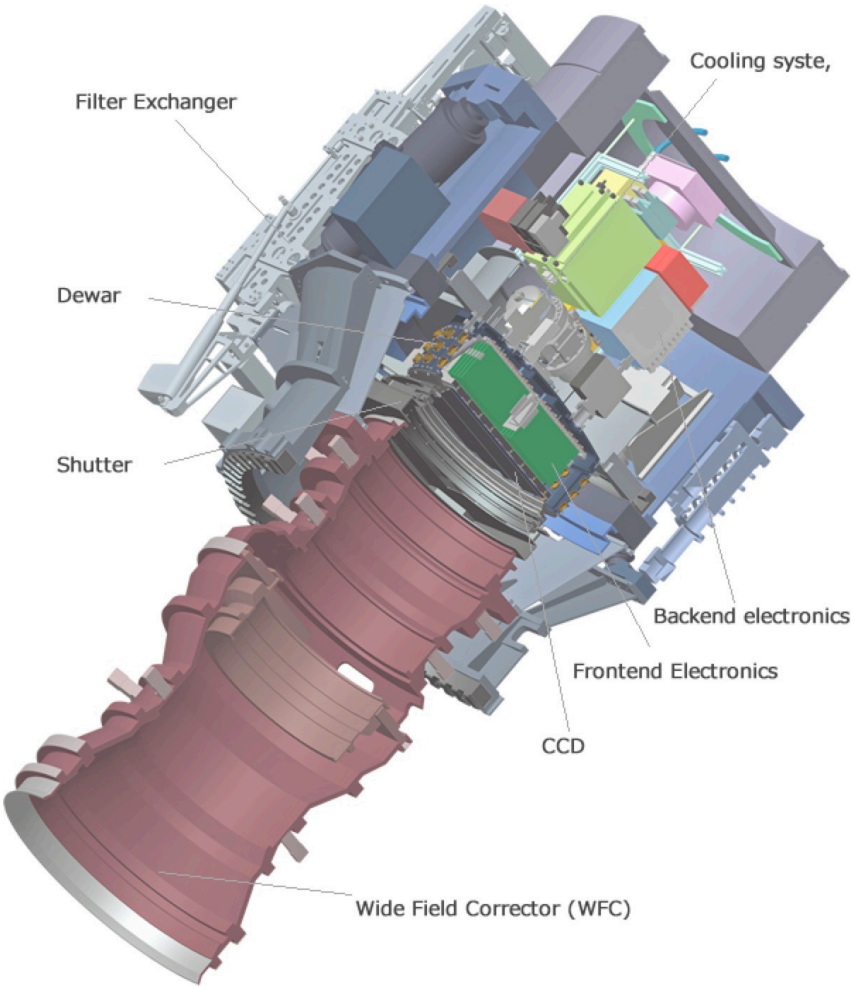

Figure 23: A cross-section view of HSC. Credit: National Astronomical Observatory of Japan.

3.1.2 The MUlti-band Subaru Survey for Early-phase SNe Ia (MUSSES)

I. Scientific objectives

There are four major scientific objectives of the MUSSES project.

(i) Searching for companion-interaction EExSNe Ia. The EExSN Ia was originally proposed as an indicator of the single-degenerate (SD) progenitor system because the interaction between a nondegenerate companion star (a red-giant or a main-sequence star) and the ejecta produced by SN explosion may account for light-curve excess in the first few days of the explosion (Kasen, 2010, Kutsuna and Shigeyama, 2015). Since 2015, a few SNe Ia which show

early light-curve excess have been reported as companion-interaction EExSNe Ia while their origins are still under debate. Given that the intensity of early excess is highly dependent on the type of nondegenerate companion and the viewing angle from the observer, a large fraction of companion-interaction EExSNe Ia may hardly be distinguished with a single-band early-phase light curve. However, simulation results suggest that the early color of companion-interaction EExSNe Ia will become significantly blue. Therefore, multiband early photometric information should be a good indicator to find companion-interaction EExSN Ia candidates.

(ii) Systematically investigating the early color evolution of different SN Ia subclasses. In order to maximize the efficiency of finding SNe, single-band transient surveys have been widely applied in the past, which prevents us from investigating the color evolution of SNe soon after their explosions. However, even with such limited information, a scatter of early color evolution is shown between subluminous, normal, and luminous SNe Ia (Figure 24). For instance, subluminous SNe Ia SN 2002es, SN 2005bl, and even the subluminous EExSN Ia iPTF14atg show much redder $B-V$ color than normal SNe Ia at very early phase. Additionally, the red $B-V$ color of iPTF14atg also contradicts the prediction of the companion-interaction scenario. One possible explanation is that subluminous SNe Ia are intrinsically red due to the deficient ^{56}Ni and slower expansion velocity compared with normal SNe Ia at early phase. Alternatively, a luminous EExSN Ia SN 2012cg may have intrinsically bluer color at early phase (e.g. more ^{56}Ni formed at the outermost region of the ejecta) rather than a companion-ejecta interaction (§4.3.2). Therefore, by investigating the early-color behavior of a number of SNe Ia we are able to build a complete picture of the early color evolution of each SN Ia subclass, and thus figure out the physical origin of the SNe Ia diversity.

(iii) Finding out new clues of the SN Ia explosion physics. Simulations based on different explosion models indicated that the element configurations in the outermost region of the SN ejecta can be very different (Maeda et al., 2011, Dessart et al., 2014a, Piro and Morozova, 2016). Although such differences cannot be well investigated with single-band photometry, early color information has been pointed out as an indicator to discriminate different models (Dessart et al., 2014b). Therefore, by investigating the early color evolution and the possible correlation between early color and light-curve/spectral properties such as the rising time, decline rate, and specific absorption features, we expect to find new clues for or against specific explosion models of SNe Ia.

(iv) Understanding the diversity issue and improving the cosmological use of SNe Ia further. Previous studies have suggested the possible connection between diversities shown in normal SNe Ia (also see §2.4.4). Given that the early-phase information on SNe Ia provides a unique perspective to understand the physical origin of such diversities, systematically inves-

tigating photometric/spectroscopic behavior of dozens of normal SNe Ia from the early phase will bring us new ideas to explain the observed diversities and further test whether all diversities have the the same origin. Finally, further understandings of the SN Ia diversity issue will enable us to improve the accuracy of the cosmological use of SNe Ia.

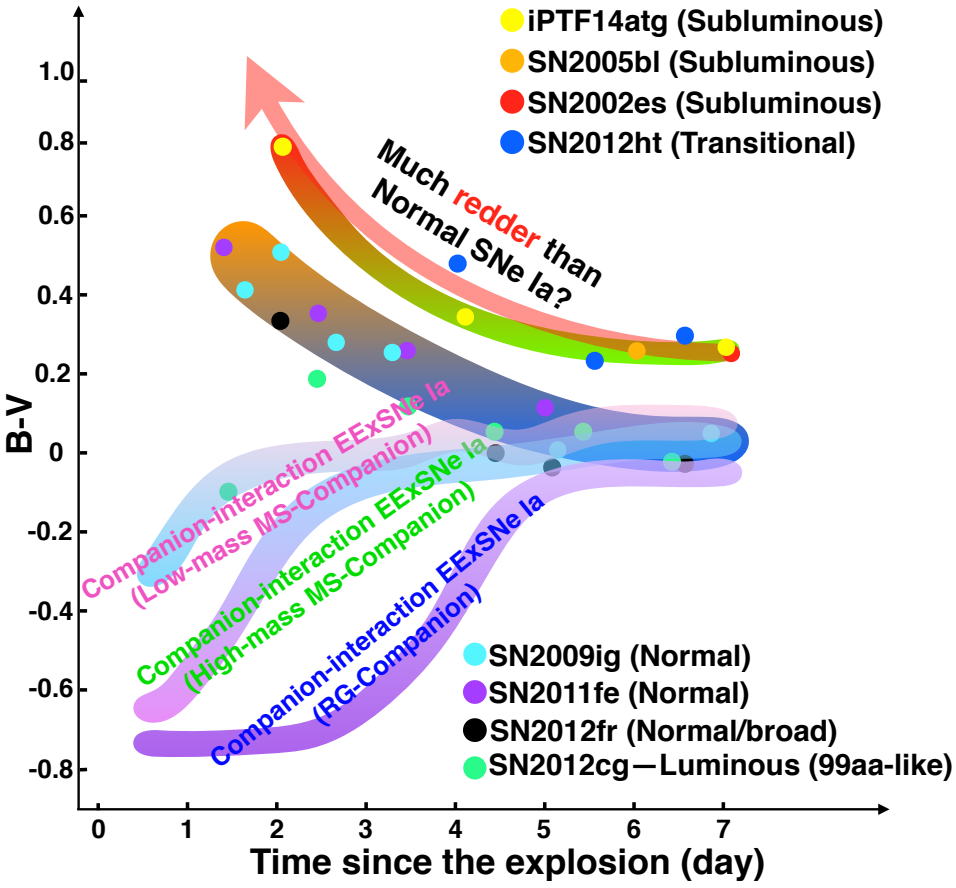

Figure 24: A schematic diagram showing the color evolution of various SN Ia subclasses within about one week of their explosions. Subluminous SNe Ia show redder $B-V$ color in the early phase compared with that of normal and luminous SNe Ia. Previous simulations indicated that the interaction between the SN ejecta and a nondegenerate companion star will lead to a very blue light-curve excess in the early phase and thus the color evolution will be significantly different from that of non-EExSNe Ia.

II. Survey design

Each MUSSES observing run includes two parts, the Subaru/HSC multiband survey and follow-up observations with more than 10 ground-based telescopes all over the world. The Subaru/HSC survey aims to discover SNe Ia within a few days of their explosions and study their early multiband (i.e. g and r band) photometric behavior. The Subaru/HSC observation is carried out in three consecutive nights/half-nights after considering a typical early-excess duration predicted by simulations and the limited available time for Subaru/HSC. Since the brightness of early-phase SNe Ia increases quickly during the HSC observation ($\lesssim -0.5$ mag day^{-1}), we can take images of the same pointings every night/half-night with different observing depths to maximize the scientific output of the 2–3-nights Subaru/HSC observation. Specifically, in the first night, the deepest HSC g-band images for over 100 deg^2 sky will be taken to search as much early-phase SNe Ia as possible. In the second and third nights (can be half-nights), multiband photometry with a shallower observing depth will be conducted for all sky region observed in the first night. By using a specific pipeline developed for quickly identifying HSC-discovered transients, follow-up observations can be triggered within one day after the HSC survey. Given that the brightness of early-phase SNe Ia will keep increasing in about two weeks and then slowly decline, intensive multiband imaging follow-ups can be achieved by using 1–4-m class telescopes (e.g. 3.5-m ARC, 2.5-m NOT, 2.5-m INT, 2-m LT, 1-m Kiso telescope, etc.) in 2–3 months. On the other hand, spectroscopies will be carried out with 6–10-m class telescopes (e.g., 10.2-m GTC, 9.2-m SALT, 8.2-m VLT, 8.1-m Gemini North/South telescope, etc.) at specific epochs. The strategy of MUSSES achieves a very large photometric dynamic range, enabling us to observe early-phase SNe Ia even to redshifts of about 0.3. The observing mode of the MUSSES is schematically shown in Figure 25.

III. A brief review of the first MUSSES observing run

The first MUSSES observing run was carried out from April to June, 2016. Our 2.5-nights ($1+1+0.5$ nights on April 4, 5, and 6, respectively) Subaru/HSC survey composed by continuous 1- and 0.5-nights multiband observations (g and r; open-use ID: S16A-106N, PI: Jian Jiang) following a 1-night HSC Strategic Survey Program (HSC SSP, Miyazaki et al., 2012, 2018) observation in g band was successfully conducted and a dozen of early-phase SN candidates were discovered in $\sim$35 deg^2 sky area with a g-band limiting magnitude of $\sim$26.0. Follow-up observations were triggered one day after the HSC survey while we suffered severe weather issues for most of follow-up observations in the first week after the HSC observation. On the other hand, due to the limited follow-up telescope resources at that time, we had to give up follow-up observations for some fainter or slower-brightening candidates. Fortunately, intensive follow-up observations have been carried out for the most interesting early-phase SN Ia, MUSSES1604D,

from the middle of April to early June. The study of MUSSES1604D is shown in §3.2.

In summary, total 12 early-phase SN candidates were discovered in our first MUSSES observing run and four of them were spectroscopically confirmed. In particular, we discovered a very interesting EExSN Ia, MUSSES1604D, within about one day of its explosion (§3.2). Additionally, we found a few transients with significant brightness variance. The physical explanation of these objects is still uncertain and a further discussion is beyond the scope of this thesis.

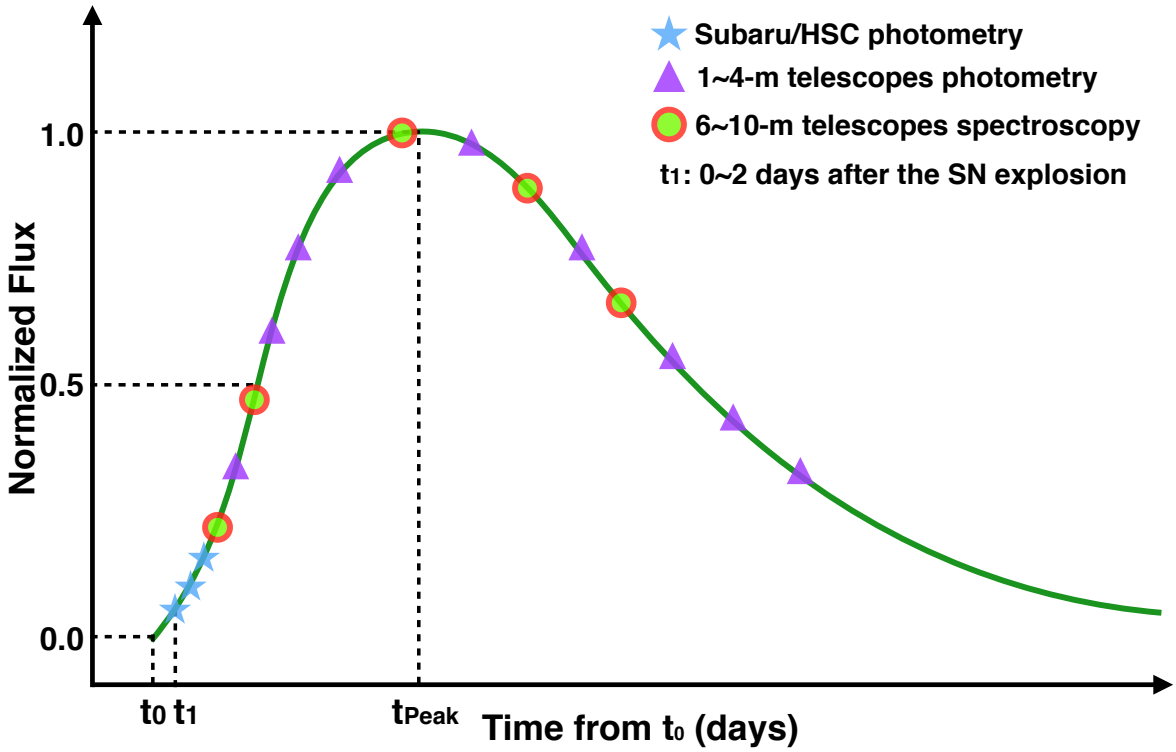

Figure 25: The observing mode of MUSSES. The Subaru/HSC survey is marked by star symbols. Other symbols represent telescopes in different apertures used for the photometric/spectroscopic follow-up observations at specific epochs. The follow-up observations can be triggered within one day after the Subaru/HSC observation.

3.2 MUSSES1604D—A Smoking Gun of the He-shell Detonation Scenario and the Multiple Origins of EExSNe Ia

3.2.1 The discovery and observational characteristics of MUSSES1604D

A faint optical transient was discovered on UT April 4.345, 2016 through the high-cadence deep-imaging multiband survey that is optimized for finding SNe Ia within a few days after explosion with the Subaru/HSC, MUSSES. Close attention has been paid to one transient because its brightness increased by ∼6.3 times within one day of the first observation. We designated this fast-rising transient as MUSSES1604D (the official IAU designation is SN 2016jhr), the fourth early-phase SN candidate found in the April 2016 observing run of MUSSES.

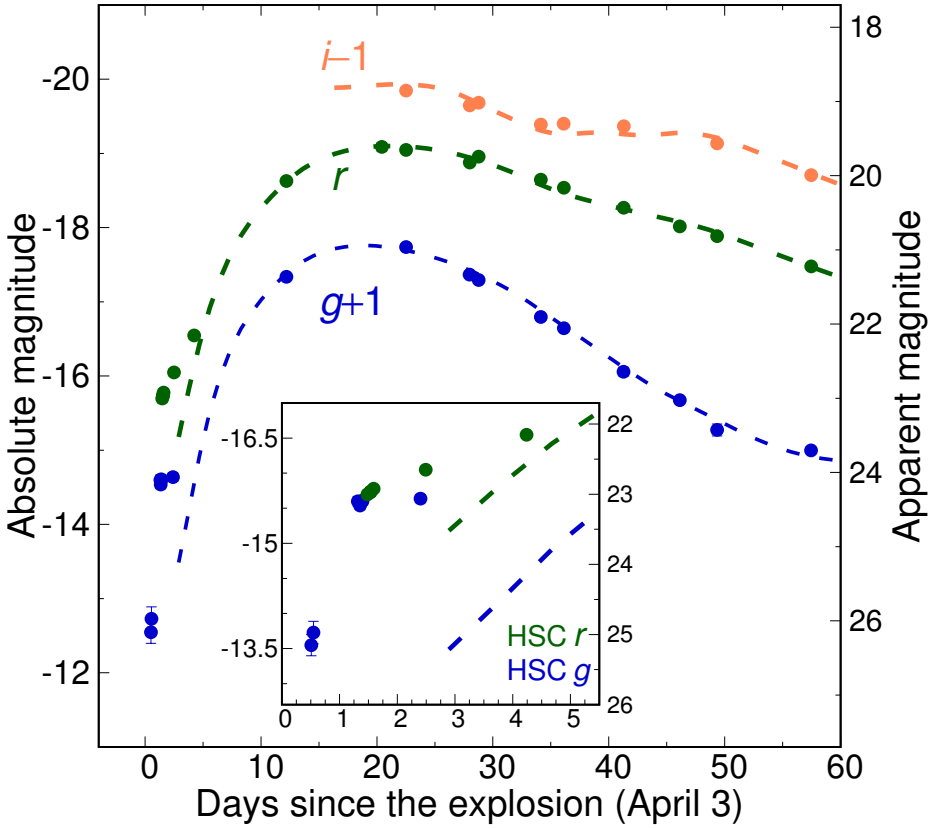

Figure 26: The multiband light curve of MUSSES1604D. Photometry in *g*, *r*, and *i* bands (observer-frame) are in the AB system. Error bars denote 1-σ uncertainties. Dashed lines are best-fitting light curves derived from the non-early-phase photometry (t$\gtrsim$12 days) with SALT2(Guy et al., 2007). The explosion epoch is estimated by adopting a classical t^2 fireball model for the early-excess phase (see §3.3.4). The inset zooms in on the early-phase multi-band light curve by Subaru/HSC, which shows that the brightening in g band "paused" after the second-night observation.

Figure 26 presents the observed *g*-, *r*-, *i*-band light curves of MUSSES1604D. The earliest photometry by Subaru/HSC indicates an apparent *g*-band magnitude of 25.14 ±0.15 on April 4.345 (MJD 57482.345). One day later, MUSSES1604D rapidly brightened to ∼23.1 and 23.0 mag in the *g* and *r* bands, respectively. More surprisingly, the *g*-band observation on April 6 indicates that the transient "paused" brightening from April 5 and shows plateau-like evolution lasting for ∼1 day. At the same time, the transient also slowed down in its rate of brightening in the *r* band.

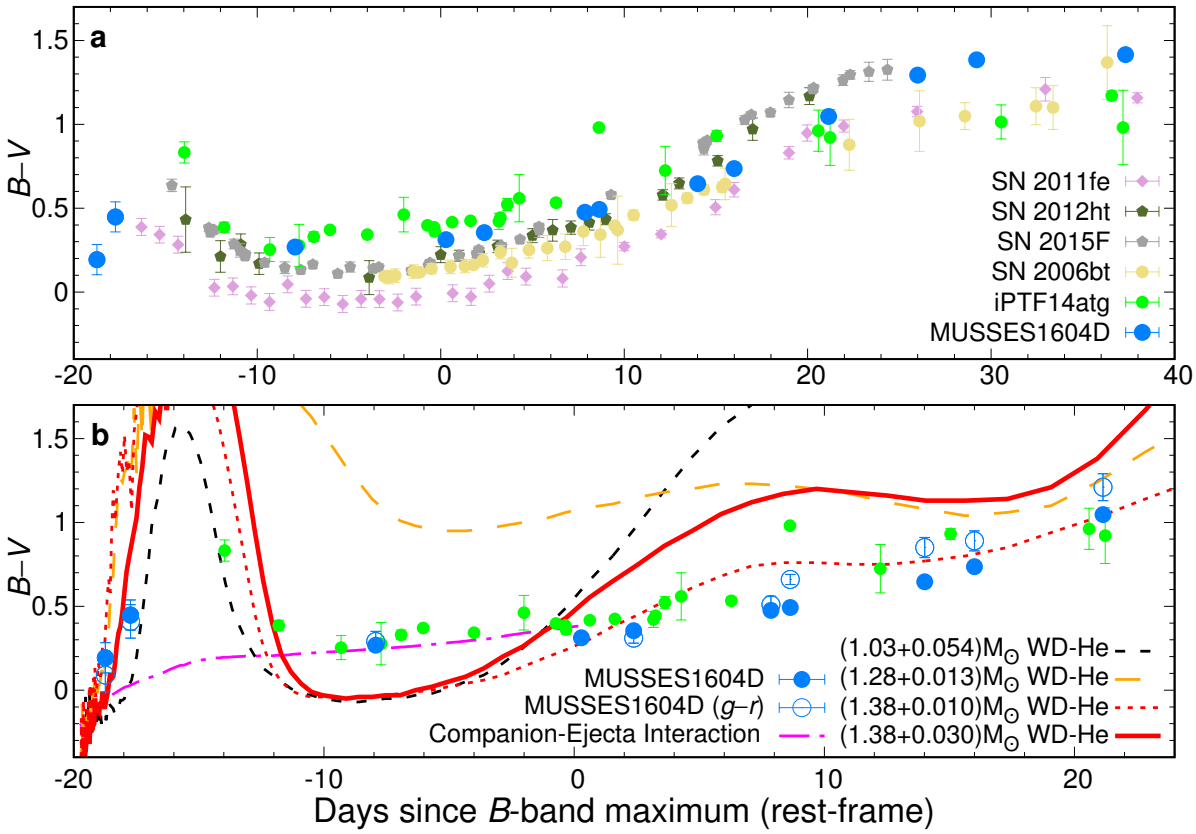

Figure 27: A comparative analysis of MUSSES1604D color evolution. The upper panel presents $B-V$ color evolution of MUSSES1604D, iPTF14atg (early-excess), SN 2006bt (MUSSES1604D-like), SN 2012ht (transitional), SN 2015F and SN 2011fe (normal-brightness). The lower panel shows the color evolution predicted by companion-interaction, He-detonation model for the sub-Chandrasekhar-mass WD and the newly proposed He-detonation models for the near-Chandrasekhar-mass WD under different He-shell mass assumptions. The *B*-band maximum occurred about 20 days after the explosion. Since the bandpass difference between the rest-frame *B*/*V* band and the observer-frame *g*/*r* band is inconspicuous at z∼0.1, the observed $g-r$ color evolution is provided for reference. Error bars represent 1-σ uncertainties.

Follow-up observations indicated that MUSSES1604D is an SN Ia with a r-band peak absolute magnitude of ~-19.1 on April 26. Adopting a host galaxy redshift (z) of 0.11737, the rest-frame light curves in the B- and V-band absolute magnitudes from $\sim$4 days after the first observation are derived by applying a K-correction based on the best-fitting model with SALT2 (Guy et al., 2007). For the early light-curve excess, we applied the K-correction through simplified spectral-energy distributions, estimated from the early color information of MUSSES1604D (see §3.3.2). The rest-frame B-band light curve shows a peak absolute magnitude of about -18.8 and $\Delta m_{15}(B)\approx0.95$ mag, indicating a normal-brightness SN Ia (Phillips, 1993).

Color evolution within a few days after the SN explosion is crucial for identifying the early excess (Kasen, 2010, Piro and Morozova, 2016). In contrast to another peculiar EExSN Ia iPTF14atg with $B-V$ color evolution obtained only from about five days after the discovery (Cao et al., 2015), the specific survey strategy of the MUSSES project enables us to obtain the color information of MUSSES1604D from about one day after the first observation (Figure 27), revealing a slightly red $B-V$ color of about 0.2 mag at first, reddening further to about 0.5 mag in one day.

3.2.2 The physical explanation of the peculiarities of MUSSES1604D

The interaction between SN ejecta and a nondegenerate companion star (the companion-interaction scenario; Kasen, 2010, Pan et al., 2012, Kutsuna and Shigeyama, 2015) or dense circumstellar material (the "CSM-ejecta interaction" scenario, hereafter CSM-interaction scenario; Levanon et al., 2015, Piro and Morozova, 2016) are popular scenarios to explain the early light-curve excess. In order to produce a prominent optical flash comparable to that of MUSSES1604D, either a companion with a very extended envelope or a large-scale CSM distribution is required. In the companion-interaction scenario, a prominent flash generated from the inner, hot region of ejecta would be observed through the hole that is carved out by a red-giant companion (Kasen, 2010, Kutsuna and Shigeyama, 2015). In the CSM-interaction scenario, a more extended CSM distribution could generate a brighter early excess but with longer diffusion time. Our best-fitting companion-interaction model (Figures 27 and 28) and previous simulations of both scenarios all indicate that the particular blue color evolution is inevitable when producing the early excess as bright as that of MUSSES1604D (§3.3.3, Figure 33), which is incompatible with the red and rapid early color evolution observed for MUSSES1604D.

Peculiar spectral features have been discovered around the peak epoch (Figure 29). At a first glance, the Si II λ6355 line, W-shaped S II feature, and Ca II H & K absorptions are reminiscent of a normal SN Ia, while the relatively weak Si II λ5972 line suggests a higher photospheric

temperature than that of an SN Ia of similar luminosity. On the other hand, prominent absorption features such as the Ti II trough around 4150 *Å*, usually attributed to low temperature, have been found at the same time, in contrast to the brightness indicated by the light curve. By inspecting near-maximum spectra of more than 800 non-subluminous SNe Ia, we found only three MUSSES1604D-like objects—SN 2006bt, SN 2007cq, and SN 2012df (§3.3, Figures 31 and 32), indicating the rarity of such hybrid supernovae.

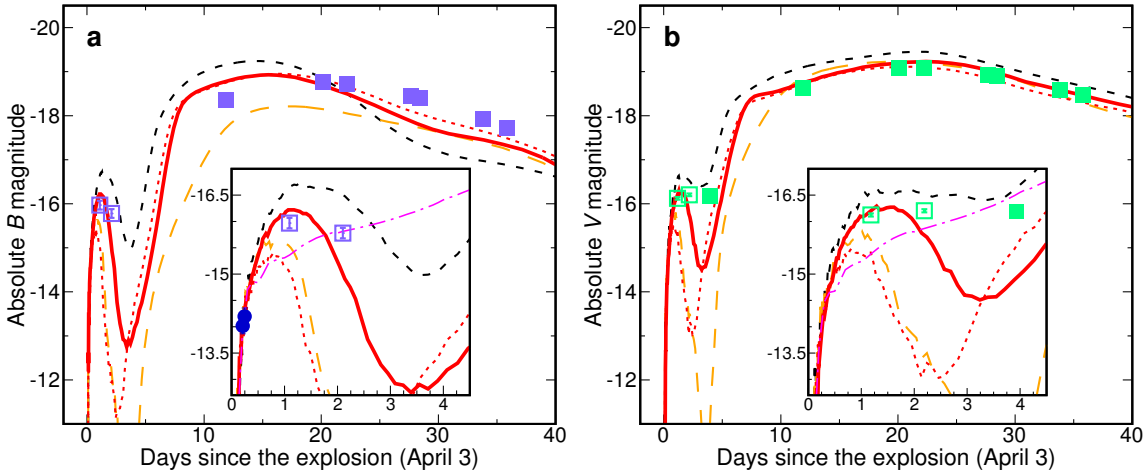

Figure 28: Rest-frame *B*- and *V*-band light curves of MUSSES1604D and simulations. K-corrections in the early-excess (open squares) and the post-early-excess phase (filled squares) are carried out with different methods. Each panel includes He-detonation models for sub-Chandrasekhar-mass WD (1.03 $M_\odot$ WD+0.054 $M_\odot$ He-shell; black dashed line) and massive WD (1.28 $M_\odot$ WD+0.013 $M_\odot$ He-shell, orange long-dashed line; 1.38 $M_\odot$ WD+0.01 $M_\odot$ He-shell, red dotted line; 1.38 $M_\odot$ WD+0.03 $M_\odot$ He-shell, red solid line) conditions. The inset zooms in on the early-excess phase and also includes our best-fitting companion-interaction model assuming a 1.05 $M_\odot$ red-giant companion (magenta dashed-dotted line). The first-night g-band data (blue circles) are included in panel a. The explosion epoch shown here is shifted (+0.3 days) from that estimated by the classical t^2 model (Figure 26) within the uncertainty from the simulations. Error bars denote 1-σ uncertainties.

The peculiar spectral features and the early excess followed by a normal-brightness light curve observed for MUSSES1604D are incompatible with predictions of classical explosion mechanisms (Nomoto et al., 1984, Khokhlov, 1991) through the hydrogen-accreting single degenerate channel, but suggested by a specific scenario in which the SN explosion is triggered by the He-shell detonation, the so-called double-detonation (DDet) scenario (Nomoto, 1982a,b, Woosley and Weaver, 1994, Fink et al., 2007, 2010, Shen and Bildsten, 2014). In principle, a He-shell detonation not only generates a shock wave propagating toward the center of the white dwarf (WD) and ignites carbon burning near the center, but also allocates ^{56}Ni and other radioactive

isotopes such as ^{52}Fe and ^{48}Cr to the outermost layers where the optical depth is relatively low (Fink et al., 2010, Kromer et al., 2010). Therefore energy deposited by decaying radioactive isotopes diffuses out and consequently results in a prominent light-curve excess in the first few days after the explosion (see §3.3.3). Observationally, the plateau-like light-curve enhancement can be detected with the day-cadence observations. At the same time, a significant amount of not only iron group elements but also intermediate-mass elements such as Ti and Ca will be produced in the outermost layers (Fink et al., 2010, Woosley and Kasen, 2011, Kromer et al., 2010). Vast numbers of absorption lines of these elements are very effective in blocking the flux in the blue part of the optical spectrum, thus leading to a relatively red $B-V$ color evolution in general. Indeed, although a substantial amount of He is left after the detonation, the expected spectrum would not show a trace of He in the optical wavelength (Boyle et al., 2017). By assuming a progenitor star with a WD mass of 1.03 $M_\odot$ and a He-shell mass as low as $\sim$0.054 $M_\odot$ (as required to trigger the He detonation on the surface of a 1.03 $M_\odot$ WD; Fink et al., 2010, Kromer et al., 2010), the prominent early excess, peculiar early color evolution and Ti II trough feature are reproduced simultaneously (Figures 27–29).

A potential issue in our simulation is the assumption of a sub-Chandrasekhar-mass WD with a thin He-shell. The amount of synthesized ^{56}Ni that determines the peak luminosity of an SN Ia is sensitive to the mass of the exploding WD. The DDet model requires a sub-Chandrasekhar-mass WD ($\sim$1 $M_\odot$) for the peak luminosity of MUSSES1604D. However, DDet happening on such a WD would lead to a fast-evolving B-band light curve, which is inconsistent with a much slower-evolving light curve observed for MUSSES1604D. In addition, the early excess that would result from the corresponding He mass of 0.054 $M_\odot$ would be brighter than that of MUSSES1604D.

We suggest two alternative scenarios that also involve He detonation to solve this issue. In the first scenario, a violent merger with another He WD (Pakmor et al., 2013) could easily trigger a detonation in a thin He shell, and could produce the light curve of MUSSES1604D, but it requires the fine-tuning for the configuration of the binary system. Whether core detonation can be triggered by the thin-He-shell detonation through the WD-WD merger is also an open question (Shen and Bildsten, 2014, Tanikawa et al., 2015). The second scenario involves a WD of near-Chandrasekhar mass, which would enable the detonation of less He on its surface, and would provide a better and more straightforward account of the light curve and spectral features of MUSSES1604D (Figures 27–29). Further investigation suggests that the best-fitting WD mass is in the range of 1.28–1.38 $M_\odot$ but with a low-yield ^{56}Ni compared with the prediction by DDet (see §3.3.3). This suggests that there could be a mechanism to reduce the mass of ^{56}Ni in the explosion triggered by the He detonation. For example, the shock wave generated by He

detonation might trigger deflagration rather than detonation near the center of the WD (Nomoto et al., 1976), because the high degeneracy pressure of a near-Chandrasekhar-mass WD would inhibit the formation of a shock wave as strong as that seen in a sub-Chandrasekhar-mass WD. Although the observed peculiarities of MUSSES1604D could be naturally explained through this scenario, it is not yet clear how a thin He shell could form on such a massive WD during binary evolution.

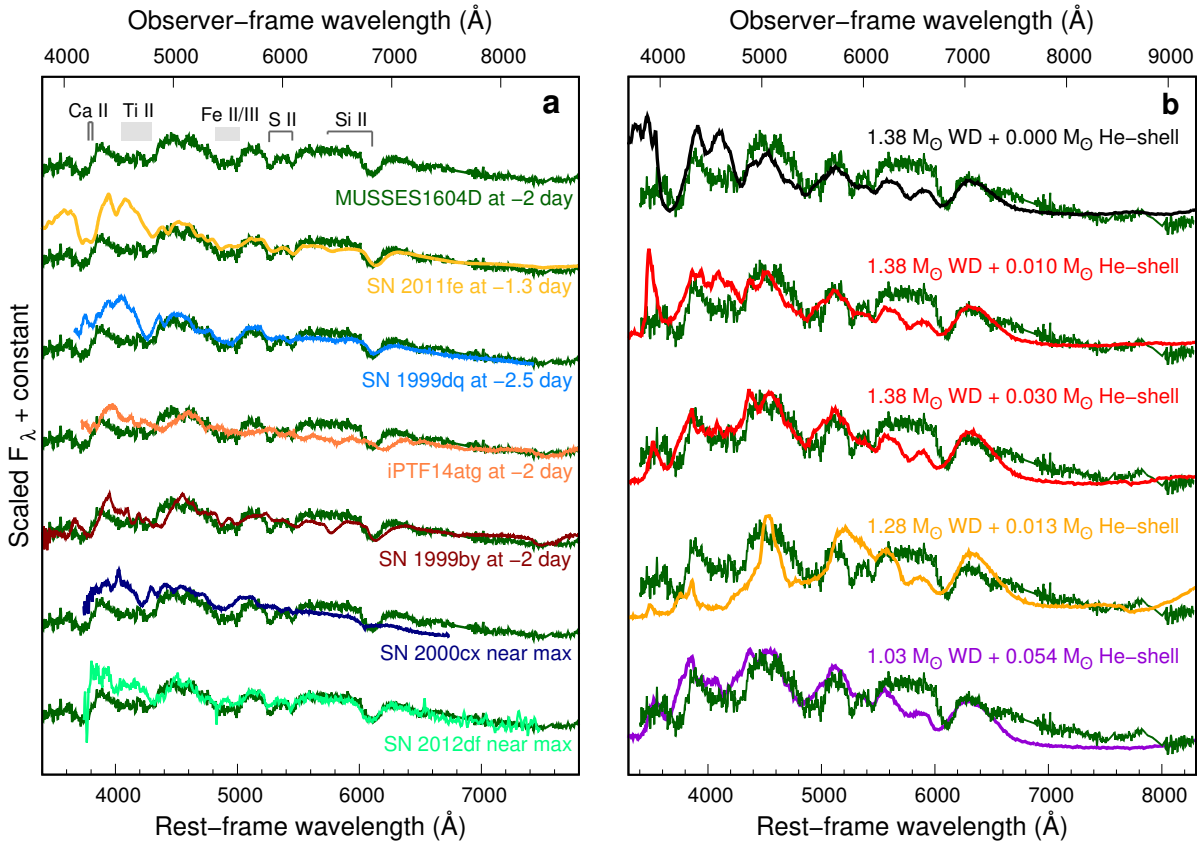

Figure 29: An around-maximum spectral comparison of MUSSES1604D, other observed SNe Ia of different subclasses, and models. In panel a, the spectrum of MUSSES1604D taken two days before the *B*-band maximum by Southern African Large Telescope (SALT) is compared with that of SN 2011fe (normal), SN 1999dq and SN 2000cx (shallow-silicon), SN 1999by (sub-luminous), iPTF14atg (early-excess), and SN 2012df (MUSSES1604D-like) at a similar epoch. Major absorption features are labeled on the spectrum of MUSSES1604D. In panel b, simulated spectra of the classical W7 deflagration model (top), the newly proposed He-detonation models with different assumed He-shell masses (middle three), and the classical double-detonation model for a sub-Chandrasekhar-mass WD (bottom) are compared with the MUSSES1604D spectrum (dark green) at the same epoch.

The discovery of MUSSES1604D suggests that the He-detonation scenario, like other popular scenarios, provides a promising explanation for EExSNe Ia (Kasen, 2010, Levanon et al., 2015, Piro and Morozova, 2016). The prominent optical excess and peculiar color evolution in the very early phase together with absorptions due to Ti II ions in around-maximum spectra can be used as indicators of this scenario. The precise He-detonation mechanism in this case is unlikely to be the classical sub-Chandrasekhar DDet model (Bildsten et al., 2007, Fink et al., 2010), because the slow-evolving *B*-band light curve of MUSSES1604D is incompatible with this scenario. Recent work shows that the sub-Chandrasekhar DDet scenario could explain a part of normal SNe Ia if only a negligible amount of He exists at the time of the He-shell detonation (Shen et al., 2018). Given that MUSSES1604D is best explained by a He shell that is thin but still more massive than that required in these models, we suggest that the He-detonation scenario might generate the observational diversity of SNe Ia, controlled by the masses of both the WD and the He shell. The discovery of MUSSES1604D provides the first observational calibration of the range and combination of these quantities realized in nature.

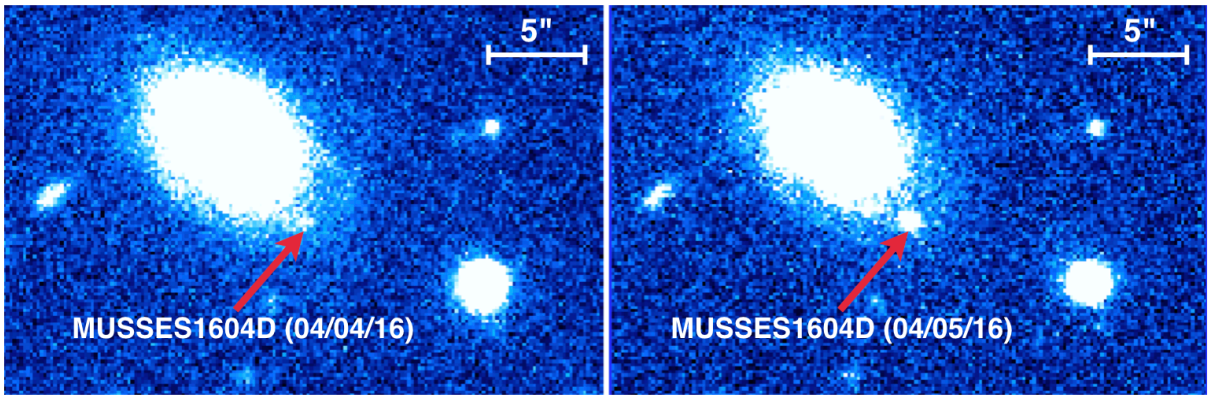

Figure 30: Early Subaru/HSC *g*-band images for MUSSES1604D. The left panel shows the earliest Subaru/HSC image of MUSSES1604D (α(J2000)=12h18m19s.85, δ(J2000)=+00°15'17.38") taken on UT April 4.345, 2016, when the *g*-band magnitude of MUSSES1604D was 25.14±0.15. The supernova then brightened rapidly to ∼23.1 mag in one day (right panel).

3.3 Further Information and Discussions on MUSSES1604D

3.3.1 Supplemental information of MUSSES1604D

To make the best use of the Subaru time, the MUSSES observing run in April 2016 adopted a specific survey mode which combines both HSC Subaru Strategic Program (HSC SSP*, 1-night g-band observation, from UT April 4.17 to UT April 4.67) and open-use observation (1.5-nights g- and r-band observation, from UT April 5.17 to 5.67 and April 6.43 to 6.67, respectively).

The supernova MUSSES1604D was discovered at α(J2000)=12h18m19s.85 and δ(J2000)= +00°15'17.38" on UT April 4.345, 2016 with a g-band magnitude of 25.14 mag upon discovery (Figure 30), and was the fourth early-phase SN candidate found in the April MUSSES observing run. MUSSES1604D was located about 5.8 arcsec (to the southwest) from the host-galaxy center. The redshift of the host galaxy is 0.11737±0.00001 (SDSS Data Release 12; Bolton et al., 2012). The distance modulus of MUSSES1604D is 38.69 mag.

The host galaxy of MUSSES1604D The red color with a visible Hα emission feature suggests that the host galaxy of MUSSES1604D is a star-forming early-type galaxy (Shimasaku et al., 2001). Further analysis with the SDSS photometry and spectroscopy shows that the stellar mass is $3-7\times10^{10}\ M_{\odot}$, which is also consistent with an early-type galaxy, e.g. an S0 galaxy.

Follow-up observations Our scheduled early follow-up observations at La Palma island and Apache Point Observatory were lost owing to poor weather conditions. With HSC SSP r-band observation conducted at two days after our Subaru/HSC observations, we successfully took another r-band image of MUSSES1604D, which provides a crucial constraint on the timescale of the early excess. Multiband follow-up observations with the 8.0-m Gemini-North telescope, the 3.5-m ARC telescope, the 2.5-m Nordic Optical Telescope (NOT), the 2.5-m Isaac Newton Telescope (INT), the 2-m Liverpool Telescope (LT), and the 1.05-m Kiso Schmidt telescope have been conducted from about -8 days to $+40$ days after the B-band maximum. For the spectroscopic observations, we triggered the 9.2-m SALT and the 8.0-m Gemini-North telescope at specific epochs to get spectral evolution from about -2 days to one month after the B-band maximum (Figure 31).

*See https://hsc.mtk.nao.ac.jp/ssp/wp-content/uploads/2016/05/hsc_ssp_rv_jan13.pdf for more details.

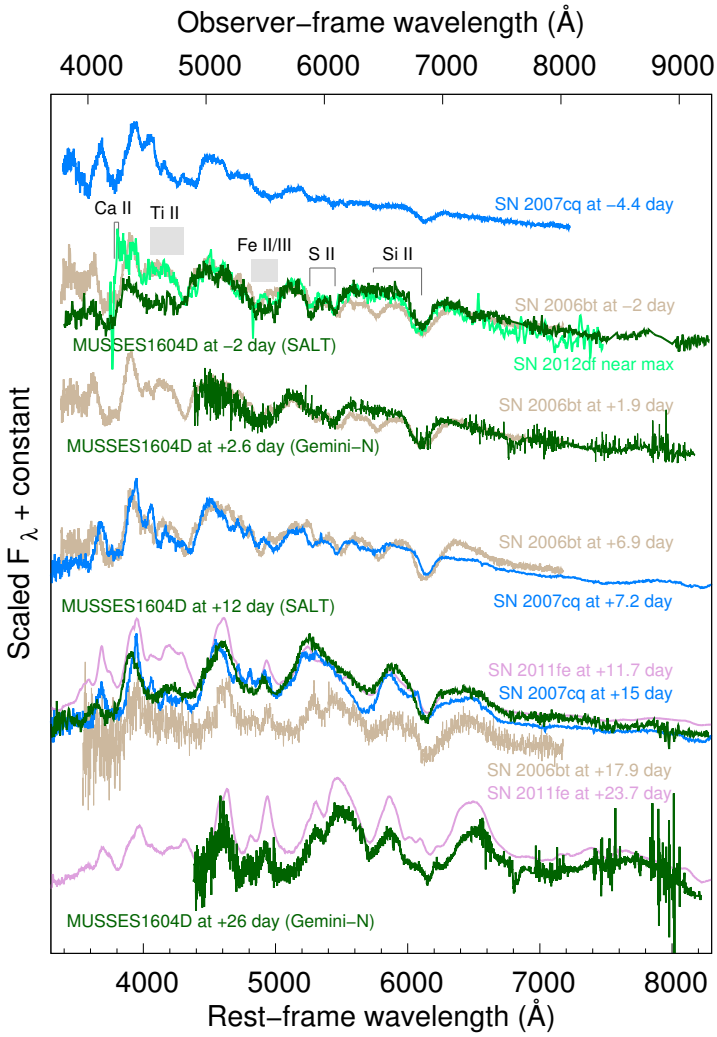

Figure 31: Spectral evolution of MUSSES1604D and analogues. Spectra for MUSSES1604D (dark green) are compared with those of the analogous SNe Ia SN 2006bt, SN 2007cq, and SN 2012df at similar epochs. Late-phase spectra of SN 2011fe are included for reference. SALT/RSS follow-up observations were carried out −2 and 12 days after the *B*-band maximum and the other two spectra were taken by Gemini-N/GMOS 3 and 26 days after the *B*-band peak.

Data reduction and photometric calibration Given that MUSSES1604D resides at the edge of the host galaxy, contamination from the host is negligible except for the photometry of the earliest Subaru/HSC observation. The morphology of the host galaxy indicates a symmetric S0 galaxy. We thus built the host template with GALFIT (Peng et al., 2010)* and performed the standard point spread function (PSF) photometry with the IRAF DAOPHOT package (Stetson, 1987) on host-subtracted images. The photometry has been tested by subtracting the SN from

*The GALFIT software can be downloaded at https://users.obs.carnegiescience.edu/peng/work/galfit/galfit.html.

the original image, using an artificial PSF star with the derived photometric magnitude. The average flux of the residual region is comparable with the surrounding region and well below the photometric error of the discovery image by Subaru/HSC (the 1-σ photometric error is 0.15 mag). PSF photometry is performed on host-subtracted images of all follow-up observations. The photometry is then calibrated to the standard SDSS photometric system by adopting a color-term correction based on field stars (Doi et al., 2010). For spectroscopic data reduction, all data were reduced with standard routines in IRAF.

3.3.2 Light-curve fitting and K-correction

Given the limited understanding of spectral features during the early-excess phase of MUSSES1604D, we adopted different methods to derive the rest-frame light curves at early-excess and post-early-excess phase, respectively. For the post-early-excess light curves, we firstly fit the observed light curves by applying the SALT2 model of SNe Ia spectrophotometric evolution which is built using a large data set including light curves and spectra of both nearby and distant SNe Ia (Guy et al., 2007). After light-curve fitting, K-correction is performed to get the rest-frame B- and V-band light curves according to the best-fitting spectral sequence model of MUSSES1604D with SNCosmo*. For the light curve in the early-excess phase (within 5 days after the explosion), we applied the color-based K-correction with a pseudo power-law spectral energy distribution (SED) function $f(\nu)$=$k\nu^{\alpha}$, where ν is the frequency of the light, k and α are parameters derived by the early color information of MUSSES1604D. Given the non-detection of Na I D absorption lines in any of our spectra ($S/N\sim$18 per resolution element near the wavelength of Na I D lines for the around-maximum spectrum) and the supernova was located far away from the center of an S0-type host, we only take into account the Galactic extinction of E$(B-V)_{MW}$=0.0263 mag (Schlegel et al., 1998). The rest-frame B- and V-band light curves are shown in Figure 32.

The K-corrected rest-frame light curve of MUSSES1604D indicates a B-band peak absolute magnitude of -18.8 but with $\Delta m_{15}(B)\approx$0.95 mag, corresponding to a slow-evolving normal-brightness SN Ia in terms of the Phillips relation (Phillips, 1993). The main-body V-band light curve of MUSSES1604D shows very good consistency with those of typical normal-brightness SNe Ia, e.g. SN 2011fe. All photometric data in observer and rest frames are listed in Table 4.

*SNCosmo is available at https://sncosmo.readthedocs.io/en/v1.6.x/.

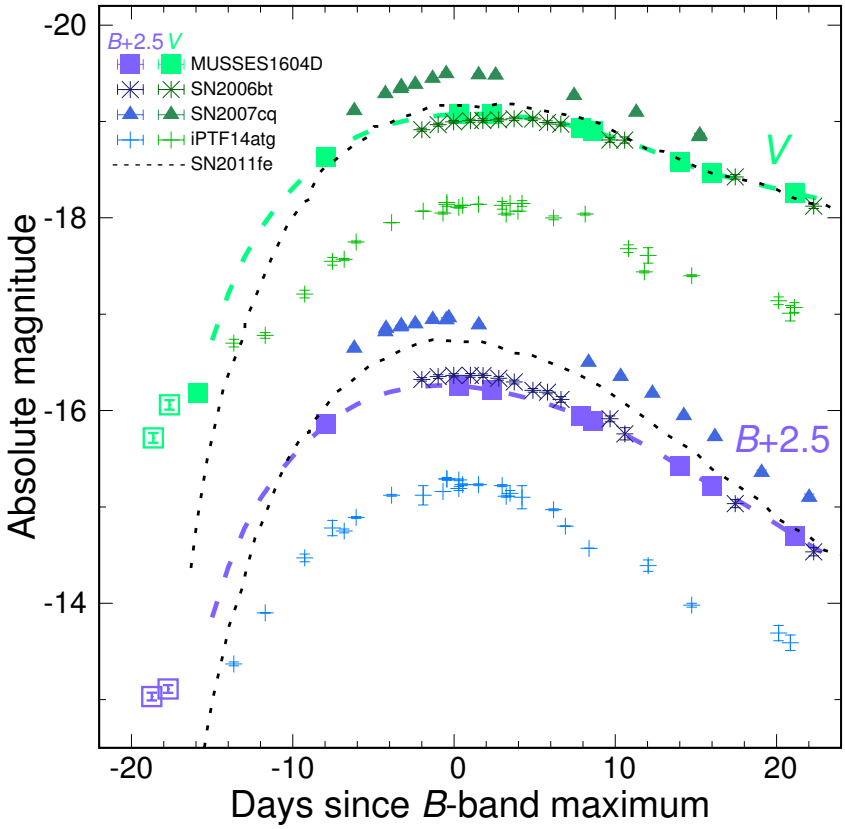

Figure 32: Rest-frame B- and V-band light curves for MUSSES1604D and other SNe Ia. K-corrections in early-excess (open squares) and post-early-excess phase (filled squares with dashed lines) of MUSSES1604D were carried out with different methods (see §3.3.2). An excellent light-curve match is shown between MUSSES1604D, SN 2006bt, and SN 2007cq. Another peculiar early-excess SN Ia iPTF14atg also shows similar light curves though its brightness is $\sim$1 magnitude fainter than that of MUSSES1604D. B- and V-band light curves of a normal SN Ia, SN 2011fe (black dotted lines) are provided for reference. Magnitudes shown here are in the Vega system and the error bars denote 1-σ uncertainties.

3.3.3 Explanations for the peculiarities of MUSSES1604D

The "peculiarities" of MUSSES1604D mainly include: **1)** a prominent optical flash with peculiar color evolution at very early time; **2)** the red $B-V$ color evolution in general; **3)** a normal-brightness SN Ia with prominent Ti II absorptions in the around-maximum spectrum; **4)** a slow-evolving light curve in blue optical wavelengths (e.g. B band). Below we compare different scenarios that may account for such peculiarities and find the best solution.

Companion-ejecta interaction

We performed two-dimensional axisymmetric radiation hydrodynamic simulations of the explosions of a WD with a Chandrasekhar mass in binary systems to obtain light curves and spectra resulting from collisions between the ejecta and the companion star (Kutsuna and Shigeyama's (K-S) companion-interaction models; Maeda et al., 2014, Kutsuna and Shigeyama, 2015). The ejecta are described by the W7 model (Nomoto et al., 1984). The best-fitting light curves presented in Figure 28 are the expected outcome of an explosion in an SD binary system with a separation of 2.5×10^{13} cm observed from the companion side. The companion star is a red giant with a mass of 1.05 $M_{\odot}$ (the core mass is 0.45 $M_{\odot}$) and a radius of 8.9×10^{12} cm, filling the Roche lobe. The initial mass of the companion was assumed to be 1.50 $M_{\odot}$. Although the companion-interaction early excess could be prominent under this condition, we cannot reproduce the early light curves and $B-V$ color evolution of MUSSES1604D because a strong but long-duration early excess will be produced after interacting with a red giant which has a more extended envelope (Kasen, 2010, Kutsuna and Shigeyama, 2015). For the spectral peculiarity (Figure 29), the prominent Ti II absorptions also contradict the predictions from typical explosion models through the hydrogen-accreting single degenerate channel (Hillebrandt and Niemeyer, 2000, Nomoto et al., 1984, Khokhlov, 1991).

Further comparisons of early-phase light curves with both Kasen's (K10) and K-S companion-interaction models (Kasen, 2010, Kutsuna and Shigeyama, 2015) are presented in panels (a)–(c) of Figure 33. Note that K10 predicts brighter early excess than K-S models because it assumes instantaneous thermalization in the shocked matter while K-S models approximately take into account thermalization processes between shocked matter and radiation (cooling of shocked matter by bremsstrahlung). As K10 noticed, the assumption of instantaneous thermalization tends to underestimate the energies of photons and also results in overestimating the emissivity from shocked matter. Therefore, K10 models produce a prominent early excess even when the companion is a low-mass main-sequence star while K-S models can only marginally produce a comparable early excess when the companion is a red giant, and generate an even fainter early excess with a main-sequence companion. However, despite the different assumptions in two companion-interaction models, both K10 and K-S models with an early excess as bright as that of MUSSES1604D predict blue color of $B-V\lesssim0.1$ in the first four days after the explosion, which is incompatible with the observational result of MUSSES1604D.

CSM-ejecta interaction

In the double-degenerate progenitor scenario where an SN Ia is generated from the merger of two WDs, a considerable amount of material from the disrupted secondary WD may get

pushed out to a large radius (Fryer et al., 2010, Shen et al., 2012) and possibly result in an early ultraviolet/optical excess due to the interaction with the ejecta (Levanon et al., 2015, Piro and Morozova, 2016). The prominent early light-curve excess of MUSSES1604D requires a very extended CSM distribution (Piro and Morozova, 2016, Levanon and Soker, 2017). Regardless of the physical possibility of creating this dense and extended CSM distribution, interactions with more extended CSM not only strengthens the early excess but also increases the diffusion time, and consequently results in a bluer and longer early-excess phase (Piro and Morozova, 2016). As can be seen in panels (d)–(f) of Figure 33, to produce an early excess with a brightness comparable to that of MUSSES1604D, blue and slow color evolution is inevitable for the CSM-ejecta interaction even after fine-tuning the CSM scale and the ^{56}Ni distribution of the inner ejecta. Therefore, the CSM-ejecta interaction cannot explain the prominent early excess with a red and rapid $B-V$ color evolution found in MUSSES1604D. More recently, a systematical investigation by Maeda et al. (2018) further indicated the clear discrepancy between early-excess features predicted by CSM- and companion-interaction scenarios and that of MUSSES1604D.

The He-detonation scenario

Another scenario is an SN Ia explosion triggered by the detonation of the He layer. The He-detonation process accommodates the radioactive materials as the nucleosynthesis ash. For example, the He detonation on the surface of the Chandrasekhar-mass WD would leave ^{56}Ni as a main energy source in this layer with the mass fraction ($X_{56\mathrm{Ni}}$) reaching to $\sim$20% (see below). The diffusion time scale (Arnett, 1996) of this He layer to optical photons is estimated to be $\sim$2 days $\times(\kappa/0.2\mathrm{cm^2g^{-1}})^{0.5}(M_{\mathrm{He}}/0.02M_{\odot})^{0.5}(V_{\mathrm{He}}/20,000\mathrm{kms^{-1}})^{-0.5}$. Here, a subscript "He" refers to quantities related to the He layer, and the He is assumed to be fully ionized. κ is the opacity. The decay power at $\sim$2 days from the ^{56}Ni in the He layer is estimated to be $\sim 2.5\times10^{41}$ erg s^{-1} $(X_{56\mathrm{Ni}}/0.2)\times(M_{\mathrm{He}}/0.02M_{\odot})$. Therefore, the radioactivity in the He-detonation ash is predicted to produce a prompt flash lasting for a few days with the peak bolometric magnitude of ~-16, assuming the He mass $M_{\mathrm{He}}\sim0.03\ M_{\odot}$. This scenario roughly explains the nature of the early excess found for MUSSES1604D. For the sub-Chandrasekhar WD, the abundance in the He ash is dominated by the other radioactive isotopes, ^{52}Fe and ^{48}Cr, and they power the early excess. Even in this case, a similar argument to that mentioned above applies.

The synthetic light curves and spectra expected for the He-shell detonation models (Figures 27–29) are simulated as follows. We constructed a series of toy one-dimensional models that mimic the results of DDet hydrodynamic simulations (Kromer et al., 2010, Woosley and Kasen, 2011). The density structure is assumed to be exponential in velocity space, where the kinetic

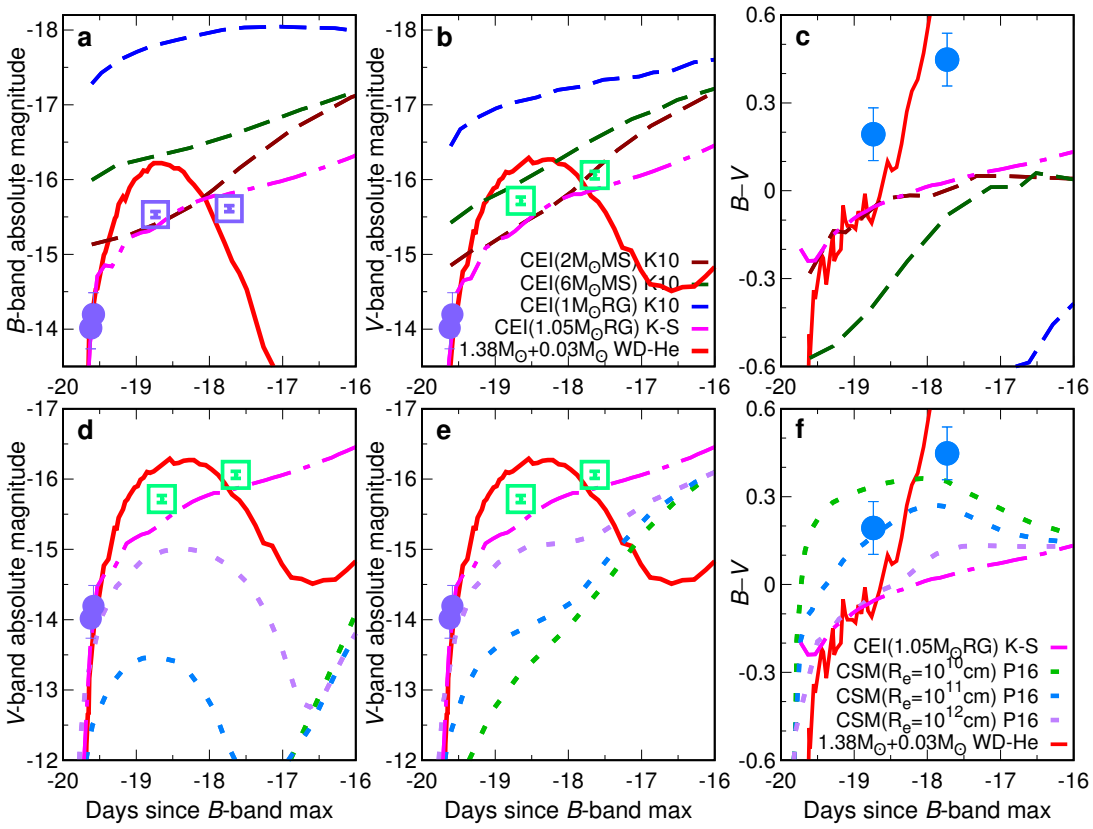

Figure 33: A comparison of MUSSES1604D observations and different model simulations at early-excess phase. Symbols for MUSSES1604D data are the same as those in Figures 26–28 and the results from our best-fitting He-detonation model (1.38 $M_\odot$ WD + 0.03 $M_\odot$ He-shell, red solid lines) are shown in each panel. Panels **a**-**c** present early B-band (**a**) and V-band (**b**) light curves and $B-V$ color evolution (**c**) predicted by different companion-interaction models observed from the companion side. Dashed lines correspond to the K10 models with different binary-system compositions (MS, main-sequence star; RG, red-giant star; Kasen, 2010). The magenta dashed-dotted line denotes our best-fitting K-S companion-interaction model (Kutsuna and Shigeyama, 2015). Although an early excess as bright as that of MUSSES1604D could be produced with specific companion-interaction models, the predicted color is very blue at the early-excess phase. Panels **d** and **e** are V-band light curves simulated by the CSM-ejecta interaction with deep (**d**) and shallow (**e**) ^{56}Ni distribution for the inner ejecta (Piro and Morozova, 2016; P16). Dotted lines correspond to an external mass of M_e=0.3 $M_\odot$ with different outer radii R_e. Panel **f** is the color evolution under the same assumptions as in **e**. Similar to companion-interaction models, combinations of early light curves and color evolution predicted by the CSM-ejecta interaction are also different from the photometric behavior of MUSSES1604D.

energy is specified by the energy generation for the assumed burned composition structure. A stratified structure in the composition and uniform abundance pattern in each layer are assumed, where the distribution of the burning products is set to represent the DDet models (Kromer et al., 2010).

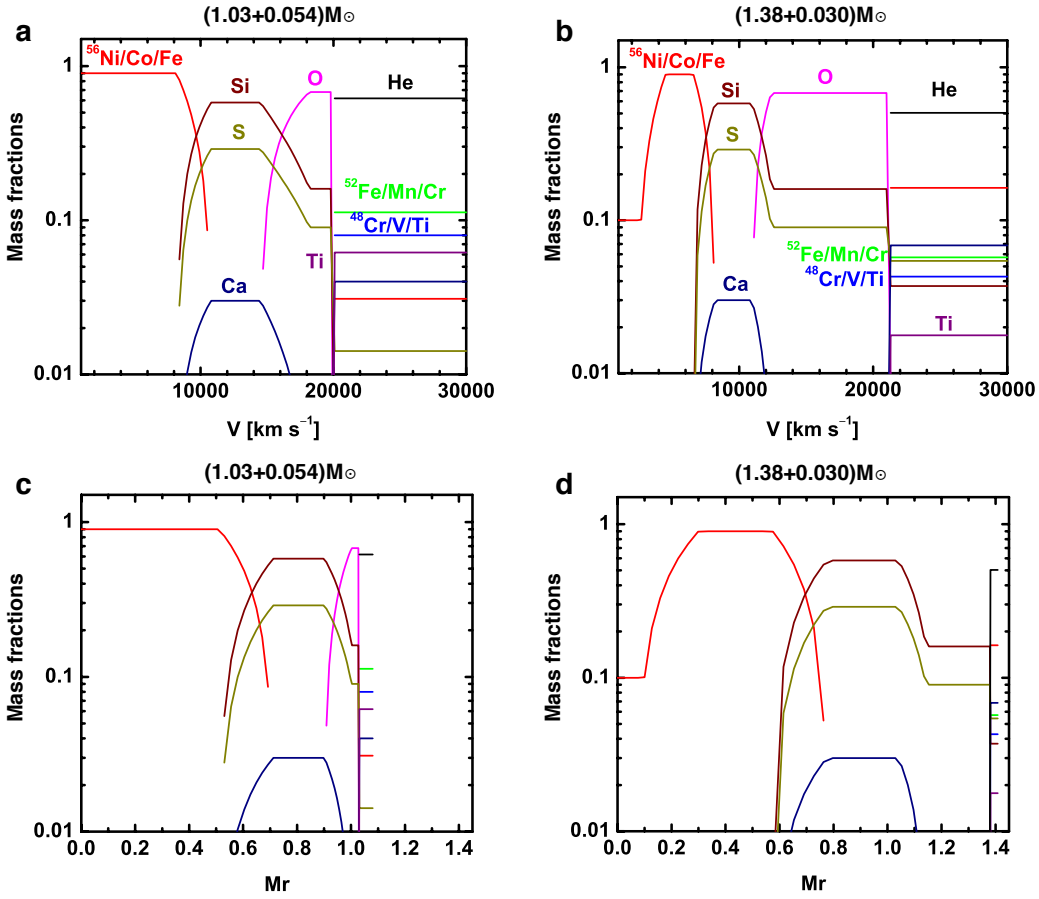

Figure 34: Composition structures of models used for radiation-transfer simulations. The composition structures shown here are He-detonation models for the sub-Chandrasekhar-mass WD (1.03 $M_\odot$ WD + 0.054 $M_\odot$ He-shell; panels **a** and **c**) and the Chandrasekhar-mass WD (1.38 $M_\odot$ WD + 0.03 $M_\odot$ He-shell; panels **b** and **d**). The mass fractions of selected elements are shown as a function of velocity (**a**, **b**) or mass coordinate (**c**, **d**). Colors used for the selected elements are same for all panels.

The model structures are shown in Figures 34 and 35. Our sub-Chandrasekhar model and the Chandrasekhar model are similar to a typical DDet model and W7 model, respectively, in the mass coordinate. For the Chandrasekhar WD model, we replace a part of ^{56}Ni-rich region by the Si-rich region, leading to a more centrally confined structure than the W7 model. Note that we assume a stable Fe/Ni region in the core of the Chandrasekhar model, the mass of which is

taken to be $\sim$0.2 $M_\odot$ similar to the W7 model. For each model, we run multi-frequency and time-dependent Monte-Carlo radiation transfer calculations (Maeda et al., 2014), which were updated to include radioactive energy input from the decay chains of ^{52}Fe/Mn/Cr and ^{48}Cr/V/Ti together with ^{56}Ni/Co/Fe. The code assumes LTE for the ionization, which is generally thought to be a good approximation in the early phase. For example, in the W7 model, LTE and NLTE simulations yield indistinguishable light curves (except for the U-band) until $\sim$25 days after the explosion, corresponding to $\sim$5 days after the B-maximum (Kasen et al., 2006, Kromer and Sim, 2009). Additionally, we do not include the non-thermal excitation of He; generally He absorption lines in optical wavelength are invisible for the DDet models even with this effect (Boyle et al., 2017).

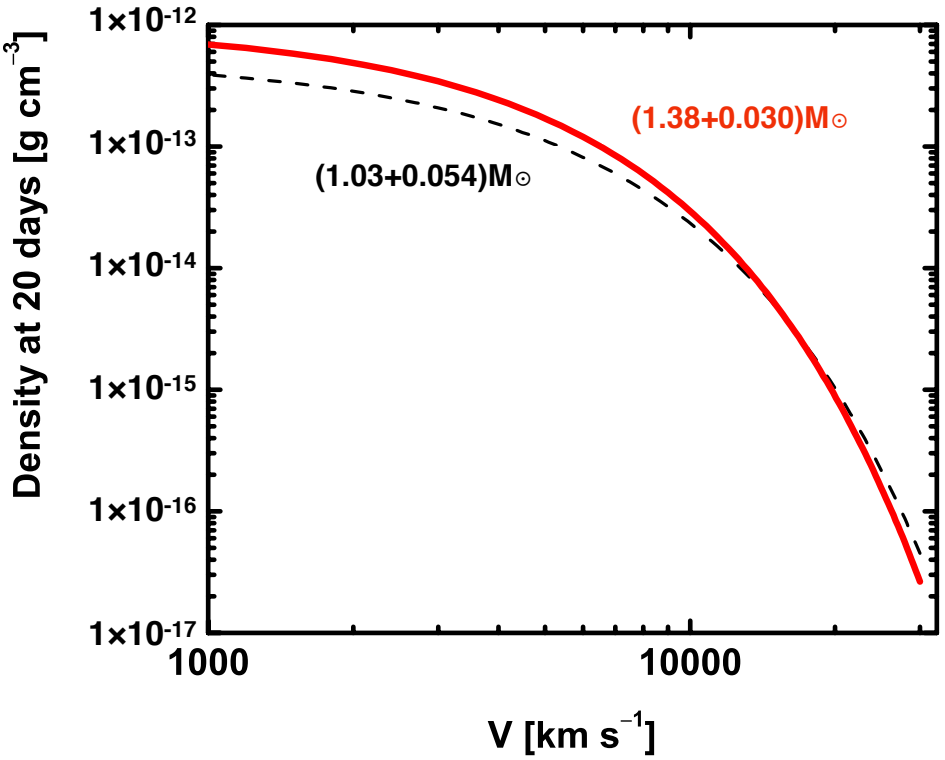

Figure 35: Density structures of the models used for radiation-transfer simulations. The density structures (as a function of velocity) shown here are He-detonation models for the sub-Chandrasekhar-mass WD (1.03 $M_\odot$ WD + 0.054 $M_\odot$ He-shell; black dashed line) and the near-Chandrasekhar-mass WD (1.38 $M_\odot$ WD + 0.03 $M_\odot$ He-shell; red solid line).

The peculiar early light curve and color evolution as well as the strong Ti II absorptions for MUSSES1604D can be naturally reproduced by the DDet scenario, as shown by the model for the 1.03 $M_\odot$ WD with 0.054 $M_\odot$ He (ash) layer in Figures 27–29. Although the sub-

Chandrasekhar DDet model can explain most of peculiarities of MUSSES1604D, it has prominent defects in the resulting fast evolution of the simulated *B*-band light curve (see also Kromer et al. 2010, Woosley and Kasen 2011). Note that the fast decline of *B*-band light curve predicted by this classical DDet scenario of the sub-Chandrasekhar-mass WD happens from $\sim$17 days after the explosion, and the magnitude becomes $\sim$1.4 mag fainter than the peak at t $\sim$25 days. The difference between the LTE and NLTE treatments in the first 25 days after the explosion is too small to account for such abnormal light-curve evolution (Kasen et al., 2006, Kromer and Sim, 2009), and thus it is unlikely that the LTE assumption accounts for this discrepancy. Another issue is that the quantity of radioactive isotopes in this model (resulting from 0.054 $M_{\odot}$ of the He layer, which is required to trigger detonation on the sub-Chandrasekhar-mass WD) produces a more prominent early light-curve excess than that of MUSSES1604D, suggesting that the observationally required amount of the He layer is smaller. To investigate the classical DDet scenario further, we ran a grid of models spanning WD masses between $\sim$0.9 and 1.4 $M_{\odot}$, but all predict very fast evolution in the *B*-band light curve and/or too bright peak luminosity.

Indeed, this fast evolution in the *B*-band light curve has been recognized as one of the issues in the (sub-Chandrasekhar) DDet model (Woosley and Kasen, 2011), since the Fe-peak and Ti/Cr in the He ash should start blocking the photons in the bluer bands once the temperature decreases after the maximum light, and this argument is not sensitive to the LTE or NLTE treatment. It has been shown that this problem could be remedied if the mass of the He layer is much smaller than that required by the classical DDet Model so as not to provide a large opacity (Sim et al., 2010, Blondin et al., 2017, Shen et al., 2018)—a suggestion based partly on an idea that such a small amount of He ($<$0.01 $M_{\odot}$) would lead to the detonation when a substantial fraction of carbon is mixed in the He layer (Shen and Bildsten, 2014). We have also confirmed from our model sequence that the light curves of sub-Chandrasekhar DDet models are indeed roughly consistent with normal (but relatively faint and fast-evolving) SNe Ia, once the He layer is removed. However, this scenario would not explain MUSSES1604D, as we do see a prominent early excess and signatures of the He ash in the around-maximum spectrum.

To remedy the abnormal fast-evolution issue in the classical DDet scenario, we investigated further models in which we allow that the relation between the WD mass and the final ^{56}Ni production expected in DDet is not necessarily fulfilled. By coordinating combinations of the WD mass, ^{56}Ni mass, and the He mass, the most straightforward choice we found is shown in Figures 27–29, where the models with 1.38 $M_{\odot}$ WD, 0.01–0.03 $M_{\odot}$ He-ash layer, and 0.43 $M_{\odot}$ of ^{56}Ni are presented. Additionally we investigated the model with 1.28 $M_{\odot}$ WD, 0.013 $M_{\odot}$ He-ash layer, and 0.44 $M_{\odot}$ of ^{56}Ni. Although such a relatively less massive WD model can also give a slow-evolving light curve, the pre-maximum $B-V$ color turns out to be too red.

Therefore, we constrain the acceptable WD mass range between 1.28 and 1.38 $M_{\odot}$. In addition, an even better consistency of the light curves and color evolution from $\sim$5 days after the B-band maximum could be expected for our preferred model (1.38$M_{\odot}$ WD + 0.03 $M_{\odot}$ He-shell) once the NLTE effects were taken into account (Kasen et al., 2006, Kromer and Sim, 2009).

From the above analyses, we suggest two scenarios that involve the He-shell detonation. The first one is the He-ignited violent merger scenario (Pakmor et al., 2013). In this case, the primary WD mass should still be $\sim$1 $M_{\odot}$ to produce the peak luminosity. The accretion stream of He during the merging process may trigger a detonation even if the He mass is low (Pakmor et al., 2013, Tanikawa et al., 2015). If the secondary is swept up by the ejecta, this would explain the slow-evolving light curve. However, there are two drawbacks to this scenario. (1) Whether the core detonation can be triggered by the thin-He-shell detonation (Shen and Bildsten, 2014, Tanikawa et al., 2015), and (2) such a scenario will involve fine-tuning of the merging configuration (e.g., masses of the WDs) to reproduce the observational features of MUSSES1604D.

The second scenario is the He detonation on the surface of a nearly Chandrasekhar-mass WD, as is motivated by our light-curve and spectral models that reproduce the observational results quite well by simply assuming the standard Chandrasekhar-mass WD without fine-tuning. In this scenario, the observationally derived mass of the He layer is sufficient to trigger the detonation. The evolutionary track of this binary system toward the He detonation on the surface of a WD more massive than 1.3 $M_{\odot}$ has never been discussed in the literature. Further investigations are needed to explore whether this scenario could be realized. Another drawback is that in the classical DDet scenario will produce too much ^{56}Ni by the core detonation, resulting in a luminous SN Ia. Still, the fact that this simple model explains all the main features of MUSSES1604D is striking, indicating that it is unlikely to be a mere coincidence. This would suggest that there could be a mechanism to reduce the mass of ^{56}Ni as compared with the prediction from the classical DDet model.

More realistic light curves and spectra might be produced if one takes into account the possible viewing angle effect related to both the violent merger scenario and the He-ignited near-Chandrasekhar-WD scenario. Our one-dimensional models only address an angle-averaged behavior. The Ti/Fe absorptions will be stronger than our one-dimensional prediction if the line of sight is to intersect a region of the He ash. The initial light-curve enhancement would also, to a lesser extent, depend on the viewing angle.

Another problem is that the Si and S features of MUSSES1604D are not very well reproduced in our spectral models. In general, while these features are qualitatively well explained, obtaining quantitatively good fits is an issue even with sophisticated NLTE modeling (Nugent et al., 1995).

We find that these features are also sensitive to detailed composition structure even in one-dimensional simulations. Providing detailed fitting for these features is beyond the scope of this study, as these features are theoretically more uncertain than the features we have analyzed here.

3.3.4 The explosion epoch of MUSSES1604D

Extrapolating the explosion epoch based on the ^{56}Ni-powered light curve is controversial because there might be a considerable "dark phase" between the explosion and the radioactive decay from SN ejecta (Piro and Nakar, 2013, 2014, Mazzali et al., 2014, Zheng et al., 2014). For example, the best-observed SN Ia so far, SN 2011fe likely has a one-day "dark phase" though the SN was discovered at the brightness of $\sim$1/1000 of its peak brightness (Nugent et al., 2011, Mazzali et al., 2014). More strict constraints on the explosion epoch require not only deep-imaging observations but also specific radiation mechanisms at early time to light up the dark phase. Thanks to the deep imaging capability of Subaru/HSC and the early excess of MUSSES1604D, the explosion time of MUSSES1604D can be pinpointed.

For the He-detonation scenario, the early optical excess is produced immediately from the radioactive decay at the surface of the SN ejecta, which is the earliest optical emission except for the instantaneous cooling emission from the shock-heated WD soon after the SN shock breakout (Piro et al., 2010, Piro and Nakar, 2013). Thus, MUSSES1604D was discovered at an earlier phase than any previously discovered SNe Ia. Given an effectively negligible dark phase before the early excess, we adopt the classical t^2 fireball model (where t is the time since the explosion) for the rising phase of the early excess, assuming that neither the photospheric temperature nor the velocity changes significantly in estimating the explosion epoch of MUSSES1604D. The result indicates that the first observation of MUSSES1604D is at $\sim 0.51^{+0.08}_{-0.06}$ days after the SN explosion. Based on the best-fitting light curves derived from the post-early-excess multiband photometry (dashed lines in Figure 26), the g-band magnitude reaches the same level of our first observation (25.14 mag) at t $\sim$3 days, suggesting that a non-negligible dark phase may exist for non-EExSNe Ia.

3.3.5 MUSSES1604D-like SNe Ia and their rarity

The rate of He-detonation SNe Ia can be constrained by estimating the fraction of MUSSES-1604D-like SNe Ia. By inspecting over 1,000 SNe Ia (varying from normal SNe Ia to various different subtypes) that have at least one good spectrum from about -6 to $+12$ days after the B-band maximum through published resources and open SN databases (Yaron and Gal-Yam, 2012,

Guillochon et al., 2017), three MUSSES1604D-like SNe Ia (without early-phase observations) have been identified. The screening criteria and detailed properties of the MUSSES1604D-like SNe Ia are listed in Table 5. In addition to three normal-brightness SNe Ia ($-19.4 \lesssim M_B \lesssim -18.7$) we mentioned here, some subluminous SNe Ia also show good similarities to MUSSES1604D (e.g. 02es-like SNe Ia, PTF10ops and SN 2010lp, which also have slow-evolving light curve and similar spectral features to those of MUSSES1604D; Maguire et al., 2011, Kromer et al., 2013). However, the limited observational information prevents us from classifying these subluminous objects conclusively. Therefore, the discussion here focuses on the best three MUSSES1604D-like SNe Ia, SN 2006bt, SN 2007cq, and SN 2012df (Foley et al., 2010, Ganeshalingam et al., 2010, Scalzo et al., 2014, Ciabattari et al., 2012).

Normal-brightness SN Ia, SN 2006bt shows good similarity with MUSSES1604D in both light curve and spectral features except for the shallow Si II λ5972 absorption found in MUSSES1604D. Because there is no Na I D feature in spectra of SN 2006bt and the SN is far away from the center of an S0/a host galaxy, the absolute magnitude is shown in Table 5 without taking into account the host extinction. Well-organized follow-up observations of SN 2006bt show pre-maximum Ti II absorptions, slow-evolving B-band light curve, and similar $B-V$ color evolution to that of MUSSES1604D.

SN 2007cq is classified as another MUSSES1604D-like SN Ia. In particular, the pre-maximum spectroscopy of SN 2007cq shows that prominent Ti II absorptions have been detected from about six days before the B-band maximum, which is consistent with the prediction of the He-detonation models (Fink et al., 2010, Kromer et al., 2010). Note that SN 2007cq shows shallower intermediate-mass-element absorptions and bluer color than those of MUSSES1604D, which can be attributed to the larger amount of ^{56}Ni generated from the core explosion of SN 2007cq.

SN 2012df was located at the edge of an S0-like galaxy. The spectrum was taken near the SN brightness peak with an unfiltered absolute magnitude of ~ -18.9 (without extinction correction). Despite the limited observational information of SN 2012df, its high spectral similarity to MUSSES1604D was found around the maximum (Figure 29). Therefore we classify SN 2012df as a MUSSES1604D-like SN Ia. Comparisons of the spectral evolution and light curves of MUSSES1604D-like SNe Ia are shown in Figures 31 and 32, respectively.

To obtain a conservative estimate of the event rate of MUSSES1604D-like SNe Ia, we eliminated all subluminous objects, even though some of them may have the same origin (Maguire et al., 2011, Kromer et al., 2013). Statistically there are four MUSSES1604D-like SNe Ia (including MUSSES1604D) out of $\sim$800 SNe Ia with B-band peak absolute magnitude $\lesssim -18.7$,

corresponding to a fraction of MUSSES1604D-like SNe Ia of $\sim$0.5%.

The traditional SN Ia classification mainly based on the SN brightness and spectral features will classify MUSSES1604D and iPTF14atg into two peculiar subclasses although both have prominent early light-curve excess, slow-evolving light curves, prominent Ti II absorptions, similar color evolution, and host environments (Cao et al., 2015, Cao et al., 2016b), suggesting that they might be intrinsically connected (Kromer et al., 2016). However, whether iPTF14atg originates from the He-detonation scenario is still an open question because the Ti II absorptions and red color of subluminous SNe Ia in post-early-excess phase can also be explained by the low temperature of ejecta, and the lack of early color information precludes further comparison with MUSSES1604D at the early-excess phase. We note that the earliest $B-V$ color of iPTF14atg at $\sim$5 days after the explosion is probably too red to be explained by companion interaction or CSM-ejecta interaction, but is in line with the predictions of He-detonation models (Figure 27). For the reference purpose, in Table 5, we list MUSSES1604D-like and iPTF14atg-like candidates selected from different SN Ia subclasses (Maguire et al., 2011, Kromer et al., 2013, Ganeshalingam et al., 2012, Li et al., 2003, Foley et al., 2013). Similarities between these objects may suggest a physical connection between SNe Ia in specific subclasses.

Table 4: Photometric information on MUSSES1604D

UT Date	Phase[a]	Telescope/Instrument	g	r	i	B[b]	V[b]
Apr 04.34	-19.62	Subaru/HSC	25.14 (15)	–	–	–	–
Apr 04.39	-19.58	Subaru/HSC	24.96 (16)	–	–	–	–
Apr 05.25	-18.82	Subaru/HSC	23.09 (07)	–	–	–	–
Apr 05.29	-18.78	Subaru/HSC	23.15 (06)	–	–	–	–
Apr 05.33	-18.74	Subaru/HSC	23.09 (05)	–	–	–	–
Apr 05.34 – 05.43	-18.74 – -18.65	Subaru/HSC	23.08 (05)	22.99 (05)	–	23.16 (04)	22.97 (05)
Apr 05.49	-18.59	Subaru/HSC	–	22.96 (06)	–	–	–
Apr 05.55	-18.54	Subaru/HSC	–	22.91 (05)	–	–	–
Apr 06.46 – 06.56	-17.73 – -17.64	Subaru/HSC	23.05 (05)	22.64 (05)	–	23.08 (04)	22.63 (05)
Apr 08.51	-15.89	Subaru/HSC	–	22.14 (04)	–	–	22.50
Apr 17.41	-7.93	ARC/ARCTIC	20.35 (03)	20.06 (03)	–	20.33	20.06
Apr 26.59	0.29	Kiso/KWFC	–	19.60 (06)	–	19.93	19.61
Apr 28.93	2.38	INT/WFC	19.95 (02)	19.64 (01)	19.84 (01)	19.98	19.61
May 05.07	7.87	NOT/ALFOSC	20.32 (03)	19.81 (02)	20.04 (02)	20.24	19.76
May 05.93	8.64	LT/IO:O	20.39 (02)	19.73 (01)	20.01 (02)	20.29	19.79
May 11.93	14.01	LT/IO:O	20.89 (03)	20.04 (03)	20.30 (04)	20.77	20.11
May 14.14	15.99	ARC/ARCTIC	21.04 (04)	20.15 (02)	20.29 (02)	20.97	20.22
May 19.89 – 19.92	21.14 – 21.16	NOT/ALFOSC	21.63 (06)	20.42 (02)	20.32 (04)	21.49	20.43
May 25.32	26.00	Gemini-N/GMOS	22.01 (02)	20.67 (02)	–	21.93	20.62
May 28.91	29.21	LT/IO:O	22.41 (08)	20.80 (03)	20.55 (03)	22.17	20.78
Jun 06.98	37.33	NOT/ALFOSC	22.69 (04)	21.21 (04)	20.98 (05)	22.68	21.26

Notes.

The magnitudes in g, r and i bands (observer-frame; AB system) have been transferred to the standard SDSS photometric system by adopting a color term correction based on field stars. Rest-frame B- and V-band magnitudes are in the Vega system. Numbers in parenthesis correspond to 1-σ statistical uncertainties in units of 1/100 mag.

[a] Days (rest-frame) relative to the estimated date of the B-band maximum, UT April 26.27, 2016.

[b] K-correction for the flash-phase (April 4–8) observations is carried out by using the power-law spectral energy distribution models derived from the color of the early flash. For post-flash observations, K-correction is performed according to the best-fitting spectral sequence model of MUSSES1604D. The Galactic extinction (E$(B-V)_{MW}$=0.0263 mag) has been corrected.

Table 5: Properties of MUSSES1604D- and iPTF14atg-like SNe Ia

SN Name	B_{Max}[a] (mag)	$\Delta m_{15}(B)$ (mag)	$B-V$ Level[b]	Ti_{II} Absorptions[c,d]	Si_{II} λ5972[c,e]	$V_{Si_{II}\lambda6355}$[c] (km s^{-1})	Ti_{II} Evolution[f]
MUSSES1604D-Like SN Ia Candidates							
MUSSES1604D	-18.8$_+$	1.0$_+$	Red$_+$	Very Deep$_+$	Shallow$_+$	11,800$_+$	Slow$_+$
SN 2012df$_+$	-18.9[g]$_+$	—	Marginal-red$_+$	Deep$_+$	Shallow$_+$	12,000$_+$	—
SN 2007cq$_+$	-19.4$_+$	1.1$_+$	Normal$_-$	Deep$_+$	Shallow$_+$	11,000$_+$	Slow$_+$
SN 2006bt$_+$	-18.9$_+$	1.1$_+$	Marginal-red$_+$	Deep$_+$	Intermediate$_-$	11,600$_+$	Slow$_+$
SN 2011fe$_-$	-19.2$_+$	1.2$_\mid$	Normal$_-$	Intermediate$_-$	Intermediate$_-$	10,300$_\mid$	Normal$_-$
iPTF14atg-Like SN Ia Candidates							
iPTF14atg	-17.7$_+$	1.3$_+$	Red$_+$	Very Deep$_+$	Deep$_+$	7,300$_+$	Normal$_+$
SN 2002es$_+$	-17.9$_+$	1.3$_+$	Red$_+$	Very Deep$_+$	Deep$_+$	6,000$_+$	Normal$_+$
SN 2010lp$_?$	-17.9$_+$	1.4$_+$	Ultra-Red$_+$	Very Deep$_+$	Deep$_+$	10,600$_-$	—
PTF10ops$_?$	-17.8$_+$	1.1$_+$	Ultra-Red$_+$	Deep$_+$	Deep$_+$	10,000$_-$	Normal$_+$
SN 2011ay$_?$	-18.1$_+$	1.3$_+$	Red$_+$	Deep$_+$	Intermediate$_\mid$	5,600$_+$	Fast$_-$
SN 2008A$_?$	-17.9$_+$	1.3$_+$	Red$_+$	Deep$_+$	Intermediate$_\mid$	6,900$_+$	Fast$_-$
SN 2005hk$_?$	-17.7$_+$	1.5$_\mid$	Marginal-red$_\mid$	Deep$_+$	Deep$_+$	6,100$_+$	Fast$_-$
SN 2008ae$_?$	-17.1$_\mid$	1.4$_+$	Ultra-Red$_+$	Deep$_+$	Intermediate$_\mid$	7,900$_+$	Fast$_-$
SN 2002cx$_?$	-17.5$_+$	1.2$_+$	Normal$_-$	Deep$_+$	Intermediate$_\mid$	5,500$_+$	Normal$_+$

Notes.

For each property, we use "+", " $\mid$ " and "-" footnotes as "support", "neutral" and "opposite" respectively to show the similarity between candidates and MUSSES1604D/iPTF14atg. For all three MUSSES1604D-like SNe Ia, the host extinction are neglected because of the relatively distant location of SNe to the center of their S0/a host galaxies and the non-detection of Na I D lines in their spectra. Galactic extinction has been applied with E$(B-V)_{MW}$ of 0.1096 mag and 0.050 mag for SN 2007cq and SN 2006bt, respectively.

[a] The absolute magnitude for iPTF14atg, 02es-like (SN 2002es, SN 2010lp, PTF10ops) and all normal-brightness SNe Ia was calculated by using cosmological parameters H_0=70.0 km s^{-1} Mpc^{-1}, Ω_m=0.30, Ω_Λ=0.70, and Ω_v=0.00. For 02cx-like SNe Ia, we adopt the value from the related paper (Foley et al., 2013).

[b] The $B-V$ color information at around the B-band maximum. Here, we define $B-V\geq$0.4 mag, 0.4 mag$>B-V\geq$0.2 mag, 0.2 mag$>B-V\geq$0.1 mag, 0.1 mag$>B-V\geq-$0.1 mag and -0.1 mag$>B-V$ as "ultra-red," "red," "marginal-red," "normal," and "blue," respectively.

[c] Spectral features at around the B-band maximum. For normal-brightness and subluminous SNe Ia, we used spectra taken on the closest epoch to t=$-$2 and t=0, respectively (relative to the B-band maximum) for the similarity comparisons.

[d] The relative strength of Ti II absorptions near the B-band maximum. The strength is relative to normal-type SNe Ia, e.g. SN 2011fe.

[e] We define the equivalent width (EW) of Si II λ5972 line as: EW(Si$_{II\lambda5972}$)$\leq$10 Å, 10 Å$<$EW(Si$_{II\lambda5972}$)$\leq$30 Å, 30 Å$<$EW(Si$_{II\lambda5972}$) as "Shallow", "Intermediate" and "Deep", respectively.

[f] The relative evolution speed of Ti II absorptions in the first 10$\pm$2 days after the B-band maximum. The evolution speed is relative to SN 2011fe and iPTF14atg for normal-brightness and subluminous SNe Ia respectively.

[g] Unfiltered photometry without considering the Galactic extinction E$(B-V)_{MW}$=0.0393 mag.

4 Further Understanding of Early-phase SNe Ia from the Statistical Perspective

With the largest sample of early-phase SNe Ia discovered until 2018, we present new evidence to further prove multiple origins of EExSNe Ia and discuss the explosion mechanism and progenitor of specific SN Ia subclasses from the early-excess perspective. This chapter is organized as follows. General information on 23 well-observed early-phase SNe Ia ("golden early-phase SNe Ia") from the subluminous to luminous subclass are summarized in §4.1, and further investigations of previously reported/unnoticed EExSNe Ia are shown in §4.2. Discussions about the multiple origins of early light-curve excess and their associated subclasses are given in §4.3, and conclusions are summarized in the last section.

4.1 Golden Early-phase SNe Ia

In this section, we systematically investigate 23 "golden early-phase SNe Ia" from published papers. In general, we define spectroscopically classified SNe Ia with single-band or multiband photometry taken from $\sim$16 days before to 15 days after the B-band maximum (in the rest frame) as golden early-phase SNe Ia. Given that some SNe Ia have intrinsically short rising phases, An SN Ia discovered at $\sim$15 days before the maximum but with a large photometric depth is also denoted as a golden sample. Here this "large photometric depth" is quantitatively defined in a way that a magnitude difference between the detection and the maximum in the same band is larger than 4 mag (LSQ12hxx, LSQ13ry, iPTF13ebh, and SN 2016coj), or a rising rate derived from the earliest photometry and the non-detection limiting magnitude is higher than about 1 mag day^{-1} (ASASSN-14lp). Note that SN 2014J (observations from early-phase to post-maximum in the same band are missing; Goobar et al., 2014) and two early-phase SNe Ia discovered by the *Kepler Space Telescope*, KSN 2012a and KSN 2011b (without spectral information; Olling et al., 2015), do not meet the criteria of golden early-phase SNe Ia.

All golden early-phase SNe Ia are further classified into "normal", "luminous," "transitional," "subluminous," and "He-det" subclasses depending on their general photometric and spectroscopic characteristics. Their basic information is listed in Table 6. We adopt $\Delta m_{15}(B)$ value and B-band apparent magnitudes at peak ($m_{B,max}$) from relevant publications. Absolute B-band magnitudes at peak ($M_{B,max}$) are derived by adopting a Hubble constant $H_0 = 70$ km s^{-1} Mpc^{-1}

and Galactic and host extinction values from Schlegel et al. (1998) and relevant publications, respectively. $M_{B,max}$ are plotted against $\Delta m_{15}(B)$ in Figure 36.

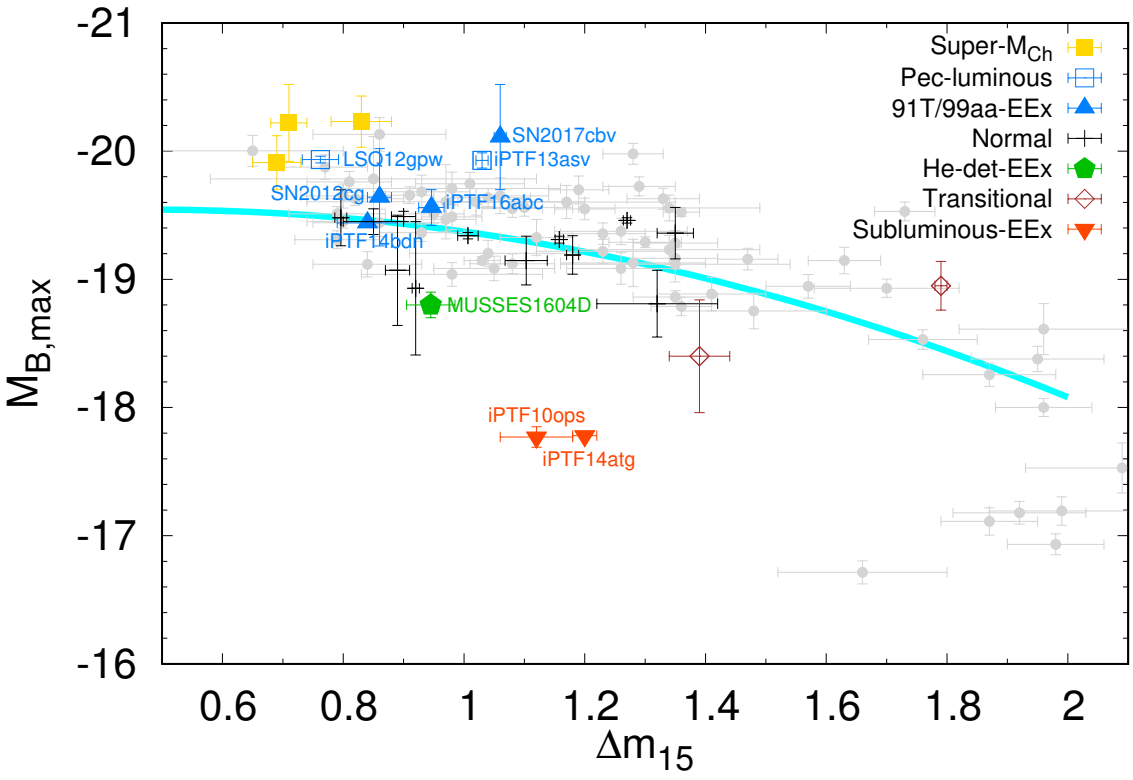

Figure 36: Absolute B-band peak magnitude ($M_{B,max}$) vs. the light-curve decline rate, expressed by the magnitude decline in 15 days from the B-band peak ($\Delta m_{15}(B)$), for 23 golden early-phase SNe Ia. Four 91T/99aa-like (blue triangles), one luminous/peculiar (blue open square), two subluminous (red inverted triangles), and one He-det (green pentagon) SNe Ia show early-excess features. Gray points are from CfA3 samples in Hicken et al. (2009). The Phillips relation is highlighted in cyan.

4.1.1 Early-phase normal and transitional SNe Ia

There are 12 normal SNe Ia in our golden sample. In general, their spectral features and luminosities well match those of normal SNe Ia. For three objects (SN 2010jn, SN 2012fr, and ASASSN-14lp) that show relatively high brightness but with normal-like spectral evolution, we classify them as normal SNe Ia at the bright end of the Phillips relation (Phillips, 1993) by following previous studies (Hachinger et al., 2013, Childress et al., 2013, Shappee et al., 2016). In addition to early optical observations, prompt *Swift*/UVOT follow-up observations

were successfully triggered for six normal SNe Ia (§4.2). However, none of the 12 normal SNe Ia show early light-curve excess in optical and UV wavelengths.

SN 2012ht and iPTF13ebh are categorized as "transitional" type based on their fast-decline light curves and relatively high luminosities as opposed to subluminous/91bg-like SNe Ia (Yamanaka et al., 2014, Hsiao et al., 2015). Although two transitional golden early-phase SNe Ia show quite different spectral features, smooth-rising light curves are found in both events at early phases.

4.1.2 Early-phase luminous SNe Ia

Our golden early-phase SN Ia sample includes six SNe Ia with bright, slow-evolving light curves and shallow absorptions by intermediate-mass elements (IME), which are grouped into "luminous/91T-like," "luminous/99aa-like," and "luminous/peculiar" subclasses in terms of their luminosities and specific spectral features.

The relatively weak IME absorptions, prominent calcium and iron lines in the premaximum spectra of three luminous SNe Ia (SN 2012cg, iPTF16abc, and SN 2017cbv) are reminiscent of 99aa-like SNe Ia. Note that iPTF14bdn has been classified as a 99aa-like SN Ia by Smitka et al. (2015). However, the early spectra dominated by iron-group elements (IGE), together with inconspicuous IME absorptions, indeed show a closer resemblance to those of 91T-like SNe Ia. Therefore, we classify iPTF14bdn as a 91T-like SN Ia.

In recent years, several SNe Ia with excessively high luminosities and broad light curves have been discovered. Since the ^{56}Ni mass required to produce such high luminosities is in conflict with that realized in the explosion of a 1.4 $M_{\odot}$ WD, they are frequently called "super-Chandrasekhar-mass" SNe Ia ("super-$M_{\rm Ch}$" SNe Ia). Spectroscopically, super-$M_{\rm Ch}$ SNe Ia commonly show persistent C II absorptions and moderately low photospheric velocities. Except for the unknown UV properties, optical photometry and spectroscopy of the golden early-phase SN Ia LSQ12gpw (Firth et al., 2014, Walker et al., 2015; spectra can be found in the Open Supernova Catalog*; Guillochon et al., 2017) indicate a high similarity to super-$M_{\rm Ch}$ SN Ia SN 2009dc (Silverman et al., 2011). We classify this 09dc-like super-$M_{\rm Ch}$ SN Ia into the luminous/peculiar subclass. Although the high peak luminosity, prominent IME absorptions, and especially the persistent carbon absorption of another golden luminous SN Ia, iPTF13asv—resemble super-$M_{\rm Ch}$ SNe Ia, its light curve evolves much faster than those of super-$M_{\rm Ch}$ and many 91T/99aa-like SNe Ia (Table 6). By following the main conclusion from Cao et al. (2016a), we classify iPTF13asv as a luminous/peculiar SN Ia.

*https://sne.space/

Table 6: Characteristics of Golden Early-phase SNe Ia

Name[a]	Subclass	$\Delta m_{15}(B)$	Peak Magnitude[b]	Redshift	Discovery Phase (days)[c]	Photometric Depth (mag)[d]	Early Excess? Optical/UV	Data Sources[e]
SN 2009ig	Normal	0.89	−19.07	0.008797	−16.4 (Unf)	4.0	N/N	(1)
SN 2010jn	Normal	0.90	−19.49	0.02602	−15.9 (*R*48)	3.4	N/–	(2)
SN 2011fe	Normal	1.10	−19.15	0.000804	−17.3 (*g*)	7.3	N/N	(3), (4)
SN 2012fr	Normal	0.85	−19.45	0.005453	−15.9 (Unf)	3.9	N/N	(5), (6)
LSQ12hxx	Normal	1.01	−19.34	0.069	−15.6 (*gr*)	4.4	N/–	(7), (8)
LSQ12hzj	Normal	1.16	−19.31	0.029	−15.9 (*gr*)	3.7	N/–	(7), (8)
LSQ13ry	Normal	1.27	−19.46	0.030	−15.7 (*gr*)	4.5	N/–	(7), (8)
iPTF13dge	Normal	1.18	−19.19	0.0159	−18.2 (*R*48)	4.1	N/N	(9)
SN 2013dy	Normal	0.92	−18.93	0.003889	−17.6 (Unf)	5.9	N/–	(10), (11)
ASASSN-14lp	Normal	0.80	−19.48	0.005101	−14.6 (*V*)	3.5	N/N	(12)
SN 2015F	Normal	1.35	−19.36	0.004846	−16.3 (*V*)	4.8	N/N	(13)
SN 2016coj	Normal	1.32	−18.81	0.004523	−15.4 (Unf)	5.1	N/–	(14), (15)
iPTF14bdn	91T-like	0.84	−19.44	0.01558	−18.0 (*R*48)	4.1	Y/Y	(16)
SN 2012cg	99aa-like	0.86	−19.64	0.00162	−17.1 (*B*)	5.2	Y/Y	(17)
iPTF16abc	99aa-like	0.95	−19.56	0.0234	−17.8 (*g*)	5.5	Y/Y	(18)
SN 2017cbv	99aa-like	1.06	−20.11	0.00399	−18.9 (*B*)	4.3	Y/Y	(19)
iPTF13asv	peculiar	1.03	−19.93	0.036	−16.2 (*R*48)	3.7	N/–	(20)
LSQ12gpw	peculiar	0.76	−19.93	0.058	−19.9 (*gr*)	3.2	Y/–	(7), (8)
SN 2012ht	Transitional	1.39	−18.40	0.003559	−15.8 (Unf)	4.3	N/N	(21)
iPTF13ebh	Transitional	1.79	−18.95	0.0133	−14.5 (*R*48)	5.9	N/N	(22)
PTF10ops	02es-like	1.12	−17.77	0.062	−15.6 (*R*48)	3.2	Y/–	(23)
iPTF14atg	02es-like	1.20	−17.78	0.0213	−18.5 (*R*48)	3.8	Y/Y	(24)
MUSSES1604D	He-det	0.95	−18.80	0.11737	−19.6 (*g*)	5.2	Y/–	(25)

Note.

[a] Names of EExSNe Ia are denoted in boldface.

[b] The peak absolute magnitude in the *B* band. Galactic extinction has been corrected for all golden early-phase SNe Ia. Reddening corrections of host galaxies are performed for SN 2010jn, SN 2012cg, SN 2013dy, SN 2015F, iPTF13ebh, iPTF16abc, and ASASSN-14lp by following related papers. For ASASSN-14lp, we tentatively adopt $R_V = 1.7$ to give a reasonable peak magnitude for this spectroscopically normal SN Ia.

[c] The "discovery phase" is the detection (the corresponding filter is shown in parentheses) time relative to the SN's *B*-band maximum in the rest frame.

[d] The "photometric depth" is defined as a magnitude difference between the detection and the maximum in the same band. Due to the lack of unfiltered (Unf) peak magnitude of SN 2012fr and SN 2012ht, their photometric depths are calculated by using the *R*-band peak magnitude.

[e] (1) Foley et al. (2012), (2) Hachinger et al. (2013), (3) Nugent et al. (2011), (4) Pereira et al. (2013), (5) Zhang et al. (2014), (6) Klotz and Conseil (2012), (7) Firth et al. (2014), (8) Walker et al. (2015), (9) Ferretti et al. (2016), (10) Zheng et al. (2013), (11) Pan et al. (2015), (12) Shappee et al. (2016), (13) Cartier et al. (2017), (14) Zheng et al. (2017), (15) Richmond and Vietje (2017), (16) Smitka et al. (2015), (17) Marion et al. (2016), (18) Miller et al. (2018), (19) Hosseinzadeh et al. (2017), (20) Cao et al. (2016a), (21) Yamanaka et al. (2014), (22) Hsiao et al. (2015), (23) Maguire et al. (2011), (24) Cao et al. (2015), (25) Jiang et al. (2017).

The UV/optical light-curve excess is found in the early phase of all 91T/99aa-like SNe Ia and LSQ12gpw, indicating an extremely high early-excess fraction of luminous SNe Ia. Detailed information for all luminous EExSNe Ia is given in §4.2.2.

4.1.3 Early-phase subluminous SNe Ia

The SN 1991bg-like, SN 2002cx-like, and SN 2002es-like SNe Ia are typical branches of subluminous SNe Ia. Mainly due to the fast-evolving light curves of 91bg-like SNe Ia, so far, none of them have been discovered at very early time. The 02cx-like SNe Ia occupy a large fraction of subluminous SNe Ia. Luminosities of 02cx-like SNe Ia show very large scatter, and their light curves evolve much slower than those of 91bg-like SNe Ia (see Foley et al. 2013 for a review). Although several 02cx-like SNe Ia have been discovered over 10 days before reaching their *B*-band maxima, we are still missing the photometric information in the first few days after their explosions. The 02es-like SNe Ia are spectroscopically similar to 91bg-like SNe Ia, indicating a low temperature and ionization for both subclasses. The main characteristics of 02es-like SNe Ia are a moderately faint ($M_{B,max} \sim -17.7 - -18.0$) but slow-evolving ($\Delta m_{15}(B) \sim 1.1$–$1.3$) light curve and lower ejecta velocity compared with those of 91bg-like SNe Ia (Ganeshalingam et al., 2012, White et al., 2015). Currently, the number of reported 02es-like SNe Ia is small ($\lesssim 10$), but two of them have been discovered at very early time. In total, only two 02es-like SNe Ia, PTF10ops and iPTF14atg, can be qualified as golden early-phase SNe Ia among published early-phase subluminous SNe Ia, and both of them show interesting early light-curve behavior (§4.2.1).

There is one early-phase supernova, iPTF14dpk, which was claimed as a 02es-like SN Ia by Cao et al. (2016b). In §4.2.4, we argue that the limited observational information cannot provide any crucial evidence for classifying iPTF14dpk as a 02es-like SN Ia; however, its peculiar early light-curve behavior indeed suggests that iPTF14dpk is more likely an early-phase core-collapse supernova (CCSN).

4.1.4 Early-phase He-det SNe Ia

As we introduced in §3.2, the characteristics of MUSSES1604D including the peculiar early light-cure excess and the Ti II trough feature shown in this normal-brightness SN Ia, can be naturally explained by assuming that the SN is triggered by a precursory detonation of a thin He layer at the surface of a progenitor WD (the so-called "He-shell-detonation" or "He-det" scenario). Currently, MUSSES1604D is the only early-phase SN Ia belonging to this class.

4.2 Early-excess SNe Ia

The definition of EExSNe Ia is schematically illustrated in Figure 37. In general, early-excess features discovered so far can be visually classified into two types. The first type is a prominent and precursory early excess occurring a few days earlier than the ^{56}Ni-powered main-body light curve (a "spike-like" EEx), which can be easily distinguished (panels a and b). The second type is a persistent (several days to more than 1 week) early excess that is coupled with the main-body light curve from the beginning (a "bump-like" EEx), which can be distinguished when the early-excess feature is prominent (panel c) or the ^{56}Ni-powered main-body light curve evolves quickly (panel d). In addition to two clear early-excess types, light curves influenced by an early-excess scenario may not have clear spike- or bump-like features but show "slow-rising" behavior in the early phase (the yellow region in panel e), which may originate from a weak bump that is covered by the main-body light curve, a weak excess observed in insensitive wavelengths or a relatively large survey cadence, and so on. Since such inconspicuous early excess will make the early light curve observationally broader, we hereafter classify these SNe as "early-broad EExSNe Ia." Given that SN 2012cg shows the weakest early-excess feature in all previously reported EExSNe Ia*, we compare our early SN sample with SN 2012cg to find out early-broad EExSNe Ia. Specifically, by shifting light curves of SNe Ia to match with that of SN 2012cg at peak, an SN Ia showing a broader rising-phase light curve and similar or narrow post-maximum light curve compared with that of SN 2012cg (the "yellow+green" region in panel e) in any wavelength will be classified as an early-broad EExSN Ia. In other words, an SN Ia which shows a generally broader light curve than that of SN 2012cg but without a spike- or bump-like early light-curve feature (the "yellow+red" region in panel e) or a fast-rising light curve (panel f) will be classified as a non-EExSN Ia. In our EExSN Ia sample (11 in total), nine of them show prominent early-excess features (Figures 38–40). The newly discovered SN Ia, SN 2017erp, and the previously reported SN 2012cg show relatively inconspicuous early-excess features.

There are eight EExSNe Ia (iPTF14atg, iPTF14bdn, iPTF16abc, LSQ12gpw, MUSSES1604D, PTF10ops, SN 2012cg, and SN 2017cbv) in our golden sample. Since a more prominent early light-curve excess in UV/NUV wavelengths is predicted by various early-excess scenarios, we further select three additional EExSNe Ia (SN 2011hr, SN 2015bq, and SN 2017erp) from 40 SNe Ia (14 of them are golden early-phase SNe Ia) that have UV/NUV light curves at relatively early phase. In addition, we introduce another two possible EExSN Ia candidates, ASASSN-15uh and SN 2015ak, in §4.2.2 but do not include them in our final sample due

*The UV light curves of SN 2012cg roughly meet the condition of panel d in Figure 37, and optical light curves are similar to the "yellow+green" region in panel e; therefore, we use SN 2012cg as the reference for selecting early-broad EExSNe Ia.

to incomplete information. Our final EExSN Ia sample includes seven luminous (91T/99aa-like and LSQ12gpw), two subluminous (02es-like), one normal (SN 2017erp), and one He-det (MUSSES1604D) SNe Ia. Their basic information is shown in Table 7.

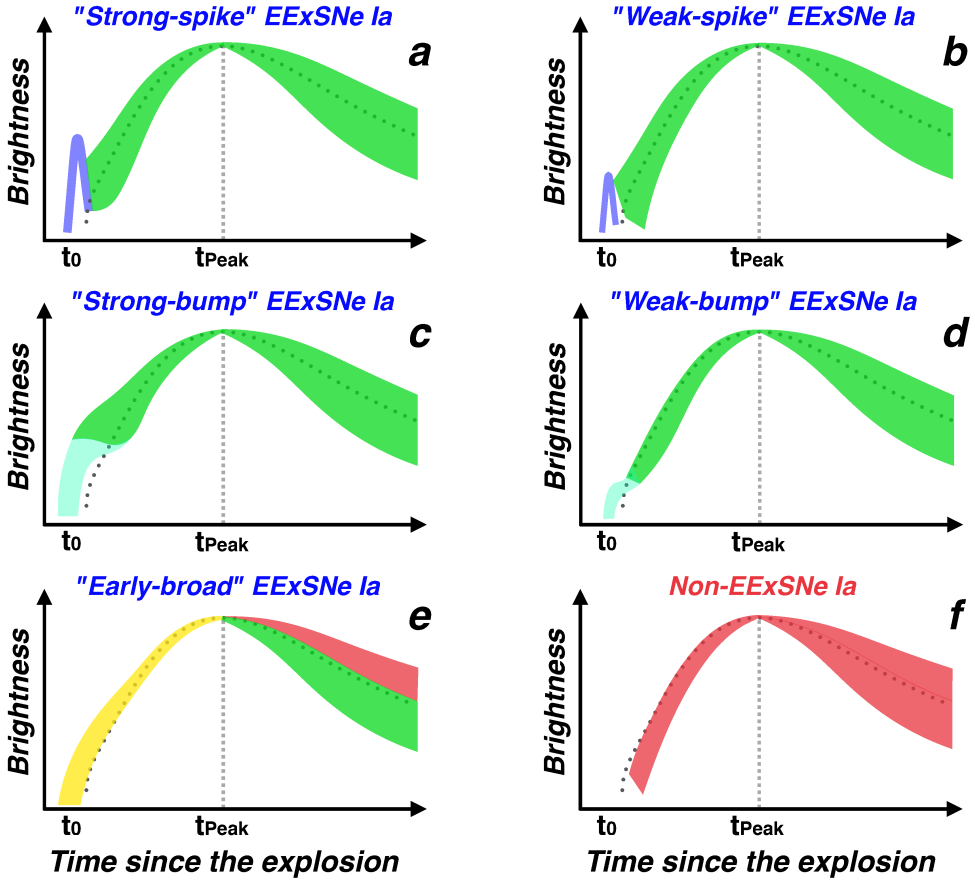

Figure 37: A schematic diagram of different shapes of early-excess features. Spike-like (panels a and b), prominent bump-like (panel c), and weak bump-like early-excess features but with a fast-evolving ^{56}Ni-powered main-body light curve (panel d) can be easily distinguished. We further use SN 2012cg (a sketchy dotted light curve is shown in each panel, and all SN light curves are shifted to match with that of SN 2012cg at peak), which shows the weakest early-excess feature as the reference for selecting other early-broad EExSNe Ia. Specifically, an SN Ia showing a broader rising-phase light curve and similar or narrow post-maximum light curve compared with that of SN 2012cg (the "yellow+green" region in panel e) in any wavelength will be classified as an early-broad EExSN Ia. SNe Ia with light curves in the "yellow+red" region (panel e) and the red region (panel f) are classified as non-EExSNe Ia.

Table 7: General Information on EExSNe Ia and Possible Candidates

Name	Subclass	$\Delta m_{15}(B)$	Discovery Phase[a]	Photometric Depth	EEx Shape[b]	EEx Duration[c]	Host Type
SN 2011hr	91T-like	0.92	-13.6 (B)	2.0	c	Long	Sb (NGC2691)
SN 2015bq	91T-like	$\sim$0.8	-13.9 (B)	2.1	c	Long	–
iPTF14bdn	91T-like	0.84	-18.0 ($R48$)	4.1	c	Long	Irr (UGC8503)
SN 2012cg	99aa-like	0.86	-17.1 (B)	5.2	d/e	Short	Sa (NGC4424)
iPTF16abc	99aa-like	0.95	-17.8 (g)	5.5	c/d	Medium	Sb (NGC5221)
SN 2017cbv	99aa-like	1.06	-18.9 (B)	4.3	c/d	Medium	SABc (NGC5643)
LSQ12gpw	Super-$M_{\rm Ch}$	0.76	-19.9 (gr)	3.2	a/c	–	–
SN 2017erp	Normal	$\sim$0.9	-17.3 (Unf)	3.6[d]	e	Medium	SABc (NGC5861)
PTF10ops	02es-like	1.12	-15.6 ($R48$)	3.2	b/d/e	–	–
iPTF14atg	02es-like	1.20	-18.5 ($R48$)	3.8	a	Medium	E (IC 831)
MUSSES1604D	He-det	0.95	-19.6 (g)	5.2	a	–	S0-like
ASASSN-15uh	99aa-like	$\sim$0.8	-9.0 (B)	1.1	–	–	Sa-like
SN 2015ak	Normal	$\sim$1.1	-15.1 (Unf)	2.2[d]	e	–	Sb (ESO 108-21)

Note.

[a] The "discovery phase" is the detection (the corresponding filter is shown in parentheses) time relative to the SN's B-band maximum in the rest frame.

[b] The early-excess shape is evaluated by using a single-band light curve, which includes the most complete early-phase information. If more than one photometric band meet the requirement, a light curve in the bluest wavelength is used. Letters correspond to the panels in Figure 37, which denote the possible early-excess shape of each SN Ia.

[c] A rough estimation of the duration of early-excess features. Light curves used for the early-excess shape evaluation and duration estimation are the same. "Long," "Medium," and "Short" correspond to the early-excess duration $T_{EEx} \gtrsim 1$ week, 0.5 week $\lesssim T_{EEx} \lesssim 1$ week, and $T_{EEx} \lesssim 0.5$ week, respectively.

[d] Due to the lack of unfiltered peak magnitude of SN 2017erp and SN 2015ak, the photometric depths of two SNe are calculated by using the *Swift*/UVOT U-band light curves started 0.6 and 1.5 days after their discoveries, respectively.

4.2.1 02es-like and He-det EExSNe Ia

The best-observed 02es-like SN Ia so far is iPTF14atg. The prominent early UV/optical excess of iPTF14atg can be basically explained by the companion-interaction scenario as proposed by Cao et al. (2015). However, it is still unclear what kind of explosion mechanism under the SD progenitor scenario can explain the faint but slow-evolving light curve and spectral evolution of 02es-like SNe Ia. On the contrary, previous simulations by Kromer et al. (2016) suggest that the merger of two sub-Chandrasekhar-mass WDs could well reproduce the spectral evolution and light curves of iPTF14atg by assuming a low-metallicity progenitor system. They thus argued that the early light-curve excess of iPTF14atg cannot be attributed to the companion-interaction scenario.

The other 02es-like golden early-phase SN Ia, PTF10ops, also shows an interesting early-phase light curve. As shown in Figure 38, although only one data point of PTF10ops was taken at early time (Maguire et al., 2011), a very likely early light-curve excess can be distinguished in comparison to other golden early-phase SNe Ia and our companion-interaction model (Kutsuna and Shigeyama, 2015; the cyan dashed curve in Figure 38), which implies that 02es-like SNe Ia may commonly show peculiar light-curve behavior in the early phase.

As mentioned in §3.3.5, the spike-like, red early excess of iPTF14atg is reminiscent of the He-det EExSN Ia MUSSES1604D, which originates from the supernova explosion triggered by the helium detonation at the surface of the progenitor. Given a significant amount of Ti production and the weak viewing angle effect predicted by the He-det scenario, the high early-excess fraction (Table 8) and strong Ti II absorptions shown in 02es-like SNe Ia can be explained with the He-det scenario. In addition, recent simulations also verify the possibility of reproducing the early light-curve excess of iPTF14atg with the He-det scenario (Maeda et al., 2018).

As the current sample size of early-phase 02es-like SNe Ia is still inadequate for statistical studies, it is uncertain that detections of early light-curve excess in both 02es-like SNe Ia is due to a viewing angle-independent early-excess scenario for 02es-like SNe Ia or is just by chance.

4.2.2 Luminous EExSNe Ia

Surprisingly, all previously discovered early-phase 91T- and 99aa-like SNe Ia show early-excess features (Figures 38–40). Even though early-excess features in optical wavelengths are inconspicuous for some 91T/99aa-like SNe Ia, all of them show more prominent early excess in UV/NUV wavelengths. In particular, 91T-like SNe Ia seem to have stronger early-excess features than 99aa-like SNe Ia (Figures 39–41).

The early-phase *R*-band light curve of a luminous golden early-phase SN Ia, iPTF13asv, does not show the early-excess feature. Since both simulations from different early-excess scenarios and previous observations suggest that observations in the *R* band are not sensitive for detecting early excess, and the earliest photometry of iPTF13asv is about 1–2 days later than that of other luminous early-phase SNe Ia, we cannot confirm that the non-detection of early excess is due to the intrinsic distinction between iPTF13asv and other luminous EExSNe Ia or the imperfectness of early-phase observations for iPTF13asv. Here, we conservatively classify iPTF13asv as a non-EExSN Ia and do not make a comparison with other luminous EExSNe Ia in §4.3.

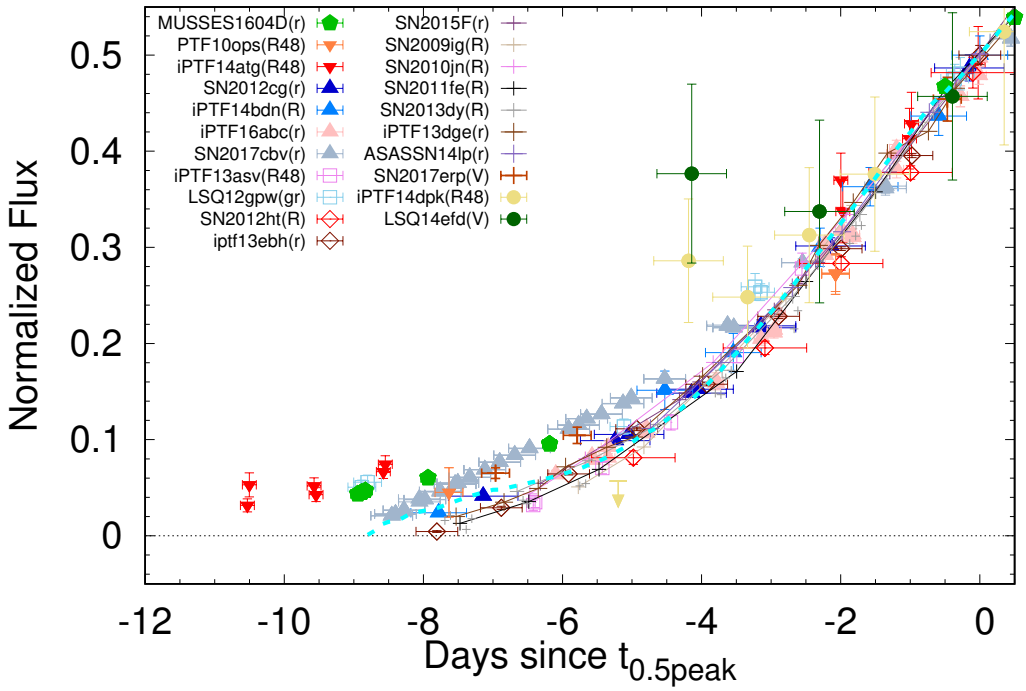

Figure 38: Early optical light curves of golden early-phase SNe Ia. Symbols are the same as in Figure 36. In order to compare early light-curve behaviors at a comparable wavelength coverage with the largest sample size, we select golden early-phase SNe Ia that have photometric information in either the PTF *R*48 band, Cousins *R* band or SDSS *r* band for comparison. Three normal SNe Ia with LSQ *gr*-band photometry are plotted with small gray crosses. Early light curves of SN 2012fr and SN 2016coj are not included due to the lack of early photometric information in a comparable wavelength coverage to other golden early-phase SNe Ia (note that neither of them shows early-excess feature even in blue wavelengths; Zhang et al., 2014, Zheng et al., 2017). As a reference of the early-excess feature of normal SNe Ia, we attached the early *Swift*/UVOT *V*-band light curve of the normal EExSN Ia, SN 2017erp. As can be seen, the early light-curve behavior of two cooling-emission CCSN candidates (filled circles), iPTF14dpk (*R*48) and LSQ14efd (*V*), are significantly different from those of golden early-phase SNe Ia. A cyan dashed curve is predicted by the interaction between SN ejecta and a 1.05 $M_{\odot}$ red-giant companion viewed from the companion side (Kutsuna and Shigeyama, 2015).

Four luminous EExSNe Ia in our sample have been well investigated before. Marion et al. (2016) claimed that the early light-curve excess of SN 2012cg originates from the companion interaction in comparison to light curves predicted by Kasen (2010). Note that such a conclusion is controversial due to the lack of simulation-based comparisons with other early-excess mechanisms. In the case of the early-excess feature of SN 2017cbv, the companion-interaction scenario is preferred based on the early-phase light-curve fitting result. However, other early-excess scenarios indeed cannot be completely excluded, as discussed by Hosseinzadeh et al. (2017). Other than SN 2012cg and SN 2017cbv, the early excess of iPTF16abc has been argued

to be incompatible with the companion interaction based on an inconsistent light-curve fitting result and strong C II absorptions at the early phase (Miller et al., 2018). Smitka et al. (2015) speculated that the blue early excess shown in a 91T-like SN Ia, iPTF14bdn, may originate from the radioactive decay in the outer-layer ejecta where the ^{56}Ni abundance is greater than normal. However, there is no attempt to fit such a prominent early light-curve excess with any early-excess scenario so far.

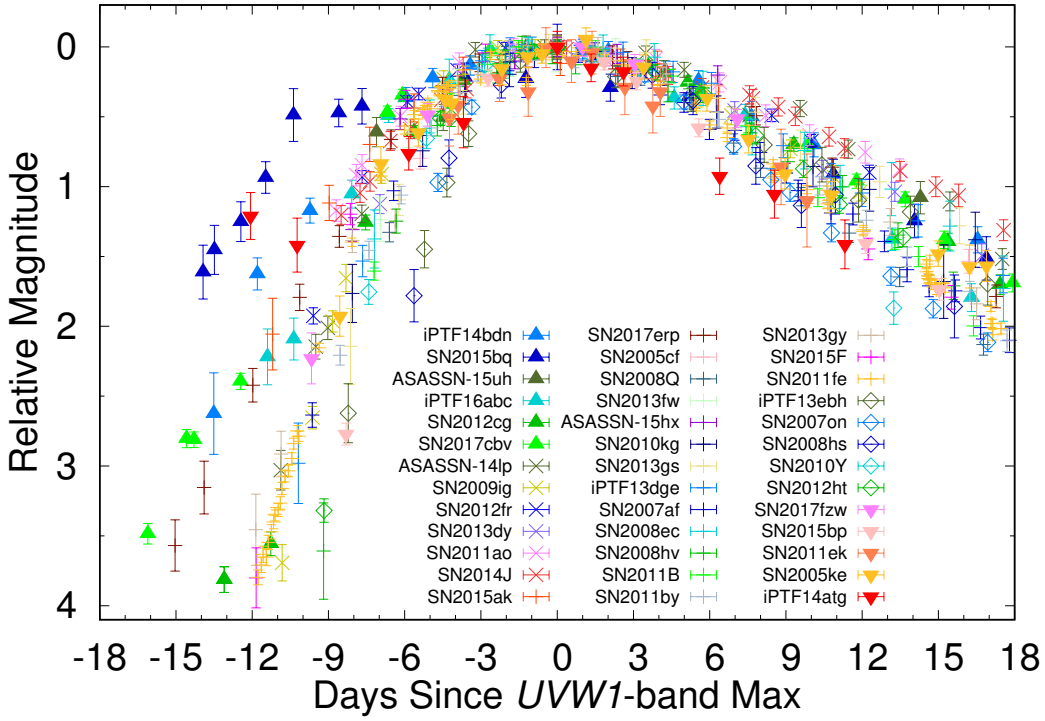

Figure 39: Early-phase *UVW*1-band light curves of different SN Ia subclasses. Symbols are the same as in Figures 36 and 38 are used (diagonal crosses are specified for normal SNe Ia with slow-decline light curves). All light curves are shifted to the same peak magnitude for comparison. The 91T- and 99aa-like SNe Ia have clear excess compared to the rest, though with large scatter. In contrast, normal SNe Ia, except for SN 2017erp and SN 2015ak, show smooth, small-scatter, rising light curves though some of them (diagonal crosses) have similar post-maximum light curves to those of 91T/99aa-like SNe Ia. So far, we have not discovered any early-excess features from transitional, 91bg-like, and 02cx-like SNe Ia, which may be due to the extremely limited early-phase information of these SN Ia subclasses.

Two other luminous EExSNe Ia, SN 2011hr and SN 2015bq, and one possible luminous EExSN Ia candidate, ASASSN-15uh, are selected from published resources and the *Swift* Optical/Ultraviolet Supernova Archive (SOUSA*; Brown et al., 2014). SN 2011hr was classified as a luminous SN

*http://swift.gsfc.nasa.gov/docs/swift/sne/swift_sn.html. The reduction is based on that of Brown et al. (2009), including subtraction of the host galaxy count rates and uses the revised UV zero points and time-dependent sensitivity from Breeveld et al. (2011).

Ia which may bridge 91T-like SNe Ia and a super-$M_{\rm Ch}$ SN Ia, SN 2007if, in terms of high luminosity (Zhang et al., 2016). Although the expected ^{56}Ni mass of SN 2011hr may be greater than the mean value of 91T-like SNe Ia, it can still be explained by the explosion of a Chandrasekhar-mass WD progenitor that experienced a more efficient detonation phase than normal SNe Ia. Additionally, the extremely high spectral similarity to SN 1991T from -13 days to 2 months after the B-band maximum indicates the physical resemblance between the two objects. In Figure 40, a prominent light-curve excess can be seen at $\sim$12 days before the U-band maximum. We therefore classify SN 2011hr as a luminous/91T-like EExSN Ia.

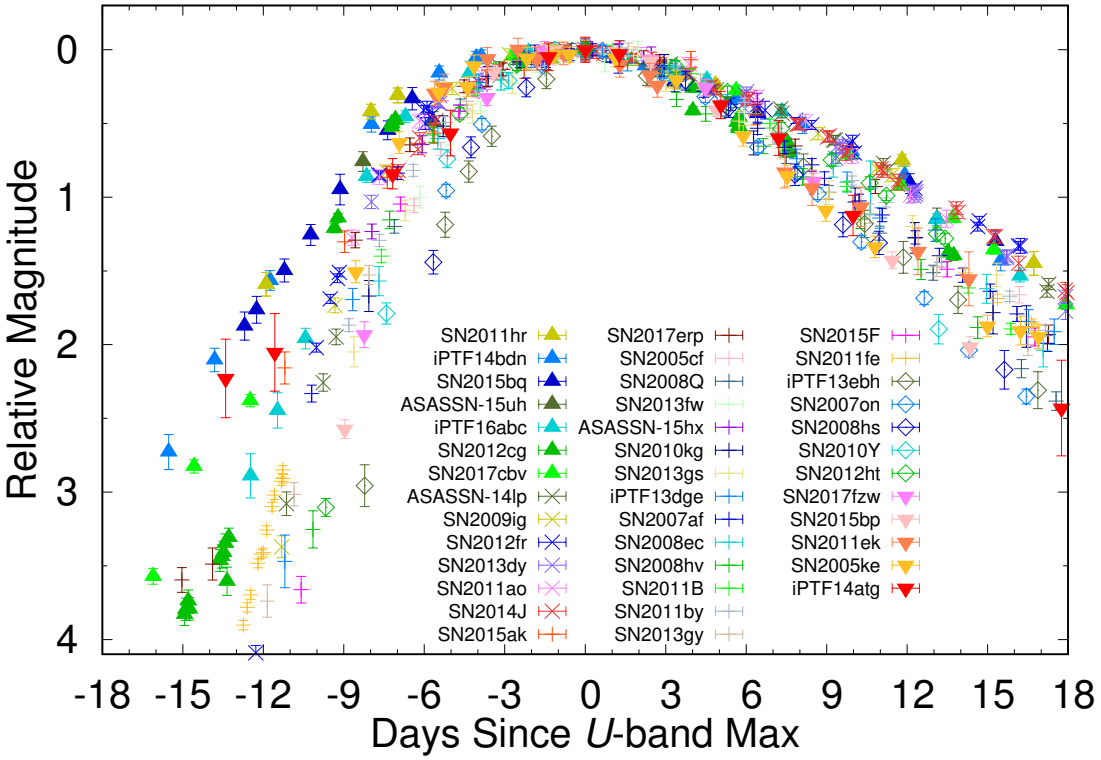

Figure 40: Early-phase U-band light curves of different SN Ia subclasses. Symbols are the same as in Figure 39. All light curves are shifted to the same peak magnitude for comparison. Early light-curve excess can still be clearly discovered in 91T/99aa-like SNe Ia and a 02es-like SN Ia, iPTF14atg. Two normal SNe Ia, SN 2017erp and SN 2015ak, show marginal early-excess features in the U band. The SNe Ia in other classes show smoothly rising light curves in the early phase.

SN 2015bq was discovered by the intermediate Palomar Transient Factory (iPTF; Law et al., 2009, Rau et al., 2009) and well followed by *Swift*/UVOT from about 2 weeks before the B-band maximum. The high-luminosity, slow-evolving light curve, together with early-phase spectra composed by prominent IGE and inconspicuous IME absorptions, indicate that SN 2015bq

is a typical 91T-like SN Ia. Interestingly, the prominent early light-curve excess of SN 2015bq shows very high similarity to two other 91T-like SNe Ia, iPTF14bdn and SN 2011hr, which indeed is much stronger than that of all 99aa-like EExSNe Ia. In §4.3.2, we discuss the intrinsic connection between 91T-like and 99aa-like EExSNe Ia and the possible explosion mechanism of these luminous objects.

ASASSN-15uh was reported as a 98es-like SN Ia by the Asiago Transient Classification Program (Tomasella et al., 2014, Turatto et al., 2015). Due to the limited photometric and spectroscopic information of both the SN and its host galaxy, we took a low-resolution spectrum of the host galaxy with the Line Imager and Slit Spectrograph (LISS; Hashiba et al., 2014) mounted on the Nayuta 2-m telescope in December 2017. We derived a host redshift of about 0.0150 by using hydrogen emission lines, which is consistent with the reported redshift of the supernova ($\sim$0.0135; Turatto et al., 2015). High UV luminosity and slow-evolving light curve match those of 91T/99aa-like SNe Ia well. Spectroscopically, shallow IME absorptions together with prominent IGE absorptions around 10 days before the *B*-band maximum are also reminiscent of 99aa-like SNe Ia. For the early-phase light curve, a possible early-excess feature can be marginally distinguished from the earliest observation at $\sim$8 days before the U-band maximum (Figure 40). Since the early-phase information of ASASSN-15uh is insufficient to determine the rising behavior, we mark ASASSN-15uh as a possible EExSN Ia candidate and do not make a quantitative comparison with other luminous EExSNe Ia in the next section.

4.2.3 SN 2017erp, the first normal EExSN Ia?

SN 2017erp was discovered at $\sim$17 days before its *B*-band maximum. Its early-phase spectral features, such as clear IME absorptions and high Si II velocity, show a good similarity to those of a normal SN Ia, SN 2003W (Jha et al., 2017). Particularly, early *Swift*/UVOT observations of SN 2017erp show interesting rising behavior in UV/optical wavelengths (Figures 38–40; see Brown et al. (2018) for more complete multiband light curves), which well meets our criteria of an early-broad EExSN Ia, especially for the $UVW1$-band light curve. Except for the peculiar early-phase light curve, a relatively slow-decline light curve toward the *B*-band peak magnitude of ~ -18.9 (Galactic extinction corrected) and the spectral evolution (Brown et al., 2018) of SN 2017erp resemble those of normal SNe Ia, such as SN 2009ig and SN 2013dy. No matter what kind of mechanism accounts for the peculiar early-phase light curve of SN 2017erp, an early-broad early excess discovered in a normal SN Ia inspires us that the early light-curve excess can also be expected in a fraction of normal SNe Ia.

The normal-type EExSNe Ia may have been discovered even earlier. The prompt *Swift*/UVOT

follow-up observation of SN 2015ak, a 99ee-like normal SN Ia identified by Hosseinzadeh et al. (2015), shows a similar early-phase light-curve behavior to that of SN 2017erp, though the photometric uncertainty is much larger. The limited post-maximum information suggests that the light-curve evolution is normal-like and the *Swift*/UVOT B-band peak magnitude is ~ -18.5 mag by adopting the redshift of the reported host galaxy. Due to the uncertainties in both the SN classification and the early-excess identification, we conservatively mark SN 2015ak as a likely normal EExSN Ia candidate.

4.2.4 iPTF14dpk, a CCSN discovered at the shock-cooling emission phase?

Cao et al. (2016b) claimed that iPTF14dpk is a 02es-like SN Ia viewed from the direction that is far away from a nondegenerate companion star based on the non-detection of early light-curve excess and moderate similarities to iPTF14atg. We argue that the identification of this object is disputable because 1) a subluminous R-band light curve and limited spectral information* prevent us from identifying whether iPTF14dpk is a 02es-like, 02cx-like SN Ia or an SN Ic; 2) a starburst host galaxy is different from the hosts of all previously discovered 02es-like SNe Ia but commonly seen in 02cx-like SNe Ia, and also CCSNe where massive stars are actively formed; 3) according to the limiting magnitude of the last non-detection of iPTF14dpk, its R-band magnitude increased to ~ -17 with a rising speed over -1.8 mag night^{-1} (Figure 38). Such a peculiar early light-curve behavior cannot be reproduced by any early-excess mechanism of SNe Ia but resembles the cooling tail of shock breakout of CCSNe, the rising phase of which is too short to be caught by a day-cadence survey (e.g. SN 2006aj, Campana et al., 2006; SN 2011dh, Arcavi et al., 2011; iPTF15dtg, Taddia et al., 2016).

Ambiguous classifications between subluminous SNe Ia and stripped-envelope CCSNe can happen sometimes. For example, although the spectral and light-curve resemblance between LSQ14efd and subluminous SNe Ia have been noticed by Barbarino et al. (2017), they classified LSQ14efd as an SN Ic based on the early-phase light curve (Figure 38) and the incompatible Si II velocity evolution to that of normal SNe Ia and a 02cx-like SN Ia, SN 2008A. We note that their argument about the velocity evolution can only exclude a part of SNe Ia but some subluminous SNe Ia (e.g. iPTF14atg) may have similar Si II velocity evolution to that of LSQ14efd. However, given that both LSQ14efd and iPTF14dpk show unique early-excess features as opposed to other EExSNe Ia and the lack of crucial evidence for the SN classification, we argue that both objects are more likely CCSNe discovered at the shock-cooling phase.

*Spectra of iPTF14dpk were obtained at -10, $+20$, and $+50$ days after the R-band maximum, which are also similar to spectra of some SNe Ic at the same epochs, e.g. SN 2004aw (Taubenberger et al., 2006).

4.3 Multiple Origins of Early-excess Type Ia Supernovae and Associated Subclasses

4.3.1 The fraction of EExSNe Ia and its implications

Current early-excess scenarios can be classified into two different types in terms of the physical mechanism: interaction-induced (i.e. companion and CSM interaction) and surface-radioactivity-induced (i.e. He-det and "surface-^{56}Ni-decay") scenarios. Recent simulations suggest that multiband photometric information during the early-excess phase is crucial for differentiating early-excess scenarios (e.g. the color evolution predicted by CSM interaction is generally faster than other scenarios, the companion-interaction may have relatively blue and slow color evolution at the early-excess phase, etc.; see Maeda et al., 2018 for details). However, the scatter of ^{56}Ni-powered early-phase light curves (Firth et al., 2014), the viewing angle effect, and uncertainties of current simulations (especially in the UV wavelength) may prevent us from differentiating early-excess scenarios in some cases. Therefore, further evidence from simulation-independent perspectives is particularly important. Since different early-excess scenarios may not only give rise to different early-excess fractions due to the viewing angle effect but also relate to specific SN Ia subclasses, statistically investigating the fraction of EExSNe Ia in each subclass can be a good starting point (Table 8).

Under the companion-interaction scenario, the early-excess feature can be observed only from specific viewing angles, which constrains the observable EExSNe Ia fraction to $\sim$10% (Kasen, 2010). Then, the probability of $\sim 10^{-6}$ for a 100% early-excess detection of six 91T/99aa-like SNe Ia suggests that the early light-curve excess of 91T/99aa-like SNe Ia should be attributed to a different early-excess scenario.

The CSM-ejecta interaction through the WD-WD merging channel is also difficult to explain early light-curve excess of 91T/99aa-like SNe Ia for the following reasons: i) short-lived carbon absorptions shown in 91T/99aa-like SNe Ia imply a low carbon-abundance environment; ii) such a high early-excess fraction suggests a spherical distribution of CSM to eliminate the viewing angle effect, which may be difficult to realize because the CSM-interaction early excess requires a short lag time between the secondary WD disruption and the SN explosion (Raskin and Kasen, 2013, Tanikawa et al., 2015, Levanon et al., 2015, 2017); iii) the long early-excess durations of some luminous SNe Ia require a tremendous amount of CSM that is difficult to be produced by disrupting a companion WD (Maeda et al., 2018). Therefore, the detection of early light-curve excess in all 91T/99aa-like SNe Ia suggests the physical connection between early excess and the explosion mechanism (which may also be related to a specific progenitor

Table 8: Supplementary Information on Early-phase SNe Ia in Different Subclasses and Their Early-excess Fractions

Subclass	Early-phase SNe Ia Golden (Final[a])	EExSNe Ia Golden (Final)	EEx Fraction Golden (Final)	Observed Rising-time Limit[b]	Photometric-depth Limit[c]	Host Type
Normal	12 (17)	0 (1)	0 (5.9%)	18.2 (iPTF13dge)	7.3 (SN 2011fe; *g*)	Various
91T/99aa-like	4 (6)	4 (6)	100% (100%)	18.9 (SN 2017cbv)	5.5 (iPTF16abc; *g*)	Late-type
Pec-luminous	2 (1)	1 (1)	50% (100%)	19.9 (LSQ12gpw)	3.7 (iPTF13asv; *R*48)	Late-type
Transitional	2	0	0	15.8 (SN 2012ht)	5.9 (iPTF13ebh; *R*48)	Various
02es-like	2	2	100%	18.5 (iPTF14atg)	3.8 (iPTF14atg; *R*48)	Early-type
He-det	1	1	100%	19.6 (MUSSES1604D)	5.2 (MUSSES1604D; *g*)	Early-type

Note.

[a] Since the earliest *R*-band photometry of iPTF13asv is about 1-2 days later than that of other luminous early-phase SNe Ia and there is no early UV/blue-optical photometry for this object, we exclude iPTF13asv from the final sample for the early-excess fraction calculation. Instead, we include five additional normal SNe Ia, SN 2007af, SN 2008hv, SN 2013gy, SN 2015ak, and SN 2017erp, and two 91T/99aa-like SNe Ia, SN 2011hr and SN 2015bq, which have the earliest UV/blue-optical information among other non-golden *Swift*/UVOT samples, in the final estimation.

[b] The "observed rising-time limit" is the longest time interval (rest-frame) from the detection to the *B*-band maximum (the champion SN's name is shown in parentheses) in each SN Ia subclass.

[c] The "photometric-depth limit" is the largest magnitude difference between the detection and the maximum in the same band (the champion SN's name and the corresponding filter are shown in parentheses) in each SN Ia subclass.

system) of these luminous objects.

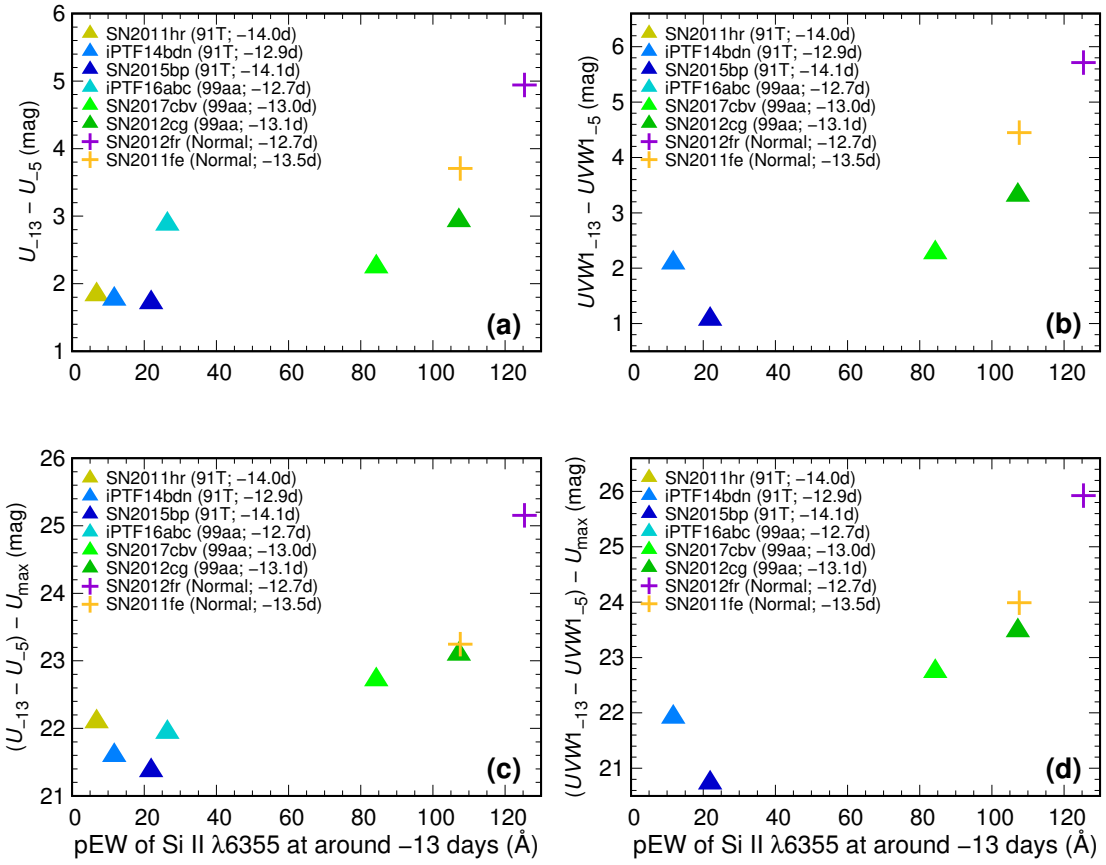

Figure 41: Early $UVW1/U$-band excess vs. the pseudo-equivalent width (pEW) of the Si II λ6355 line at about 13 days before the B-band peak of 91T/99aa-like EExSNe Ia. In order to maximize the sample size of 91T/99aa-like EExSNe Ia for the comparison, we use the magnitude variance from about -13 to -5 days after the peak epoch in the $UVW1/U$ band to describe the early-excess strength (panels (a) and (b)). Two normal SNe Ia that have both photometric and spectroscopic information at a similar epoch are included as references. In panels (c) and (d), the correlation between the pEW of the early Si II λ6355 line and the early-excess strength is still clear after normalizing the magnitude variance to the U-band peak magnitude for each SN, suggesting that the proposed correlation is unlikely to be related to the SN's intrinsic brightness. The epoch (relative to the B-band maximum) of each spectrum used for the pEW calculation is shown in the legend.

Although early excess is always shown in 91T/99aa-like SNe Ia, a large scatter of the early-excess strength can be found in Figures 39 and 40, which is barely related to the luminosity of main-body light curves. Instead, a likely correlation between the early-excess strength and the equivalent width of the Si II λ6355 line* is shown in Figure 41: a 91T/99aa-like SN Ia with

*In order to maximize the sample size of 91T/99aa-like EExSNe Ia for comparison, we use the magnitude variance from about -13 to -5 days after the peak epoch in the $UVW1/U$ band to describe the early-excess strength. The smaller the magnitude variance, the stronger the early light-curve excess. Spectra used for the pseudo-equivalent width (pEW) calculation were taken around -14–-13 days after their B-band

a shallower Si II λ6355 absorption has more prominent EEx. In other words, 91T-like SNe Ia generally have stronger early-excess features than 99aa-like SNe Ia. Such a correlation is independent of the peak luminosity (panels (c) and (d) in Figure 41).

Defining a "non-EExSN Ia" is tricky, as it depends not only on the performed early-phase observations (cadence, imaging quality, wavelengths, etc.) but also on the strength of the early excess itself. By using the golden early-phase SNe Ia and other SNe Ia which have early-enough UV/NUV information, we try to present the currently "best" non-EExSN Ia sample for the early-excess fraction estimation. However, we note that even for some golden early-phase SNe Ia (e.g. SN 2010jn), it still remains a possibility that the non-EEx detection is due to the dimness of the early excess and/or unfavorable observing wavelengths (e.g. V and R band). In other words, the early-excess fraction shown in this thesis is a somewhat lower limit due to the probable incompleteness of early-excess detections from previous observations. Therefore, an early-excess fraction of 5.9% (one of a total of 17 normal early-phase SNe Ia, which include 12 golden SNe Ia and five additional SNe Ia, SN 2007af, SN 2008hv, SN 2013gy, SN 2015ak, and SN 2017erp, that have the earliest UV/blue-optical photometric data among other non-golden normal SNe Ia*) or 11.8% (by counting both SN 2017erp and SN 2015ak as normal EExSNe Ia) for normal SNe Ia cannot exclude any early-excess scenario.

There were several attempts at searching for EExSNe Ia with datasets from large supernova survey projects (Hayden et al., 2010, Bianco et al., 2011, Ganeshalingam et al., 2011), but none of them reported a positive early-excess detection. We argue that the previous studies are not in conflict with the high early-excess fraction of 91T/99aa-like SNe Ia proposed in this thesis for the following reasons. i) Since the purpose of those studies is to find significant early-excess features for testing the companion-interaction scenario (especially for the red-giant companion condition) by comparing their early-phase light curves with the model light curve predicted by Kasen (2010), they do not further investigate the "small" early light-curve scatter in their plots. ii) Although only six 91T/99aa-like SNe Ia with very limited early-phase data points are included in Ganeshalingam et al. (2011; see Figure 3 therein), it is clearly shown that the large light-curve scatter at early phase is related to 91T/99aa-like SNe Ia. iii) The early light-curve scatter shown in Figure 1 of both Hayden et al. (2010) and Bianco et al. (2011) is similar to the scatter in Figure 38 of this thesis, which may also relate to 91T/99aa-like SNe Ia in their samples. Since the sample composition in both papers is not clearly mentioned, further analysis of those samples may increase the total number of EExSNe Ia and improve the EEx-fraction estimation. Indeed, our finding about the correlation between early light-curve excess

maxima.

*Given that some normal SNe Ia in our *Swift*/UVOT sample are not early enough for the non-EEx classification, we only include 12 golden normal SNe Ia and five additional normal SNe Ia, SN 2007af, SN 2008hv, SN 2013gy, SN 2015ak, and SN 2017erp, which have UV/blue-optical information at about 10 days before their maxima in the same band.

and 91T/99aa-like SNe Ia can be further supported by a very recent work by Stritzinger et al. (2018), which suggests that 91T/99aa-like SNe Ia tend to show very blue $B-V$ color evolution in the early phase. In addition to statistical studies, early-phase photometries of two *Kepler*-discovered SNe Ia, KSN 2012a and KSN 2012b, give good constraints on the non-EEx detection of two SNe (Olling et al., 2015), although we exclude them from the fraction calculation due to a lack of the spectroscopic identification. Given that both are more like normal SNe Ia in terms of the light-curve behavior, the non-EEx detections of two SNe should not influence the early-excess fraction of 91T/99aa-like SNe Ia but may slightly decrease the early-excess fraction of normal SNe Ia.

4.3.2 From normal to super-$M_{\rm Ch}$ SNe Ia, the diversity and their intrinsic connections

In order to explain the IGE-dominant absorptions in the early spectra of 91T/99aa-like SNe Ia, a more efficient detonation reaching the outermost region of the ejecta is frequently proposed (e.g. Zhang et al., 2016). This may account for the early light-curve enhancement due to high ^{56}Ni production in the outer layer of the ejecta (Piro and Morozova, 2016). However, as opposed to a spike-like early excess powered by a large amount of fast-decay radioactive elements from a precursory detonation of a thin He-shell predicted by the He-det scenario, a broadened, possibly bump-like early-phase light curve will be formed due to the radioactivity of substantial ^{56}Ni at the outermost region of the ejecta. Such a prediction is indeed reminiscent of the early-rising behavior of luminous EExSNe Ia (Figures 39 and 40).

Such an efficient detonation is expected in an extreme case of the delayed-detonation model, represented by the so-called gravitationally confined detonation (GCD; Plewa et al., 2004, Townsley et al., 2007, Jordan IV et al., 2008, Meakin et al., 2009). The buoyantly rising deflagration bubble ignited near the stellar core will finally trigger a detonation at the opposite pole from the breakout location of the deflagration bubble. Thanks to the mild expansion before the bubble reaches the surface, the detonation is more efficient than the traditional delayed-detonation scenario (Niemeyer and Woosley, 1997) and thus results in a larger amount of ^{56}Ni extended to the ejecta's surface. According to Jordan IV et al. (2012), the detonation happens at the antipodal point from where the star ejected the ash from its interior, giving rise to approximately azimuthal symmetry upon the system. Therefore, the diversity of element distribution due to the viewing angle effect can be expected, e.g. more ^{56}Ni will be generated at the surface on the opposite side of the off-center ignition point. Since the asymmetry of the detonation becomes smaller when getting to the inner region of the WD, the viewing angle effect in the earlier phase is more prominent. Such a prediction is basically in line with recent 3D simulations

(Seitenzahl et al., 2016).

Although spectra produced by Seitenzahl et al. (2016) show clear distinctions from SN 1991T after taking into account the viewing angle effect, shallower-than-normal IME absorptions and luminous and slow-evolving light curves are qualitatively consistent with typical features of 99aa-like SNe Ia. Nevertheless, their simulation shows that only UV/NUV light curves and spectral features at wavelengths $\lesssim 5000$ Å highly depend on the viewing angle, which suggests that a main spectral difference between 91T- and 99aa-like SNe Ia, the Si II absorptions, cannot be completely attributed to the viewing angle effect through the GCD scenario.

Simulations of the GCD scenario also indicate that by switching the offset distance of the ignition point, the total ^{56}Ni amount (and thus the early-excess strength) and spectral features can be varied. In order to explain the extreme spectral features of 91T-like SNe Ia with the GCD scenario, an intuitive extrapolation is that 91T-like SNe Ia that have the strongest early excess and shallowest IME features correspond to the most extreme offset condition. By taking into account both the off-center level and the viewing angle effect, spectral differences between 91T- and 99aa-like SNe Ia, the correlation between the early-excess strength and the equivalent width of the Si II λ6355 line, and the luminosity scatter shown in 91T/99aa-like SNe Ia could be promisingly explained with the GCD scenario. In order to further testify to the GCD scenario and its relation to luminous SNe Ia, it is encouraged to investigate the upper limit of the initial offset and multiple-bubbles-triggered GCD models in future simulations.

For the progenitor system of 91T/99aa-like SNe Ia, since the GCD-induced early excess can be realized through both single- and double-degenerate channels if the mass of merged WDs can reach the Chandrasekhar mass limit, early-excess features of 91T/99aa-like SNe Ia may not provide direct information on their progenitor systems.

A further question is whether both 91T/99aa-like and normal SNe Ia have the same origin. In principle, the luminosity and spectral features of normal SNe Ia can be reproduced by decreasing the offset distance of the ignition point so that the GCD scenario will finally get back to the traditional delayed-detonation scenario, which can also give rise to the smooth, small-scatter rising light curves that we see in normal SNe Ia. For the progenitor system of two SN Ia subclasses, non-detections of a surviving companion star and hydrogen emission lines in the nebular phase spectra of normal SNe Ia so far are in conflict with predictions by the SD progenitor scenario (Schaefer and Pagnotta, 2012, Mattila et al., 2005, Leonard, 2007, Shappee et al., 2013, Lundqvist et al., 2013, Maguire et al., 2016), which is in opposition to the growing evidence of the possible connection between 91T/99aa-like SNe Ia and the SD progenitor scenario (Leloudas et al., 2015). Therefore, even with the same explosion physics (note that GCD in

nature is a special case of the delayed-detonation scenario), normal and luminous SNe Ia may originate from different progenitor systems (Fisher and Jumper, 2015).

If the amount of surface ^{56}Ni is moderate compared with that of 91T/99aa-like SNe Ia, we may see an early-broad EExSN Ia instead of a bump-like one, which not only is in line with the early-phase light curve of SN 2017erp and previous simulations (Piro and Morozova, 2016) qualitatively but may also explain some "slow rising," "fast decline" light curves found in previous statistical studies (Hayden et al., 2010, Ganeshalingam et al., 2011). However, if the surface-^{56}Ni-decay scenario accounts for the early excess of the normal SN Ia SN 2017erp and the candidate SN 2015ak, a further question is why the ^{56}Ni radiation through the traditional delayed-detonation scenario can realize such a large early light-curve scatter in normal SNe Ia. One possible explanation is that a small offset degree of the ignition point may also exist even under the traditional delayed-detonation scenario (Maeda et al., 2010). In order to further understand the origin of such inconspicuous early excess shown in normal SNe Ia, a comprehensive investigation of SN 2017erp and SN 2015ak is highly recommended.

As we mentioned in §4.1.2, early light-curve excess is also found in a 09dc-like SN Ia, LSQ12gpw, at $\sim$20 days before the B-band maximum. Although the explosion mechanism and progenitor system of super-$M_{\rm Ch}$ SNe Ia are still under debate, previous observations show evidence of dense CSM around super-$M_{\rm Ch}$ SNe Ia. Yamanaka et al. (2016) reported the near-infrared light echo from $\sim$40 to 110 days after the B-band maximum of a super-$M_{\rm Ch}$ SN Ia candidate, SN 2012dn, suggesting the presence of a wind from the pre-explosion system, possibly through the SD channel. If such a dense CSM can be formed nearer to the explosion site, not only the companion interaction but also the CSM interaction may explain the early light-curve excess of LSQ12gpw under the SD progenitor scenario.

On the other hand, Taubenberger et al. (2013) pointed out that the discrepancy between the extremely luminous peak and the faint light-curve tail of the super-$M_{\rm Ch}$ SN Ia SN 2009dc may require additional energy injection at early phase (see also Maeda and Iwamoto, 2009), i.e. the interaction between SN ejecta and nearby CSM. Such confined CSM could be realized through the double-degenerate (DD) channel as the envelope predicted by the merger scenario would be ejected soon after the disruption of the secondary WD (Levanon et al., 2015, Tanikawa et al., 2015). Under the CSM-interaction scenario through the DD channel, not only the prominent early light-curve excess of LSQ12gpw but also the persistent C II features that are commonly shown in super-$M_{\rm Ch}$ SNe Ia could be explained. Furthermore, although only one early-phase super-$M_{\rm Ch}$ SN Ia (i.e. LSQ12gpw) has been found, the discovery of early excess in this super-$M_{\rm Ch}$ SN Ia may imply an early-excess scenario that is weakly affected by the viewing angle effect. Therefore, we speculate that the early light-curve excess in super-$M_{\rm Ch}$ SNe Ia is more

likely powered by the CSM interaction through either the DD or the SD channel. Given that the CSM components are possibly dominated by different materials in two progenitor systems, spectroscopy at the early-excess phase may provide new evidence of the progenitor system of super-$M_{\rm Ch}$ SNe Ia.

4.3.3 The companion-interaction EExSNe Ia

The statistical study of EExSNe Ia not only further supports the multiple origins of previously discovered early excess but also reduces the possibility of the connection between luminous EExSNe Ia and the companion-interaction scenario to a large extent.* However, as opposed to the bump-like early excess of 91T/99aa-like SNe Ia, a spike-like early excess of the subluminous EExSN Ia, iPTF14atg, cannot be interpreted by the ^{56}Ni radioactivity from the outermost layer of the ejecta. Additionally, recent simulations by Maeda et al. (2018) also indicate a significant discrepancy between the early-phase light curve of iPTF14atg and their CSM-interaction models.

Although the early excess of iPTF14atg seems to be promisingly reproduced with the companion interaction (Cao et al., 2015, Maeda et al., 2018), whether its spectral evolution and general light-curve behavior can be reproduced through the SD channel is still under debate (Kromer et al., 2016). Alternatively, as we discussed in §4.2.1 (also see Maeda et al. 2018), in terms of the spectral and early-excess resemblance between MUSSES1604D and iPTF14atg, the He-det scenario is also promising for explaining 02es-like EExSNe Ia. As the current early-phase information of 02es-like SNe Ia is too limited to make a comparative analysis or give a stringent constraint from the statistical perspective, finding more early-phase 02es-like SNe Ia through ongoing transient surveys will shed light on the nature of this peculiar SN Ia subclass.

4.4 Summary of Chapter 4

In this chapter, we present general information on published, well-observed early-phase SNe Ia so far and summarize the characteristics of 11 (six reported and five unnoticed) EExSNe Ia in different subclasses. In particular, by investigating the connections and differences between these EExSNe Ia, new evidence of multiple origins of early light-curve excess and the implication for the explosion mechanism of 91T/99aa-like SNe Ia are presented.

*Note that if 91T/99aa-like SNe Ia truly originate from the SD progenitor system, it remains a possibility that the early light-curve excess of a small fraction of luminous SNe Ia may have multiple components.

We found that a 100% early-excess detection in six early-phase 91T/99aa-like SNe Ia is significantly in conflict with the prediction of the companion-interaction scenario but can be promisingly explained by the radioactive decay of a ^{56}Ni-abundant outer layer or, alternatively (but less likely), interacting with spherically distributed CSM. In addition, the discovered correlation between the Si II absorption feature and the strength of early excess also suggests an intrinsic connection between the explosion mechanism and the early light-curve excess of 91T/99aa-like SNe Ia. By investigating the early-excess behavior, post-EEx photometric/spectroscopic properties, and explosion models proposed for luminous SNe Ia, the surface-^{56}Ni-decay scenario is preferred for interpreting 91T/99aa-like EExSNe Ia. Specifically, we argue that the gravitationally confined detonation is a promising scenario for producing 91T/99aa-like SNe Ia with such a high early-excess fraction. Also, spectral and early-excess differences between 91T- and 99aa-like SNe Ia and their intrinsic luminosity scatters could be qualitatively explained by taking into account the variation of the off-center distance of the initial ignition point and the viewing angle effect. In contrast to the high early-excess fraction of luminous SNe Ia, early light-curve excess discovered in a normal SN Ia, SN 2017erp, and a possible candidate, SN 2015ak, so far suggests that early excess may accompany with a fraction of normal SNe Ia. Whether the early excess shown in normal SNe Ia is attributed to surface ^{56}Ni decay through the traditional delayed-detonation mechanism requires further investigation.

Even though about a dozen of EExSNe Ia were successfully discovered in various SN Ia subclasses, we have not found any crucial evidence to support the companion-interaction scenario, even for the most promising candidate, iPTF14atg. The multiple origins of early light-curve excess suggest that EExSNe Ia may not be a superior indicator of the SD progenitor system as we originally expected, and we need to be more cautious when interpreting any newly discovered EExSNe Ia. A schematic diagram of the possible connections between different early-excess scenarios and their corresponding SN Ia subclasses based on our studies (Chapters 3 and 4) is shown in Figure 42. Further understanding of the early-excess scenarios relies not only on individual studies of well-observed EExSNe Ia but also on systematical investigations of the early-phase light-curve behavior of each SN Ia subclass, which can be realized with ongoing survey projects such as the Zwicky Transient Facility (ZTF; Smith et al., 2014), MUSSES (Chapter 3), and forthcoming transient surveys with the Tomo-e Gozen Camera mounted on the 1.05-m Kiso Schmidt telescope (Sako et al., 2018) and the Large Synoptic Survey Telescope (LSST; Ivezić et al., 2008) in the near future.

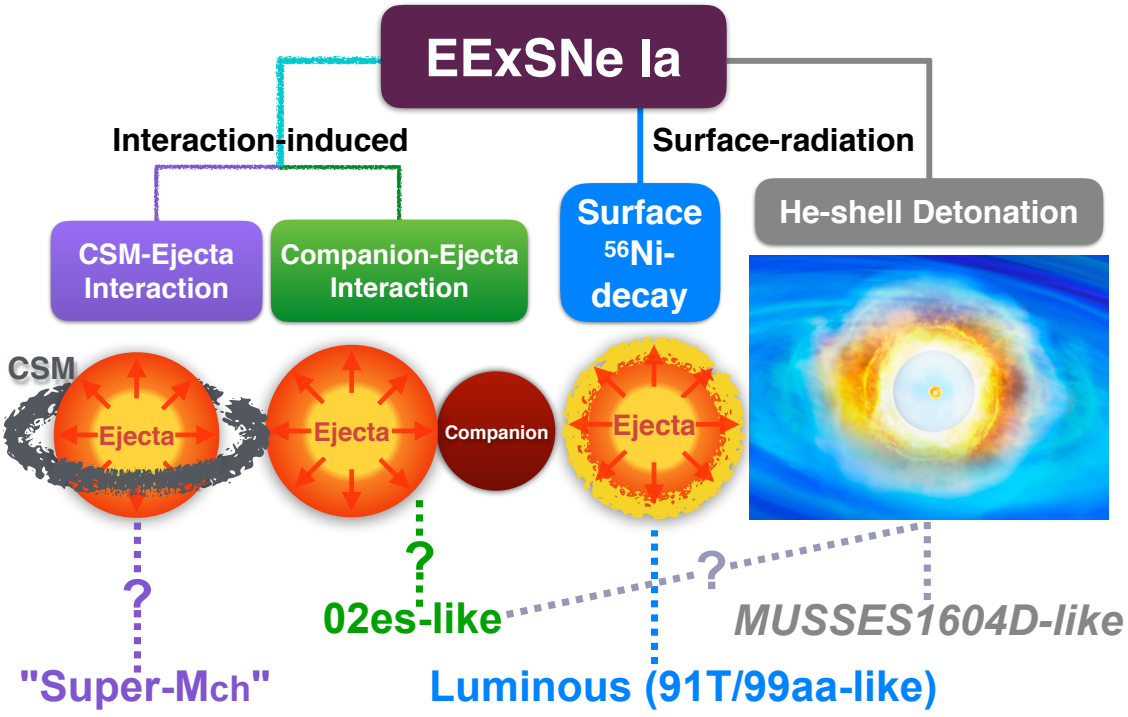

Figure 42: A schematic diagram showing the possible connections between different early-excess scenarios and their corresponding SN Ia subclasses. For luminous 91T/99aa-like SNe Ia, their early-excess features can be well explained by the surface-^{56}Ni-decay scenario. Interaction between extended CSM and ejecta can explain both early excess and ultra-high luminosity of super-$M_{\rm Ch}$ SNe Ia qualitatively. Whether or not the early light-curve excess shown in 02es-like subluminous SNe Ia originates from the companion-ejecta interaction is still under debate. The He-shell detonation scenario is likely related to specific SN Ia subclasses, such as MUSSES1604D-like and possibly, 02es-like SNe Ia.

5 A Future Plan of Early-phase SNe Ia Study in the HSC–Tomo-e Era

As the broad adoption of large-array CCD cameras in astronomical observations, great breakthroughs in time-domain astronomy have been made through various transient survey programs in the last decade (Nugent et al., 2011, Cao et al., 2015, Dong et al., 2016, Smartt et al., 2017). In 2019, Japanese astronomical community will have both "deep-wide" (Subaru/HSC) and "shallow-wide" (Kiso/Tomo-e; Sako et al., 2018) survey facilities. We are now stepping into a golden era of time-domain astronomy.

Thanks to the large telescope aperture and field of view of Subaru/HSC and the extremely high survey efficiency of Kiso/Tomo-e, transient studies especially for early-phase SNe and other faint, rapidly rising transients can be well carried out with these powerful survey facilities. Therefore, future transient surveys will aim for not only early-phase SNe Ia but also various kinds of transients that show significant brightness variance in days, hours, or even shorter timescales (hereafter "rapid transients"), which can be classified into early-phase SNe and tidal disruption events (TDEs), fast-evolving luminous transients, kilonovae, and unknown types in general. Rapid transient surveys with HSC and Tomo-e will help us to figure out the nature of these high-energy phenomena in the Universe.

5.1 Early-phase SNe Ia Study with the Tomo-e Gozen Camera

The next-generation wide-field camera, the Tomo-e Gozen camera (or Tomo-e for short), will be put into use for the Kiso 1.05-m Schmidt telescope from April 2019. In contrast to traditional CCD cameras, the negligible readout time of the CMOS sensor enables us to carry out unique high-cadence survey observations with Tomo-e.

5.1.1 The Tomo-e Gozen camera

The Tomo-e Gozen camera is a mosaic CMOS camera with a field-of-view of about 20.7 deg^2 covered by 84 chips of 2k $\times$ 1k CMOS image sensors (Figure 43). The camera consists of four quadrant units symmetrical to each other, named as Q1, Q2, Q3, and Q4. Each camera unit has 21 chips of the CMOS sensor. A picture of the camera units Q1 and Q3 are shown in Figure 44. The sensor chips are fixed on a camera base along the spherical focal-plane of the Kiso Schmidt telescope via height adjustment plates (HAPs), the tops of which are diagonally cut.

A top cover, a window frame, and a bottom part are attached to the camera base. The window frame has 21 rectangle apertures where transparent windows, optical filters, and grism elements are installed. Electronics boards for sensor readout are attached on the bottom part. The four camera units are fixed on a focal plane interface (FPI) unit. The total weight of Tomo-e fixed on the focal plane of the telescope is about 57 kg. The data production rate of total four camera units is $\sim$830 MB sec^{-1} at 2-frame-per-second (fps) sampling, corresponding to approximately 30 TB in one night. GPS times are recorded at the beginning and the end of exposures of a frame set. Camera units Q1 and Q3 have been put into use since November 2018. The other two units will be completed by April 2019.

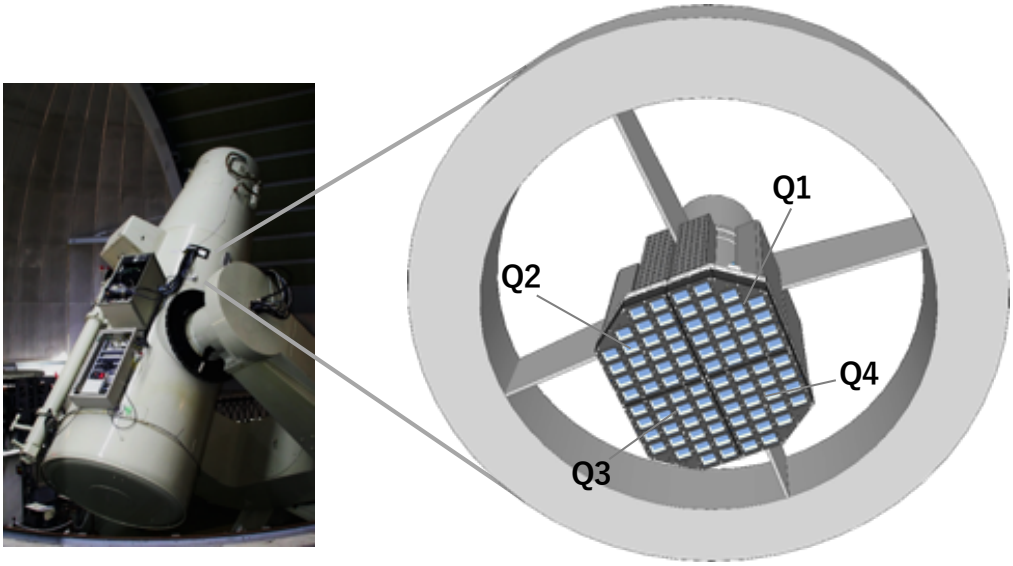

Figure 43: The Kiso Schmidt telescope and a schematic diagram of the front-side view of the Tomo-e Gozen camera. Q1, Q2, Q3, and Q4 correspond to four quadrant units of the camera (with 84 CMOS sensors in total). The complete Tomo-e Gozen camera will be mounted on the 1.05-m Kiso Schmidt telescope in April 2019.

5.1.2 The Tomo-e Gozen transient survey project

In order to maximize the detection efficiency of rapid transients, we plan to carry out a wide-field, high-cadence transient survey with Tomo-e from 2019. In general, Tomo-e will monitor $\sim$7,000 deg^2 sky area with the elevation higher than 40 deg at least 3 times per night.

Specifically, the on-source exposure time is 6 seconds per visit, reaching a limiting magnitude (5-σ) of 20 in a dark, clear night. In contrast to Pan-STARRS and ZTF, since the Tomo-e Gozen survey is designed to find brighter transients, we are able to easily carry out imaging follow-up observations with 1-m-class telescopes and spectroscopies with 2–4 m telescopes through domestic and international collaborations. The excellent instrument performance and the special survey mode make the Tomo-e Gozen transient survey one of the most powerful rapid transient surveys in the world.

During the Tomo-e Gozen transient survey, more than 1,000 SNe are expected every year. Particularly, several of them will be discovered within a few days of their explosions. Thanks to the high-cadence observing mode, a statistical investigation of the intra-night variability of a dozen of early-phase SNe Ia can be achieved by the end of 2020. In addition to early-phase SNe, other kinds of rapid transients can be investigated with Tomo-e as well. From 2019 to 2024, we expect to discover over 60 rapid transients through the Tomo-e Gozen transient survey.

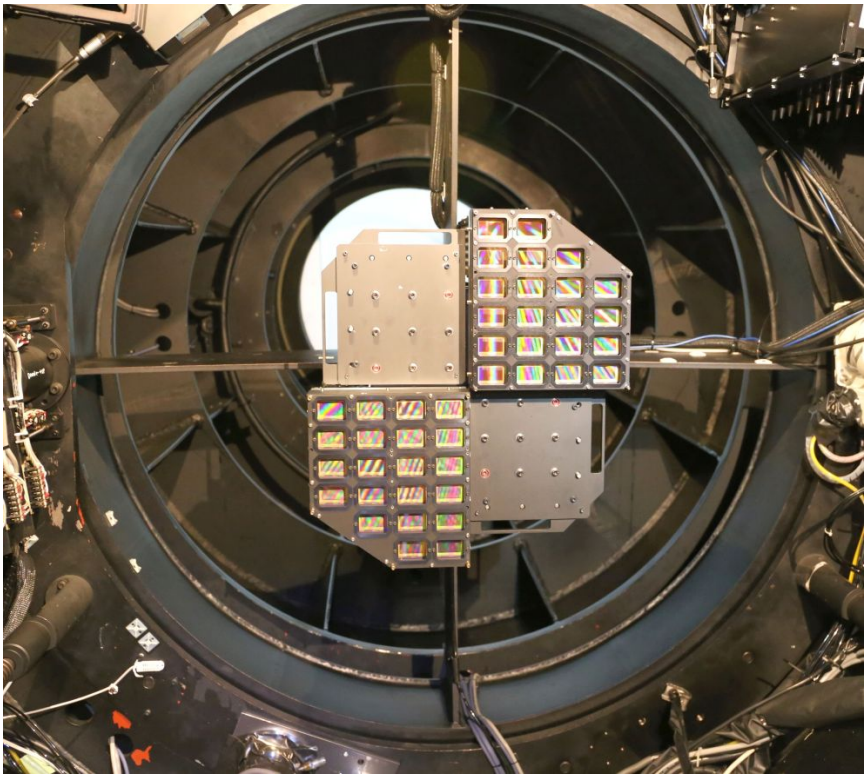

Figure 44: The camera units Q1 and Q3, mounted on the focal plane of the 1.05-m Kiso Schmidt telescope. Counterweights are installed on focal plane areas of Q2 and Q4 units. North and west directions on the sky correspond to upside and right-side on the sensors in this picture, respectively. Credit: Institute of Astronomy, the University of Tokyo.

5.2 MUSSES-FAST: A New-generation Transient Survey for Early-phase, Rapidly Brightening Transients

5.2.1 The innovation of Japanese time-domain surveys

Even though lots of scientific outputs have been achieved through time-domain surveys with a wide, shallow, and day(s)-cadence observing mode in the last decade, its limited observing depth (i.e. limiting magnitude) and low time resolution indeed prevent us from discovering early-phase SNe and other faint, rapid transients (e.g. kilonovae, Smartt et al., 2017; SN shock breakout, Campana et al., 2006, etc.) efficiently. Thanks to the large telescope aperture of Subaru, such interesting objects can be easily discovered with Subaru/HSC. In particular, as the brightness of those objects increases promptly, the efficiency of HSC survey can be further enhanced by running an synergetic survey with Kiso/Tomo-e. Based on this idea and our original HSC survey project led by the author, MUSSES (§3.2), we propose an innovative observing mode to further improve the survey capability of early-phase SNe with Subaru/HSC—the **MU**ltiple **S**imultaneous **S**urveys for **E**arly-phase **S**Ne and **FAS**ter **T**ransients (**MUSSES-FAST**).

5.2.2 MUSSES-FAST: A low-cost and high-yield rapid-transient survey

In general, MUSSES-FAST enables us to make the best use of both HSC and Tomo-e to study not only early-phase SNe but other rapid transients which show even shorter timescales. In each observing run, we plan to carry out three full/half-nights multiband Subaru/HSC observations to cover $\sim$200 deg^2 sky with a g-band limiting magnitude $\gtrsim$25.5. Simultaneously, Tomo-e will monitor the same region with a 45-min cadence (10–13 runs per night; a limiting magnitude of $\sim$22.5 for 4-runs (20 min exposure) stacked images) for about one week to catch HSC-discovered/undiscovered rapid transients (Figure 45). Once a rapid transient is discovered, multiband photometric and spectroscopic follow-up observations with over 10 telescopes all over the world will be triggered immediately. Such a global follow-up network has been well trained in previous Subaru/HSC observations.

MUSSES-FAST's advantages mainly include: 1) A unique combination of Subaru/HSC and Kiso/Tomo-e; The special locations of two telescopes and the high-cadence Tomo-e monitoring observations enable the proposed project to not only study the early-excess behavior (few-days duration) in great detail but also discover rapid transients with even shorter characteristic timescales (i.e. from minutes to hours). 2) An extremely high scientific productivity; We expect

to find around 50 early-phase SNe (SNe Ia & core-collapse SNe) and a dozen of other rapid transients every year (two observing runs). 3) A low dependence on the weather condition; Even if a portion of HSC observations are canceled out due to the weather issue, the synergetic observations by Tomo-e will ensure the discovery of some rapid transients. On the other hand, if the Tomo-e survey suffers the weather issue, MUSSES-FAST will transform to our original HSC survey mode (MUSSES) and the early-phase SNe Ia study can be carried out as usual.

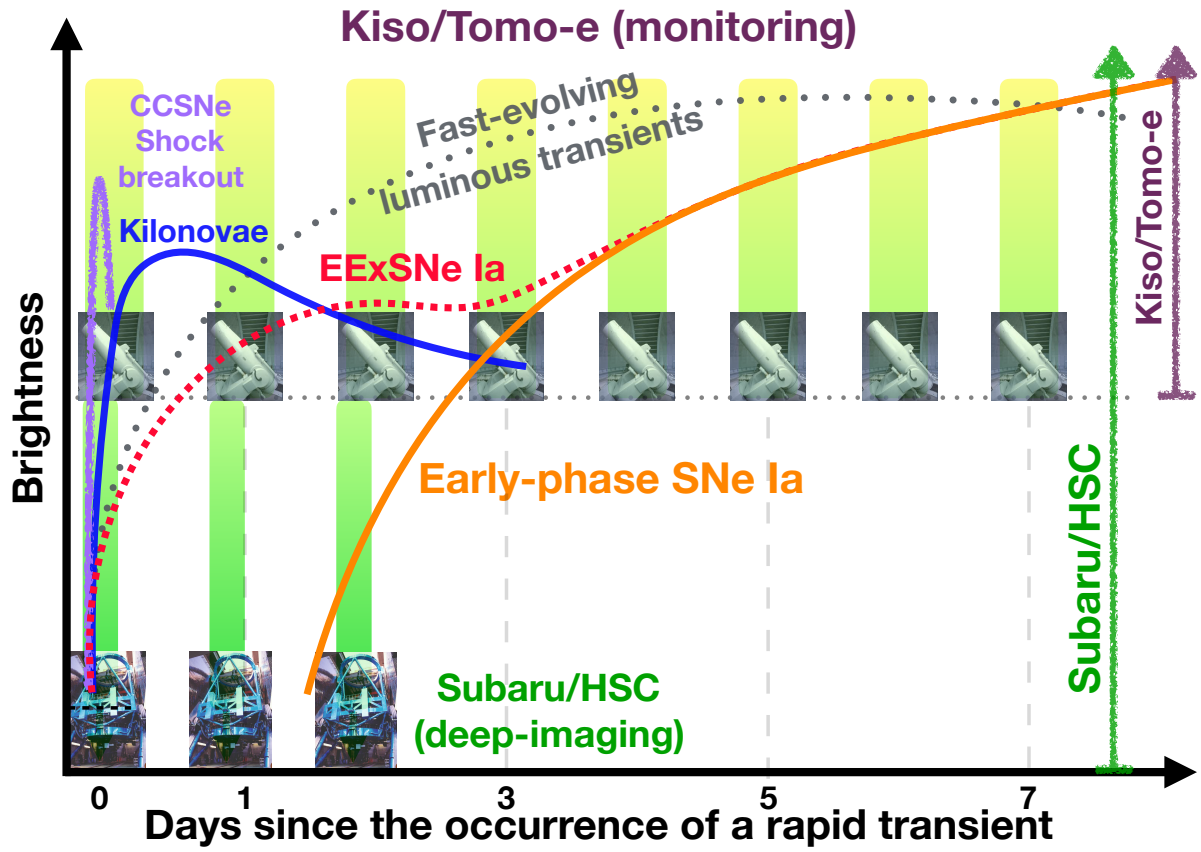

Figure 45: The observing mode of MUSSES-FAST. During the multiband HSC survey, Tomo-e will monitor all HSC-targeted regions every 45 minutes to catch HSC-discovered/undiscovered rapid transients. Most of rapid transients will be discovered by Tomo-e in the first few days of the monitoring observations (lasting for about one week). Light curves of typical rapid transients are shown in the plot.

5.2.3 The early-phase SNe Ia study with MUSSES-FAST

MUSSES-FAST is designed for studying not only early-phase SNe but also other transients that show significant brightening in a short timescale. In the thesis, only early-phase SNe Ia-related scientific objectives are given as follows.

I. A further investigation of the He-det SNe Ia

The discovery of a peculiar EExSN Ia, MUSSES1604D, clearly indicates that the so-called He-det scenario can also produce EExSNe Ia (§3.2). Therefore, the early-excess feature is important for studying not only the progenitor system but also the explosion mechanism of SNe Ia. As the first robust evidence of a specific kind of explosion mechanism of SNe Ia, further questions about the He-det scenario have also been emerged after the discovery of MUSSES1604D.

(i) What is the exact physical mechanism that triggers the He-shell detonation? Although a general He-det scenario can explain MUSSES1604D quite well, whether such a He-shell detonation is triggered by accreting mass from a He star (i.e. the double-detonation scenario, Nomoto, 1982a,b, Woosley and Weaver, 1994, Fink et al., 2007, 2010) or merging with a less massive white dwarf (i.e. the violent merger scenario, Shen and Bildsten, 2014, Shen et al., 2018) is still an open question. (ii) What kinds of SNe Ia originating from the He-det scenario and their proportions among all SNe Ia? A recent study of hypervelocity WDs which have been proposed as good candidates of survived WDs through the violent-merger He-det scenario implies that SNe Ia originating from the He-det scenario may occupy a considerable number of total SNe Ia (Shen et al., 2018). Figuring out the role that the He-det scenario plays in making SNe Ia is particularly important for the understanding of the origin of the SN Ia diversity and thus enables us to further purify SN Ia samples used for the measurement of the cosmological expansion. With MUSSES-FAST, above issues can be well studied by carrying out systematic investigations (e.g. not only multiband photometry but spectroscopy during the early-excess phase) of MUSSES1604D-like SNe Ia discovered in the near future.

II. Surface ^{56}Ni decay, the dominant early-excess scenario of SNe Ia?

Our recent work suggested that the majority of early light-curve excesses discovered so far are likely powered by the radiation from a large amount of ^{56}Ni formed at the outermost region of the ejecta, known as the surface-^{56}Ni-decay scenario (see Chapter 4 for details). Although such a scenario can explain the high early-excess fraction of luminous SNe Ia quite well, a further question is whether the surface-^{56}Ni-decay scenario commonly exists in various kinds of SNe Ia or exclusively associates with the luminous subclass, the answer of which is crucial to under-

stand if SNe Ia in different subclasses share the same explosion mechanism. In order to unveil the physical origin of the surface-^{56}Ni-decay scenario and its associated SN Ia subclass(es), we are planning to carry out more complete statistical analysis of the early light-curve behavior and estimate the early-excess fraction of each SN subclass with an enlarged early-phase SN Ia sample made by MUSSES-FAST.

III. Companion-interaction EExSNe Ia, discovered or not yet?

The debate between two popular progenitor scenarios of SNe Ia (i.e. the single-degenerate (SD) and the double-degenerate (DD) scenario) has been lasted for a long time. Recently, a growing number of studies suggested the existence of both scenarios in the Universe, while it is still an open question that which scenario plays a leading role in making SNe Ia. From the early-excess perspective, our recent study pointed out that almost all discovered EExSNe Ia are unlikely related to the companion-interaction scenario, thus implying a low possibility of the leading position of the SD scenario. Although the early-excess feature of iPTF14atg might be reproduced by the companion-interaction scenario (Cao et al., 2015, Maeda et al., 2018), whether or not its spectral evolution and the main-body light curve can be realized through the SD channel is still under debate (Kromer et al., 2016). Moreover, early-excess detections in both early-phase 02es-like SNe Ia, PTF10ops and iPTF14atg, may indicate an early-excess scenario that is less affected by the viewing angle effect. In terms of the weak viewing-angle dependence of the He-det scenario and the early-excess resemblance between MUSSES1604D and iPTF14atg, the He-det scenario may be more promising to explain iPTF14atg and other 02es-like EExSNe Ia. In order to figure out the progenitor system of this peculiar SN Ia subclass, an effective way is to give a more strict constraint on its early-excess fraction and make a further comparative analysis by using several early-phase 02es-like SNe Ia discovered by MUSSES-FAST in the near future.

Given that only a certain percentage of early-phase SNe Ia can show early-excess feature through the companion-interaction channel due to the viewing angle effect, a large number of non-EExSNe Ia discovered by MUSSES-FAST can be used to further test and improve the current companion-interaction models. Also, we hope to find robust evidence of the single-degenerate progenitor system by catching reliable companion-interaction EExSNe Ia in the next few years.

IV. A more advanced purification of the cosmologically used SNe Ia

Figuring out the long-standing diversity issue of SNe Ia is not only one of the ultimate goals of SNe Ia study but also crucial for the SN cosmology. In order to confirm the absolute magnitude of SNe Ia for the distance measurement, light-curve fitting based on previously well-observed

SN Ia samples are required. In principle, an SN Ia with a larger stretch factor should correspond to bluer color. However, as more and more SNe Ia have been discovered in recent years, a fraction of SNe Ia, such as MUSSES1604D, show intrinsically redder color while their light-curve stretch factors are also large. Such kind of objects may introduce the systematical error when applying SNe Ia as the distance indicator because their intrinsic brightness can be overestimated during the light-curve fitting. Therefore, figuring out the origin and fraction of such "red-broad" SNe Ia is important to further improve the accuracy of the cosmological use of SNe Ia. Since the early-phase information on SNe Ia provides a unique perspective to understand the physical origin of the SNe Ia diversity, by systematically investigating more than 50 early-phase SNe Ia in different subclasses, we aim to formulate more stringent selection criteria of the cosmologically used SNe Ia.

5.2.4 Scientific expectations and prospects

In the next few years, MUSSES-FAST will enable us to build the largest sample of early-phase SNe Ia. Thanks to the well-established follow-up network, about 32 early-phase SNe Ia can be investigated every year (assuming two MUSSES-FAST observing runs per year). Statistical studies of early-phase photometric/spectroscopic behavior can be achieved even for rare SN Ia subclasses after the three-years survey. For the EExSNe Ia study, assuming an early-excess fraction of 37.9% from previous observations (11/29), $\sim$12.1 EExSNe Ia can be expected every year. Given a large scatter of the early-excess fraction shown in different SN Ia subclass, we derive a lower-limit expected number of $\sim$5.2 by applying a specific early-excess fraction for each SN Ia subclass based on the result shown in Chapter 4, which is still an impressive number compared with the number of EExSNe Ia discovered so far. With over 15 EExSNe Ia discovered in the next three years, new breakthroughs on the physical mechanisms that account for the He-det and the surface-^{56}Ni-decay early-excess scenarios will be achieved. On the other hand, a few of companion-interaction EExSNe Ia can be expected if the single-degenerate scenario truly dominates the progenitor channel of SNe Ia. In addition to EExSNe Ia, a larger number of non-EExSNe Ia will be used to study the intrinsic early light-curve scatter and to improve the estimation of early-excess fraction in each SN Ia subclass. Finally, new understandings of the SNe Ia diversity will enable us to further improve the accuracy of using SNe Ia in cosmology.

In addition to the remarkable outcome from early-phase SNe Ia, following studies for other interesting rapid transients can be carried out. (1) Core-collapse SNe at the shock breakout phase. (2) The so-called fast-evolving luminous transients, a kind of peculiar transients which may originate from shock breakouts within dense circumstellar materials surrounding progenitor stars (Tanaka et al., 2016). (3) Kilonovae; given the light curve of the first kilo-

nova EM170817 (the electromagnetic counterpart of the gravitational wave event GW170817, Smartt et al., 2017), MUSSES-FAST is able to not only discover EM170817-like kilonovae at redshift reaching to $\sim$0.1 (far beyond the detection limit of the LIGO-Virgo collaboration) but catch their ephemeral rising phases in optical wavelengths thanks to the unique observing mode. (4) Other unexpected transients; unknown rapid transients that could be optical counterparts of neutron star – black hole merger events, fast radio bursts or even something beyond our current knowledge are potential targets of MUSSES-FAST. Since the duration and intrinsic brightness of those rapid transients are very uncertain, uninterruptedly monitoring the HSC-observed region is the best way to catch them. Such an observing mode can be achieved by MUSSES-FAST thanks to the extremely large field-of-view of Tomo-e and a negligible time interval between the HSC and Tomo-e survey. Even though the possibility to find these mysterious transients might be small due to the large uncertainties of their photometric behavior and event rates, we are still very looking forward to what kind of "byproducts" can be discovered through this innovative survey project.

6 Conclusions

In this thesis, the study of early-phase SNe Ia discovered by well-designed early-phase SNe Ia surveys with Kiso/KWFC and Subaru/HSC (Chapters 2 and 3) and the statistical investigation with previously discovered/unnoticed EExSNe Ia (Chapter 4) are presented. Further investigations of early-phase SNe Ia can be well conducted by making the best use of Subaru/HSC and Kiso/Tomo-e in the near future (Chapter 5). The main conclusions of the thesis are summarized as follows.

6.1 KWFC-related Early-phase SNe Ia Study

In order to test the feasibility of running an early-phase SNe Ia-targeted survey, a series of observations were carried out through two supernova projects with Kiso/KWFC, KISS and SKYS, in 2015. During the seven-months observations, total 13 SN candidates were discovered and four of them were confirmed as early-phase supernovae. Light curves and spectra obtained from KWFC and other follow-up facilities indicate that three of them are early-phase SNe Ia (KISS15m, KISS15n, and SKYS6) and the other one (SKYS9) is an early-phase type IIP supernova. In particular, three KWFC early-phase SNe Ia, KISS15m, KISS15n, and SKYS6, belong to subluminous, luminous, and normal type, respectively. The sample diversity enables us to investigate the early photometric behavior of SNe Ia in different subclasses.

KISS15m is one of the youngest 91bg-like subluminous SNe Ia so far. Although KISS15m does not show peculiar photometric behavior in the early phase, by comparing KISS15m with a 02es-like subluminous EExSN Ia iPTF14atg and other subluminous non-EExSNe Ia, we proposed a set of observables (i.e. the rising time, the post-maximum light-curve profile, and the early color evolution) for identifying inconspicuous early-excess features. Subluminous EExSNe Ia discovered in the near future will bring us new ideas about the physical connection between subluminous SNe Ia and specific early-excess scenario(s).

The high spectral similarity between a luminous early-phase SN Ia, KISS15n, and a super-$M_{\rm Ch}$ SN Ia candidate SN 2006gz suggests the same physical origin of two objects. Given a comparable brightness but distinct spectral features to those of 91T/99aa-like luminous SNe Ia, KISS15n (or 06gz-like SNe Ia) probably is a transitional type that bridges the super-$M_{\rm Ch}$ and 91T/99aa-like SNe Ia. By statistically investigating the early-phase observational properties of luminous SNe Ia, we may find out the intrinsic difference/connection between these luminous

SN Ia subclasses.

The spectral information of an early-phase normal SN Ia, SKYS6, may support a likely correlation between the low Si II velocity feature and the carbon footprint for normal SNe Ia. We proposed that the "diversities" shown in normal SNe Ia including the early light-curve dispersion, carbon-footprint difference, Si II velocity scatter, and disperse NUV−optical color evolution may originate from the off-center explosion scenario. Future 3D numerical simulations will help us to understand whether or not such diversities can be attributed to the viewing angle effect caused by the off-center explosion.

6.2 HSC-related Early-phase SNe Ia Study

The discovery of three early-phase SNe Ia in our KWFC observations demonstrated the feasibility of conducting early-phase SNe Ia-targeted survey with wide-field imagers and thus inspired us to further investigate early-phase SNe Ia with the best survey facility in the world, the Subaru/HSC. With the experience accumulated from KISS and SKYS, the advanced early-phase SNe Ia survey project with Subaru/HSC, MUSSES, was launched out in April, 2016.

The MUSSES project includes survey observations with the 8.2-m Subaru telescope and follow-up observations with 1–10-m ground-based telescopes. In order to carry out such a large project, building a global collaboration is necessary. International collaborations with astronomers from different countries enable us to carry out real-time follow-up observations with more than 10 large aperture telescopes all over the world.

The first MUSSES observing run has been successfully carried out in April 2016. We discovered 12 early-phase SN candidates soon after the HSC survey, and especially, a very special early-phase SN Ia, the so-called MUSSES1604D (or SN 2016jhr), attracted our attention. The multiband Subaru/HSC survey and follow-up observations indicated that a prominent but red early flash followed with peculiar spectral features of MUSSES1604D are in conflict with predictions by previously proposed physical mechanisms (e.g. the interaction between the SN ejecta and a companion star or CSM). Further analysis with numerous computational simulations suggested that all peculiarities of MUSSES1604D can be naturally explained by a supernova explosion that is triggered by a detonation of a thin helium shell of its progenitor star (the so-called He-shell detonation scenario). This finding not only indicates the multiple origins of the light-curve excess found in early-phase SNe Ia but provides robust evidence of one kind of explosion mechanism of SNe Ia for the first time.

6.3 Statistical Study of Early-excess SNe Ia

Inspired by the discovery of MUSSES1604D, further investigations of early-phase SNe Ia that show additional brightness enhancements (i.e. EExSNe Ia) were carried out through the statistical analysis.

With the largest sample of early-phase SNe Ia discovered until 2018, we presented independent evidence to further prove multiple origins of EExSNe Ia and discuss the explosion mechanism and progenitor of specific SN Ia subclasses from the early-excess perspective in Chapter 4. We systematically investigated 11 early-excess SNe Ia from subluminous to luminous subclasses. Eight of them were selected from 23 SNe Ia with extremely early-phase optical light curves ("golden" early-phase SNe Ia), and three of them were selected from 40 SNe Ia (including 14 golden samples) with early-phase UV/NUV light curves. We found that previously discovered EExSNe Ia show a clear preference for specific SN Ia subclasses. In particular, the early-excess feature shown in all six luminous (91T- and 99aa-like) SNe Ia is in conflict with the viewing angle dependence predicted by the companion-interaction scenario. Instead, such a high early-excess fraction is likely related to the explosion physics of luminous SNe Ia; i.e. a more efficient detonation happening in the progenitor of luminous SNe Ia may consequently account for the early-excess feature powered by the radiation from a ^{56}Ni-abundant outer layer. The diversity of early-excess features shown in different SN Ia subclasses suggests multiple origins of the discovered early-excess SNe Ia, challenging their applicability as a robust progenitor indicator. Further understanding of the early-excess diversity relies not only on multiband photometry and prompt-response spectroscopy of individual early-excess SNe Ia but also on investigations of the general early-phase light-curve behavior of each SN Ia subclass.

6.4 Future Plan and Prospects

In the next decade, time-domain astronomy will become one of the most popular branches in astronomy and pioneering work on rapid transients can be achieved by using Subaru/HSC and Kiso/Tomo-e in the next few years. With the forthcoming Tomo-e Gozen transient survey and an innovative rapid transient survey, the MUSSES-FAST that uniquely combines two top-level survey facilities (i.e. Subaru/HSC and Kiso/Tomo-e) to further improve the survey capability of early-phase SNe, we plan to build the largest sample of early-phase SNe in next 3–5 years. Thanks to the well-established follow-up network, we are able to carry out systematical investigations of over 100 rapid transients for the first time. With over 15 EExSNe Ia discovered by HSC and Tomo-e (more than all EExSNe Ia discovered so far), new breakthroughs on the

physical mechanisms of the He-det and the surface-^{56}Ni-decay early-excess scenarios will be made. Additionally, several companion-interaction EExSNe Ia can be expected if the SD scenario truly dominates the progenitor system of SNe Ia. Finally, further understanding of the diversity of SNe Ia will help us to improve the accuracy of their cosmological use.

The Universe is full of surprises. In addition to scientific outputs from early-phase SNe Ia study with ongoing and forthcoming time-domain surveys, other interesting transients including the fast-evolving luminous transients, SN shock breakouts, optical counterparts of gravitational wave events and fast radio bursts, and even something beyond our current knowledge can be discovered with these amazing survey projects. Great progress in time-domain astronomy thus can be expected by using Subaru/HSC and Kiso/Tomo-e in the near future.

7 Appendix: Supplementary Information on SKYS Supernovae and Candidates

A-1) Non-early-phase Supernovae and Candidates

During the SKYS observation, nine around/post-peak supernova candidates are selected based on their relative locations to host galaxies, absolute magnitude, and light-curve behavior. Two of them (SKYS5 and SKYS7) have been spectroscopically confirmed and another two (SKYS3 and SKYS4) are classified as SNe with relatively low confidence.

We only conducted *g*-band follow-up observations with the Kiso/KWFC for nine around/post-peak supernova candidates due to our limited follow-up time. As KWFC was removed on Nov. 24 and the onset of the poor observational condition since Nov. 21, all follow-up observations with KWFC were terminated since then. Basic information of each object is shown as follows. Their photometric and spectroscopic results are summarized in Tables 9 and 10 at the end of this section, respectively.

SKYS1

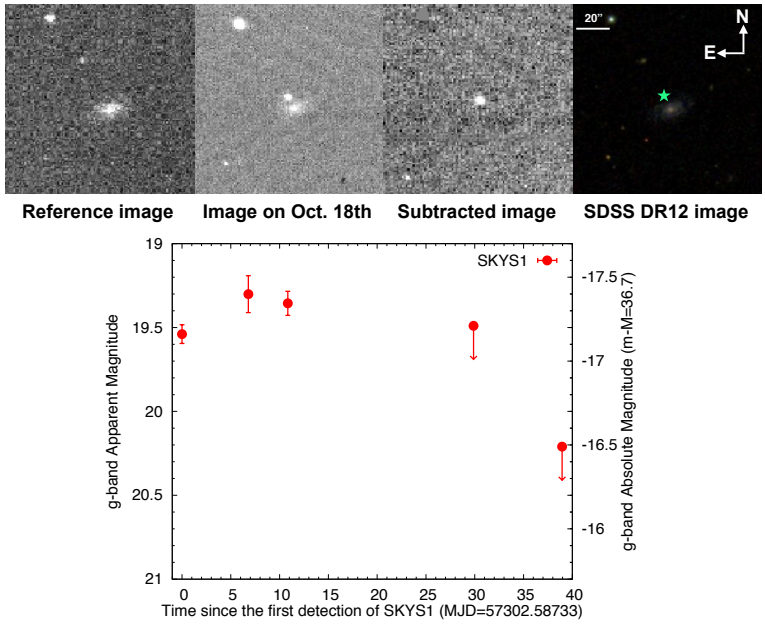

Figure 46: *g*-band observations of SKYS1. The upper panel (from left to right) shows the SDSS *g*-band reference image, the KWFC *g*-band image taken on Oct. 18, the subtracted image and the SDSS DR12 color image at the same region. The position of SKYS1 (RA $23^h12^m55^s.85$, Dec +00:21:55.5) is marked by a cyan star symbol. The lower panel is the KWFC *g*-band light curve.

SKYS1 is the first SN that was discovered in the second night of the SKYS observation (Oct. 7). Since SKYS1 is far away from the host center, we are able to exclude the possibility of an AGN. The spectrum of the host galaxy indicates that the host is a star-forming galaxy at redshift of 0.049. The g-band absolute magnitude of SKYS1 is about -17.4 mag around the peak and we could not discover SKYS1 during our November observing run due to its low brightness. The photometric behavior of SKYS1 showed the similarity with two Type II SNe, PTF10uls and PTF12gnn (Khazov et al. 2015).

SKYS2

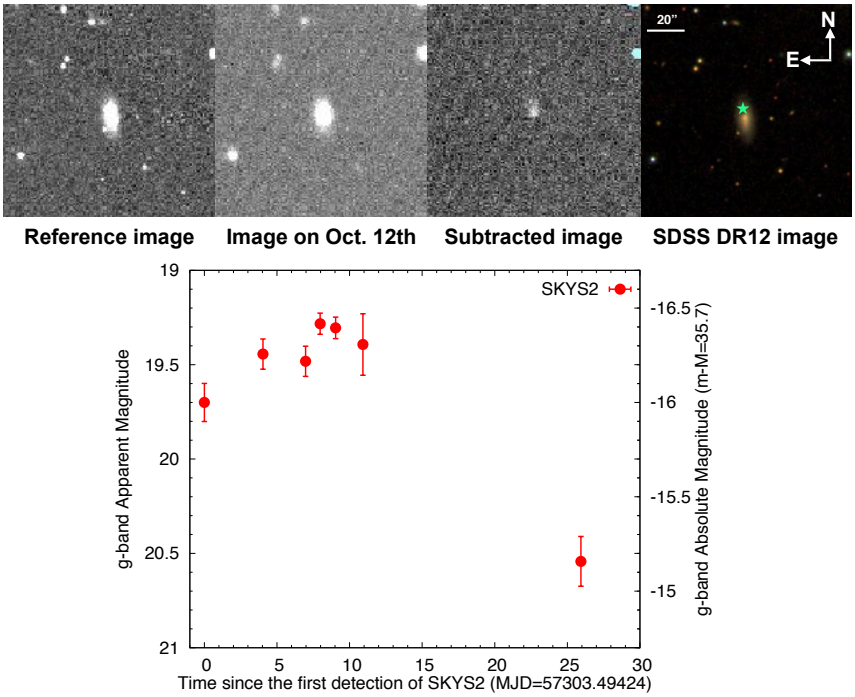

Figure 47: g-band observations of SKYS2. The upper panel (from left to right) shows the SDSS g-band reference image, the KWFC g-band image taken on Oct. 12, the subtracted image and the SDSS DR12 color image at the same region of SKYS2. The position of SKYS2 (RA $21^h14^m41^s.15$, Dec -00:24:37.7) is marked by a cyan star symbol. The lower panel is the KWFC g-band light curve.

SKYS2 was discovered on Oct. 8. The spectrum of the host galaxy indicates that the host is a late-type galaxy at redshift of 0.032. The g-band absolute magnitude of SKYS2 is about -16.5 mag around the peak. According to the luminosity and light-curve profile of SKYS2, it is likely to be a CCSN. The light curve of SKYS2 also suggests that our first detection was within about 10 days after the explosion.

SKYS3

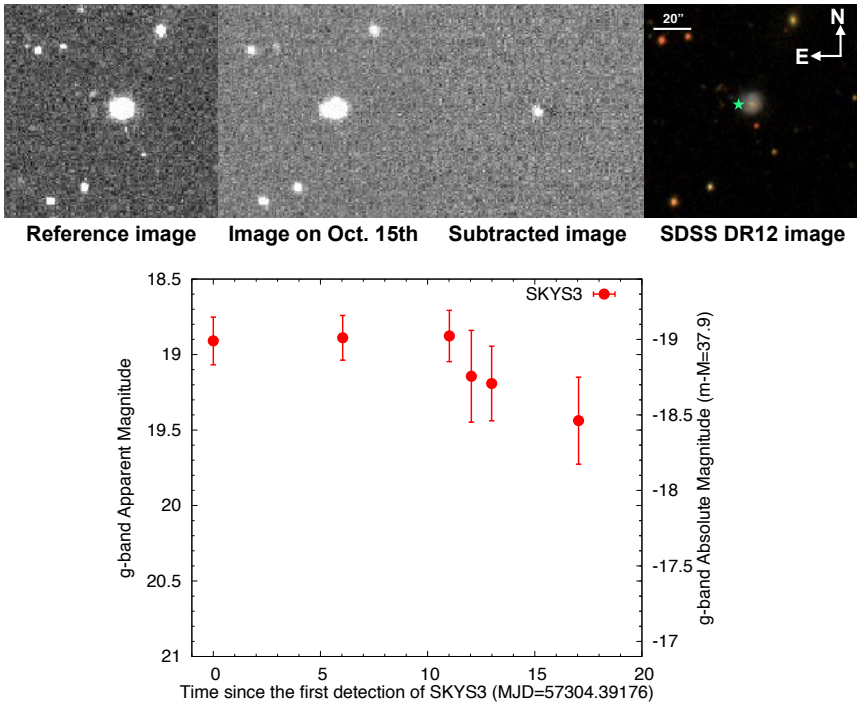

Figure 48: g-band observations of SKYS3. The upper panel (from left to right) includes the SDSS g-band reference image, the KWFC g-band image taken on Oct. 15, the subtracted image and the SDSS DR12 color image at the same region. The position of SKYS3 (RA $16^h39^m46^s.56$, Dec +40:50:18.4) is marked by a cyan star symbol. The lower panel is the KWFC g-band light curve.

SKYS3 was discovered on Oct. 9. The image clearly showed that SKYS3 located at the edge of the host galaxy. According to the photometric redshift of the host galaxy (photo-z $\sim$0.085) we calculated the g-band absolute magnitude of SKYS3 is about -19.1 mag around the peak, which is a typical value of a normal SN Ia. Given that the visible time of SKYS3 is too short in November, we could not successfully follow up SKYS3 during the November observing run. However, since the absolute magnitude of SKYS3 was derived by using the photometric redshift of the host and the light-curve behavior of SKYS3 is quite strange compared to normal SNe Ia around the peak, SKYS3 could be a CCSN or a non-SN transient, e.g. a foreground luminous blue variable (LBV, Smith et al. 2010, 2011).

SKYS4

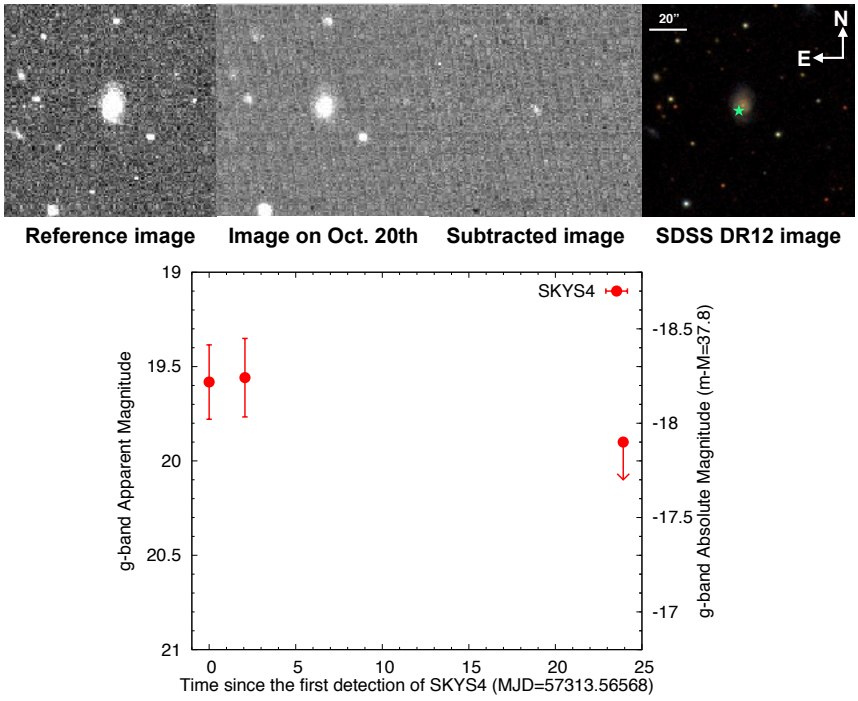

Figure 49: g-band observations of SKYS4. The upper panel (from left to right) shows the SDSS g-band reference image, the KWFC g-band image taken on Oct. 20, the subtracted image and the SDSS DR12 color image at the same region. The position of SKYS4 (RA $22^h07^m24^s.92$, Dec +22:08:40.7) is marked by a cyan star symbol. The lower panel is the KWFC g-band light curve.

SKYS4 is the last SN found in the October observing run. Since there was no observing time from Oct. 22 to Nov. 5, the follow-up observation of SKYS4 cannot be well performed. According to the photometric redshift of the host galaxy (photo-z $\sim$0.08) we calculated the g-band absolute magnitude of SKYS4 is around -18.3 mag on Oct. 20. In addition, SKYS4 was fainter than the observational limit during the November observation. The relatively high declining speed of SKYS4 also suggests that SKYS4 could be a post-maximum SN or quickly varying transient. Given the limited information of SKYS4 and its host galaxy and the relatively close distance of SKYS4 to the center of its host galaxy, we cannot rule out the possibility that SKYS4 is a non-SN transient, e.g. a rapidly varying AGN.

SKYS5

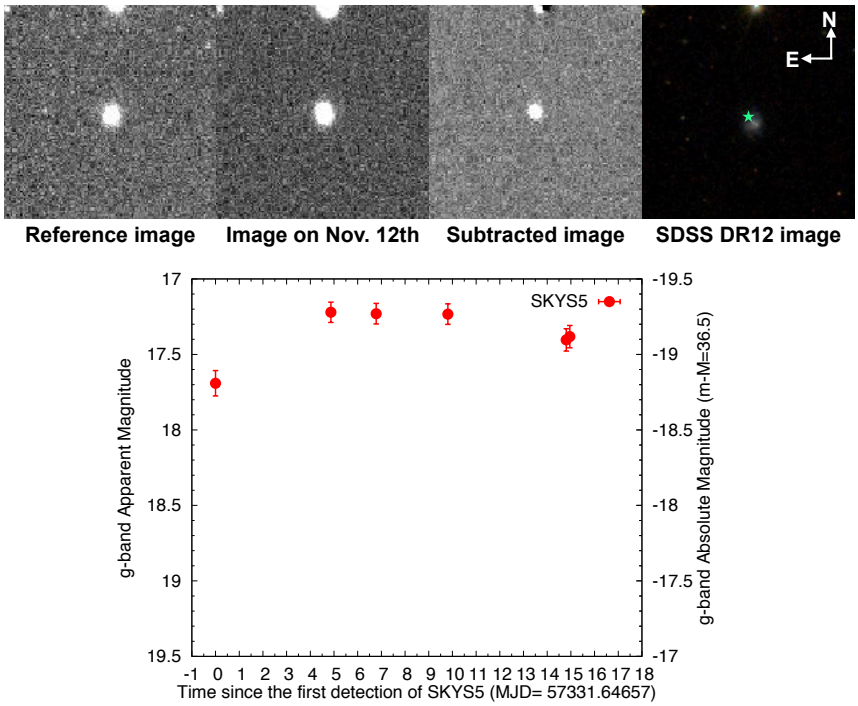

Figure 50: *g*-band observations of SKYS5. The upper panel (from left to right) shows the SDSS *g*-band reference image, the KWFC *g*-band image taken on Nov. 12, the subtracted image and the SDSS DR12 color image at the same region. The position of SKYS5 (RA $01^h10^m24^s.10$, Dec +23:21:27.0) is marked by a cyan star symbol. The lower panel is the KWFC *g*-band light curve.

SKYS5 was discovered in the first day of our November observing run (Nov. 5) and spectroscopically followed by the LT/SPRAT on Nov. 13. The spectral fitting suggests that SKYS5 is a 91T-like SN Ia in a few days after the peak or a normal SN Ia at about -7 days to the *B*-band maximum mainly due to a blue SED and relatively weak Si II λ6355 absorption feature (Figure 51). The redshift predicted by the spectral fitting is about 0.048. Given a *g*-band peak absolute magnitude of -19.3 and a slow evolving light curve, we suggest SKSY5 is more likely a 91T-like SN Ia.

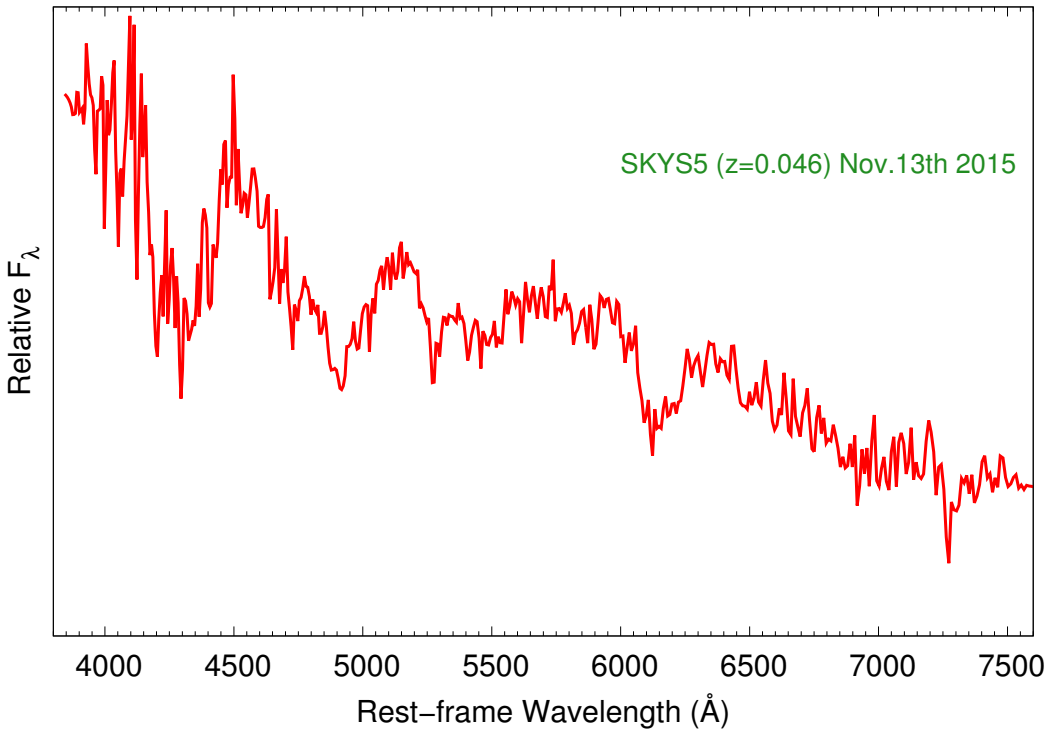

Figure 51: A spectrum of SKYS5 taken by SPectrograph for the Rapid Acquisition of Transients (SPRAT) mounted on the Liverpool Telescope (LT) on Nov. 13 (Table 10). Clear Si II and other IME absorptions indicate that SKYS5 is an SN Ia. However, the relatively weak SiII 6355 line suggests it could be either a 91T-like SN Ia around the peak epoch or an early phase normal SN Ia. By combining with the light curve profile of SKYS5, we finally confirmed SKYS5 is a 91T-like SN Ia discovered at about one week before the *B*-band maximum.

SKYS7

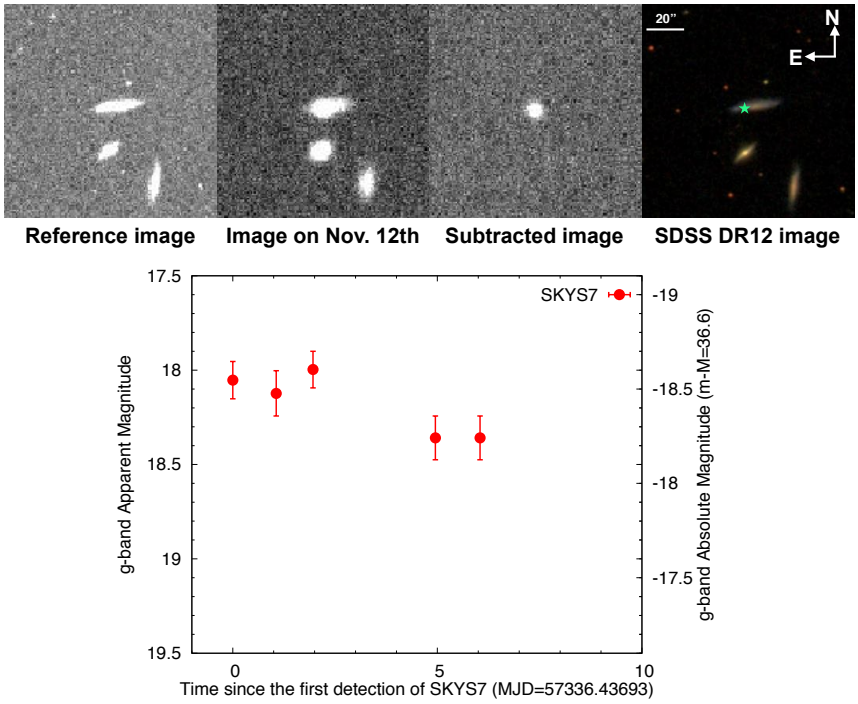

Figure 52: g-band observations of SKYS7. The upper panel (from left to right) shows the SDSS g-band reference image, the KWFC g-band image taken on Nov. 12, the subtracted image and the SDSS DR12 color image at the region of SKYS7. The position of SKYS7 (RA $22^h04^m02^s.75$, Dec +09:30:50.0) is marked by a cyan star symbol. The lower panel is the KWFC g-band light curve.

SKYS7 was detected on Nov. 10 and spectroscopically followed by the LT/SPRAT on Nov. 15. The relatively red spectrum and blended S II and Si II absorption features indicate that SKYS7 could be a 91T-like or normal-type SN Ia around two-weeks after the maximum (z=0.048). By using common $\Delta m_{15}(B)$ value of 91T-like SN Ia ($\sim$0.8), we obtained that the g-band peak absolute magnitude of SKYS7 (-19 mag) is too faint in terms of a 91T-like SN Ia. Therefore, we classified SKYS7 as a normal SN Ia. However, Given that SKYS7 is embedded in the host galaxy, we cannot completely rule out that SKYS7 is a luminous SN Ia by taking into account the possible extinction from the host galaxy.

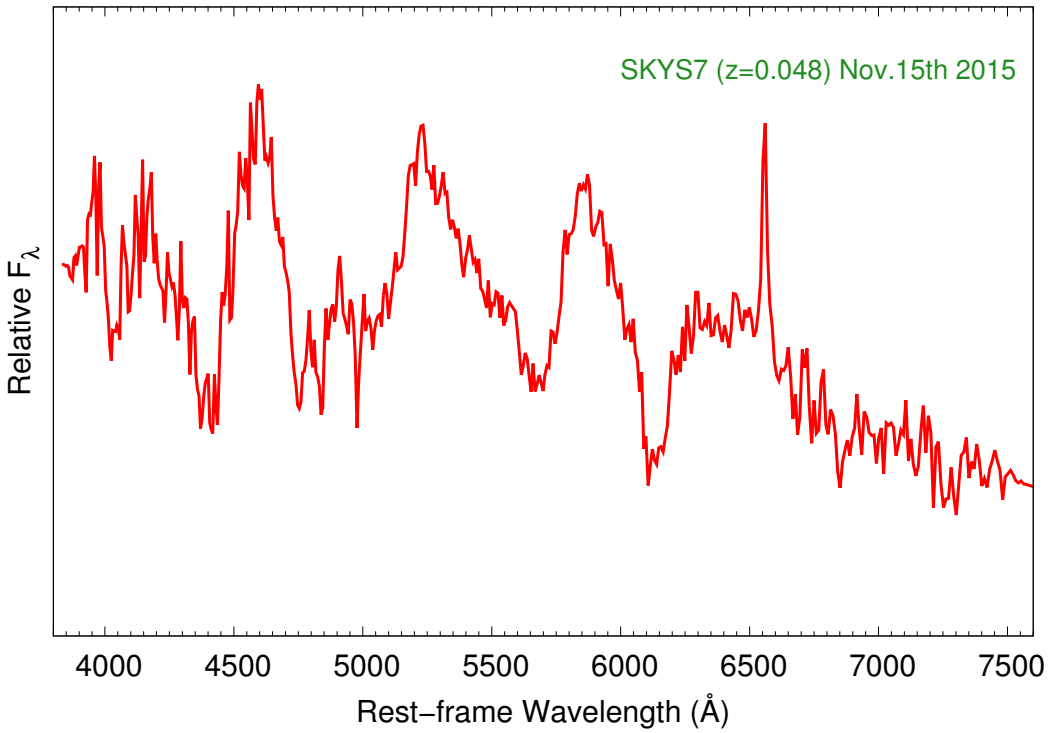

Figure 53: A spectrum of SKYS7 taken by LT/SPRAT on Nov. 15 (Table 10). The blended S II and Si II absorption features around 5600 Å and the red SED imply that SKYS7 was a post-maximum SN Ia during our observation. However, such a late-phase spectrum prevents us from confirming SKYS7 is a normal-type or a 91T-like SN Ia. According to a g-band absolute magnitude of SKYS7 around two weeks after the maximum (-18.2) and a typical $\Delta m_{15}(B)$ value of a 91T-like SN Ia, we finally classified SKYS7 as a normal-type SN Ia which was discovered around 10 days after the B-band maximum.

SKYS8

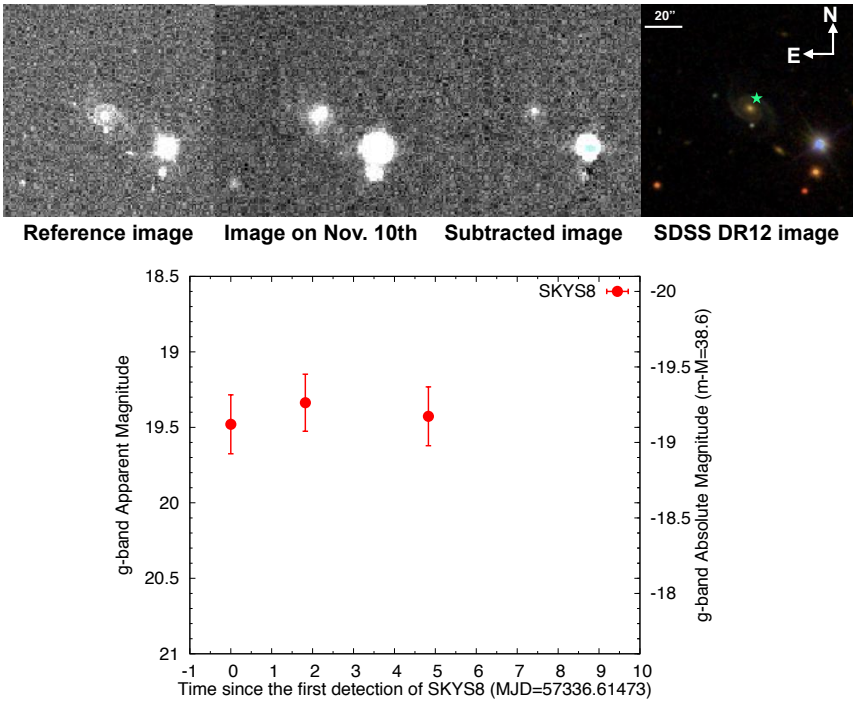

Figure 54: *g*-band observations of SKYS8. The upper panel (from left to right) shows the SDSS *g*-band reference image, the KWFC *g*-band image taken on Nov. 10, the subtracted image and the SDSS DR12 color image at the same region. The position of SKYS8 (RA $23^h48^m24^s.37$, Dec +15:50:44.2) is marked by a cyan star symbol. The lower panel is the KWFC *g*-band light curve.

SKYS8 located at the spiral arm of the host galaxy at z=0.113 was also discovered on Nov. 10. We only observed SKYS8 on Nov. 10, 12, and 15 due to the limited KWFC follow-up time in our November observing run. However, a light curve around the peak can be easily distinguished even with three data points, suggesting a *g*-band peak absolute magnitude of about -19.3. Therefore, we classified SKYS8 as a normal SN Ia candidate.

SKYS10

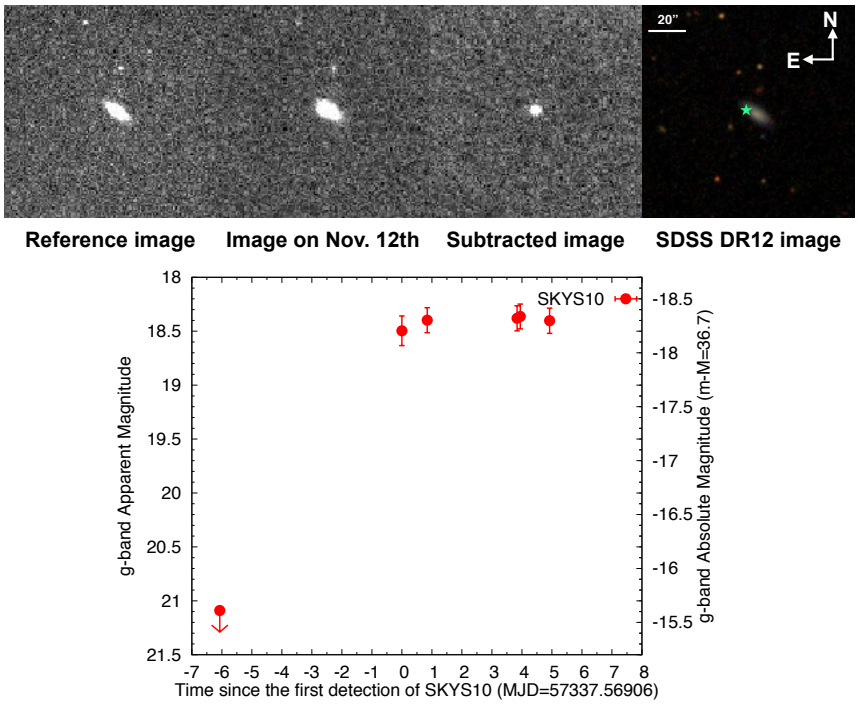

Figure 55: *g*-band observations of SKYS10. The upper panel (from left to right) shows the SDSS *g*-band reference image, the KWFC *g*-band image taken on Nov. 12, the subtracted image and the SDSS DR12 color image at the same region. The position of SKYS10 (RA $22^h37^m02^s.12$, Dec +20:42:31.9) is marked by a cyan star symbol. The lower panel is the KWFC *g*-band light curve.

SKYS10 showed a peculiar light-curve behavior during our observations. We discovered SKYS10 on Nov. 12 and did not find any signature at the same position in the 6-days-earlier image of which the limiting magnitude is about 21.1 mag. Such a finding implied that SKYS10 should be a very early SN during our first observation. According to the photometric redshift of the host galaxy (z=0.059), the absolute magnitude of SKYS10 during the discovery is about -18.2. However, SKYS8 did not show significant brightness variation in our follow-up observations, in contrast to our expectation that SKYS10 is an early-phase SN Ia. The light curve of SKYS10 is more similar to a fast rising early-phase SN IIP with a relatively high luminosity than normal SNe IIP. One possible reason is an over-estimation of the host redshift. However, due to the missing of the spectroscopy of SKYS10, it is hard to fully exclude the possibility that SKYS10 is a supernova imposter, e.g. a foreground LBV.

SKYS11

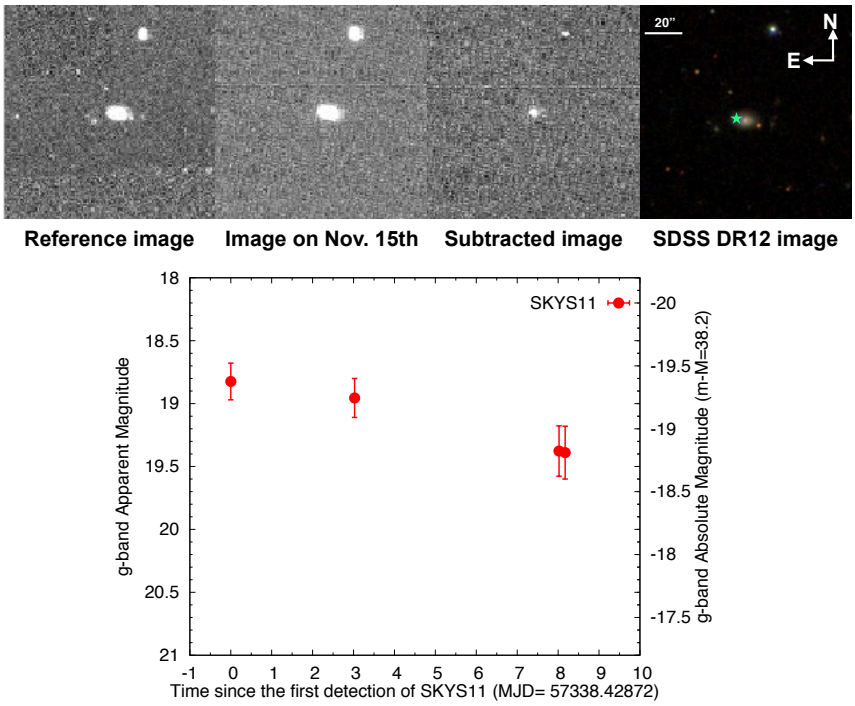

Figure 56: *g*-band observations of SKYS11. The upper panel (from left to right) shows the SDSS *g*-band reference image, the KWFC *g*-band image taken on Nov. 15, the subtracted image and the SDSS DR12 color image at the same region. The position of SKYS11 (RA $01^h05^m47^s.75$, Dec +24:59:01.0) is marked by a cyan star symbol. The lower panel is the KWFC *g*-band light curve.

The last SN candidate of SKYS, SKYS11 was discovered on Nov. 12. We ruled out the possibility that SKYS11 is an AGN in terms of its far distance to the host center. The light curve of SKYS11 suggests that our first observation was close to the peak by adopting an absolute magnitude derived from a photometric redshift of the host (z=0.094). We reported that SKYS11 is a normal SN Ia because the light-curve declining speed is comparable or slightly higher than another normal SN Ia, SKYS7.

Table 9: Photometric Information on KWFC Non-early-phase SNe and Candidates

Object	MJD[a]	UT[a]	Filter	Magnitude[b]	Exp. Time (s)	Telescope
SKYS1	57302.59	2015 Oct. 07	*g*	19.54 ± 0.06	180	Kiso/KWFC
SKYS1	57309.39	2015 Oct. 14	*g*	19.54 ± 0.06	180	Kiso/KWFC
SKYS1	57313.43	2015 Oct. 18	*g*	19.54 ± 0.06	180	Kiso/KWFC
SKYS1	57332.47	2015 Nov. 06	*g*	> 19.49[c]	180	Kiso/KWFC
SKYS1	57341.54	2015 Nov. 15	*g*	> 20.21[c]	180	Kiso/KWFC
SKYS2	57303.49	2015 Oct. 08	*g*	19.70 ± 0.10	180	Kiso/KWFC
SKYS2	57307.53	2015 Oct. 12	*g*	19.44 ± 0.08	180	Kiso/KWFC
SKYS2	57310.47	2015 Oct. 15	*g*	19.48 ± 0.08	180	Kiso/KWFC
SKYS2	57311.47	2015 Oct. 16	*g*	19.28 ± 0.06	180	Kiso/KWFC
SKYS2	57312.53	2015 Oct. 17	*g*	19.31 ± 0.06	180	Kiso/KWFC
SKYS2	57314.42	2015 Oct. 19	*g*	19.39 ± 0.16	180	Kiso/KWFC
SKYS2	57329.43	2015 Nov. 03	*g*	20.54 ± 0.13	180	Kiso/KWFC
SKYS3	57304.39	2015 Oct. 09	*g*	18.91 ± 0.16	180	Kiso/KWFC
SKYS3	57310.43	2015 Oct. 15	*g*	18.89 ± 0.15	180	Kiso/KWFC
SKYS3	57315.41	2015 Oct. 20	*g*	18.88 ± 0.17	180	Kiso/KWFC
SKYS3	57316.43	2015 Oct. 21	*g*	19.14 ± 0.30	180	Kiso/KWFC
SKYS3	57317.38	2015 Oct. 22	*g*	19.19 ± 0.25	180	Kiso/KWFC
SKYS3	57321.44	2015 Oct. 26	*g*	19.44 ± 0.29	180	Kiso/KWFC
SKYS4	57313.57	2015 Oct. 18	*g*	19.58 ± 0.20	180	Kiso/KWFC
SKYS4	57315.63	2015 Oct. 20	*g*	19.56 ± 0.20	180	Kiso/KWFC
SKYS4	57337.49	2015 Nov. 11	*g*	> 19.90[c]	180	Kiso/KWFC
SKYS5	57331.65	2015 Nov. 05	*g*	17.69 ± 0.08	180	Kiso/KWFC
SKYS5	57336.52	2015 Nov. 10	*g*	17.22 ± 0.07	180	Kiso/KWFC
SKYS5	57338.43	2015 Nov. 12	*g*	17.23 ± 0.07	180	Kiso/KWFC
SKYS5	57341.45	2015 Nov. 15	*g*	17.23 ± 0.07	180	Kiso/KWFC
SKYS5	57346.45	2015 Nov. 20	*g*	17.40 ± 0.07	180	Kiso/KWFC
SKYS5	57346.60	2015 Nov. 20	*g*	17.38 ± 0.07	180	Kiso/KWFC
SKYS7	57336.44	2015 Nov. 10	*g*	18.05 ± 0.10	180	Kiso/KWFC
SKYS7	57337.50	2015 Nov. 11	*g*	18.12 ± 0.12	180	Kiso/KWFC
SKYS7	57338.40	2015 Nov. 12	*g*	18.00 ± 0.10	180	Kiso/KWFC
SKYS7	57341.39	2015 Nov. 15	*g*	18.36 ± 0.12	180	Kiso/KWFC
SKYS7	57342.48	2015 Nov. 16	*g*	18.36 ± 0.12	180	Kiso/KWFC

Note:

[a] The median time for a single exposure.

[b] AB magnitudes for SDSS *g*-band filter.

[c] 5σ upper limit.

Object	MJD[a]	UT[a]	Filter	Magnitude[b]	Exp. Time (s)	Telescope
SKYS8	57336.61	2015 Nov. 10	*g*	19.48 ± 0.20	180	Kiso/KWFC
SKYS8	57338.44	2015 Nov. 12	*g*	19.34 ± 0.19	180	Kiso/KWFC
SKYS8	57341.44	2015 Nov. 15	*g*	19.43 ± 0.20	180	Kiso/KWFC
SKYS10	57331.50	2015 Nov. 05	*g*	>21.09[c]	180	Kiso/KWFC
SKYS10	57337.57	2015 Nov. 11	*g*	18.50 ± 0.14	180	Kiso/KWFC
SKYS10	57338.41	2015 Nov. 12	*g*	18.40 ± 0.12	180	Kiso/KWFC
SKYS10	57341.41	2015 Nov. 15	*g*	18.38 ± 0.12	180	Kiso/KWFC
SKYS10	57341.52	2015 Nov. 15	*g*	18.36 ± 0.12	180	Kiso/KWFC
SKYS10	57342.49	2015 Nov. 16	*g*	18.40 ± 0.12	180	Kiso/KWFC
SKYS11	57338.43	2015 Nov. 12	*g*	18.82 ± 0.15	180	Kiso/KWFC
SKYS11	57341.45	2015 Nov. 15	*g*	18.96 ± 0.16	180	Kiso/KWFC
SKYS11	57346.45	2015 Nov. 20	*g*	19.38 ± 0.20	180	Kiso/KWFC
SKYS11	57346.60	2015 Nov. 20	*g*	19.39 ± 0.21	180	Kiso/KWFC

Note:
[a] The median time for a single exposure.
[b] AB magnitudes for SDSS *g*-band filter.
[c] 5σ upper limit.

Table 10: A Summary of Spectroscopic Follow-ups of SKYS5 and SKYS7

Object	UT	Exp. Time (s)	Telescope	slit width (")	grism/filter
SKYS5	2015 Nov. 13	1800	LT/SPRAT	1.8	Red/4020longpass[a]
SKYS7	2015 Nov. 15	1800	LT/SPRAT	1.8	Red/4020longpass[a]

Note:
[a] LT/SPART Red configuration has much better performance above $\sim$6000Å, "4020longpass" is the abbreviation of "Edmund Optics 400nm longpass filter". The wavelength coverage and resolution is 400-800 nm and 350 respectively.

A-2) SKYS9, an Early-phase Type IIP Supernova

An early-phase SN IIP, SKYS9, has been well followed by space/ground-based telescopes from UV to NIR wavelengths. In this section, we show a part of preliminarily reduced data and briefly introduce the observational properties of SKYS9. Photometric and spectroscopic information on SKYS9 is summarized in Tables 11 and 12 at the end of this section, respectively.

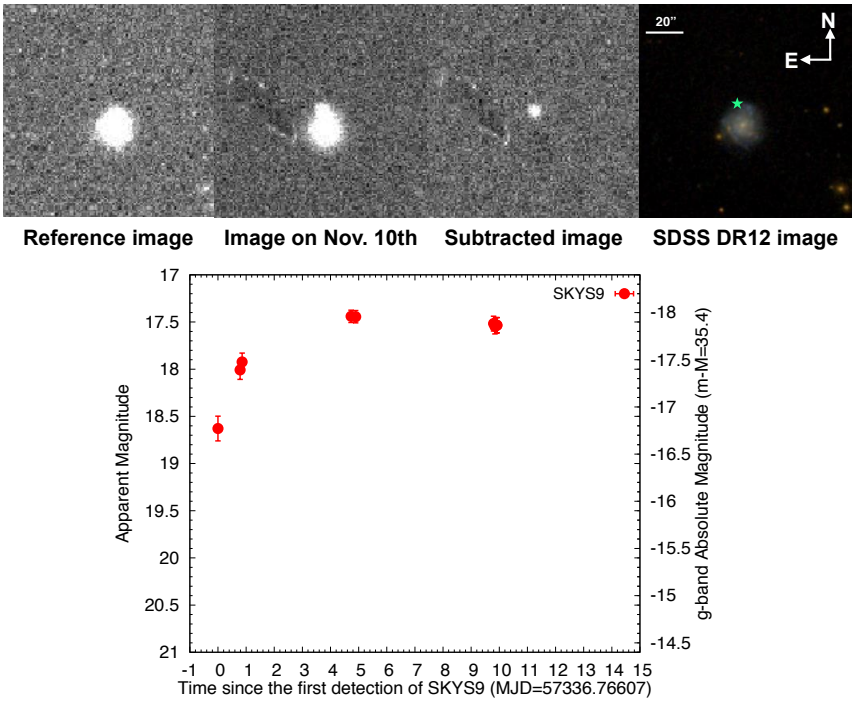

Figure 57: g-band observations of SKYS9. The upper panel (from left to right) shows the SDSS g-band reference image, the KWFC g-band image taken on Nov. 10, the subtracted image and the SDSS DR12 color image at the same region. The position of SKYS9 (RA $03^h11^m16^s.73$, Dec +01:11:35.1) is marked by a cyan star symbol. The lower panel is the KWFC g-band light curve. The fast brightening suggests that SKYS9 is an early-phase SN candidate.

SKYS9 was classified as an early-phase SN candidate one day after the discovery. Multi-band photometric follow-ups have been conducted by Kiso/KWFC, LJT/YFOSC, and OISTER members. In particular, we triggered *Swift*/UVOT UV+optical follow-up observation lasted for about one month. The complete spectral evolution of SKYS9 has been obtained by using LJT/YFOSC, LT/SPRAT, and Subaru/FOCAS. Finally we confirmed that SKYS9 is an SN IIP discovered in a few days after the explosion based on both photometric and spectroscopic information. A part of preliminarily reduced data are given in section.

A very bright object was discovered at the edge of a likely host galaxy on Nov. 10, 2015. According to the spectroscopic redshift of the host galaxy candidate (z=0.027), the g-band absolute magnitude of the object was about -16.8 mag during the discovery, implying a (either early-phase or post-early-phase) CCSN or an early-phase SN Ia candidate. Therefore, we carried out both g- and r-band follow-up observations with KWFC in the second night and the photometry showed that the g-band magnitude was increasing with a speed of about -1 mag day^{-1}. Such a fast brightening light curve suggests this object is a very likely early-phase SN and we immediately required SKYS collaborators to carry out multiband imaging and spectroscopic follow-up observations for this amazing transient, SKYS9.

The first spectrum of SKYS9 was taken by LJT/YFOSC on Nov. 12, 2015 (Figure 58, Table 12). The featureless blue continuum suggests that SKYS9 is an early-phase CCSN candidate. Given the importance of the early UV information in supernova study, we immediately triggered the UV/Optical Telescope (UVOT) mounted on the *Swift* satellite to carry out 6-bands imaging observations as a complement of our ground-based follow-up observations. As we expected, KWFC follow-up observations clearly showed that the brightness of SKYS9 quickly reached the peak and then became relatively stable, which makes a reminiscent of an SN IIP. Until Nov. 23, the Hα emission line and other Balmer line features were identified in the spectrum of SKYS9, indicating the identity of a typical SN IIP.

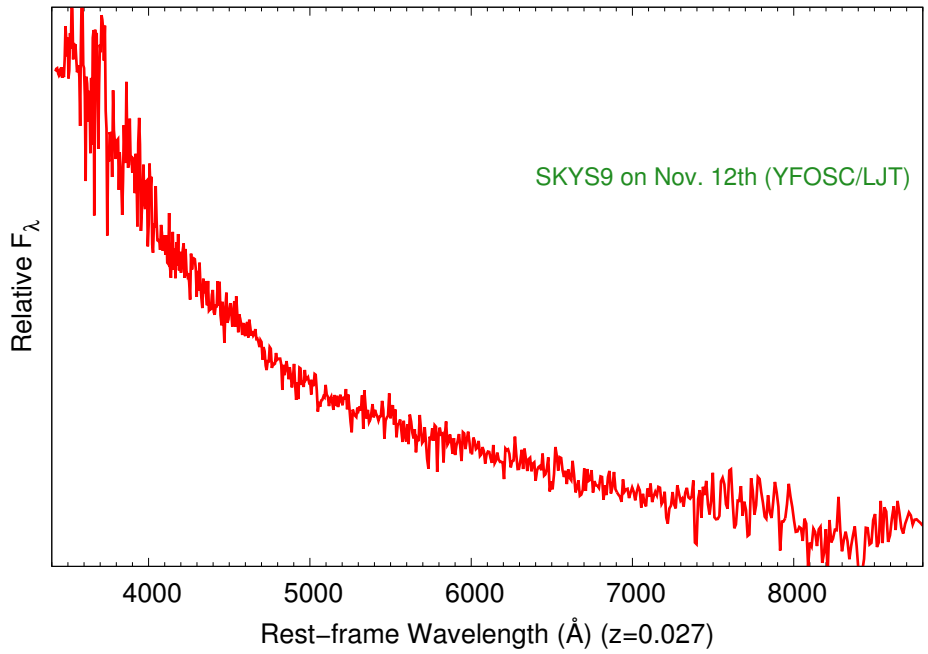

Figure 58: The first spectrum of SKYS9 taken by LJT/YFOSC on Nov. 12, 2015. The featureless blue continuum makes a reminiscent of an early-phase CCSN.

Ground-based multiband photometries of SKYS9

As what we mentioned in Chapter 2, the OISTER and LJT/YFOSC were in charge of the photometric follow-up (both optical and NIR) of early-phase SN candidates discovered by SKYS. Figure 59 presents the first 23-days multiband light curves of SKYS9 taken by KWFC and MITSuME.

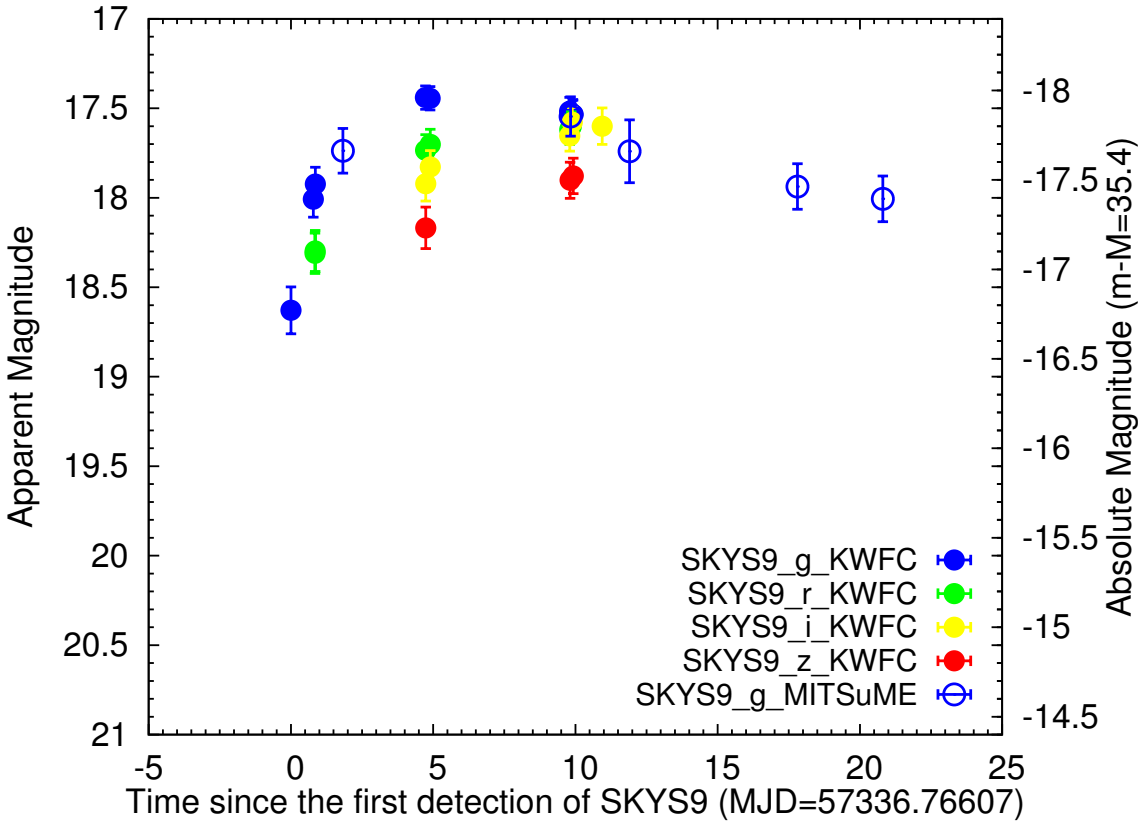

Figure 59: Multiband light curves of SKYS9 taken by KWFC and MITSuME in the first 23 days after the discovery. According to the *g*-band light curve, a "plateau" phase of SKYS9 happened at about 12 days after the discovery. For the multiband light curves, a longer rising phase can be found in redder wavelengths.

UV/optical photometry with *Swift*/UVOT

Given that the early-phase spectrum indicates a blue featureless continuum of SKYS9, we immediately triggered the *Swift*/UVOT observation from 5 days after the discovery to further investigate SKYS9 with the early-phase UV photometric information. The preliminary *Swift*/UVOT UV/optical light curves are shown in Figure 60.

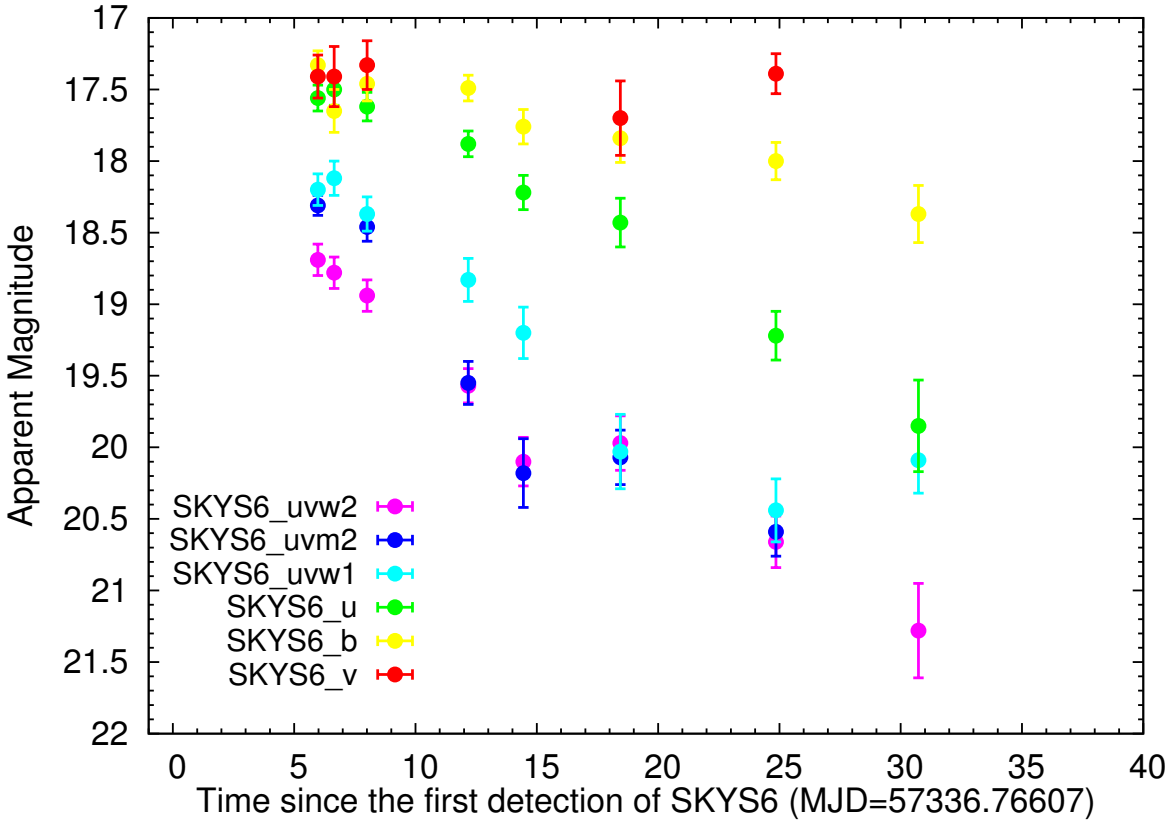

Figure 60: One-month UV/optical light curves of SKYS9 taken by *Swift*/UVOT. The UV and *u*-band brightness of SKYS9 keep declining in the first month with relatively high decline rate. In contrast, the *b*- and *v*-band light curves show slow evolution during the observation.

Spectral evolution of SKYS9

We did spectroscopy for SKYS9 from very early phase by using LJT/YFOSC and LT/SPRAT. The spectral evolution from Nov. 12, 2015 to Jan. 7, 2016 is shown in Figure 61.

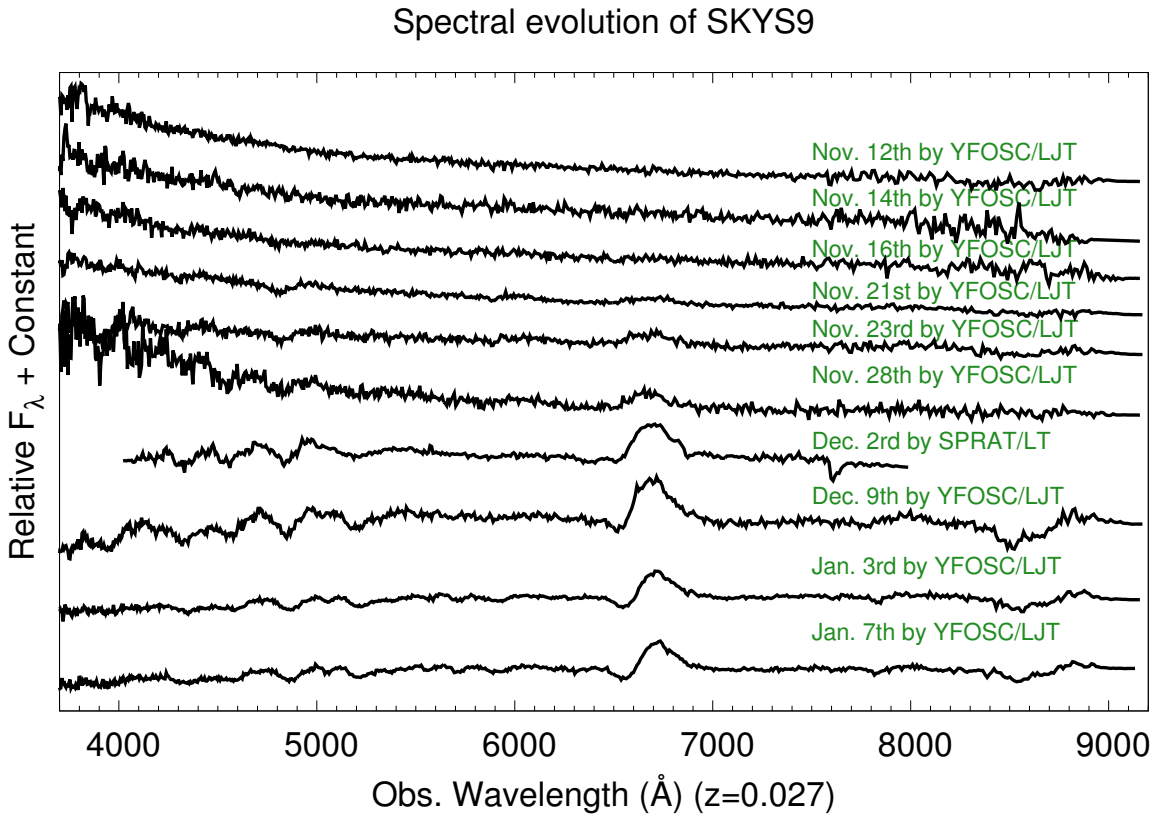

Figure 61: The two-month spectral evolution of SKYS9. At the beginning, a blue featureless continuum SED lasted more than one week after the explosion. About 10 days later, the weak Balmer series can be marginally discriminated and we finally confirmed that SKYS9 is a Type IIP supernova based on both light curve and spectral features.

Table 11: Photometric Information on SKYS9

Object	MJD[a]	UT[a]	Filter	Magnitude[b]	Exp. Time (s)	Telescope
SKYS9	57336.77	2015 Nov 10	*g*	18.63 ± 0.13	180	Kiso/KWFC
SKYS9	57337.55	2015 Nov 11	*g*	18.01 ± 0.10	180	Kiso/KWFC
SKYS9	57337.62	2015 Nov 11	*g*	17.92 ± 0.09	180	Kiso/KWFC
SKYS9	57341.50	2015 Nov 15	*g*	17.44 ± 0.03	180	Kiso/KWFC
SKYS9	57341.66	2015 Nov 15	*g*	17.44 ± 0.03	180	Kiso/KWFC
SKYS9	57346.56	2015 Nov 20	*g*	17.52 ± 0.08	180	Kiso/KWFC
SKYS9	57346.61	2015 Nov 20	*g*	17.55 ± 0.08	180	Kiso/KWFC
SKYS9	57346.67	2015 Nov 20	*g*	17.65 ± 0.08	180	Kiso/KWFC
SKYS9	57346.68	2015 Nov 20	*g*	17.62 ± 0.08	180	Kiso/KWFC
SKYS9	57337.62	2015 Nov 11	*r*	18.31 ± 0.11	180	Kiso/KWFC
SKYS9	57337.62	2015 Nov 11	*r*	18.30 ± 0.12	180	Kiso/KWFC
SKYS9	57341.50	2015 Nov 15	*r*	17.73 ± 0.09	180	Kiso/KWFC
SKYS9	57341.66	2015 Nov 15	*r*	17.70 ± 0.09	180	Kiso/KWFC
SKYS9	57346.57	2015 Nov 20	*r*	17.62 ± 0.08	180	Kiso/KWFC
SKYS9	57346.62	2015 Nov 20	*r*	17.60 ± 0.08	180	Kiso/KWFC
SKYS9	57341.64	2015 Nov 15	*i*	17.92 ± 0.10	180	Kiso/KWFC
SKYS9	57346.63	2015 Nov 15	*i*	17.83 ± 0.09	180	Kiso/KWFC
SKYS9	57346.68	2015 Nov 20	*i*	17.65 ± 0.09	220	Kiso/KWFC
SKYS9	57331.70	2015 Nov 20	*i*	17.58 ± 0.08	220	Kiso/KWFC
SKYS9	57338.47	2015 Nov 21	*i*	17.60 ± 0.10	220	Kiso/KWFC
SKYS9	57341.51	2015 Nov 15	*z*	18.17 ± 0.12	180	Kiso/KWFC
SKYS9	57346.58	2015 Nov 20	*z*	17.90 ± 0.10	220	Kiso/KWFC
SKYS9	57346.69	2015 Nov 20	*z*	17.88 ± 0.10	220	Kiso/KWFC
SKYS9	57353.46	2015 Nov 12	*g*	18.38 ± 0.15	60	MITSuME
SKYS9	57354.55	2015 Nov 20	*g*	18.47 ± 0.16	60	MITSuME
SKYS9	57357.46	2015 Nov 22	*g*	18.72 ± 0.17	60	MITSuME
SKYS9	57353.46	2015 Nov 28	*g*	18.38 ± 0.15	60	MITSuME
SKYS9	57354.55	2015 Dec 01	*g*	18.47 ± 0.16	60	MITSuME

Note:

[a] Median time for single exposure.

[b] AB magnitudes for SDSS ugriz filter.

Table 12: A Summary of Spectroscopic Follow-ups of SKYS9

Object	UT	Exp. Time (s)	Telescope	slit width (")	grism/filter
SKYS9	2015 Nov. 12	2400	LJT/YFOSC	2.51	#3[a]
SKYS9	2015 Nov. 14	2400	LJT/YFOSC	2.51	#3[a]
SKYS9	2015 Nov. 16	2400	LJT/YFOSC	2.51	#3[a]
SKYS9	2015 Nov. 21	2400	LJT/YFOSC	2.51	#3[a]
SKYS9	2015 Nov. 23	2400	LJT/YFOSC	2.51	#3[a]
SKYS9	2015 Dec. 02	1800	LT/SPRAT	1.8	Red/4020longpass[b]
SKYS9	2015 Dec. 09	2400	LJT/YFOSC	2.51	#3[a]
SKYS9	2016 Jan. 03	2400	LJT/YFOSC	2.51	#3[a]
SKYS9	2016 Jan. 07	2400	LJT/YFOSC	2.51	#3[a]

Note:

[a] The wavelength coverage and resolution of Grism#3 on LJT/YFOSC is 340-910 nm and 150 respectively.

[b] LT/SPART Red configuration has much better performance above $\sim$6000Å, "4020longpass" is the abbreviation of "Edmund Optics 400nm longpass filter". The wavelength coverage and resolution is 400-800 nm and 350 respectively.

References

Iair Arcavi, Avishay Gal-Yam, Ofer Yaron, Assaf Sternberg, Itay Rabinak, Eli Waxman, Mansi M Kasliwal, Robert M Quimby, Eran O Ofek, Assaf Horesh, et al. Sn 2011dh: discovery of a type iib supernova from a compact progenitor in the nearby galaxy m51. *ApJL*, 742 (2):L18, 2011.

David Arnett. *Supernovae and Nucleosynthesis: An Investigation of the History of Matter from the Big Bang to the Present*. 1996.

David Arnett and Eli Livne. The Delayed-Detonation Model of Type IA Supernovae I. The Deflagration Phase. *ApJ*, 427:314, May 1994.

W. D. Arnett. Type I supernovae. I - Analytic solutions for the early part of the light curve. *ApJ*, 253:785–797, February 1982.

W. David Arnett. A Possible Model of Supernovae: Detonation of ^{12}C. *ApJS*, 5:180–212, October 1969.

W. Baade and F. Zwicky. On Super-novae. *Proceedings of the National Academy of Science*, 20:254–259, May 1934. doi: 10.1073/pnas.20.5.254.

D. D. Balam and M. L. Graham. ATel 7529: DAO spectroscopic classification of PSN J13003230+2758411 in the Coma Cluster. *ATel*, 7529:1, May 2015.

C. Barbarino, M. T. Botticella, M. Dall'Ora, M. Della Valle, S. Benetti, J. D. Lyman, S. J. Smartt, I. Arcavi, C. Baltay, D. Bersier, M. Dennefeld, N. Ellman, M. Fraser, A. Gal-Yam, G. Hosseinzadeh, D. A. Howell, C. Inserra, E. Kankare, G. Leloudas, K. Maguire, C. McCully, A. Mitra, R. McKinnon, F. Olivares E., G. Pignata, D. Rabinowitz, S. Rostami, K. W. Smith, M. Sullivan, S. Valenti, O. Yaron, and D. Young. LSQ14efd: observations of the cooling of a shock break-out event in a type Ic Supernova. *MNRAS*, 471:2463–2480, October 2017.

K. Barbary, G. Aldering, R. Amanullah, M. Brodwin, N. Connolly, K. S. Dawson, M. Doi, P. Eisenhardt, L. Faccioli, V. Fadeyev, H. K. Fakhouri, A. S. Fruchter, D. G. Gilbank, M. D. Gladders, G. Goldhaber, A. Goobar, T. Hattori, E. Hsiao, X. Huang, Y. Ihara, N. Kashikawa, B. Koester, K. Konishi, M. Kowalski, C. Lidman, L. Lubin, J. Meyers, T. Morokuma, T. Oda, N. Panagia, S. Perlmutter, M. Postman, P. Ripoche, P. Rosati, D. Rubin, D. J. Schlegel, A. L. Spadafora, S. A. Stanford, M. Strovink, N. Suzuki, N. Takanashi, K. Tokita, N. Yasuda, and Supernova Cosmology Project. The Hubble Space Telescope Cluster Supernova Survey. VI. The Volumetric Type Ia Supernova Rate. *ApJ*, 745:31, January 2012.

Cesare Barbieri. The Galileo Italian National Telescope and its Instrumentation. *Experimental Astronomy*, 7:257–279, January 1997.

S. Benetti, E. Cappellaro, P. A. Mazzali, M. Turatto, G. Altavilla, F. Bufano, N. Elias-Rosa, R. Kotak, G. Pignata, M. Salvo, and V. Stanishev. The Diversity of Type Ia Supernovae: Evidence for Systematics? *ApJ*, 623:1011–1016, April 2005.

E. Bertin and S. Arnouts. SExtractor: Software for source extraction. *A&AS*, 117:393–404, June 1996.

Emmanuel Bertin. SWarp: Resampling and Co-adding FITS Images Together. Astrophysics Source Code Library, October 2010.

FB Bianco, DA Howell, M Sullivan, A Conley, D Kasen, S González-Gaitán, J Guy, P Astier, C Balland, RG Carlberg, et al. Constraining type ia supernovae progenitors from three years of supernova legacy survey data. *ApJ*, 741(1):20, 2011.

Lars Bildsten, Ken J. Shen, Nevin N. Weinberg, and Gijs Nelemans. Faint Thermonuclear Supernovae from AM Canum Venaticorum Binaries. *ApJ*, 662:L95–L98, June 2007.

Stéphane Blondin and John L. Tonry. Determining the Type, Redshift, and Age of a Supernova Spectrum. *ApJ*, 666:1024–1047, September 2007.

Stéphane Blondin, Luc Dessart, D. John Hillier, and Alexei M. Khokhlov. Evidence for sub-Chandrasekhar-mass progenitors of Type Ia supernovae at the faint end of the width-luminosity relation. *MNRAS*, 470:157–165, September 2017.

Adam S. Bolton, David J. Schlegel, Éric Aubourg, Stephen Bailey, Vaishali Bhardwaj, Joel R. Brownstein, Scott Burles, Yan-Mei Chen, Kyle Dawson, Daniel J. Eisenstein, James E. Gunn, G. R. Knapp, Craig P. Loomis, Robert H. Lupton, Claudia Maraston, Demitri Muna, Adam D. Myers, Matthew D. Olmstead, Nikhil Padmanabhan, Isabelle Pâris, Will J. Percival, Patrick Petitjean, Constance M. Rockosi, Nicholas P. Ross, Donald P. Schneider, Yiping Shu, Michael A. Strauss, Daniel Thomas, Christy A. Tremonti, David A. Wake, Benjamin A. Weaver, and W. Michael Wood-Vasey. Spectral Classification and Redshift Measurement for the SDSS-III Baryon Oscillation Spectroscopic Survey. *AJ*, 144:144, November 2012.

Aoife Boyle, Stuart A. Sim, Stephan Hachinger, and Wolfgang Kerzendorf. Helium in double-detonation models of type Ia supernovae. *A&A*, 599:A46, March 2017.

AA Breeveld, W Landsman, ST Holland, P Roming, NPM Kuin, and MJ Page. An updated ultraviolet calibration for the swift/uvot. In *AIP Conference Proceedings*, volume 1358, pages 373–376. AIP, 2011.

Peter J Brown, Stephen T Holland, Stefan Immler, Peter Milne, Peter WA Roming, Neil Gehrels, John Nousek, Nino Panagia, Martin Still, and DANIEL VANDEN BERk. Ultraviolet light curves of supernovae with the swift ultraviolet/optical telescope. *AJ*, 137(5): 4517, 2009.

Peter J Brown, Alice A Breeveld, Stephen Holland, Paul Kuin, and Tyler Pritchard. Sousa: the swift optical/ultraviolet supernova archive. *APSS*, 354(1):89–96, 2014.

Peter J. Brown, Griffin Hosseinzadeh, Saurabh W. Jha, David Sand, Ethan Vieira, Xiaofeng Wang, Mi Dai, Kyle G. Dettman, Syed Uddin, Lifan Wang, Iair Arcavi, Tiara Diamond, Daichi Hiramatsu, D. Andrew Howell, E. Y. Hsiao, G. H. Marion, Curtis McCully, Peter A. Milne, Davron Mirzaqulov, Stefano Valenti, and Xiang Danfeng. Red and Reddened: Ultraviolet through Near-Infrared Observations of Type Ia Supernova 2017erp. *ArXiv e-prints*, art. arXiv:1808.04729, August 2018.

Sergio Campana, Vanessa Mangano, AJ Blustin, P Brown, David N Burrows, Guido Chincarini, JR Cummings, Giancarlo Cusumano, Massimo Della Valle, Daniele Malesani, et al. The association of grb 060218 with a supernova and the evolution of the shock wave. *Nature*, 442 (7106):1008, 2006.

Yi Cao, SR Kulkarni, D Andrew Howell, Avishay Gal-Yam, Mansi M Kasliwal, Stefano Valenti, Joel Johansson, Rahman Amanullah, Ariel Goobar, Jesper Sollerman, et al. A strong ultraviolet pulse from a newborn type ia supernova. *Nature*, 521(7552):328, 2015.

Yi Cao, J. Johansson, Peter E. Nugent, A. Goobar, Jakob Nordin, S. R. Kulkarni, S. Bradley Cenko, Ori D. Fox, Mansi M. Kasliwal, C. Fremling, R. Amanullah, E. Y. Hsiao, D. A. Perley, Brian D. Bue, Frank J. Masci, William H. Lee, and Nicolas Chotard. Absence of Fast-moving Iron in an Intermediate Type Ia Supernova between Normal and Super-Chandrasekhar. *ApJ*, 823:147, June 2016a.

Yi Cao, S. R. Kulkarni, Avishay Gal-Yam, S. Papadogiannakis, P. E. Nugent, Frank J. Masci, and Brian D. Bue. SN2002es-like Supernovae from Different Viewing Angles. *ApJ*, 832:86, November 2016b.

R. Cartier, M. Sullivan, R. E. Firth, G. Pignata, P. Mazzali, K. Maguire, M. J. Childress, I. Arcavi, C. Ashall, B. Bassett, S. M. Crawford, C. Frohmaier, L. Galbany, A. Gal-Yam, G. Hosseinzadeh, D. A. Howell, C. Inserra, J. Johansson, E. K. Kasai, C. McCully, S. Prajs, S. Prentice, S. Schulze, S. J. Smartt, K. W. Smith, M. Smith, S. Valenti, and D. R. Young. Early observations of the nearby Type Ia supernova SN 2015F. *MNRAS*, 464:4476–4494, February 2017.

N. K. Chakradhari, D. K. Sahu, S. Srivastav, and G. C. Anupama. Supernova SN 2012dn: a spectroscopic clone of SN 2006gz. *MNRAS*, 443:1663–1679, September 2014.

M. J. Childress, R. A. Scalzo, S. A. Sim, B. E. Tucker, F. Yuan, B. P. Schmidt, S. B. Cenko, J. M. Silverman, C. Contreras, E. Y. Hsiao, M. Phillips, N. Morrell, S. W. Jha, C. McCully, A. V. Filippenko, J. P. Anderson, S. Benetti, F. Bufano, T. de Jaeger, F. Forster, A. Gal-Yam, L. Le Guillou, K. Maguire, J. Maund, P. A. Mazzali, G. Pignata, S. Smartt, J. Spyromilio, M. Sullivan, F. Taddia, S. Valenti, D. D. R. Bayliss, M. Bessell, G. A. Blanc, D. J. Carson, K. I. Clubb, C. de Burgh-Day, T. D. Desjardins, J. J. Fang, O. D. Fox, E. L. Gates, I. T. Ho, S. Keller, P. L. Kelly, C. Lidman, N. S. Loaring, J. R. Mould, M. Owers, S. Ozbilgen, L. Pei, T. Pickering, M. B. Pracy, J. A. Rich, B. E. Schaefer, N. Scott, M. Stritzinger, F. P. A. Vogt, and G. Zhou. Spectroscopic Observations of SN 2012fr: A Luminous, Normal Type Ia Supernova with Early High-velocity Features and a Late Velocity Plateau. *ApJ*, 770:29, June 2013.

F. Ciabattari, E. Mazzoni, G. Petroni, L. Tomasella, A. Pastorello, S. Valenti, S. Benetti, E. Cappellaro, M. Turatto, and P. Ochner. Supernova 2012df = Psn J17481875+5218023. *CBET*, 3161:1, July 2012.

Tomas Dahlen, Louis-Gregory Strolger, and Adam G. Riess. The Extended HST Supernova Survey: The Rate of SNe Ia at z > 1.4 Remains Low. *ApJ*, 681:462–469, July 2008.

Luc Dessart, Stéphane Blondin, D. John Hillier, and Alexei Khokhlov. Constraints on the explosion mechanism and progenitors of Type Ia supernovae. *MNRAS*, 441:532–550, June 2014a.

Luc Dessart, D. John Hillier, Stéphane Blondin, and Alexei Khokhlov. Critical ingredients of Type Ia supernova radiative-transfer modelling. *MNRAS*, 441:3249–3270, July 2014b.

Carolyn L. Doherty, Pilar Gil-Pons, Lionel Siess, John C. Lattanzio, and Herbert H. B. Lau. Super- and massive AGB stars - IV. Final fates - initial-to-final mass relation. *MNRAS*, 446: 2599–2612, January 2015.

Mamoru Doi, Masayuki Tanaka, Masataka Fukugita, James E. Gunn, Naoki Yasuda, Željko Ivezić, Jon Brinkmann, Ernst de Haars, S. J. Kleinman, Jurek Krzesinski, and R. French Leger. Photometric Response Functions of the Sloan Digital Sky Survey Imager. *AJ*, 139: 1628–1648, April 2010.

Subo Dong, B. J. Shappee, J. L. Prieto, S. W. Jha, K. Z. Stanek, T. W. S. Holoien, C. S. Kochanek, T. A. Thompson, N. Morrell, I. B. Thompson, U. Basu, J. F. Beacom, D. Bersier, J. Brimacombe, J. S. Brown, F. Bufano, Ping Chen, E. Conseil, A. B. Danilet, E. Falco,

D. Grupe, S. Kiyota, G. Masi, B. Nicholls, F. Olivares E., G. Pignata, G. Pojmanski, G. V. Simonian, D. M. Szczygiel, and P. R. Woźniak. ASASSN-15lh: A highly super-luminous supernova. *Science*, 351:257–260, January 2016.

R. Ferretti, R. Amanullah, A. Goobar, J. Johansson, P. M. Vreeswijk, R. P. Butler, Y. Cao, S. B. Cenko, G. Doran, A. V. Filippenko, E. Freeland, G. Hosseinzadeh, D. A. Howell, P. Lundqvist, S. Mattila, J. Nordin, P. E. Nugent, T. Petrushevska, S. Valenti, S. Vogt, and P. Wozniak. Time-varying sodium absorption in the Type Ia supernova 2013gh. *A&A*, 592: A40, Jul 2016.

Alexei V. Filippenko, Michael W. Richmond, David Branch, Martin Gaskell, William Herbst, Charles H. Ford, Richard R. Treffers, Thomas Matheson, Luis C. Ho, Arjun Dey, Wallace L. W. Sargent, Todd A. Small, and Wil J. M. van Breugel. The Subluminous, Spectroscopically Peculiar Type 1a Supernova 1991bg in the Elliptical Galaxy NGC 4374. *AJ*, 104:1543, October 1992.

M. Fink, W. Hillebrandt, and F. K. Röpke. Double-detonation supernovae of sub-Chandrasekhar mass white dwarfs. *A&A*, 476:1133–1143, December 2007.

M. Fink, F. K. Röpke, W. Hillebrandt, I. R. Seitenzahl, S. A. Sim, and M. Kromer. Double-detonation sub-Chandrasekhar supernovae: can minimum helium shell masses detonate the core? *A&A*, 514:A53, May 2010.

A. Finzi and R. A. Wolf. Type i Supernovae. *ApJ*, 150:115, October 1967.

RE Firth, M Sullivan, A Gal-Yam, DA Howell, K Maguire, P Nugent, AL Piro, C Baltay, U Feindt, E Hadjiyksta, et al. The rising light curves of type ia supernovae. *MNRAS*, 446(4): 3895–3910, 2014.

Robert Fisher and Kevin Jumper. Single-degenerate type ia supernovae are preferentially overluminous. *The Astrophysical Journal*, 805(2):150, 2015.

Gastón Folatelli, M. M. Phillips, Nidia Morrell, Masaomi Tanaka, Keiichi Maeda, Ken'ichi Nomoto, Maximilian Stritzinger, Christopher R. Burns, Mario Hamuy, Paolo Mazzali, Luis Boldt, Abdo Campillay, Carlos Contreras, Sergio González, Miguel Roth, Francisco Salgado, W. L. Freedman, Barry F. Madore, S. E. Persson, and Nicholas B. Suntzeff. Unburned Material in the Ejecta of Type Ia Supernovae. *ApJ*, 745:74, January 2012.

Ryan J. Foley and Daniel Kasen. Measuring Ejecta Velocity Improves Type Ia Supernova Distances. *ApJ*, 729:55, March 2011.

Ryan J. Foley, Gautham Narayan, Peter J. Challis, Alexei V. Filippenko, Robert P. Kirshner, Jeffrey M. Silverman, and Thea N. Steele. SN 2006bt: A Perplexing, Troublesome, and Possibly Misleading Type Ia Supernova. *ApJ*, 708:1748–1759, January 2010.

Ryan J. Foley, Nathan E. Sanders, and Robert P. Kirshner. Velocity Evolution and the Intrinsic Color of Type Ia Supernovae. *ApJ*, 742:89, December 2011.

Ryan J. Foley, P. J. Challis, A. V. Filippenko, M. Ganeshalingam, W. Landsman, W. Li, G. H. Marion, J. M. Silverman, R. L. Beaton, V. N. Bennert, S. B. Cenko, M. Childress, P. Guhathakurta, L. Jiang, J. S. Kalirai, R. P. Kirshner, A. Stockton, E. J. Tollerud, J. Vinkó, J. C. Wheeler, and J. H. Woo. Very Early Ultraviolet and Optical Observations of the Type Ia Supernova 2009ig. *ApJ*, 744:38, January 2012.

Ryan J Foley, Peter J Challis, Ryan Chornock, Mohan Ganeshalingam, W Li, GH Marion, Nidia I Morrell, G Pignata, Maximillian D Stritzinger, Jeffrey M Silverman, et al. Type iax supernovae: a new class of stellar explosion. *ApJ*, 767(1):57, 2013.

Ryan J. Foley, Curtis McCully, Saurabh W. Jha, Lars Bildsten, Wen-fai Fong, Gautham Narayan, Armin Rest, and Maximilian D. Stritzinger. Possible Detection of the Stellar Donor or Remnant for the Type Iax Supernova 2008ha. *ApJ*, 792:29, September 2014.

Chris L. Fryer, Ashley J. Ruiter, Krzysztof Belczynski, Peter J. Brown, Filomena Bufano, Steven Diehl, Christopher J. Fontes, Lucille H. Frey, Stephen T. Holland, Aimee L. Hungerford, Stefan Immler, Paolo Mazzali, Casey Meakin, Peter A. Milne, Cody Raskin, and Francis X. Timmes. Spectra of Type Ia Supernovae from Double Degenerate Mergers. *ApJ*, 725: 296–308, December 2010.

Vadim N. Gamezo, Alexei M. Khokhlov, Elaine S. Oran, Almadena Y. Chtchelkanova, and Robert O. Rosenberg. Thermonuclear Supernovae: Simulations of the Deflagration Stage and Their Implications. *Science*, 299:77–81, January 2003.

Mohan Ganeshalingam, Weidong Li, Alexei V. Filippenko, Carmen Anderson, Griffin Foster, Elinor L. Gates, Christopher V. Griffith, Bryant J. Grigsby, Niels Joubert, Joel Leja, Thomas B. Lowe, Brent Macomber, Tyler Pritchard, Patrick Thrasher, and Dustin Winslow. Results of the Lick Observatory Supernova Search Follow-up Photometry Program: BVRI Light Curves of 165 Type Ia Supernovae. *ApJS*, 190:418–448, October 2010.

Mohan Ganeshalingam, Weidong Li, and Alexei V Filippenko. The rise-time distribution of nearby type ia supernovae. *MNRAS*, 416(4):2607–2622, 2011.

Mohan Ganeshalingam, Weidong Li, Alexei V Filippenko, Jeffrey M Silverman, Ryan Chornock, Ryan J Foley, Thomas Matheson, Robert P Kirshner, Peter Milne, Mike Calkins, et al. The low-velocity, rapidly fading type ia supernova 2002es. *ApJ*, 751(2):142, 2012.

Suvi Gezari, Luc Dessart, Stéphane Basa, D. Chris Martin, James D. Neill, S. E. Woosley, D. John Hillier, Gurvan Bazin, Karl Forster, Peter G. Friedman, Jérémy Le Du, Alain Mazure, Patrick Morrissey, Susan G. Neff, David Schiminovich, and Ted K. Wyder. Probing Shock Breakout with Serendipitous GALEX Detections of Two SNLS Type II-P Supernovae. *ApJ*, 683:L131, August 2008.

Ariel Goobar, Joel Johansson, Rahman Amanullah, Yi Cao, DA Perley, MM Kasliwal, Raphael Ferretti, PE Nugent, C Harris, A Gal-Yam, et al. The rise of sn 2014j in the nearby galaxy m82. *ApJL*, 784(1):L12, 2014.

O. Graur, D. Poznanski, D. Maoz, N. Yasuda, T. Totani, M. Fukugita, A. V. Filippenko, R. J. Foley, J. M. Silverman, A. Gal-Yam, A. Horesh, and B. T. Jannuzi. Supernovae in the Subaru Deep Field: the rate and delay-time distribution of Type Ia supernovae out to redshift 2. *MNRAS*, 417:916–940, October 2011.

James Guillochon, Jerod Parrent, Luke Zoltan Kelley, and Raffaella Margutti. An Open Catalog for Supernova Data. *ApJ*, 835:64, January 2017.

J. Guy, P. Astier, S. Baumont, D. Hardin, R. Pain, N. Regnault, S. Basa, R. G. Carlberg, A. Conley, S. Fabbro, D. Fouchez, I. M. Hook, D. A. Howell, K. Perrett, C. J. Pritchet, J. Rich, M. Sullivan, P. Antilogus, E. Aubourg, G. Bazin, J. Bronder, M. Filiol, N. Palanque-Delabrouille, P. Ripoche, and V. Ruhlmann-Kleider. SALT2: using distant supernovae to improve the use of type Ia supernovae as distance indicators. *A&A*, 466:11–21, April 2007.

S Hachinger, PA Mazzali, M Sullivan, RS Ellis, K Maguire, A Gal-Yam, DA Howell, PE Nugent, E Baron, J Cooke, et al. The uv/optical spectra of the type ia supernova sn 2010jn: a bright supernova with outer layers rich in iron-group elements. *MNRAS*, 429(3):2228–2248, 2013.

N. J. Hammer, H. Th. Janka, and E. Müller. Three-dimensional Simulations of Mixing Instabilities in Supernova Explosions. *ApJ*, 714:1371–1385, May 2010.

Yasuhito Hashiba, Mamoru Doi, Shigeyuki Sako, Tomoki Morokuma, Hanindyo Kuncarayakti, Mitsuru Kokubo, Kazuma Mitsuda, Hidenori Takahashi, Ken Tateuchi, Makoto Watanabe, et al. A fabry-perot and grism imaging spectrograph liss (line imager and slit spectrograph). In *SPIE*, volume 9147, page 91472J. International Society for Optics and Photonics, 2014.

Brian T Hayden, Peter M Garnavich, Richard Kessler, Joshua A Frieman, Saurabh W Jha, Bruce Bassett, David Cinabro, Benjamin Dilday, Daniel Kasen, John Marriner, et al. The rise and fall of type ia supernova light curves in the sdss-ii supernova survey. *ApJ*, 712(1):350, 2010.

M. Hicken, P. M. Garnavich, J. L. Prieto, S. Blondin, D. L. DePoy, R. P. Kirshner, and J. Parrent. The Luminous and Carbon-rich Supernova 2006gz: A Double Degenerate Merger? *ApJ*, 669: L17–L20, November 2007.

Malcolm Hicken, Peter Challis, Saurabh Jha, Robert P Kirshner, Tom Matheson, Maryam Modjaz, Armin Rest, W Michael Wood-Vasey, Gaspar Bakos, Elizabeth J Barton, et al. Cfa3: 185 type ia supernova light curves from the cfa. *ApJ*, 700(1):331, 2009.

Wolfgang Hillebrandt and Jens C. Niemeyer. Type IA Supernova Explosion Models. *ARA&A*, 38:191–230, January 2000.

P. Höflich and A. Khokhlov. Explosion Models for Type IA Supernovae: A Comparison with Observed Light Curves, Distances, H 0, and Q 0. *ApJ*, 457:500, February 1996.

P. Höflich, A. M. Khokhlov, and J. C. Wheeler. Delayed Detonation Models for Normal and Subluminous Type IA Supernovae: Absolute Brightness, Light Curves, and Molecule Formation. *ApJ*, 444:831, May 1995.

P. Höflich, J. C. Wheeler, and F. K. Thielemann. Type Ia Supernovae: Influence of the Initial Composition on the Nucleosynthesis, Light Curves, and Spectra and Consequences for the Determination of Ω_M and Λ. *ApJ*, 495:617–629, March 1998.

Peter Höflich, Christopher L. Gerardy, Robert A. Fesen, and Shoko Sakai. Infrared Spectra of the Subluminous Type Ia Supernova SN 1999by. *ApJ*, 568:791–806, April 2002.

G. Hosseinzadeh, I. Arcavi, S. Valenti, C. McCully, and D. A. Howell. FLOYDS Classification of PSN J22151967-6532534 as a Young Type Ia Supernova. *ATel*, 7928:1, August 2015.

Griffin Hosseinzadeh, David J Sand, Stefano Valenti, Peter Brown, D Andrew Howell, Curtis McCully, Daniel Kasen, Iair Arcavi, K Azalee Bostroem, Leonardo Tartaglia, et al. Early blue excess from the type ia supernova 2017cbv and implications for its progenitor. *ApJL*, 845(2):L11, 2017.

EY Hsiao, CR Burns, C Contreras, P Höflich, D Sand, GH Marion, MM Phillips, M Stritzinger, S González-Gaitán, RE Mason, et al. Strong near-infrared carbon in the type ia supernova iptf13ebh. *A&A*, 578:A9, 2015.

Jr. Iben, I. and A. V. Tutukov. Supernovae of type I as end products of the evolution of binaries with components of moderate initial mass. *ApJS*, 54:335–372, February 1984.

Željko Ivezić, Steven M. Kahn, J. Anthony Tyson, Bob Abel, Emily Acosta, Robyn Allsman, David Alonso, Yusra AlSayyad, Scott F. Anderson, John Andrew, James Roger P. Angel, George Z. Angeli, Reza Ansari, Pierre Antilogus, Constanza Araujo, Robert Armstrong, Kirk T. Arndt, Pierre Astier, Éric Aubourg, Nicole Auza, Tim S. Axelrod, Deborah J. Bard, Jeff D. Barr, Aurelian Barrau, James G. Bartlett, Amanda E. Bauer, Brian J. Bauman, Sylvain Baumont, Andrew C. Becker, Jacek Becla, Cristina Beldica, Steve Bellavia, Federica B. Bianco, Rahul Biswas, Guillaume Blanc, Jonathan Blazek, Roger D. Blandford, Josh S. Bloom, Joanne Bogart, Tim W. Bond, Anders W. Borgland, Kirk Borne, James F. Bosch, Dominique Boutigny, Craig A. Brackett, Andrew Bradshaw, William Nielsen Brandt, Michael E. Brown, James S. Bullock, Patricia Burchat, David L. Burke, Gianpietro Cagnoli, Daniel Calabrese, Shawn Callahan, Alice L. Callen, Srinivasan Chandrasekharan, Glenaver Charles-Emerson, Steve Chesley, Elliott C. Cheu, Hsin-Fang Chiang, James Chiang, Carol Chirino, Derek Chow, David R. Ciardi, Charles F. Claver, Johann Cohen-Tanugi, Joseph J. Cockrum, Rebecca Coles, Andrew J. Connolly, Kem H. Cook, Asantha Cooray, Kevin R. Covey, Chris Cribbs, Wei Cui, Roc Cutri, Philip N. Daly, Scott F. Daniel, Felipe Daruich, Guillaume Daubard, Greg Daues, William Dawson, Francisco Delgado, Alfred Dellapenna, Robert de Peyster, Miguel de Val- Borro, Seth W. Digel, Peter Doherty, Richard Dubois, Gregory P. Dubois-Felsmann, Josef Durech, Frossie Economou, Michael Eracleous, Henry Ferguson, Enrique Figueroa, Merlin Fisher- Levine, Warren Focke, Michael D. Foss, James Frank, Michael D. Freemon, Emmanuel Gangler, Eric Gawiser, John C. Geary, Perry Gee, Marla Geha, Charles J. B. Gessner, Robert R. Gibson, D. Kirk Gilmore, Thomas Glanzman, William Glick, Tatiana Goldina, Daniel A. Goldstein, Iain Goodenow, Melissa L. Graham, William J. Gressler, Philippe Gris, Leanne P. Guy, Augustin Guyonnet, Gunther Haller, Ron Harris, Patrick A. Hascall, Justine Haupt, Fabio Hernandez, Sven Herrmann, Edward Hileman, Joshua Hoblitt, John A. Hodgson, Craig Hogan, Dajun Huang, Michael E. Huffer, Patrick Ingraham, Walter R. Innes, Suzanne H. Jacoby, Bhuvnesh Jain, Fabrice Jammes, James Jee, Tim Jenness, Garrett Jernigan, Darko Jevremović, Kenneth Johns, Anthony S. Johnson, Margaret W. G. Johnson, R. Lynne Jones, Claire Juramy-Gilles, Mario Jurić, Jason S. Kalirai, Nitya J. Kallivayalil, Bryce Kalmbach, Jeffrey P. Kantor, Pierre Karst, Mansi M. Kasliwal, Heather Kelly, Richard Kessler, Veronica Kinnison, David Kirkby, Lloyd Knox, Ivan V. Kotov, Victor L. Krabbendam, K. Simon Krughoff, Petr Kubánek, John Kuczewski, Shri Kulkarni, John Ku, Nadine R. Kurita, Craig S. Lage, Ron Lambert, Travis Lange, J. Brian Langton, Laurent Le Guillou, Deborah Levine, Ming Liang, Kian-Tat Lim, Chris J. Lintott, Kevin E. Long, Margaux Lopez, Paul J. Lotz, Robert H. Lupton, Nate B. Lust, Lauren A. MacArthur, Ashish Mahabal, Rachel Mandelbaum, Darren S. Marsh, Philip J. Marshall, Stuart Marshall, Morgan May, Robert McKercher, Michelle McQueen, Joshua Meyers, Myriam Migliore, Michelle Miller, David J. Mills, Connor Miraval, Joachim Moeyens, David G. Monet, Marc Moniez,

Serge Monkewitz, Christopher Montgomery, Fritz Mueller, Gary P. Muller, Freddy Muñoz Arancibia, Douglas R. Neill, Scott P. Newbry, Jean-Yves Nief, Andrei Nomerotski, Martin Nordby, Paul O'Connor, John Oliver, Scot S. Olivier, Knut Olsen, William O'Mullane, Sandra Ortiz, Shawn Osier, Russell E. Owen, Reynald Pain, Paul E. Palecek, John K. Parejko, James B. Parsons, Nathan M. Pease, J. Matt Peterson, John R. Peterson, Donald L. Petravick, M. E. Libby Petrick, Cathy E. Petry, Francesco Pierfederici, Stephen Pietrowicz, Rob Pike, Philip A. Pinto, Raymond Plante, Stephen Plate, Paul A. Price, Michael Prouza, Veljko Radeka, Jayadev Rajagopal, Andrew P. Rasmussen, Nicolas Regnault, Kevin A. Reil, David J. Reiss, Michael A. Reuter, Stephen T. Ridgway, Vincent J. Riot, Steve Ritz, Sean Robinson, William Roby, Aaron Roodman, Wayne Rosing, Cecille Roucelle, Matthew R. Rumore, Stefano Russo, Abhijit Saha, Benoit Sassolas, Terry L. Schalk, Pim Schellart, Rafe H. Schindler, Samuel Schmidt, Donald P. Schneider, Michael D. Schneider, William Schoening, German Schumacher, Megan E. Schwamb, Jacques Sebag, Brian Selvy, Glenn H. Sembroski, Lynn G. Seppala, Andrew Serio, Eduardo Serrano, Richard A. Shaw, Ian Shipsey, Jonathan Sick, Nicole Silvestri, Colin T. Slater, J. Allyn Smith, R. Chris Smith, Shahram Sobhani, Christine Soldahl, Lisa Storrie-Lombardi, Edward Stover, Michael A. Strauss, Rachel A. Street, Christopher W. Stubbs, Ian S. Sullivan, Donald Sweeney, John D. Swinbank, Alexander Szalay, Peter Takacs, Stephen A. Tether, Jon J. Thaler, John Gregg Thayer, Sandrine Thomas, Vaikunth Thukral, Jeffrey Tice, David E. Trilling, Max Turri, Richard Van Berg, Daniel Vanden Berk, Kurt Vetter, Francoise Virieux, Tomislav Vucina, William Wahl, Lucianne Walkowicz, Brian Walsh, Christopher W. Walter, Daniel L. Wang, Shin-Yawn Wang, Michael Warner, Oliver Wiecha, Beth Willman, Scott E. Winters, David Wittman, Sidney C. Wolff, W. Michael Wood-Vasey, Xiuqin Wu, Bo Xin, Peter Yoachim, Hu Zhan, and for the LSST Collaboration. LSST: from Science Drivers to Reference Design and Anticipated Data Products. *ArXiv e-prints*, art. arXiv:0805.2366, May 2008.

Koichi Iwamoto, Franziska Brachwitz, Ken'ICHI Nomoto, Nobuhiro Kishimoto, Hideyuki Umeda, W. Raphael Hix, and Friedrich-Karl Thielemann. Nucleosynthesis in Chandrasekhar Mass Models for Type IA Supernovae and Constraints on Progenitor Systems and Burning-Front Propagation. *ApJS*, 125:439–462, December 1999.

S. W. Jha, Y. Camacho, K. Dettman, Y. C. Pan, R. J. Foley, A. Rest, D. Scolnic, and R. Skelton. SALT spectroscopic classification of SN 2017erp as a type-Ia supernova well before maximum light. *ATel*, 10490:1, June 2017.

Ji-an Jiang, Mamoru Doi, Keiichi Maeda, Toshikazu Shigeyama, Kenichi Nomoto, Naoki Yasuda, Saurabh W Jha, Masaomi Tanaka, Tomoki Morokuma, Nozomu Tominaga, et al. A hybrid type ia supernova with an early flash triggered by helium-shell detonation. *Nature*, 550(7674):80, 2017.

Ji-an Jiang, Mamoru Doi, Keiichi Maeda, and Toshikazu Shigeyama. Surface Radioactivity or Interactions? Multiple Origins of Early-excess Type Ia Supernovae and Associated Subclasses. *ApJ*, 865:149, October 2018. doi: 10.3847/1538-4357/aadb9a.

George C Jordan IV, RT Fisher, DM Townsley, AC Calder, C Graziani, S Asida, DQ Lamb, and JW Truran. Three-dimensional simulations of the deflagration phase of the gravitationally confined detonation model of type ia supernovae. *ApJ*, 681(2):1448, 2008.

George C Jordan IV, C. Graziani, R. T. Fisher, D. M. Townsley, C. Meakin, K. Weide, L. B. Reid, J. Norris, R. Hudson, and D. Q. Lamb. The detonation mechanism of the pulsationally assisted gravitationally confined detonation model of type ia supernovae. *ApJ*, 759(1):53, 2012.

D. Kasen, F. K. Röpke, and S. E. Woosley. The diversity of type Ia supernovae from broken symmetries. *Nature*, 460:869–872, August 2009.

Daniel Kasen. Seeing the collision of a supernova with its companion star. *ApJ*, 708(2):1025, 2010.

Daniel Kasen, R. C. Thomas, and P. Nugent. Time-dependent Monte Carlo Radiative Transfer Calculations for Three- dimensional Supernova Spectra, Light Curves, and Polarization. *ApJ*, 651:366–380, November 2006.

Nobunari Kashikawa, Kentaro Aoki, Ryo Asai, Noboru Ebizuka, Motoko Inata, Masanori Iye, Koji S. Kawabata, George Kosugi, Youichi Ohyama, Kiichi Okita, Tomohiko Ozawa, Yoshihiko Saito, Toshiyuki Sasaki, Kazuhiro Sekiguchi, Yasuhiro Shimizu, Hiroko Taguchi, Tadafumi Takata, Yasushi Yadoumaru, and Michitoshi Yoshida. FOCAS: The Faint Object Camera and Spectrograph for the Subaru Telescope. *PASJ*, 54:819–832, December 2002.

M. M. Kasliwal, E. O. Ofek, A. Gal-Yam, A. Rau, P. J. Brown, S. B. Cenko, P. B. Cameron, R. Quimby, S. R. Kulkarni, L. Bildsten, P. Milne, and G. Bryngelson. SN 2007ax: An Extremely Faint Type Ia Supernova. *ApJ*, 683:L29, August 2008.

Koji S. Kawabata, Osamu Nagae, Shingo Chiyonobu, Hiroyuki Tanaka, Hidehiko Nakaya, Mariko Suzuki, Yukiko Kamata, Satoshi Miyazaki, Kazuyoshi Hiragi, Hisashi Miyamoto, Masayuki Yamanaka, Akira Arai, Takuya Yamashita, Makoto Uemura, Takashi Ohsugi, Mizuki Isogai, Yoshiaki Ishitobi, and Shuji Sato. Wide-field one-shot optical polarimeter: HOWPol. In *SPIE*, volume 7014, page 70144L, July 2008.

A. M. Khokhlov. Delayed detonation model for type IA supernovae. *A&A*, 245:114–128, May 1991.

A. Klotz and E. Conseil. PSN J03333599-3607377 a supernova candidate by TAROT in NGC 1365. *ATel*, 4523:1, October 2012.

Masahiro Konishi, Kentaro Motohara, Ken Tateuchi, Hidenori Takahashi, Yutaro Kitagawa, Natsuko Kato, Shigeyuki Sako, Yuka K. Uchimoto, Koji Toshikawa, Ryou Ohsawa, Tomoyasu Yamamuro, Kentaro Asano, Yoshifusa Ita, Takafumi Kamizuka, Shinya Komugi, Shintaro Koshida, Sho Manabe, Noriyuki Matsunaga, Takeo Minezaki, Tomoki Morokuma, Asami Nakashima, Toshinobu Takagi, Toshihiko Tanabé, Mizuho Uchiyama, Tsutomu Aoki, Mamoru Doi, Toshihiro Handa, Daisuke Kato, Kimiaki Kawara, Kotaro Kohno, Takashi Miyata, Tomohiko Nakamura, Kazushi Okada, Takao Soyano, Yoichi Tamura, Masuo Tanaka, Ken'ichi Tarusawa, and Yuzuru Yoshii. ANIR: Atacama near-infrared camera for the 1.0 m miniTAO telescope. *PASJ*, 67:4, February 2015.

R. Kotak, W. P. S. Meikle, G. Pignata, M. Stehle, S. J. Smartt, S. Benetti, W. Hillebrandt, D. J. Lennon, P. A. Mazzali, F. Patat, and M. Turatto. Spectroscopy of the type Ia supernova SN 2002er: Days -11 to +215. *A&A*, 436:1021–1031, June 2005.

T. Kotani, N. Kawai, K. Yanagisawa, J. Watanabe, M. Arimoto, H. Fukushima, T. Hattori, M. Inata, H. Izumiura, J. Kataoka, H. Koyano, K. Kubota, D. Kuroda, M. Mori, S. Nagayama, K. Ohta, T. Okada, K. Okita, R. Sato, Y. Serino, Y. Shimizu, T. Shimokawabe, M. Suzuki, H. Toda, T. Ushiyama, Y. Yatsu, A. Yoshida, and M. Yoshida. MITSuME—Multicolor Imaging Telescopes for Survey and Monstrous Explosions. *NCimC*, 28:755, July 2005.

Kevin Krisciunas, Nicholas B. Suntzeff, Mark M. Phillips, Pablo Candia, José Luis Prieto, Roberto Antezana, Robin Chassagne, Hsiao-Wen Chen, Mark Dickinson, Peter R. Eisenhardt, Juan Espinoza, Peter M. Garnavich, David González, Thomas E. Harrison, Mario Hamuy, Vladimir D. Ivanov, Wojtek Krzemiński, Craig Kulesa, Patrick McCarthy, Amaya Moro-Martín, César Muena, Alberto Noriega-Crespo, S. E. Persson, Philip A. Pinto, Miguel Roth, Eric P. Rubenstein, S. Adam Stanford, Guy S. Stringfellow, Abner Zapata, Alain Porter, and Marina Wischnjewsky. Optical and Infrared Photometry of the Type Ia Supernovae 1991T, 1991bg, 1999ek, 2001bt, 2001cn, 2001cz, and 2002bo. *AJ*, 128:3034–3052, December 2004.

M. Kromer and S. A. Sim. Time-dependent three-dimensional spectrum synthesis for Type Ia supernovae. *MNRAS*, 398:1809–1826, October 2009.

M. Kromer, S. A. Sim, M. Fink, F. K. Röpke, I. R. Seitenzahl, and W. Hillebrandt. Double-detonation Sub-Chandrasekhar Supernovae: Synthetic Observables for Minimum Helium Shell Mass Models. *ApJ*, 719:1067–1082, August 2010.

M. Kromer, R. Pakmor, S. Taubenberger, G. Pignata, M. Fink, F. K. Röpke, I. R. Seitenzahl,

S. A. Sim, and W. Hillebrandt. SN 2010lp—a Type Ia Supernova from a Violent Merger of Two Carbon-Oxygen White Dwarfs. *ApJ*, 778:L18, November 2013.

Markus Kromer, Christoffer Fremling, R Pakmor, S Taubenberger, Rahman Amanullah, SB Cenko, Claes Fransson, Ariel Goobar, G Leloudas, Francesco Taddia, et al. The peculiar type ia supernova iptf14atg: Chandrasekhar-mass explosion or violent merger? *MNRAS*, 459 (4):4428–4439, 2016.

M. Kuhlen, S. E. Woosley, and G. A. Glatzmaier. Carbon Ignition in Type Ia Supernovae. II. A Three-dimensional Numerical Model. *ApJ*, 640:407–416, March 2006.

Masamichi Kutsuna and Toshikazu Shigeyama. Revealing progenitors of type ia supernovae from their light curves and spectra. *PASJ*, 67(3):54, 2015.

N. Kuznetsova, K. Barbary, B. Connolly, A. G. Kim, R. Pain, N. A. Roe, G. Aldering, R. Amanullah, K. Dawson, M. Doi, V. Fadeyev, A. S. Fruchter, R. Gibbons, G. Goldhaber, A. Goobar, A. Gude, R. A. Knop, M. Kowalski, C. Lidman, T. Morokuma, J. Meyers, S. Perlmutter, D. Rubin, D. J. Schlegel, A. L. Spadafora, V. Stanishev, M. Strovink, N. Suzuki, L. Wang, N. Yasuda, and Supernova Cosmology Project. A New Determination of the High-Redshift Type Ia Supernova Rates with the Hubble Space Telescope Advanced Camera for Surveys. *ApJ*, 673:981–998, February 2008.

Nicholas M Law, Shrinivas R Kulkarni, Richard G Dekany, Eran O Ofek, Robert M Quimby, Peter E Nugent, Jason Surace, Carl C Grillmair, Joshua S Bloom, Mansi M Kasliwal, et al. The palomar transient factory: system overview, performance, and first results. *PASP*, 121 (886):1395, 2009.

Bruno Leibundgut, Robert P. Kirshner, Mark M. Phillips, Lisa A. Wells, N. B. Suntzeff, Mario Hamuy, R. A. Schommer, A. R. Walker, L. Gonzalez, P. Ugarte, R. E. Williams, G. Williger, Mercedes Gomez, Ronald Marzke, Brian P. Schmidt, Barbara Whitney, Nelson Coldwell, J. Peters, F. H. Chaffee, Craig B. Foltz, D. Rehner, L. Siciliano, T. G. Barnes, K. P. Cheng, P. M. N. Hintzen, Y. C. Kim, Jose Maza, J. Wm. Parker, A. C. Porter, P. C. Schmidtke, and George Sonneborn. SN 1991bg: A Type IA Supernova With a Difference. *AJ*, 105:301, January 1993.

G. Leloudas, E. Y. Hsiao, J. Johansson, K. Maeda, T. J. Moriya, J. Nordin, T. Petrushevska, J. M. Silverman, J. Sollerman, M. D. Stritzinger, F. Taddia, and D. Xu. Supernova spectra below strong circumstellar interaction. *A&A*, 574:A61, February 2015.

Douglas C. Leonard. Constraining the type ia supernova progenitor: The search for hydrogen in nebular spectra. *ApJ*, 670(2):1275, 2007.

Naveh Levanon and Noam Soker. Early uv emission from disc-originated matter (dom) in type ia supernovae in the double-degenerate scenario. *MNRAS*, 470(2):2510–2516, 2017.

Naveh Levanon, Noam Soker, and Enrique García-Berro. Constraining the double-degenerate scenario for Type Ia supernovae from merger ejected matter. *MNRAS*, 447:2803–2809, March 2015.

Weidong Li, Alexei V. Filippenko, Ryan Chornock, Edo Berger, Perry Berlind, Michael L. Calkins, Peter Challis, Chris Fassnacht, Saurabh Jha, Robert P. Kirshner, Thomas Matheson, Wallace L. W. Sargent, Robert A. Simcoe, Graeme H. Smith, and Gordon Squires. SN 2002cx: The Most Peculiar Known Type Ia Supernova. *PASP*, 115:453–473, April 2003.

Weidong Li, Joshua S Bloom, Philipp Podsiadlowski, Adam A Miller, S Bradley Cenko, Saurabh W Jha, Mark Sullivan, D Andrew Howell, Peter E Nugent, Nathaniel R Butler, et al. Exclusion of a luminous red giant as a companion star to the progenitor of supernova sn 2011fe. *Nature*, 480(7377):348, 2011.

Weidong Li, Ryan Chornock, Jesse Leaman, Alexei V. Filippenko, Dovi Poznanski, Xiaofeng Wang, Mohan Ganeshalingam, and Filippo Mannucci. Nearby supernova rates from the Lick Observatory Supernova Search - III. The rate-size relation, and the rates as a function of galaxy Hubble type and colour. *MNRAS*, 412:1473–1507, April 2011.

Eli Livne. Numerical Simulations of the Convective Flame in White Dwarfs. *ApJ*, 406:L17, March 1993. doi: 10.1086/186776.

Eli Livne and Ami S. Glasner. Geometrical Effects in Off-Center Detonation of Helium Shells. *ApJ*, 361:244, September 1990.

P. Lundqvist, A. Nyholm, F. Taddia, J. Sollerman, J. Johansson, C. Kozma, N. Lundqvist, C. Fransson, P. M. Garnavich, M. Kromer, B. J. Shappee, and A. Goobar. No trace of a single-degenerate companion in late spectra of supernovae 2011fe and 2014J. *A&A*, 577: A39, May 2015.

Peter Lundqvist, Seppo Mattila, Jesper Sollerman, Cecilia Kozma, E. Baron, Nick L. J. Cox, Claes Fransson, Bruno Leibundgut, and Jason Spyromilio. Hydrogen and helium in the spectra of Type Ia supernovae. *MNRAS*, 435:329–345, October 2013.

K Maeda, S Benetti, M Stritzinger, FK Röpke, G Folatelli, Jesper Sollerman, S Taubenberger, K Nomoto, G Leloudas, M Hamuy, et al. An asymmetric explosion as the origin of spectral evolution diversity in type ia supernovae. *Nature*, 466(7302):82, 2010.

Keiichi Maeda and Koichi Iwamoto. Observational characteristics and possible asphericity of overluminous Type Ia supernovae. *MNRAS*, 394:239–249, March 2009.

Keiichi Maeda and Yukikatsu Terada. Progenitors of type Ia supernovae. *International Journal of Modern Physics D*, 25:1630024, July 2016.

Keiichi Maeda, Giorgos Leloudas, Stefan Taubenberger, Maximilian Stritzinger, Jesper Sollerman, Nancy Elias- Rosa, Stefano Benetti, Mario Hamuy, Gaston Folatelli, and Paolo A. Mazzali. Effects of the explosion asymmetry and viewing angle on the Type Ia supernova colour and luminosity calibration. *MNRAS*, 413:3075–3094, June 2011.

Keiichi Maeda, Masamichi Kutsuna, and Toshikazu Shigeyama. Signatures of a companion star in type ia supernovae. *ApJ*, 794(1):37, 2014.

Keiichi Maeda, Ji-an Jiang, Toshikazu Shigeyama, and Mamoru Doi. Type ia supernovae in the first few days: Signatures of helium detonation versus interaction. *ApJ*, 861(2):78, 2018.

K. Maguire, S. Taubenberger, M. Sullivan, and P. A. Mazzali. Searching for swept-up hydrogen and helium in the late-time spectra of 11 nearby Type Ia supernovae. *MNRAS*, 457:3254–3265, April 2016.

Kate Maguire, Mark Sullivan, Rollin C Thomas, P Nugent, D Andrew Howell, Avishay Gal-Yam, Iair Arcavi, Sagi Ben-Ami, Sarah Blake, Janos Botyanszki, et al. Ptf10ops–a subluminous, normal-width light curve type ia supernova in the middle of nowhere. *MNRAS*, 418(2): 747–758, 2011.

Dan Maoz, Filippo Mannucci, and Gijs Nelemans. Observational Clues to the Progenitors of Type Ia Supernovae. *ARA&A*, 52:107–170, August 2014.

GH Marion, Peter J Brown, Jozsef Vinkó, Jeffrey M Silverman, David J Sand, Peter Challis, Robert P Kirshner, J Craig Wheeler, Perry Berlind, Warren R Brown, et al. Sn 2012cg: Evidence for interaction between a normal sn ia and a non-degenerate binary companion. *ApJ*, 820(2):92, 2016.

T. Matheson, R. P. Kirshner, P. Challis, S. Jha, P. M. Garnavich, P. Berlind, M. L. Calkins, S. Blondin, Z. Balog, A. E. Bragg, N. Caldwell, K. Dendy Concannon, E. E. Falco, G. J. M. Graves, J. P. Huchra, J. Kuraszkiewicz, J. A. Mader, A. Mahdavi, M. Phelps, K. Rines, I. Song, and B. J. Wilkes. Optical Spectroscopy of Type ia Supernovae. *AJ*, 135:1598–1615, April 2008.

S. Mattila, P. Lundqvist, J. Sollerman, C. Kozma, E. Baron, C. Fransson, B. Leibundgut, and K. Nomoto. Early and late time VLT spectroscopy of SN 2001el - progenitor constraints for a type Ia supernova. *A&A*, 443:649–662, November 2005.

P. A. Mazzali, M. Sullivan, S. Hachinger, R. S. Ellis, P. E. Nugent, D. A. Howell, A. Gal-Yam, K. Maguire, J. Cooke, R. Thomas, K. Nomoto, and E. S. Walker. Hubble Space Telescope

spectra of the Type Ia supernova SN 2011fe: a tail of low-density, high-velocity material with Z < Z. *MNRAS*, 439:1959–1979, April 2014.

Curtis McCully, Saurabh W. Jha, Ryan J. Foley, Lars Bildsten, Wen-Fai Fong, Robert P. Kirshner, G. H. Marion, Adam G. Riess, and Maximilian D. Stritzinger. A luminous, blue progenitor system for the type Iax supernova 2012Z. *Nature*, 512:54–56, August 2014.

Casey A Meakin, Ivo Seitenzahl, Dean Townsley, George C Jordan IV, James Truran, and Don Lamb. Study of the detonation phase in the gravitationally confined detonation model of type ia supernovae. *ApJ*, 693(2):1188, 2009.

A. A. Miller, Y. Cao, A. L. Piro, N. Blagorodnova, B. D. Bue, S. B. Cenko, Suhail Dhawan, Raphael Ferretti, O. D. Fox, Christoffer Fremling, et al. Early observations of the type ia supernova iptf 16abc: A case of interaction with nearby, unbound material and/or strong ejecta mixing. *ApJ*, 852(2):100, 2018.

Peter A. Milne, Peter J. Brown, Peter W. A. Roming, Filomena Bufano, and Neil Gehrels. Grouping Normal Type Ia Supernovae by UV to Optical Color Differences. *ApJ*, 779:23, December 2013.

Peter A. Milne, Ryan J. Foley, Peter J. Brown, and Gautham Narayan. The Changing Fractions of Type Ia Supernova NUV–Optical Subclasses with Redshift. *ApJ*, 803:20, April 2015.

Takeo Minezaki, Daisuke Kato, Shigeyuki Sako, Masahiro Konishi, Shintaro Koshida, Natsuko Mitani, Tsutomu Aoki, Mamoru Doi, Toshihiro Handa, Yoshifusa Ita, Kimiaki Kawara, Kotaro Kohno, Takashi Miyata, Kentaro Motohara, Takao Soyano, Toshihiko Tanabé, Masuo Tanaka, Ken'ichi Tarusawa, Yuzuru Yoshii, Leonardo Bronfman, Maria T. Ruiz, and Mario Hamuy. The University of Tokyo Atacama 1.0-m Telescope. In *SPIE*, volume 7733, page 773356, July 2010.

S. Miyazaki, Y. Komiyama, S. Kawanomoto, Y. Doi, H. Furusawa, T. Hamana, Y. Hayashi, H. Ikeda, Y. Kamata, H. Karoji, M. Koike, T. Kurakami, S. Miyama, T. Morokuma, F. Nakata, K. Namikawa, H. Nakaya, K. Nariai, Y. Obuchi, Y. Oishi, N. Okada, Y. Okura, P. Tait, T. Takata, Y. Tanaka, M. Tanaka, T. Terai, D. Tomono, F. Uraguchi, T. Usuda, Y. Utsumi, Y. Yamada, H. Yamanoi, H. Aihara, H. Fujimori, S. Mineo, H. Miyatake, M. Oguri, T. Uchida, M. M. Tanaka, N. Yasuda, M. Takada, H. Murayama, A. J. Nishizawa, N. Sugiyama, M. Chiba, T. Futamase, S.-Y. Wang, H.-Y. Chen, P. T. P. Ho, E. J. Y. Liaw, C.-F. Chiu, C.-L. Ho, T.-C. Lai, Y.-C. Lee, D.-Z. Jeng, S. Iwamura, R. Armstrong, S. Bickerton, J. Bosch, J. E. Gunn, R. H. Lupton, C. Loomis, P. Price, S. Smith, M. A. Strauss, E. L. Turner, H. Suzuki, Y. Miyazaki, M. Muramatsu, K. Yamamoto, M. Endo, Y. Ezaki, N. Ito, N. Kawaguchi, S. Sofuku, T. Taniike, K. Akutsu, N. Dojo, K. Kasumi, T. Matsuda, K. Imoto, Y. Miwa, M. Suzuki,

K. Takeshi, and H. Yokota. Hyper Suprime-Cam: System design and verification of image quality. *PASJ*, 70:S1, January 2018.

Satoshi Miyazaki, Yutaka Komiyama, Hidehiko Nakaya, Yukiko Kamata, Yoshi Doi, Takashi Hamana, Hiroshi Karoji, Hisanori Furusawa, Satoshi Kawanomoto, Tomoki Morokuma, Yuki Ishizuka, Kyoji Nariai, Yoko Tanaka, Fumihiro Uraguchi, Yousuke Utsumi, Yoshiyuki Obuchi, Yuki Okura, Masamune Oguri, Tadafumi Takata, Daigo Tomono, Tomio Kurakami, Kazuhito Namikawa, Tomonori Usuda, Hitomi Yamanoi, Tsuyoshi Terai, Hatsue Uekiyo, Yoshihiko Yamada, Michitaro Koike, Hiro Aihara, Yuki Fujimori, Sogo Mineo, Hironao Miyatake, Naoki Yasuda, Jun Nishizawa, Tomoki Saito, Manobu Tanaka, Tomohisa Uchida, Nobu Katayama, Shiang-Yu Wang, Hsin-Yo Chen, Robert Lupton, Craig Loomis, Steve Bickerton, Paul Price, Jim Gunn, Hisanori Suzuki, Yasuhito Miyazaki, Masaharu Muramatsu, Koei Yamamoto, Makoto Endo, Yutaka Ezaki, Noboru Itoh, Yoshinori Miwa, Hideo Yokota, Toru Matsuda, Ryuichi Ebinuma, and Kunio Takeshi. Hyper Suprime-Cam. In *SPIE*, volume 8446, page 84460Z, September 2012.

Maryam Modjaz, Weidong Li, Alexei V. Filippenko, Jennifer Y. King, Douglas C. Leonard, Thomas Matheson, Richard R. Treffers, and Adam G. Riess. The Subluminous Type Ia Supernova 1998de in NGC 252. *PASP*, 113:308–325, March 2001.

Tomoki Morokuma, Nozomu Tominaga, Masaomi Tanaka, Kensho Mori, Emiko Matsumoto, Yuki Kikuchi, Takumi Shibata, Shigeyuki Sako, Tsutomu Aoki, Mamoru Doi, Naoto Kobayashi, Hiroyuki Maehara, Noriyuki Matsunaga, Hiroyuki Mito, Takashi Miyata, Yoshikazu Nakada, Takao Soyano, Ken'ichi Tarusawa, Satoshi Miyazaki, Fumiaki Nakata, Norio Okada, Yuki Sarugaku, Michael W. Richmond, Hiroshi Akitaya, Greg Aldering, Ko Arimatsu, Carlos Contreras, Takashi Horiuchi, Eric Y. Hsiao, Ryosuke Itoh, Ikuru Iwata, Koji S. Kawabata, Nobuyuki Kawai, Yutaro Kitagawa, Mitsuru Kokubo, Daisuke Kuroda, Paolo Mazzali, Toru Misawa, Yuki Moritani, Nidia Morrell, Rina Okamoto, Nikolay Pavlyuk, Mark M. Phillips, Elena Pian, Devendra Sahu, Yoshihiko Saito, Kei Sano, Maximilian D. Stritzinger, Yutaro Tachibana, Francesco Taddia, Katsutoshi Takaki, Ken Tateuchi, Akihiko Tomita, Dmitry Tsvetkov, Takahiro Ui, Nobuharu Ukita, Yuji Urata, Emma S. Walker, and Taketoshi Yoshii. Kiso Supernova Survey (KISS): Survey strategy. *PASJ*, 66:114, December 2014.

Tomoki Morokuma, Paolo Mazzali, Andrzej Piascik, Chris Ashall, Simon Prentice, Francesco Taddia, Maximilian Stritzinger, Ditte Slumstrup, Maria. R. Drout, Philip S. Cowperthwaite, Nozomu Tominaga, Masaomi Tanaka, Dmitry Tsvetkov, Nickolay Pavlyuk, Yuki Sarugaku, Yoshihiko Saito, Masafumi Yagi, Ji-an Jiang, Takumi Shibata, Katsuhiko Mameta, and

Masanori Takeishi. ATel 7532: KISS: Discovery and Identification of a young SN Ia KISS15n in the Coma cluster. *ATel*, 7532:1, May 2015.

Kentaro Motohara, Masahiro Konishi, Koji Toshikawa, Natsuko Mitani, Shigeyuki Sako, Yuka K. Uchimoto, Tomoyasu Yamamuro, Takeo Minezaki, Toshihiko Tanabe, Takashi Miyata, Shintaro Koshida, Daisuke Kato, Ryo Ohsawa, Tomohiko Nakamura, Kentaro Asano, Yuzuru Yoshii, Mamoru Doi, Kotaro Kohno, Masuo Tanaka, Kimiaki Kawara, Toshihiro Handa, Tsutomu Aoki, Takao Soyano, Ken'ichi Tarusawa, and Yoshifusa Ita. First Paschen alpha imaging from the ground: the first light of Atacama Near-Infrared Camera on the mini-TAO 1m telescope. In *SPIE*, volume 7735, page 77353K, July 2010.

Jeremy R. Mould, John P. Huchra, Wendy L. Freedman, Jr. Kennicutt, Robert C., Laura Ferrarese, Holland C. Ford, Brad K. Gibson, John A. Graham, Shaun M. G. Hughes, Garth D. Illingworth, Daniel D. Kelson, Lucas M. Macri, Barry F. Madore, Shoko Sakai, Kim M. Sebo, Nancy A. Silbermann, and Peter B. Stetson. The Hubble Space Telescope Key Project on the Extragalactic Distance Scale. XXVIII. Combining the Constraints on the Hubble Constant. *ApJ*, 529:786–794, February 2000.

J. C. Niemeyer and S. E. Woosley. The thermonuclear explosion of chandrasekhar mass white dwarfs. *ApJ*, 475(2):740, 1997.

K. Nomoto. Accreting white dwarf models for type I supernovae. I - Presupernova evolution and triggering mechanisms. *ApJ*, 253:798–810, February 1982a.

K. Nomoto. Accreting white dwarf models for type I supernovae. II. Off-center detonation supernovae. *ApJ*, 257:780–792, June 1982b.

K. Nomoto. Nucleosynthesis in Type-I Supernovae - Carbon Deflagration and Helium Detonation Models. In C. Chiosi and A. Renzini, editors, *Stellar Nucleosynthesis*, volume 109, page 205, January 1984.

K. Nomoto and Jr. Iben, I. Carbon ignition in a rapidly accreting degenerate dwarf - A clue to the nature of the merging process in close binaries. *ApJ*, 297:531–537, October 1985.

K. Nomoto, D. Sugimoto, and S. Neo. Carbon Deflagration Supernova, an Alternative to Carbon Detonation. *ApJS*, 39:L37, February 1976.

K. Nomoto, F. K. Thielemann, and K. Yokoi. Accreting white dwarf models for type I supern. III. Carbon deflagration supernovae. *ApJ*, 286:644–658, November 1984.

Peter Nugent, Mark Phillips, E. Baron, David Branch, and Peter Hauschildt. Evidence for a Spectroscopic Sequence among Type 1a Supernovae. *ApJL*, 455:L147, December 1995.

Peter E Nugent, Mark Sullivan, S Bradley Cenko, Rollin C Thomas, Daniel Kasen, D Andrew Howell, David Bersier, Joshua S Bloom, SR Kulkarni, Michael T Kandrashoff, et al. Supernova sn 2011fe from an exploding carbon–oxygen white dwarf star. *Nature*, 480(7377):344, 2011.

Rob P Olling, Richard Mushotzky, Edward J Shaya, Armin Rest, Peter M Garnavich, Brad E Tucker, Daniel Kasen, Steve Margheim, and Alexei V Filippenko. No signature of ejecta interaction with a stellar companion in three type ia supernovae. *Nature*, 521(7552):332, 2015.

R. Pakmor, M. Kromer, S. Taubenberger, and V. Springel. Helium-ignited Violent Mergers as a Unified Model for Normal and Rapidly Declining Type Ia Supernovae. *ApJ*, 770:L8, June 2013.

Rüdiger Pakmor, Markus Kromer, Friedrich K. Röpke, Stuart A. Sim, Ashley J. Ruiter, and Wolfgang Hillebrandt. Sub-luminous type Ia supernovae from the mergers of equal-mass white dwarfs with mass ˜0.9M_{solar}. *Nature*, 463:61–64, January 2010.

Kuo-Chuan Pan, Paul M. Ricker, and Ronald E. Taam. Impact of Type Ia Supernova Ejecta on Binary Companions in the Single- degenerate Scenario. *ApJ*, 750:151, May 2012.

Y-C Pan, RJ Foley, Markus Kromer, OD Fox, W Zheng, P Challis, KI Clubb, AV Filippenko, Gaston Folatelli, ML Graham, et al. 500 days of sn 2013dy: spectra and photometry from the ultraviolet to the infrared. *MNRAS*, 452(4):4307–4325, 2015.

J. T. Parrent, D. A. Howell, B. Friesen, R. C. Thomas, R. A. Fesen, D. Milisavljevic, F. B. Bianco, B. Dilday, P. Nugent, E. Baron, I. Arcavi, S. Ben-Ami, D. Bersier, L. Bildsten, J. Bloom, Y. Cao, S. B. Cenko, A. V. Filippenko, A. Gal-Yam, M. M. Kasliwal, N. Konidaris, S. R. Kulkarni, N. M. Law, D. Levitan, K. Maguire, P. A. Mazzali, E. O. Ofek, Y. Pan, D. Polishook, D. Poznanski, R. M. Quimby, J. M. Silverman, A. Sternberg, M. Sullivan, E. S. Walker, Dong Xu, C. Buton, and R. Pereira. Analysis of the Early-time Optical Spectra of SN 2011fe in M101. *ApJL*, 752:L26, June 2012.

Jerod T. Parrent, R. C. Thomas, Robert A. Fesen, G. H. Marion, Peter Challis, Peter M. Garnavich, Dan Milisavljevic, Jòzsef Vinkò, and J. Craig Wheeler. A Study of Carbon Features in Type Ia Supernova Spectra. *ApJ*, 732:30, May 2011.

F. Patat, S. Benetti, E. Cappellaro, I. J. Danziger, M. della Valle, P. A. Mazzali, and M. Turatto. The type IA supernova 1994D in NGC 4526: the early phases. *MNRAS*, 278:111–124, January 1996.

Chien Y. Peng, Luis C. Ho, Chris D. Impey, and Hans-Walter Rix. Detailed Decomposition of Galaxy Images. II. Beyond Axisymmetric Models. *AJ*, 139:2097–2129, June 2010.

R. Pereira, R. C. Thomas, G. Aldering, P. Antilogus, C. Baltay, S. Benitez-Herrera, S. Bongard, C. Buton, A. Canto, F. Cellier-Holzem, J. Chen, M. Childress, N. Chotard, Y. Copin, H. K. Fakhouri, M. Fink, D. Fouchez, E. Gangler, J. Guy, W. Hillebrandt, E. Y. Hsiao, M. Kerschhaggl, M. Kowalski, M. Kromer, J. Nordin, P. Nugent, K. Paech, R. Pain, E. Pécontal, S. Perlmutter, D. Rabinowitz, M. Rigault, K. Runge, C. Saunders, G. Smadja, C. Tao, S. Taubenberger, A. Tilquin, and C. Wu. Spectrophotometric time series of SN 2011fe from the Nearby Supernova Factory. *A&A*, 554:A27, June 2013.

S. Perlmutter, S Gabi, G Goldhaber, A Goobar, DE Groom, IM Hook, AG Kim, MY Kim, JC Lee, R Pain, et al. Measurements* of the cosmological parameters ω and λ from the first seven supernovae at z 0.35. *ApJ*, 483(2):565, 1997.

S. Perlmutter, G. Aldering, G. Goldhaber, R. A. Knop, P. Nugent, P. G. Castro, S. Deustua, S. Fabbro, A. Goobar, D. E. Groom, I. M. Hook, A. G. Kim, M. Y. Kim, J. C. Lee, N. J. Nunes, R. Pain, C. R. Pennypacker, R. Quimby, C. Lidman, R. S. Ellis, M. Irwin, R. G. McMahon, P. Ruiz-Lapuente, N. Walton, B. Schaefer, B. J. Boyle, A. V. Filippenko, T. Matheson, A. S. Fruchter, N. Panagia, H. J. M. Newberg, W. J. Couch, and The Supernova Cosmology Project. Measurements of Omega and Lambda from 42 High-Redshift Supernovae. *ApJ*, 517:565, jun 1999.

M. M. Phillips. The Absolute Magnitudes of Type IA Supernovae. *ApJ*, 413:L105, August 1993.

Anthony L. Piro. Radioactively Powered Rising Light Curves of Type Ia Supernovae. *ApJ*, 759: 83, November 2012.

Anthony L Piro and Viktoriya S Morozova. Exploring the potential diversity of early type ia supernova light curves. *ApJ*, 826(1):96, 2016.

Anthony L. Piro and Ehud Nakar. What can we Learn from the Rising Light Curves of Radioactively Powered Supernovae? *ApJ*, 769:67, May 2013.

Anthony L. Piro and Ehud Nakar. Constraints on Shallow ^{56}Ni from the Early Light Curves of Type Ia Supernovae. *ApJ*, 784:85, March 2014.

Anthony L. Piro, Philip Chang, and Nevin N. Weinberg. Shock Breakout from Type Ia Supernova. *ApJ*, 708:598–604, January 2010.

Tomasz Plewa, AC Calder, and DQ Lamb. Type ia supernova explosion: Gravitationally confined detonation. *ApJL*, 612(1):L37, 2004.

Iu. P. Pskovskii. Light curves, color curves, and expansion velocity of type I supernovae as functions of the rate of brightness decline. *Soviet Astronomy*, 21:675, December 1977.

Yu. P. Pskovskii. Photometric classification and basic parameters of type I supernovae. *Soviet Astronomy*, 28:658–664, December 1984.

Cody Raskin and Daniel Kasen. Tidal tail ejection as a signature of type ia supernovae from white dwarf mergers. *ApJ*, 772(1):1, 2013.

Arne Rau, Shrinivas R. Kulkarni, Nicholas M. Law, Joshua S. Bloom, David Ciardi, George S. Djorgovski, Derek B. Fox, Avishay Gal-Yam, Carl C. Grillmair, Mansi M. Kasliwal, Peter E. Nugent, Eran O. Ofek, Robert M. Quimby, William T. Reach, Michael Shara, Lars Bildsten, S. Bradley Cenko, Andrew J. Drake, Alexei V. Filippenko, David J. Helfand, George Helou, D. Andrew Howell, Dovi Poznanski, and Mark Sullivan. Exploring the Optical Transient Sky with the Palomar Transient Factory. *PASP*, 121:1334, December 2009.

M. Richmond and B. Vietje. BVRI Photometry of SN 2016coj in NGC 4125. *Journal of the American Association of Variable Star Observers (JAAVSO)*, 45:65, June 2017.

M. W. Richmond and H. A. Smith. BVRI Photometry of SN 2011fe in M101. *Journal of the American Association of Variable Star Observers (JAAVSO)*, 40:872, April 2012.

A. G. Riess, A. V. Filippenko, P. Challis, A. Clocchiatti, A. Diercks, P. M. Garnavich, R. L. Gilliland, C. J. Hogan, S. Jha, R. P. Kirshner, B. Leibundgut, M. M. Phillips, D. Reiss, B. P. Schmidt, R. A. Schommer, R. C. Smith, J. Spyromilio, C. Stubbs, N. B. Suntzeff, and J. Tonry. Observational Evidence from Supernovae for an Accelerating Universe and a Cosmological Constant. *AJ*, 116:1009–1038, sep 1998.

Adam G. Riess, Alexei V. Filippenko, Weidong Li, and Brian P. Schmidt. Is there an Indication of Evolution of Type IA Supernovae from their Rise Times? *AJ*, 118:2668–2674, December 1999a.

Adam G. Riess, Alexei V. Filippenko, Weidong Li, Richard R. Treffers, Brian P. Schmidt, Yulei Qiu, Jingyao Hu, Mark Armstrong, Chuck Faranda, Eric Thouvenot, and Christian Buil. The Rise Time of Nearby Type IA Supernovae. *AJ*, 118:2675–2688, December 1999b.

Steven A. Rodney, Adam G. Riess, Louis-Gregory Strolger, Tomas Dahlen, Or Graur, Stefano Casertano, Mark E. Dickinson, Henry C. Ferguson, Peter Garnavich, Brian Hayden, Saurabh W. Jha, David O. Jones, Robert P. Kirshner, Anton M. Koekemoer, Curtis McCully, Bahram Mobasher, Brandon Patel, Benjamin J. Weiner, S. Bradley Cenko, Kelsey I. Clubb, Michael Cooper, Alexei V. Filippenko, Teddy F. Frederiksen, Jens Hjorth, Bruno Leibundgut, Thomas Matheson, Hooshang Nayyeri, Kyle Penner, Jonathan Trump, Jeffrey M. Silverman,

Vivian U, K. Azalee Bostroem, Peter Challis, Abhijith Rajan, Schuyler Wolff, S. M. Faber, Norman A. Grogin, and Dale Kocevski. Type Ia Supernova Rate Measurements to Redshift 2.5 from CANDELS: Searching for Prompt Explosions in the Early Universe. *AJ*, 148:13, July 2014.

F. K. Röpke, S. E. Woosley, and W. Hillebrandt. Off-Center Ignition in Type Ia Supernovae. I. Initial Evolution and Implications for Delayed Detonation. *ApJ*, 660:1344–1356, May 2007.

Hideyuki Saio and Ken'ichi Nomoto. Inward Propagation of Nuclear-burning Shells in Merging C-O and He White Dwarfs. *ApJ*, 500:388–397, June 1998.

Kiyoshi Sakimoto, Hiroshi Akitaya, Takuya Yamashita, Koji S. Kawabata, Hidehiko Nakaya, Hisashi Miyamoto, Tatsuya Harao, Ryosuke Itoh, Risako Matsui, Yuki Moritani, Asami Nakashima, Takashi Ohsugi, Mahito Sasada, Katsutoshi Takaki, Issei Ueno, Takahiro Ui, Takeshi Urano, and Michitoshi Yoshida. An optical and near-infrared multipurpose instrument HONIR. In *SPIE*, volume 8446, page 844673, September 2012.

Masao Sako, Bruce Bassett, Andrew Becker, David Cinabro, Fritz DeJongh, D. L. Depoy, Ben Dilday, Mamoru Doi, Joshua A. Frieman, Peter M. Garnavich, Craig J. Hogan, Jon Holtzman, Saurabh Jha, Richard Kessler, Kohki Konishi, Hubert Lampeitl, John Marriner, Gajus Miknaitis, Robert C. Nichol, Jose Luis Prieto, Adam G. Riess, Michael W. Richmond, Roger Romani, Donald P. Schneider, Mathew Smith, Mark SubbaRao, Naohiro Takanashi, Kouichi Tokita, Kurt van der Heyden, Naoki Yasuda, Chen Zheng, John Barentine, Howard Brewington, Changsu Choi, Jack Dembicky, Michael Harnavek, Yutaka Ihara, Myungshin Im, William Ketzeback, Scott J. Kleinman, Jurek Krzesiński, Daniel C. Long, Elena Malanushenko, Viktor Malanushenko, Russet J. McMillan, Tomoki Morokuma, Atsuko Nitta, Kaike Pan, Gabrelle Saurage, and Stephanie A. Snedden. The Sloan Digital Sky Survey-II Supernova Survey: Search Algorithm and Follow-up Observations. *AJ*, 135:348–373, January 2008.

Shigeyuki Sako, Tsutomu Aoki, Mamoru Doi, Nobuyuki Ienaka, Naoto Kobayashi, Noriyuki Matsunaga, Hiroyuki Mito, Takashi Miyata, Tomoki Morokuma, Yoshikazu Nakada, Takao Soyano, Ken'ichi Tarusawa, Satoshi Miyazaki, Fumiaki Nakata, Norio Okada, Yuki Sarugaku, and Michael W. Richmond. KWFC: four square degrees camera for the Kiso Schmidt Telescope. In *SPIE*, volume 8446, page 84466L, September 2012.

Shigeyuki Sako, Ryou Ohsawa, Hidenori Takahashi, Yuto Kojima, Mamoru Doi, Naoto Kobayashi, Tsutomu Aoki, Noriaki Arima, Ko Arimatsu, Makoto Ichiki, et al. The tomo-e gozen wide field cmos camera for the kiso schmidt telescope. In *SPIE*, volume 10702, page 107020J. International Society for Optics and Photonics, 2018.

R. Scalzo, G. Aldering, P. Antilogus, C. Aragon, S. Bailey, C. Baltay, S. Bongard, C. Buton, F. Cellier-Holzem, M. Childress, N. Chotard, Y. Copin, H. K. Fakhouri, E. Gangler, J. Guy, A. G. Kim, M. Kowalski, M. Kromer, J. Nordin, P. Nugent, K. Paech, R. Pain, E. Pecontal, R. Pereira, S. Perlmutter, D. Rabinowitz, M. Rigault, K. Runge, C. Saunders, S. A. Sim, G. Smadja, C. Tao, S. Taubenberger, R. C. Thomas, B. A. Weaver, and Nearby Supernova Factory. Type Ia supernova bolometric light curves and ejected mass estimates from the Nearby Supernova Factory. *MNRAS*, 440:1498–1518, May 2014.

Bradley E. Schaefer and Ashley Pagnotta. An absence of ex-companion stars in the type Ia supernova remnant SNR 0509-67.5. *Nature*, 481:164–166, January 2012.

Kevin Schawinski, Stephen Justham, Christian Wolf, Philipp Podsiadlowski, Mark Sullivan, Katrien C. Steenbrugge, Tony Bell, Hermann-Josef Röser, Emma S. Walker, Pierre Astier, Dave Balam, Christophe Balland, Ray Carlberg, Alex Conley, Dominique Fouchez, Julien Guy, Delphine Hardin, Isobel Hook, D. Andrew Howell, Reynald Pain, Kathy Perrett, Chris Pritchet, Nicolas Regnault, and Sukyoung K. Yi. Supernova Shock Breakout from a Red Supergiant. *Science*, 321:223–226, July 2008.

Edward F. Schlafly and Douglas P. Finkbeiner. Measuring Reddening with Sloan Digital Sky Survey Stellar Spectra and Recalibrating SFD. *ApJ*, 737:103, August 2011.

David J Schlegel, Douglas P Finkbeiner, and Marc Davis. Maps of dust infrared emission for use in estimation of reddening and cosmic microwave background radiation foregrounds. *ApJ*, 500(2):525, 1998.

Ivo R. Seitenzahl, Markus Kromer, Sebastian T. Ohlmann, Franco Ciaraldi-Schoolmann, Kai Marquardt, Michael Fink, Wolfgang Hillebrandt, Rüdiger Pakmor, Friedrich K. Röpke, Ashley J. Ruiter, Stuart A. Sim, and Stefan Taubenberger. Three-dimensional simulations of gravitationally confined detonations compared to observations of SN 1991T. *A&A*, 592:A57, July 2016.

Benjamin J. Shappee, K. Z. Stanek, R. W. Pogge, and P. M. Garnavich. No Stripped Hydrogen in the Nebular Spectra of Nearby Type Ia Supernova 2011fe. *ApJL*, 762:L5, January 2013.

Benjamin J Shappee, A. L. Piro, T. W.-S Holoien, J. L. Prieto, C. Contreras, K. Itagaki, C. R. Burns, C. S. Kochanek, K. Z. Stanek, E. Alper, et al. The young and bright type ia supernova asassn-14lp: Discovery, early-time observations, first-light time, distance to ngc 4666, and progenitor constraints. *ApJ*, 826(2):144, 2016.

Benjamin J. Shappee, A. L. Piro, K. Z. Stanek, S. G. Patel, R. A. Margutti, V. M. Lipunov, and R. W. Pogge. Strong evidence against a non-degenerate companion in sn 2012cg. *ApJ*, 855 (1):6, 2018.

Ken J. Shen and Lars Bildsten. Unstable Helium Shell Burning on Accreting White Dwarfs. *ApJ*, 699:1365–1373, July 2009.

Ken J. Shen and Lars Bildsten. The Ignition of Carbon Detonations via Converging Shock Waves in White Dwarfs. *ApJ*, 785:61, April 2014.

Ken J Shen, Lars Bildsten, Daniel Kasen, and Eliot Quataert. The long-term evolution of double white dwarf mergers. *ApJ*, 748(1):35, 2012.

Ken J. Shen, Daniel Kasen, Broxton J. Miles, and Dean M. Townsley. Sub-Chandrasekhar-mass White Dwarf Detonations Revisited. *ApJ*, 854:52, February 2018.

Kazuhiro Shimasaku, Masataka Fukugita, Mamoru Doi, Masaru Hamabe, Takashi Ichikawa, Sadanori Okamura, Maki Sekiguchi, Naoki Yasuda, Jon Brinkmann, István Csabai, Shin-Ichi Ichikawa, Zeljko Ivezić, Peter Z. Kunszt, Donald P. Schneider, Gyula P. Szokoly, Masaru Watanabe, and Donald G. York. Statistical Properties of Bright Galaxies in the Sloan Digital Sky Survey Photometric System. *AJ*, 122:1238–1250, September 2001.

Takashi Shimokawabe, Nobuyuki Kawai, Taro Kotani, Yoichi Yatsu, Takuto Ishimura, Nicolas Vasquez, Yuki Mori, Yusuke Kudo, Michitoshi Yoshida, Kenshi Yanagisawa, Shogo Nagayama, Hiroyuki Toda, Yasuhiro Shimozu, Daisuke Kuroda, Junichi Watanabe, Hideo Fukushima, and Masaki Mori. MITSuME: multicolor optical/NIR telescopes for GRB afterglows. In M. Galassi, David Palmer, and Ed Fenimore, editors, *AIPC*, volume 1000, pages 543–546, May 2008. doi: 10.1063/1.2943527.

L. Siess. Evolution of massive AGB stars. I. Carbon burning phase. *A&A*, 448:717–729, March 2006.

Jeffrey M. Silverman and Alexei V. Filippenko. Berkeley Supernova Ia Program - IV. Carbon detection in early-time optical spectra of Type Ia supernovae. *MNRAS*, 425:1917–1933, September 2012.

Jeffrey M. Silverman, Mohan Ganeshalingam, Weidong Li, Alexei V. Filippenko, Adam A. Miller, and Dovi Poznanski. Fourteen months of observations of the possible super-Chandrasekhar mass Type Ia Supernova 2009dc. *MNRAS*, 410:585–611, January 2011.

S. A. Sim, F. K. Röpke, W. Hillebrandt, M. Kromer, R. Pakmor, M. Fink, A. J. Ruiter, and I. R. Seitenzahl. Detonations in Sub-Chandrasekhar-mass C+O White Dwarfs. *ApJ*, 714: L52–L57, May 2010.

S. J. Smartt, T. W. Chen, A. Jerkstrand, M. Coughlin, E. Kankare, S. A. Sim, M. Fraser, C. Inserra, K. Maguire, K. C. Chambers, M. E. Huber, T. Krühler, G. Leloudas, M. Magee,

L. J. Shingles, K. W. Smith, D. R. Young, J. Tonry, R. Kotak, A. Gal-Yam, J. D. Lyman, D. S. Homan, C. Agliozzo, J. P. Anderson, C. R. Angus, C. Ashall, C. Barbarino, F. E. Bauer, M. Berton, M. T. Botticella, M. Bulla, J. Bulger, G. Cannizzaro, Z. Cano, R. Cartier, A. Cikota, P. Clark, A. De Cia, M. Della Valle, L. Denneau, M. Dennefeld, L. Dessart, G. Dimitriadis, N. Elias-Rosa, R. E. Firth, H. Flewelling, A. Flörs, A. Franckowiak, C. Frohmaier, L. Galbany, S. González-Gaitán, J. Greiner, M. Gromadzki, A. Nicuesa Guelbenzu, C. P. Gutiérrez, A. Hamanowicz, L. Hanlon, J. Harmanen, K. E. Heintz, A. Heinze, M. S. Hernandez, S. T. Hodgkin, I. M. Hook, L. Izzo, P. A. James, P. G. Jonker, W. E. Kerzendorf, S. Klose, Z. Kostrzewa- Rutkowska, M. Kowalski, M. Kromer, H. Kuncarayakti, A. Lawrence, T. B. Lowe, E. A. Magnier, I. Manulis, A. Martin-Carrillo, S. Mattila, O. McBrien, A. Müller, J. Nordin, D. O'Neill, F. Onori, J. T. Palmerio, A. Pastorello, F. Patat, G. Pignata, Ph. Podsiadlowski, M. L. Pumo, S. J. Prentice, A. Rau, A. Razza, A. Rest, T. Reynolds, R. Roy, A. J. Ruiter, K. A. Rybicki, L. Salmon, P. Schady, A. S. B. Schultz, T. Schweyer, I. R. Seitenzahl, M. Smith, J. Sollerman, B. Stalder, C. W. Stubbs, M. Sullivan, H. Szegedi, F. Taddia, S. Taubenberger, G. Terreran, B. van Soelen, J. Vos, R. J. Wainscoat, N. A. Walton, C. Waters, H. Weiland, M. Willman, P. Wiseman, D. E. Wright, Ł. Wyrzykowski, and O. Yaron. A kilonova as the electromagnetic counterpart to a gravitational-wave source. *Nature*, 551:75–79, November 2017.

Roger M. Smith, Richard G. Dekany, Christopher Bebek, Eric Bellm, Khanh Bui, John Cromer, Paul Gardner, Matthew Hoff, Stephen Kaye, Shrinivas Kulkarni, Andrew Lambert, Michael Levi, and Dan Reiley. The Zwicky transient facility observing system. In *SPIE*, volume 9147, page 914779, July 2014.

Michael T Smitka, Peter J Brown, Nicholas B Suntzeff, Jujia Zhang, Qian Zhai, Xiaofeng Wang, Jun Mo, and Tianmeng Zhang. The 1999aa-like type ia supernova iptf14bdn in the ultraviolet and optical. *ApJ*, 813(1):30, 2015.

W. M. Sparks and T. P. Stecher. Supernova: The Result of the Death Spiral of a White Dwarf into a Red Giant. *ApJ*, 188:149, February 1974.

Peter B. Stetson. DAOPHOT: A Computer Program for Crowded-Field Stellar Photometry. *PASP*, 99:191, March 1987.

Maximilian D Stritzinger, Benjamin J Shappee, Anthony L Piro, Christopher Ashall, E Baron, Peter Hoeflich, Simon Holmbo, Thomas W-S Holoien, MM Phillips, CR Burns, et al. Red versus blue: Early observations of thermonuclear supernovae reveal two distinct populations? *ApJL*, 864(2):L35, 2018.

Francesco Taddia, Christoffer Fremling, Jesper Sollerman, A Corsi, A Gal-Yam, Emir

Karamehmetoglu, R Lunnan, B Bue, Mattias Ergon, M Kasliwal, et al. iptf15dtg: a double-peaked type ic supernova from a massive progenitor. *A&A*, 592:A89, 2016.

N. Takanashi, M. Doi, N. Yasuda, H. Kuncarayakti, K. Konishi, D. P. Schneider, D. Cinabro, and J. Marriner. Photometric properties of intermediate-redshift Type Ia supernovae observed by the Sloan Digital Sky Survey-II Supernova Survey. *MNRAS*, 465:1274–1288, February 2017.

Masaomi Tanaka, Nozomu Tominaga, Tomoki Morokuma, Naoki Yasuda, Hisanori Furusawa, Petr V. Baklanov, Sergei I. Blinnikov, Takashi J. Moriya, Mamoru Doi, Ji-an Jiang, Takahiro Kato, Yuki Kikuchi, Hanindyo Kuncarayakti, Tohru Nagao, Ken'ichi Nomoto, and Yuki Taniguchi. Rapidly Rising Transients from the Subaru Hyper Suprime-Cam Transient Survey. *ApJ*, 819:5, March 2016.

Ataru Tanikawa, Naohito Nakasato, Yushi Sato, Kenichi Nomoto, Keiichi Maeda, and Izumi Hachisu. Hydrodynamical evolution of merging carbon–oxygen white dwarfs: Their pre-supernova structure and observational counterparts. *ApJ*, 807(1):40, 2015.

S. Taubenberger, S. Hachinger, G. Pignata, P. A. Mazzali, C. Contreras, S. Valenti, A. Pastorello, N. Elias-Rosa, O. Bärnbantner, H. Barwig, S. Benetti, M. Dolci, J. Fliri, G. Folatelli, W. L. Freedman, S. Gonzalez, M. Hamuy, W. Krzeminski, N. Morrell, H. Navasardyan, S. E. Persson, M. M. Phillips, C. Ries, M. Roth, N. B. Suntzeff, M. Turatto, and W. Hillebrandt. The underluminous Type Ia supernova 2005bl and the class of objects similar to SN 1991bg. *MNRAS*, 385:75–96, March 2008.

S. Taubenberger, S. Benetti, M. Childress, R. Pakmor, S. Hachinger, P. A. Mazzali, V. Stanishev, N. Elias-Rosa, I. Agnoletto, F. Bufano, M. Ergon, A. Harutyunyan, C. Inserra, E. Kankare, M. Kromer, H. Navasardyan, J. Nicolas, A. Pastorello, E. Prosperi, F. Salgado, J. Sollerman, M. Stritzinger, M. Turatto, S. Valenti, and W. Hillebrandt. High luminosity, slow ejecta and persistent carbon lines: SN 2009dc challenges thermonuclear explosion scenarios. *MNRAS*, 412:2735–2762, April 2011.

S. Taubenberger, M. Kromer, S. Hachinger, P. A. Mazzali, S. Benetti, P. E. Nugent, R. A. Scalzo, R. Pakmor, V. Stanishev, J. Spyromilio, F. Bufano, S. A. Sim, B. Leibundgut, and W. Hillebrandt. 'Super-Chandrasekhar' Type Ia Supernovae at nebular epochs. *MNRAS*, 432: 3117–3130, July 2013.

Stefan Taubenberger, A Pastorello, PA Mazzali, S Valenti, G Pignata, DN Sauer, A Arbey, O Bärnbantner, S Benetti, A Della Valle, et al. Sn 2004aw: confirming diversity of type ic supernovae. *MNRAS*, 371(3):1459–1477, 2006.

R. C. Thomas, G. Aldering, P. Antilogus, C. Aragon, S. Bailey, C. Baltay, S. Bongard, C. Buton, A. Canto, M. Childress, N. Chotard, Y. Copin, H. K. Fakhouri, E. Gangler, E. Y. Hsiao, M. Kerschhaggl, M. Kowalski, S. Loken, P. Nugent, K. Paech, R. Pain, E. Pecontal, R. Pereira, S. Perlmutter, D. Rabinowitz, M. Rigault, D. Rubin, K. Runge, R. Scalzo, G. Smadja, C. Tao, B. A. Weaver, C. Wu, P. J. Brown, P. A. Milne, and Nearby Supernova Factory. Type Ia Supernova Carbon Footprints. *ApJ*, 743:27, December 2011.

Todd A. Thompson. Accelerating Compact Object Mergers in Triple Systems with the Kozai Resonance: A Mechanism for "Prompt" Type Ia Supernovae, Gamma- Ray Bursts, and Other Exotica. *ApJ*, 741:82, November 2011.

F. X. Timmes and S. E. Woosley. The Conductive Propagation of Nuclear Flames. I. Degenerate C + O and O + NE + MG White Dwarfs. *ApJ*, 396:649, September 1992.

F. X. Timmes, Edward F. Brown, and J. W. Truran. On Variations in the Peak Luminosity of Type Ia Supernovae. *ApJ*, 590:L83–L86, June 2003.

Lina Tomasella, Stefano Benetti, Enrico Cappellaro, Andrea Pastorello, Massimo Turatto, Roberto Barbon, Nancy Elias-Rosa, Avet Harutyunyan, Paolo Ochner, Leonardo Tartaglia, et al. Asiago supernova classification program: Blowing out the first two hundred candles. *Astronomische Nachrichten*, 335(8):841–849, 2014.

N. Tominaga, S. Blinnikov, P. Baklanov, T. Morokuma, K. Nomoto, and T. Suzuki. Properties of Type II Plateau Supernova SNLS-04D2dc: Multicolor Light Curves of Shock Breakout and Plateau. *ApJL*, 705:L10–L14, November 2009.

N. Tominaga, T. Morokuma, S. I. Blinnikov, P. Baklanov, E. I. Sorokina, and K. Nomoto. Shock Breakout in Type II Plateau Supernovae: Prospects for High- Redshift Supernova Surveys. *ApJS*, 193:20, March 2011.

Tomonori Totani, Tomoki Morokuma, Takeshi Oda, Mamoru Doi, and Naoki Yasuda. Delay Time Distribution Measurement of Type Ia Supernovae by the Subaru /XMM-Newton Deep Survey and Implications for the Progenitor. *PASJ*, 60:1327, December 2008.

DM Townsley, AC Calder, SM Asida, IR Seitenzahl, F Peng, N Vladimirova, DQ Lamb, and JW Truran. Flame evolution during type ia supernovae and the deflagration phase in the gravitationally confined detonation scenario. *ApJ*, 668(2):1118, 2007.

M. Turatto, P. Ochner, S. Benetti, L. Tomasella, E. Cappellaro, N. Elias-Rosa, A. Pastorello, L. Tartaglia, and G. Terreran. Asiago spectroscopic observation of the two SN candidates ASASSN-15ug and ASASSN-15uh. *ATel*, 8439:1, December 2015.

Hideyuki Umeda, Ken'ichi Nomoto, Hitoshi Yamaoka, and Shinya Wanajo. Evolution of 3-9 M_{solar} Stars for Z=0.001-0.03 and Metallicity Effects on Type Ia Supernovae. *ApJ*, 513: 861–868, March 1999.

Pieter G. van Dokkum. Cosmic-Ray Rejection by Laplacian Edge Detection. *PASP*, 113:1420–1427, November 2001.

J. Vinkó, L. L. Kiss, B. Csák, G. Fúrész, R. Szabó, J. R. Thomson, and S. W. Mochnacki. The Peculiar Type Ia Supernova 1999by: Spectroscopy at Early Epochs. *AJ*, 121:3127–3132, June 2001.

E. S. Walker, C. Baltay, A. Campillay, C. Citrenbaum, C. Contreras, N. Ellman, U. Feindt, C. González, M. L. Graham, E. Hadjiyska, E. Y. Hsiao, K. Krisciunas, R. McKinnon, K. Ment, N. Morrell, P. Nugent, M. M. Phillips, D. Rabinowitz, S. Rostami, J. Serón, M. Stritzinger, M. Sullivan, and B. E. Tucker. First Results from the La Silla-QUEST Supernova Survey and the Carnegie Supernova Project. *ApJS*, 219:13, July 2015.

X. Wang, A. V. Filippenko, M. Ganeshalingam, W. Li, J. M. Silverman, L. Wang, R. Chornock, R. J. Foley, E. L. Gates, B. Macomber, F. J. D. Serduke, T. N. Steele, and D. S. Wong. Improved Distances to Type Ia Supernovae with Two Spectroscopic Subclasses. *ApJL*, 699: L139–L143, July 2009a.

X. Wang, W. Li, A. V. Filippenko, R. J. Foley, R. P. Kirshner, M. Modjaz, J. Bloom, P. J. Brown, D. Carter, A. S. Friedman, A. Gal-Yam, M. Ganeshalingam, M. Hicken, K. Krisciunas, P. Milne, J. M. Silverman, N. B. Suntzeff, W. M. Wood-Vasey, S. B. Cenko, P. Challis, D. B. Fox, D. Kirkman, J. Z. Li, T. P. Li, M. A. Malkan, M. R. Moore, D. B. Reitzel, R. M. Rich, F. J. D. Serduke, R. C. Shang, T. N. Steele, B. J. Swift, C. Tao, D. S. Wong, and S. N. Zhang. The Golden Standard Type Ia Supernova 2005cf: Observations from the Ultraviolet to the Near-Infrared Wavebands. *ApJ*, 697:380–408, May 2009b.

R. F. Webbink. Double white dwarfs as progenitors of R Coronae Borealis stars and type I supernovae. *ApJ*, 277:355–360, February 1984.

John Whelan and Jr. Iben, Icko. Binaries and Supernovae of Type I. *ApJ*, 186:1007–1014, December 1973.

Christopher J White, Mansi M Kasliwal, Peter E Nugent, Avishay Gal-Yam, D Andrew Howell, Mark Sullivan, Ariel Goobar, Anthony L Piro, Joshua S Bloom, Shrinivas R Kulkarni, et al. Slow-speed supernovae from the palomar transient factory: two channels. *ApJ*, 799(1):52, 2015.

S. E. Woosley and Daniel Kasen. Sub-Chandrasekhar Mass Models for Supernovae. *ApJ*, 734: 38, June 2011.

S. E. Woosley and Thomas A. Weaver. Sub–Chandrasekhar Mass Models for Type IA Supernovae. *ApJ*, 423:371, March 1994.

S. E. Woosley, R. E. Taam, and T. A. Weaver. Models for Type I Supernova. I. Detonations in White Dwarfs. *ApJ*, 301:601, February 1986.

Masayuki Yamanaka, Keiichi Maeda, Miho Kawabata, Masaomi Tanaka, Katsutoshi Takaki, Issei Ueno, Kazunari Masumoto, Koji S Kawabata, Ryosuke Itoh, Yuki Moritani, et al. Early-phase photometry and spectroscopy of transitional type ia sn 2012ht: Direct constraint on the rise time. *ApJL*, 782(2):L35, 2014.

Masayuki Yamanaka, Keiichi Maeda, Masaomi Tanaka, Nozomu Tominaga, Koji S Kawabata, Katsutoshi Takaki, Miho Kawabata, Tatsuya Nakaoka, Issei Ueno, Hiroshi Akitaya, et al. Oister optical and near-infrared observations of the super-chandrasekhar supernova candidate sn 2012dn: Dust emission from the circumstellar shell. *PASJ*, 68(5):68, 2016.

Kenshi Yanagisawa, Daisuke Kuroda, Michitoshi Yoshida, Yasuhiro Shimizu, Shogo Nagayama, Hiroyuki Toda, Kouji Ohta, and Nobuyuki Kawai. Six years of GRB follow up with MITSuME Okayama Telescope. In Nobuyuki Kawai and Shigehiro Nagataki, editors, *AIPC*, volume 1279, pages 466–468, October 2010.

Ofer Yaron and Avishay Gal-Yam. WISeREP—An Interactive Supernova Data Repository. *PASP*, 124:668, July 2012.

Yoichi Yatsu, Nobuyuki Kawai, Takashi Shimokawabe, Nicolas Vasquez, Takuto Ishimura, Taro Kotani, Kenshi Yanagisawa, Michitoshi Yoshida, Sinngo Nagayama, Hiroyasu Shimizu, Hiroyuki Toda, and Daisuke Kuroda. Development of MITSuME—Multicolor imaging telescopes for survey and monstrous explosions. *PhyE*, 40:434–437, December 2007.

Michitoshi Yoshida. Current Status of the Instruments, Instrumentation and Open Use of Okayama Astrophysical Observatory. *JKAS*, 38:117–120, June 2005.

Ju-Jia Zhang, Xiao-Feng Wang, Jin-Ming Bai, Tian-Meng Zhang, Bo Wang, Zheng-Wei Liu, Xu-Lin Zhao, and Jun-Cheng Chen. Optical and ultraviolet observations of the narrow-lined type ia sn 2012fr in ngc 1365. *AJ*, 148(1):1, 2014.

Ju-Jia Zhang, Xiao-Feng Wang, Michele Sasdelli, Tian-Meng Zhang, Zheng-Wei Liu, Paolo A. Mazzali, Xiang-Cun Meng, Keiichi Maeda, Jun-Cheng Chen, Fang Huang, Xu-Lin Zhao, Kai-Cheng Zhang, Qian Zhai, Elena Pian, Bo Wang, Liang Chang, Wei-Min Yi, Chuan-Jun

Wang, Xue-Li Wang, Yu-Xin Xin, Jian-Guo Wang, Bao-Li Lun, Xiang-Ming Zheng, Xi-Liang Zhang, Yu-Feng Fan, and Jin-Ming Bai. A Luminous Peculiar Type Ia Supernova SN 2011hr: More Like SN 1991T or SN 2007if? *ApJ*, 817:114, February 2016.

WeiKang Zheng, Jeffrey M Silverman, Alexei V Filippenko, Daniel Kasen, Peter E Nugent, Melissa Graham, Xiaofeng Wang, Stefano Valenti, Fabrizio Ciabattari, Patrick L Kelly, et al. The very young type ia supernova 2013dy: Discovery, and strong carbon absorption in early-time spectra. *ApJL*, 778(1):L15, 2013.

WeiKang Zheng, Isaac Shivvers, Alexei V. Filippenko, Koichi Itagaki, Kelsey I. Clubb, Ori D. Fox, Melissa L. Graham, Patrick L. Kelly, and Jon C. Mauerhan. Estimating the First-light Time of the Type Ia Supernova 2014J in M82. *ApJ*, 783:L24, March 2014.

WeiKang Zheng, Alexei V. Filippenko, Jon Mauerhan, Melissa L. Graham, Heechan Yuk, Griffin Hosseinzadeh, Jeffrey M. Silverman, Liming Rui, Ron Arbour, Ryan J. Foley, Bela Abolfathi, Louis E. Abramson, Iair Arcavi, Aaron J. Barth, Vardha N. Bennert, Andrew P. Brandel, Michael C. Cooper, Maren Cosens, Sean P. Fillingham, Benjamin J. Fulton, Goni Halevi, D. Andrew Howell, Tiffany Hsyu, Patrick L. Kelly, Sahana Kumar, Linyi Li, Wenxiong Li, Matthew A. Malkan, Christina Manzano-King, Curtis McCully, Peter E. Nugent, Yen-Chen Pan, Liuyi Pei, Bryan Scott, Remington Oliver Sexton, Isaac Shivvers, Benjamin Stahl, Tommaso Treu, Stefano Valenti, H. Alexander Vogler, Jonelle L. Walsh, and Xiaofeng Wang. Discovery and Follow-up Observations of the Young Type Ia Supernova 2016coj. *ApJ*, 841: 64, May 2017.